

70490

**FINITE ELEMENT ANALYSIS OF STRIP AND
CIRCULAR PLATE ANCHORS**

A Thesis Submitted
in Partial Fulfilment of the Requirements
for the Degree of
DOCTOR OF PHILOSOPHY

By
C. VIJAYAN

to the
DEPARTMENT OF CIVIL ENGINEERING
INDIAN INSTITUTE OF TECHNOLOGY, KANPUR
JANUARY, 1981

I. I. T. KANPUR
CENTRAL LIBRARY
Acc. No. A 70490

16 APR 1982

CE-1981-D-VJ-FIN

To

MY PARENTS



iii

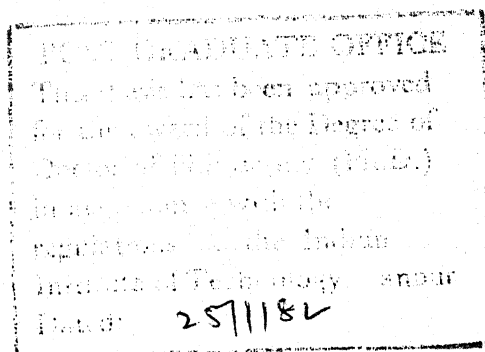
CERTIFICATE

Certified that this work on 'FINITE ELEMENT ANALYSIS OF STRIP AND CIRCULAR PLATE ANCHORS' has been carried out under my supervision and that it has not been submitted elsewhere for a degree.

(N.S.V. Kameswara Rao) 9/1/81

Professor and Head
Department of Civil Engineering
Indian Institute of Technology
Kanpur.

January, 1981



ACKNOWLEDGEMENTS

The author expresses his deep sense of gratitude to Dr. N.S.V. Kameswara Rao, Professor and Head, Department of Civil Engineering, Indian Institute of Technology, Kanpur for the able guidance and continuous encouragement throughout the present investigation.

The author is thankful to Dr. M.R. Madhav, Dr. Yudhbir, Dr. Umesh Dayal and Mr. K.V. Lakshmidhar for their encouragement during this work.

The author is thankful to his friends Anirudhan, Venkataramani and Remeshchandra for their valuable help during the preparation of this thesis.

The author is thankful to Mr. C.M. Abraham for careful and efficient typing of this thesis. The tracing work done by Mr. J.C. Verma and the cyclostyling work done by Mr. R.S. Dwivedi are gratefully acknowledged.

The author wishes to record his appreciation and thanks for the excellent computational facilities provided by Computer Centre, IIT, Kanpur for carrying out this work.

The author is deeply indebted to his wife Prema for her patience and understanding during this work and to his children Mini and Pradeep for brightening many a gloomy day by their love and cheer.

CONTENTS

	Page
LIST OF TABLES	viii
LIST OF FIGURES	xi
NOMENC LATURE	xix
SYNOPSIS	xxii
 CHAPTER 1	
INTRODUCTION	1
1.1 General	1
1.2 Scope of the Present Investigation	7
 CHAPTER 2	
LITERATURE REVIEW	13
2.1 Introduction	13
2.2 Analytical Methods	13
2.2.1 Elastic Analysis	13
2.2.2 Elasto-Plastic Analysis of Progressive Deformation and Collapse	17
2.2.3 Theoretical Approaches for the Computation of Ultimate Capacity of Anchors	24
2.3 Experimental Investigations	39
 CHAPTER 3	
ANALYTICAL MODEL, METHODS OF SOLUTION	49
3.1 Introduction	49
3.2 Finite Element Method	50
3.2.1 Physical Interpretation	51
3.2.2 Finite Element Displacement Formulation of an Elastic Continuum	53
3.2.3 Convergence in Finite Element Method	57
3.3 Displacement Formulation of Elements Used	58
3.3.1 Continuum Elements	58
3.3.2 Structural Elements	74
3.3.3 Interface Elements	85

3.4	Elasto-Plastic Analysis	96
3.4.1	Some Basic Concepts	
3.4.2	Derivation of Elasto-Plastic Matrix	102
3.4.3	The 'Initial Stress' Computational Method	109
3.4.4	Convergence Criteria and Increment Size	111
3.5	Kotter's Equation for Circular Rupture Surface	112
CHAPTER 4	HORIZONTAL STRIP ANCHORS	115
4.1	Introduction	115
4.2	Finite Element Model	117
4.2.1	Elastic Analysis	117
4.2.2	Elasto-Plastic Analysis	120
4.3	Results and Discussions	126
4.3.1	Elastic Analysis	126
4.3.2	Elasto-Plastic Analysis	141
4.4	Conclusions	159
CHAPTER 5	VERTICAL STRIP ANCHORS	205
5.1	Introduction	205
5.2	Elasto-Plastic Analysis	206
5.3	Results and Discussions	208
5.4	Conclusions	222
CHAPTER 6	CIRCULAR ANCHORS	236
6.1	Introduction	236
6.2	Finite Element Models	238
6.2.1	Elastic Analysis	238
6.2.2	Elasto-Plastic Analysis	240
6.3	Results and Discussions	244
6.3.1	Elastic Analysis	244
6.3.2	Elasto-Plastic Analysis	255
6.4	Conclusions	264

	Page
CHAPTER 7 THEORETICAL RESULTS OF BREAKOUT RESISTANCE OF HORIZONTAL STRIP AND CIRCULAR ANCHORS	287
7.1 General	287
7.2 Horizontal Strip Anchor	289
7.2.1 Strip Theory-1 (ST-1)	290
7.2.2 Strip Theory-2 (ST-2)	293
7.2.3 Breakout Factors Using Meyerhof and Adams's Theory (58)	296
7.2.4 Comparison of Strip Anchor Theories	297
7.3 Circular Anchors	298
7.3.1 Circular Anchor Theory-1 (CIR-1)	299
7.3.2 Balla's Theory-Recomputation of Factors	303
7.3.3 Breakout Factors Using Meyerhof and Adams's Theory	306
7.3.4 Breakout Factors Using Mariupol'skii's Theory	307
7.3.5 Breakout Factors for Matsuo's Theory	307
7.3.6 Breakout Factors - Earth Cone Method	309
7.3.7 Comparison of Different Theories	309
7.4 Results and Discussions	311
7.4.1 Horizontal Strip Anchor	311
7.4.2 Circular Anchor	314
7.5 Conclusions	320
7.5.1 Horizontal Strip Anchor	320
7.5.2 Circular Anchor	321
CHAPTER 8 CONCLUSIONS AND RECOMMENDATIONS	353
8.1 Introduction	353
8.2 Conclusions	353
8.3 Recommendations	357
REFERENCES	359
APPENDIX A	369
APPENDIX B	372

List of Tables

Table No.		Page
2.1	Limiting Values of D/B Beyond which No Increase in Uplift Resistance is Observed	26
3.1	Invariant Derivatives for Various Yield Conditions	108
4.1	Influence Factors for Vertical Displacement of Flexible Strip, Uniformly Distributed Uplift Load	128
4.2	Influence Factors for Vertical Displacement of Flexible Strip, Uniformly Distributed Uplift Load	129
4.3	Influence Factors for Vertical Displacement of Rigid Strip	132
4.4	Influence Factors for Vertical Displacement of Rigid Strip	132
4.5	Influence Factors for Vertical Displacement of Strip Anchor - Continuum Element and Beam-Column Element Anchor Discretisation	134
4.6	Elasto-Plastic Undrained Analysis - Horizontal Strip Anchor	142
4.7	Elasto-Plastic Undrained Analysis - Horizontal Strip, Von-Mises Criterion	145
4.8	Results from Strip Anchor Theories	152
4.9	Elasto-Plastic Drained Analysis - Horizontal Strip Anchor - Mohr-Coulomb Model	154
4.10	Comparison of Uplift Load	158
5.1	Elasto-Plastic Undrained Analysis - Vertical Strip Anchor	209
5.2	Elasto-Plastic Undrained Analysis - Vertical Strip, Von-Mises Criterion	212

Table No.		Page
6.1	Influence Factors for Vertical Displacement of Flexible Circle, Uniformly Distributed Uplift Load	245
6.2	Influence Factors for Vertical Displacement of Flexible Circle, Uniformly Distributed Uplift Load	247
6.3	Influence Factors for Vertical Displacement of Rigid Circle	249
6.4	Influence Factors for Vertical Displacement of Rigid Circle	249
6.5	Influence Factors for Vertical Displacement of Circular Anchor - Continuum Element and Plate Element Discretisation	251
6.6	Elasto-Plastic Undrained Analysis - Circular Anchor	256
6.7	Elasto-Plastic Undrained Analysis - Circular Anchor	258
6.8	Results from Circular Anchor Theories	261
6.9	Elasto-Plastic Drained Analysis-Mehr-Coulomb Model	262
6.10	Comparison of Breakout Load	263
7.1	Breakout Factors for Strip Plate Anchor, - F_c and F_q for ST-1	323
7.2	Breakout Factors for Strip Plate Anchor - F_c and F_q for ST-2	324
7.3	Breakout Factors for Strip Plate Anchor - F_c and F_q for Meyerhof and Adam's Theory(58)	325
7.4	Breakout Factors for Circular Plate Anchor - F_c and F_q for CIR-1	326
7.5	Uplift Capacity Factors $F_1(\phi, \lambda)$, $F_2(\phi, \lambda)$ and $F_3(\phi, \lambda)$ for Circular Plate Anchor - Balla's Theory (6)	327
7.6	Breakout Factors for Circular Plate Anchor - F_c and F_q for Balla's Theory (6)	328

Table No.		Page
7.7	Breakout Factors for Circular Plate Anchor - F_c and F_q for Meyerhof and Adams's Theory (58)	329
7.8	Breakout Factors for Circular Plate Anchor - F_c and F_q for Mariupol'skii's Theory(51)	330
7.9	Breakout Factors for Circular Plate Anchor - F_c and F_q for Matsuo's Theory (52)	331
7.10	Breakout Factors for Circular Plate Anchor - F_q for Earth Cone Method (44)	332
7.11	Comparison of Circular Anchor Pull-out Results with Theory - Small Scale Laboratory Tests	333
7.12	Comparison of Anchor Pull-out Results with Theory - Large Scale Tests in Laboratory and Field	337

List of Figures

Figure No.		Page
1.1	Horizontal and Vertical Anchors	2
2.1	Elastic Perfectly Plastic Models for Non-Frictional Soil Behaviour	19
2.2	Drucker-Prager and Mohr-Coulomb Criteria for Frictional Soil Behaviour	20
2.3	Limit Analysis and Stress Characteristic Solution, Vertical Strip Anchor	28
2.4	Theoretical Methods for the Estimate of Uplift Capacity - Circular Anchor	35-37
2.5	Comparison of Theoretical, Model Test and Site Results	42
2.6	Breakout Factor F_q in Sands	43
2.7	Breakout Factor F_c in Clays	44
2.8	Comparison of Theoretical and Test Results	44
3.1	Four Noded Linear Isoparametric Quadrilateral Element for Two Dimensional Analysis	61
3.2	Eight Noded Parabolic Isoparametric Element for Two Dimensional Analysis	66
3.3	Four Noded Isoparametric Quadrilateral Ring Element for Axisymmetric Analysis	69
3.4	Eight Noded Isoparametric Quadrilateral Ring Element for Axisymmetric Analysis	73
3.5	Beam-Column Element Used for Two Dimensional Analysis	75
3.6	Co-ordinate Systems, Axisymmetric Thin Plate Element	78
3.7	Four Noded and Six Noded Interface Elements for Two Dimensional Analysis	88

Figure No.		Page
3.8	Four Noded and Six Noded Interface Ring Elements for Axisymmetric Analysis	93
3.9	Uniaxial Behaviour	98
3.10	Yield Surface and Normality Concept	101
3.11	Circular Rupture Surface	113
4.1	Simulation of Anchor Behaviour	163
4.2	Discretised Model of Soil Layer of Finite Depth Underlain by Rough Rigid Base, Mesh for Elastic Analysis, Full Bonding Case	164
4.3	Discretised Model of Soil Layer of Finite Depth Underlain by Rough Rigid Base, Mesh for Elastic Analysis, Full Separation	165
4.4	Variation of Vertical Displacement with Depth (Horizontal Strip, Full Bonding, $H/B = 2.0$, $D/B = 0.5$)	166
4.5	Variation of Vertical Displacement with Depth (Horizontal Strip, Full Bonding, $H/B = 2.0$, $D/B = 1.0$)	167
4.6	Variation of Vertical Displacement with Depth (Horizontal Strip, Full Bonding, $H/B = 2.0$, $D/B = 1.5$)	168
4.7	Variation of Vertical Displacement with Depth (Horizontal Strip, Full Separation, $H/B = 2.0$, $D/B = 0.5$)	169
4.8	Variation of Vertical Displacement with Depth (Horizontal Strip, Full Separation, $H/B = 2.0$, $D/B = 1.0$)	170
4.9	Variation of Vertical Displacement with Depth (Horizontal Strip, Full Separation, $H/B = 2.0$, $D/B = 1.5$)	171
4.10	Variation of σ_y with Depth Along Centre Line (Flexible Horizontal Strip, Full Bonding, UDL, $\nu = 0.3$)	172

Figure No.		Page
4.11	Variation of σ_y with Depth Along Centre Line (Flexible Horizontal Strip, Full Separation, UDL, $\nu = 0.3$)	173
4.12	Variation of Vertical Contact Stress (Horizontal Strip, Flexible and Rigid Anchors, $\nu = 0.3$)	174
4.13	Variation of Vertical Contact Stress (Horizontal Strip, Flexible and Rigid Anchors, $\nu = 0.49$)	175
4.14	Variation of Central Vertical Displacement of Anchor with Relative Stiffness (Full Bonding, Continuum Element)	176
4.15	Variation of Central Vertical Displacement of Anchor with Relative Stiffness (Full Separation, Continuum Element)	177
4.16	Variation of Maximum Differential Displacement of Anchor with Relative Stiffness (Full Bonding, Continuum Element)	178
4.17	Variation of Maximum Differential Displacement of Anchor with Relative Stiffness (Full Separation, Continuum Element)	179
4.18	Variation of Vertical Contact Stress Distribution (Horizontal Strip, Continuum Element, Full Bonding, Full Separation, $\nu = 0.30$)	180
4.19	Variation of Vertical Contact Stress Distribution (Horizontal Strip, Continuum Element, Full Bonding, Full Separation, $\nu = 0.49$)	181
4.20	Variation of Central Vertical Displacement of Anchor with Relative Stiffness (Full Bonding, Beam-Column Element)	182
4.21	Variation of Central Vertical Displacement of Anchor with Relative Stiffness (Full Separation, Beam-Column Element)	183
4.22	Variation of Maximum Differential Displacement of Anchor with Relative Stiffness (Full Bonding, Beam-Column Element)	184

Figure No.		Page
4.23	Variation of Maximum Differential Displacement of Anchor with Relative Stiffness (Full Separation, Beam-Column Element)	185
4.24	Variation of Vertical Contact Stress (Horizontal Strip, Beam-Column Element, Full Bonding, Full Separation, $\nu = 0.3$)	186
4.25	Variation of Vertical Contact Stress (Horizontal Strip, Beam-Column Element, Full Bonding, Full Separation, $\nu = 0.49$)	187
4.26	Bending Moment Distribution (Horizontal Strip, Beam-Column Element, Uniform Load, Full Bonding)	188
4.27	Bending Moment Distribution (Horizontal Strip, Beam-Column Element, Uniform Load, Full Separation)	189
4.28	Bending Moment Distribution Due to Concentrated and Uniform Load on Anchor (Horizontal Strip, Beam-Column Element)	190
4.29	Elasto-Plastic Displacement Response of Thick Walled Cylinder, Von-Mises and Tresca Criteria	191
4.30	Discretised Model of Soil Layer of Finite Depth Underlain by Rough Rigid Base, Elasto-Plastic Analysis	192
4.31	Load Displacement Response, Horizontal Strip Anchor, Von-Mises Model	194
4.32	Load Displacement Response, Horizontal Strip Anchor, Von-Mises and Tresca Models	195
4.33	Load Displacement Response, Horizontal Strip Anchor: $K_r = 1, 10, 100$, Full Separation, Von-Mises Model	196
4.34	Spread of Plastic Zone, Horizontal Strip Anchor, Von-Mises Model, Full Bonding	197
4.35	Spread of Plastic Zone, Horizontal Strip Anchor, Von-Mises Model, Full Separation	198

Figure No.		Page
4.36	Velocity Field at Limit Load, Von-Mises Criterion	199
4.37	Velocity Field at Numerical Limit Load, Von-Mises Criterion, Full Separation	200
4.38	Load Displacement Response, Horizontal Strip, Mohr-Coulomb Model	201
4.39	Spread of Plastic Zone, Horizontal Strip, Mohr-Coulomb Model, Full Bonding	202
4.40	Spread of Plastic Zone, Horizontal Strip, Mohr-Coulomb Model, Full Separation	203
4.41	Velocity Field at Limit Load, Mohr-Coulomb Model, Full Separation, $\phi = 30^\circ$	204
5.1	Discretised Model of Soil Layer and Anchor, Elasto-Plastic Analysis	225
5.2	Load Displacement Response of Vertical Anchor for $K_r = 1, 10, 50$ (Full Bonding, Von-Mises Model)	226
5.3	Load Displacement Response of Vertical Anchor for $D/B = 1.0, 1.5, 2.0$ (Full Bonding, Von-Mises Model)	227
5.4	Load Displacement Response of Vertical Anchor for $D/B = 1.0, 1.5, 2.0$ (Tresca Model)	228
5.5	Load Displacement Response of Vertical Anchor for $D/B = 1.0, 1.5, 2.0$ (Full Separation, Von-Mises Model)	229
5.6	Spread of Plastic Zone (Vertical Anchor, $D/B = 1.0$, Full Bonding, Von-Mises Model)	230
5.7	Spread of Plastic Zone (Vertical Anchor, $D/B = 1.5$, Full Bonding, Von-Mises Model)	231
5.8	Spread of Plastic Zone (Vertical Anchor, $D/B = 2.0$, Full Bonding, Von-Mises Model)	232
5.9	Yield Zone at Failure Load (Vertical Anchor, $D/B = 1.0, 1.5, 2.0$, Full Separation, Von-Mises Model)	233

Figure No.		Page
5.10	Velocity Field at Collapse Load (Vertical Anchor, Full Separation, Von-Mises Model, $D/B = 1.5$)	234
5.11	Resistance of Plastic Clay to Anchor Blocks, Summary of Experimental and Theoretical Results	235
6.1	Variation of Vertical Displacement with Depth (Circular Anchor, Full Bonding, $H/B = 2.0$, $D/B = 0.5$)	268
6.2	Variation of Vertical Displacement with Depth (Circular Anchor, Full Bonding, $H/B = 2.0$, $D/B = 1.0$)	269
6.3	Variation of Vertical Displacement with Depth (Circular Anchor, Full Bonding, $H/B = 2.0$, $D/B = 1.5$)	270
6.4	Variation of Vertical Displacement with Depth (Circular Anchor, Full Separation, $H/B = 2.0$, $D/B = 1.0$)	271
6.5	Variation of Vertical Stress with Depth (Circular Anchor, Full Bonding, $H/B = 2.0$)	272
6.6	Variation of Vertical Stress with Depth (Circular Anchor, Full Separation, $H/B = 2.0$)	273
6.7	Variation of Vertical Contact Stress Distribution (Circular Anchor, Flexible and Rigid, $\nu = 0.3$)	274
6.8	Variation of Central Vertical Displacement with K_r (Circular Anchor, Full Bonding, Continuum Element)	275
6.9	Variation of Central Vertical Displacement with K_r (Circular Anchor, Full Separation, Continuum Element)	276
6.10	Variation of Vertical Contact Stress Dis- tribution (Circular Anchor, Continuum Element, $\nu = 0.3$)	277
6.11	Variation of Central Vertical Displacement with K_r (Circular Anchor, Plate Element)	278

Figure No.		Page
6.12	Variation of Vertical Contact Stress Distribution (Circular Anchor, Plate Element, $\nu = 0.3$)	279
6.13	Radial Bending Moment Distribution (Circular Anchor, Plate Element, Uniform Load, Full Bonding)	280
6.14	Radial Bending Moment Distribution (Circular Anchor, Plate Element Uniform Load, Full Separation)	281
6.15	Elasto-Plastic Displacement Response of Thick Walled Cylinder Von-Mises, Tresca Criteria	282
6.16	Elastic-Plastic Stress Distribution Through Thickness of Thick Walled Cylinder at $p = 8.44 \text{ N/cm}^2$	283
6.17	Load Displacement Response, Circular Anchor, Von-Mises and Tresca Models	284
6.18	Spread of Plastic Zone, Circular Anchor, Von-Mises Model	285
6.19	Velocity Field at Limit Load, Von-Mises Criterion	286
7.1	General Geometry and Symbols	338
7.2	Weight Calculation of Breaking out Earth Body	338
7.3	Shearing Resistance on Rupture Surface for ST-1	339
7.4	Resultant of Normal Stress and Shear Stress on Rupture Surface for ST-2	339
7.5	Breakout Factors for Horizontal Strip, F_c for ST-1	340
7.6	Breakout Factors for Horizontal Strip, F_q for ST-1	341
7.7	Breakout Factors for Horizontal Strip, F_c for ST-2	342

Figure No.		Page
7.8	Breakout Factors for Horizontal Strip, F_q for ST-2	343
7.9	Comparison of Strip Anchor Theories, $C=0$	344
7.10	Comparison of Strip Anchor Theories, $\phi=0$	345
7.11	Shearing Resistance on Rupture Surface, Circular Anchor - Balla's Theory	346
7.12	Breakout Factors for Circular Anchor, F_c for CIR-1	347
7.13	Breakout Factors for Circular Anchor, F_q for CIR-1	348
7.14	Breakout Factors for Circular Anchor, F_c for Balla's Theory	349
7.15	Breakout Factors for Circular Anchor, F_q for Balla's Theory	350
7.16	Comparison of Circular Anchor Theories, $C=0$	351
7.17	Comparison of Circular Anchor Theories, $\phi=0$	352
B.1	Flow Chart : Main Program : ELPLP1	375
B.2	Flow Chart : ASEMBL Program: ELPLP1	376
B.3	Flow Chart : Stress Program : ELPLP1	377

NOMENC LATURE

A	Area of cross section of the member
$\{a\}$	Nodal displacement vector
B	Width of strip anchor and diameter of circular anchor
B_o	Diameter of anchor shaft
$[B]$	Strain displacement matrix
$\{b\}$	Vector of body force components
C	Cohesion
C_u	Undrained shear strength
C_1	Radial shear at inner periphery
D	Depth of anchor be
$[D]$	Stress-strain matrix
$[D_{ep}^*]$	Elasto-plastic matrix
E	Elastic modulus of soil
E_p	Elastic modulus of anchor material
E_u	Undrained soil modulus
$\{F\}$	Nodal force vector
F_c, F_q	Breakout factors
F_c', F_q'	Cylindrical cavity expansion factors
F_u	Ultimate uplift capacity factor
F_1, F_2, F_3	Non-dimensional parameters
f_o	Unit skin resistance
G	Shear modulus
I	Moment of inertia
I_r	Rigidity index of soil

$[J]$	Jacobian matrix of transformation
$[K]$	Stiffness matrix
K'	Coefficient of lateral earth pressure
K_o	Coefficient of lateral earth pressure at rest
K_r	Relative stiffness of anchor
K_s, K_n	Shearing and normal material properties for interface element
K_u	Nominal uplift coefficient of earth pressure on vertical plane through footing edge
L	Length
M_r, M_t	Radial and tangential bending moment per unit length
$[N]$	Shape function matrix
NEL	Number of elements
N_c	Bearing capacity factor for deep foundations
n	Empirical coefficient
P	Maximum resistance to lateral displacement
P_u	Breakout load
P	Vector of forces/unit length along joint element
p_u	Intensity of ultimate uplift pressure
p_y	Yield stress
$\{R\}$	Load vector
\bar{T}	Surface traction
W_b	Weight of base slab
W_f	Effective weight of foundation
W_{sf}	Weight of lifted soil mass and foundation
α_i, α_j	Gaussian quadrature weights
β	Semi-vertical angle of cone
γ	Unit weight of soil

γ_f	Unit weight of material of foundation
δ	Displacement
ε	Strain
ε_0	Initial strain
ε_p	Plastic strain
κ	Hardening parameter
λ	Embedment ratio
ν	Poisson's ratio
ξ'_v	Volume change factor
σ	Stress
σ_0	Initial stress
σ_{yield}	Uniaxial yield
τ_f	Shear stress on rupture surface
ϕ	Angle of internal friction

SYNOPSIS

FINITE ELEMENT ANALYSIS OF STRIP AND
CIRCULAR PLATE ANCHORS
A Thesis submitted
In Partial Fulfilment of the Requirements
for the Degree of
DOCTOR OF PHILOSOPHY
by
C. VIJAYAN
Department of Civil Engineering
Indian Institute of Technology, Kanpur
January 1981

The present work is an analytical study of the response of strip and circular plate anchors subjected to static loading. Horizontal and vertical strip anchor behaviour is studied. Finite element displacement formulation is used to analyse the elastic response and to predict the load deformation behaviour upto collapse using elastic perfectly plastic models for soil. Provision to carry out non-linear elasto-plastic analysis using Von-Mises, Tresca and associated Mohr-Coulomb laws is made. Linear and parabolic isoparametric elements are used for continuum discretisation and interface elements are used to model breakaway at anchor bottom. Also, conventional formulations for the determination of ultimate uplift capacity of horizontal strip and circular anchors have been carried out on the basis of assumed slip surfaces. The results from the anchor theories for the calculation of uplift capacity of horizontal anchors are presented in the form of breakout factors for easy use and comparison.

In Chapter 1, the problem is introduced. The motivation for and scope of the work carried out have been discussed. In Chapter 2, literature review of theoretical and experimental work pertaining to plate anchors is made. A review of the application of elasto-plastic analysis to geotechnical engineering problems is made. In Chapter 3, the models and methods used in the present investigation are presented. The elements used for discretising continuum, anchor structure and interface are presented and the derivation of elasto-plastic matrix and the 'initial stress' computational technique used for non-linear analysis are explained.

In Chapter 4, the finite element elastic and elasto-plastic analysis of horizontal strip anchor is carried out. Elastic response due to uniformly distributed uplift load on flexible strip and load on rigid strip are studied. The effect of anchor stiffness on elastic response is studied by using continuum elements and beam-column elements to discretise the anchor. The undrained behaviour is simulated by Von-Mises perfectly plastic model and limited results using Tresca criterion are also analysed for comparison of the two models. Effects of anchor stiffness and anchor breakaway from underlying soil on deformation response and collapse load are studied. The effect of convergence criterion, increment size, and mesh refinement on the numerical limit load obtained from elasto-plastic analysis is investigated. The drained analysis is carried out

by the use of Mohr-Coulomb associated plasticity model. The results from undrained and drained analyses carried out are compared with conventional strip anchor theories.

In Chapter 5, the elasto-plastic undrained analysis of shallow vertical strips are carried out using Von-Mises model. Tresca criterion is also used in limited cases for comparison. The effects of anchor embedment depth, anchor breakaway from soil behind the anchor on deformation response and collapse loads are studied.

In Chapter 6, the finite element elastic and elasto-plastic analysis of circular anchor embedded in a soil medium and underlain by a rough rigid base are carried out. Elastic analysis of a uniformly loaded flexible anchor and a rigid anchor are performed to study the effects of anchor embedment, Poisson's ratio and anchor breakaway from soil below it. The anchor is discretised by continuum elements and axisymmetric plate bending elements to study the effect of anchor stiffness on response. Non-linear undrained deformation analysis using Von-Mises model is carried out to study the effect of interface separation, anchor rigidity, initial stresses due to weight etc. on the ultimate breakout load. Frictional behaviour is modelled by Mohr-Coulomb criterion. The results obtained from the use of these models are compared with the results from conventional theories.

The breakout load of horizontal strip and circular anchors are computed using conventional theories in Chapter 7. Kotter's equation is used to get the variation of soil resistance on assumed rupture surface. The results from all the important shallow anchor theories are recast in the form of breakout factors which gives a common basis for comparison of different theories.

Based on the elastic analysis of horizontal strip and circular anchors it can be inferred that the response of an embedded foundation under uplift loads is significantly affected by factors like embedment ratio, layer depth below anchor, Poisson's ratio of the material and the condition at interface below the anchor. The deformation response as well as the stress distributions above and below the anchor are influenced by the anchor separation from soil below it. The maximum bending moment in the anchor depends on the Poisson's ratio of the soil as well as anchor interface conditions.

It can generally be concluded that for the case of anchors embedded inside the soil, the anchor stiffness affects the load deformation response curve but does not significantly alter numerical limit loads obtained. It is observed that the Tresca model gives a deformation response curve which falls below that obtained from Von-Mises model. The load at which the soil medium reaches plastic state and limit loads obtained are smaller for Tresca model. The full anchor bonding gives loads which are

much higher than obtained from approximate theories. Case of full breakaway conditions gives numerical limit loads which compare reasonably with the shallow anchor theories.

The onset of yield in soil with the use of the associated Mohr-Coulomb model for purely frictional soils takes place at low load levels. For the cases of purely frictional soils analysed for strip and circular anchors the full bonding case gives loads higher than those predicted by conventional theories.

In an incremental iterative method like 'initial stress' technique used in the non-linear elasto-plastic analysis of the anchor problem, the maximum number of iterations specified within an increment and the convergence criterion both have a direct bearing on the numerical limit loads obtained and the computer time needed for the solution of the problem.

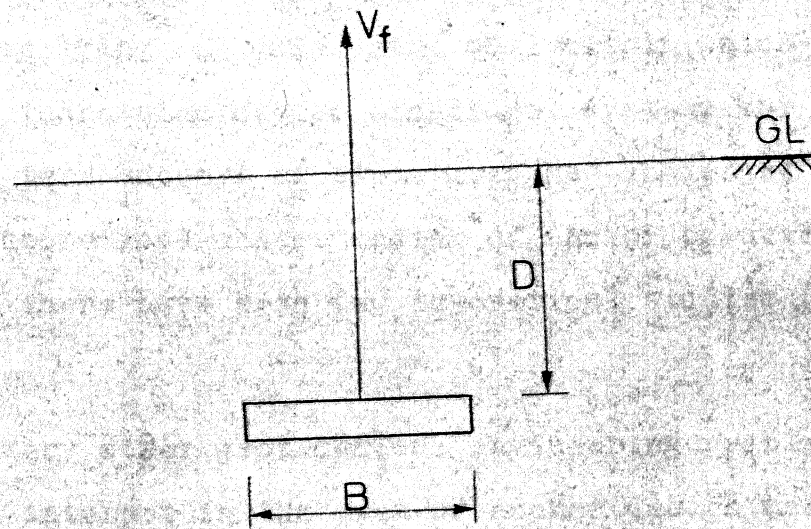
CHAPTER 1

INTRODUCTION

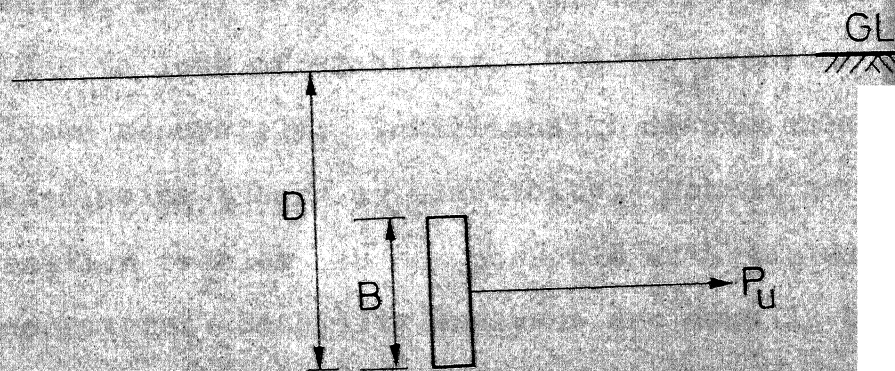
1.1 General :

On land and offshore, increasingly complex structures are planned and built, which are to be designed to withstand not only large compressive forces but also considerable tensile forces acting on their foundations. Buried earth anchors have provided the necessary uplift resistance for engineering structures such as high mast transmission towers, utility poles, aircraft moorings, submerged tunnels, pipe lines etc. Anchors are also provided for tie back resistance of retaining structures. In ocean environment mooring system for surface or submerged platforms owes its stability to ocean bottom anchors. Plate anchor is one of the common types of anchors used in practice.

The common shape of the anchor slab may be rectangular or circular and they may be positioned horizontally, vertically (Fig. 1.1) or in an inclined direction inside the soil medium. The loads experienced may be monotonically increasing, decreasing or cyclic in character. The embedment of the anchor slab inside the soil medium subjected to uplift load makes the horizontal anchor problem more complicated than a footing problems where a downward load is applied on the surface of the footing. Response of anchors to applied loads depends very much on the geometry and the distance of the top free boundary of the soil, the rigidity



a. Horizontal anchor



b. Vertical anchor

FIG.11 HORIZONTAL AND VERTICAL ANCHORS

of the anchor and the interface condition between the anchor slab and the overlying and underlying soil within which it is embedded. The increasing use of anchorage systems for both short and long term support of structures has indicated a need for a better theoretical understanding of anchor behaviour. Until recently there have been few theoretical studies (26,31,69, 80,87).

As with every other geotechnical engineering problem, the main points of interest in the area of anchor design are the prediction of displacements and stresses in the soil mass due to change in loading. The general stress deformation problem can be classified as i) failure due to excessive displacements ii) failure due to loss of stability. The two problems are usually analysed separately. Traditionally displacements have been calculated using theory of elasticity. Non-linear analysis of the deformation problem is now possible with the advent of high speed computers. Stability analyses are usually based on the limit theorems of perfect plasticity assuming that the soil acts as a rigid plastic material with no deformation till loss of equilibrium at failure, followed by large deformations at failure state. The main short comings in the above approaches are i) except for small strains soil does not behave elastically, ii) the limit theorems of plasticity ignore the deformations occurring prior to the loss of stability.

General constitutive relations for the stress-strain behavior of soil are needed in order to trace the load deformation

history from the onset of loading upto collapse and to predict the deformation behaviour at any intermediate load realistically. These general deformation states can be recognised for a foundation subjected to service loads as i) an immediate deformation under constant volume where the changes in total stresses are carried by pore fluid ii) a consolidation settlement during which load is gradually transferred from pore fluid to numerical skeleton, thus decreasing the excess pore pressure and changing the volume iii) all the deformations occurring after the excess pore pressures have been dissipated completely. A general displacement formulation should be able to unify all the above three formulations. But for convenience and on account of special situations where a separate treatment may be better, the undrained deformation problem, the consolidation problem and the drained deformation problem are formulated and analysed separately. For soils with high permeability value and situations where the loading rate is not very fast, the need for carrying out the first two stages of analysis does not arise because pore pressure build up during loading may not take place. Carrying out drained analysis alone in such situations is more reasonable and practical.

There is power elegance and usefulness in any method which can trace the load deformation behaviour upto collapse incorporating a reasonable material constitutive relationship. The incremental theory of plasticity implemented in finite difference and

finite element methods has been used with success in achieving the above objective. The finite element method is more powerful and versatile in the sense that anisotropy, non-homogeneity and non-linearity of material models or difficult boundary, loading and interface conditions can be implemented in the general program without much added effort. In a finite element analysis of deformation problem with a realistic constitutive relation the allowable and ultimate resistance are simply recorded as two points on the load deformation response curve and there is no longer any need to adopt basically different analysis for ultimate bearing pressure and settlement.

The undrained deformation problem is a special situation in geotechnical engineering called $\phi = 0$, case. The undrained shear strength values are determined directly from appropriate in-situ or laboratory tests. The undrained modulus and undrained strength defines the constants for an elastic perfectly plastic analysis. The initiation of yield is defined by a yield criterion. The two simple models used for elastic-perfectly plastic non-frictional behaviour are the classical models of Von-Mises and Tresca suggested for metal plasticity. These models have been used to analyse the undrained load settlement behaviour and ultimate bearing pressure for footing problem (21, 41, 43, 99). The analysis illustrated how the yielding under footing is initiated, the contained plastic zone expanded and settlements accrued and also how the load settlement curve asymptotically approached the ultimate load.

It is the frictional behaviour of soils as compared to the idealised perfectly 'cohesive' behaviour of metals that makes the plasticity formulation for soil material much more complex. The shear strength of the soil medium is a function of the effective normal stress on the potential failure plane at the time of failure. The Mohr-Coulomb and Drucker-Prager generalised form of yield criteria have been used to solve boundary value problems in soil mechanics (10,35,75,89,106,108).

The implementation of incremental theory of plasticity in the finite element method can reasonably trace the progressive deformation depending upon the accurate description of the material constitutive relation for soil. Notable contributions have been made in the development of better constitutive equations and their implementation in numerical methods (25,42,47,70,71,72,76,77,78,79,84,86,91,92,107). Although the above methods can trace the load deformation history upto collapse the use of approximate and reliable techniques for the determination of breakout capacity are also essential, atleast to make a first design estimate. The approximate approaches are derived based on simplifying assumptions for special situations and their reliability in predicting correct failure loads has to be verified on comparison with experimental results and also with results from sophisticated analyses.

The elastic analysis to determine the short term undrained deformation or long term drained deformation problem with the

use of appropriate parameters is useful in many practical situations. The non-linear elasto-plastic analysis, implementing incremental theory of plasticity with a realistic constitutive law in displacement finite element analysis to trace progressive deformation upto failure and approximate analytical methods for determination of ultimate capacities developed based on experimental observations, are both useful in predicting the behaviour and design of anchors.

Scope of the Present Investigation :

The present work is related to the elastic analysis and analysis of progressive deformation upto collapse using finite element technique with incremental theory of plasticity models, of strip and circular horizontal plate anchors subjected to static loads. Undrained behaviour of vertical anchors is also analysed. The work also focusses attention on the calculation of breakout load of shallow horizontal strip and circular anchors on the basis of assumed geometry of rupture surfaces (approximate approaches). The loading and geometric nature of problems analysed are such that they reduce to two dimensional plane strain and axisymmetric field problems.

The finite element displacement formulation with two-dimensional and axisymmetric elements are used to solve the problems mentioned above. To discretise the soil continuum, isoparametric elements are used. Four noded elements with linear variation of displacement and eight noded elements with quadratic

variation of displacement are used in both two-dimensional and axisymmetric cases. A beam-column element and an axisymmetric thin plate element are also used to model the anchor in plane strain and axisymmetric cases respectively. Interface elements are derived which can be used with four noded and eight noded two-dimensional and axisymmetric elements to model the interface behaviour. Full bonding at interface of anchor and soil, partial normal and shear slip or full breakaway can be modelled by these elements.

The elastic analysis is carried out for limited cases to study the effects of embedment depth, anchor rigidity, soil layer depth etc. on response. The analysis is done for horizontal strip and circular earth anchors. Full bonding and complete breakaway at anchor soil interface are studied as two extreme cases. The undrained elasto-plastic analysis to trace the progressive deformation with loads is carried out using mainly Von-Mises model. Tresca criterion is used in limited cases for comparison. Poisson's ratio equal to 0.48 is specified in the above analysis. The effect of the anchor stiffness, the initial stresses, interface breakaway etc. are also studied. The frictional behaviour is modelled by implementing associated Mohr-Coulomb law into displacement finite element program. The effects of variation of angle of internal friction and interface breakaway on response and ultimate loads are studied.

Calculation of ultimate uplift capacity of horizontal strip and circular anchors based on assumed shape of rupture surface is done. The resulting uplift loads obtained are presented in the form of breakout factors. Attempts to unify the mode of presentation of results from different shallow anchor theories in the form of breakout factors are made. This will be useful for comparison of different shallow anchor theories and for purposes of design.

A chapterwise description of the work that has been carried out in the present thesis is given below :

In Chapter 2 a literature review of theoretical work on elastic and elasto-plastic analysis of plate anchors is presented. A critical review of existing methods for the prediction of breakout resistance is made. The laboratory and field tests performed on strip and circular slab anchors are also reviewed.

Chapter 3 summarises the models and methods used in the present work. Displacement formulation in finite element method is explained. The elements used for discretisation, namely, four noded and eight noded isoparametric two-dimensional and axisymmetric elements for continuum, the beam-column and axisymmetric plate element for anchor and the interface elements to be used with the above elements are presented. Method of derivation of incremental elasto-plastic matrix and the 'initial stress' computational technique used in carrying out the

non-linear elasto-plastic analysis is described. Kotter's equation for circular rupture surface used in the computation of ultimate uplift load by approximate methods is presented.

In Chapter 4 the finite element elastic and elasto-plastic analysis on horizontal strip anchor is presented. Elastic response due to a uniformly distributed uplift load on flexible anchor and uplift load on a rigid strip are studied. Full bonding and full separation at the level of anchor are considered. The effect of anchor stiffness on factors like contact pressure, displacement and bending moments are studied by the use of beam-column element. Alternately the anchor is also modelled by continuum elements and the effect of anchor stiffness on response is studied. The undrained behaviour is simulated by Von-Mises model and limited results using Tresca criterion are also analysed for comparison of the two models. Effects of interface separation, anchor stiffness and 'initial stresses' on response and collapse load are analysed. The elasto-plastic drained analysis using Mohr-Coulomb criterion is carried out to investigate effect of angle of internal friction, cohesion, initial stresses, anchor breakaway etc. on load deformation response and break-out load.

In Chapter 5, the finite element elasto-plastic undrained analysis of vertical strip anchor is presented. Undrained response using Von-Mises model is analysed to trace yielding zones and collapse load. Tresca criterion is used for comparison in

limited cases. Effects of, anchor rigidity, embedment depth of anchor, interface separation and initial stresses on behaviour are studied.

In Chapter 6, the finite element elastic and elasto-plastic analyses of circular anchor embedded in a soil medium of limited depth and underlain by a rough rigid base are carried out. Elastic response due to uniformly distributed uplift load on a flexible anchor and uplift load on a rigid anchor are studied. The anchor is discretised by continuum elements and also by axisymmetric plate bending elements to study the effect of anchor rigidity on response due to uplift loads. Non-linear elasto-plastic analysis using Von-Mises criterion is carried out to study the effect of interface separation, initial stresses on response and ultimate breakout load. Tresca criterion is also used for few cases. Frictional behaviour is modelled by Mohr-Coulomb criterion and the results obtained are compared with approximate anchor theories.

In Chapter 7, breakout load of horizontal strip and circular anchors are computed. The results for strip and circular anchors are presented in the form of breakout factors. Emphasis is on a unified mode of presentation of the results from various theories for an easier comparison and use. Some of the

important laboratory and field test results are compared with the theoretical predictions for circular anchors.

In Chapter 8, the conclusions from the present investigation are summarised. The suggestions for future work are listed.

CHAPTER 2

LITERATURE REVIEW

2.1 Introduction :

The reported literature in the area of plate anchors is reviewed under two main heads, namely, analytical methods and experimental investigations. Elastic solutions available on anchor problem are listed. Developments in non-linear elastic-plastic solutions using incremental plasticity theory are reviewed. The examples of application of the above approach to soil anchor problem are presented. Theoretical results for computation of ultimate capacity of shallow and deep strip and circular anchors and experience gained from laboratory and field tests must both be utilised in proportioning anchors. Important shallow and deep anchor theories already in use are reviewed and experimental work done on anchor behaviour are briefly described.

2.2 Analytical Methods :

2.2.1 Elastic Analysis :

The solutions for vertical and horizontal line loads acting beneath the surface of an elastic semi-infinite homogeneous isotropic mass were given by Melan (54). Chikkanagappa (15) carried out the integration of vertical stress (σ_z) beneath the surface of a strip subjected to uniform pressure acting at a finite depth below the surface. For a flexible strip anchor

which is embedded and bonded to the medium subjected to vertical uniform upward load, the above solution can be used to obtain the distribution of vertical stress beneath the anchor with a sign reversal in vertical stress. Fotiyeva and Litkin (30) determined the relative displacements and contact pressure distribution of deep anchor plates in plane strain conditions. The problem was treated as the case of a rigid anchor plate on the upper edge of a slit in an infinite medium, the lower edge being free of all stresses. Repnikov and Gorbunov-Posadov (74) solved the problem of an absolutely rigid smooth strip which lies parallel to the free surface of a semi-infinite elastic plane at a finite depth below the surface and subjected to a concentrated uplift force. Considering the breakaway at the plate anchor interface beneath the anchor, ^{they} he obtained approximate solutions for relative settlements of slit below anchor and contact pressure distribution above anchor. Bosakov (11) presented the results of analysis of a deep anchor plate of finite rigidity under plane strain conditions acted on by a central concentrated line load. The internal forces in plate section were also obtained.

Mindlin's (59) solution for a point load acting inside a semi-infinite continuous mass has been integrated to obtain displacements and stresses due to a flexible loaded area. Fox (31) has obtained solutions for relationship between the mean vertical displacement of a uniformly loaded flexible

rectangle acting inside a semi-infinite mass to the mean surface displacement of an identical rectangle on the surface. Skopek (90) obtained the expressions for vertical stress beneath an embedded flexible rectangle and also obtained as a limiting case the vertical stress beneath the central axis of a strip. Nishida (65) gave explicit expressions for the vertical displacement beneath the edge of a circular area acted on by uniform intensity of load. The vertical stress beneath the centre and edge of the circle for different Poisson's ratios and depths below the loaded level were tabulated. Chapman and Groth (14) integrated Mindlin's solution to obtain vertical displacement of a uniformly loaded flexible rectangle. Geddes (32) tabulated the vertical stress beneath the centre line for axially symmetric distribution of uniform, triangular and parabolic loading acting inside the medium. All work mentioned above for flexible circular and rectangular horizontal loaded areas were done for downward loads acting beneath the surface. The same solutions are equally valid for a load acting in the upward direction on horizontal loaded areas, with necessary change in signs.

Douglas and Davis (26) solved for the horizontal displacement of a uniformly loaded, vertical flexible rectangular area embedded inside a semi-infinite mass by using the Mindlin's solution for horizontal displacement due to a horizontal point load acting inside the medium.

Butterfield and Banerjee (13) solved the problem of rigid rectangular and circular areas embedded inside semi-infinite elastic continuum at a finite depth below the surface.

Selvadurai (87) obtained closed-form solution for the axially symmetric problem of an infinite elastic solid containing a bonded symmetrically loaded rigid inclusion. The problem essentially pertains to a deep anchor of spheroidal shape.

A general method of analysis of horizontally embedded anchors in an elastic soil medium has been presented by Rowe and Booker (80). The solution has the following features. The solution can handle any general shape of anchor buried at depth D , below the surface inside an elastic layer. The anchor may be perfectly flexible or completely rigid while anchor soil interface may be either smooth or rough. Provision for slip between anchor and soil as well as breakaway of anchor from underlying soil is permitted. Influence charts for rigid circular and strip anchors are presented to illustrate the effect of parameters under study like embedment ratio, layer depth, Poisson's ratio, anchor roughness, anchor breakaway etc. The analysis proposed, because of the smaller number of equations to be solved for comparable accuracy, especially for deep anchors and deep soil layers is claimed to have computational savings when compared to finite element method. Rowe and Booker (81) studied the effect of anchor inclination upon elastic behaviour of rigid anchor plates.

2.2.2 Elasto-Plastic Analysis of Progressive Deformation and Collapse :

Because of the considerable efforts needed in computations involved in the numerical solution of the problems, the elasto-plastic analysis of realistic problems using incremental theory of plasticity were attempted only after the advent of high speed computers.

The classical papers of Allen and Southwell (3) and Jacobs (45) in which tension plates with holes and notch plates were considered, represent pioneering efforts in the numerical solution of elasto-plastic problems in accordance with the incremental theory of plasticity. Ang and Harper (4) considered similar problems with the help of a physical model of the governing finite difference equations. Pope (68) used the finite element elasto-plastic analysis to solve for stresses in tension plates subjected to edge loads. Marcal and King (50) suggested a partial stiffness concept for elasto-plastic finite element method. The concept was used to study simple problems in plane stress, plane strain and axisymmetric problems in solid mechanics. In all the above approaches Von-Mises criterion was used. Explicit form of elasto-plastic matrix which takes the place of elasticity matrix in incremental analysis was introduced by Yamada and Yoshimura (103) and Zienkiewicz et al. (108). The former by inverting the Prandtl-Reuss equations of plasticity theory derived the general elasto-plastic matrix for three

dimensional case in incremental form for strain hardening Von-Mises material. The incremental form of elasto-plastic matrix for plane stress problems was also presented.

Zienkiewicz et al. (108) presented a general method for the derivation of the elasto-plastic matrix for evaluating the stress increments from those of stress for any yield surface with an associated flow rule. The material model can be perfectly plastic or strain hardening. Another major contribution of the paper was the presentation of the computational process called 'initial stress' approach which used a 'constant elastic matrix' for solution instead of the conventional variable tangent stiffness approach. This is an iterative technique where the corrections are based on stress. A further refinement of 'initial stress' method was proposed by Nayak and Zienkiewicz (63) in order to accelerate convergence of original 'initial stress' technique.

As theory of plasticity was originally developed for metals, it was necessary to adapt and extend it to model soil behaviour. Since the earlier works of Drucker and Prager (27) this adaptation process is going on. Classical models used to simulate non-frictional behaviour and frictional behaviour of soils are shown in Fig. 2.1 and Fig. 2.2 respectively.

Ideal plastic materials employing well known Tresca or Von-Mises criteria were used to analyse undrained loading on clayey soils. Settlement of strip load on elasto-plastic

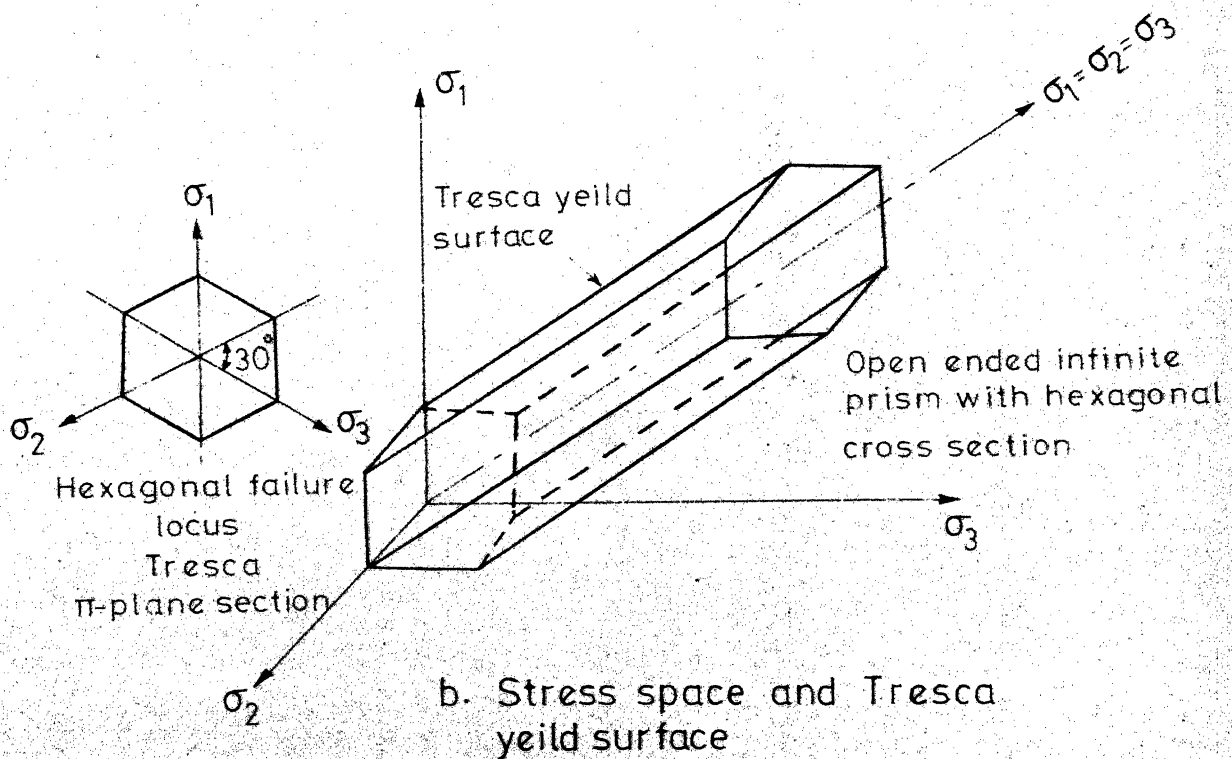
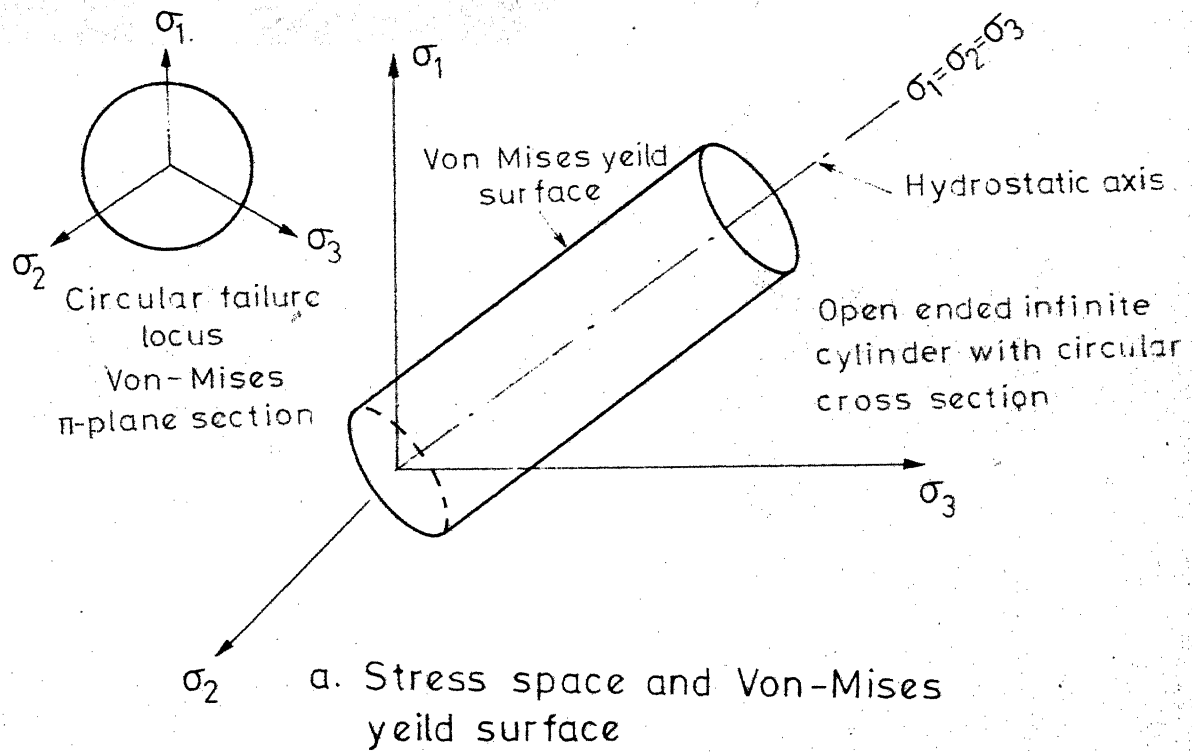
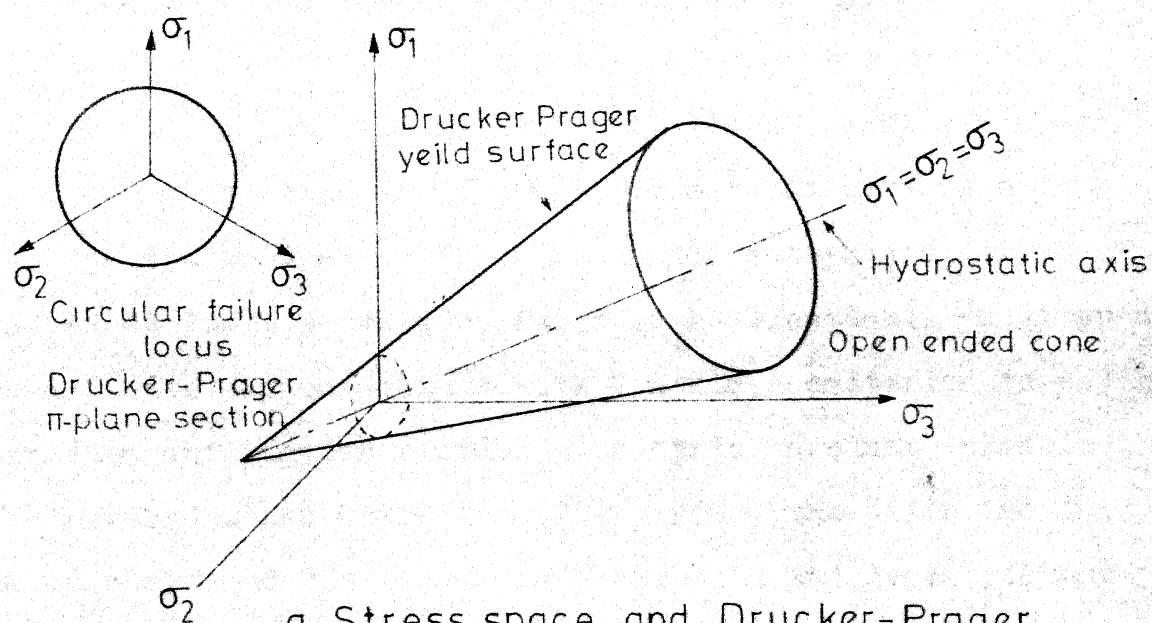
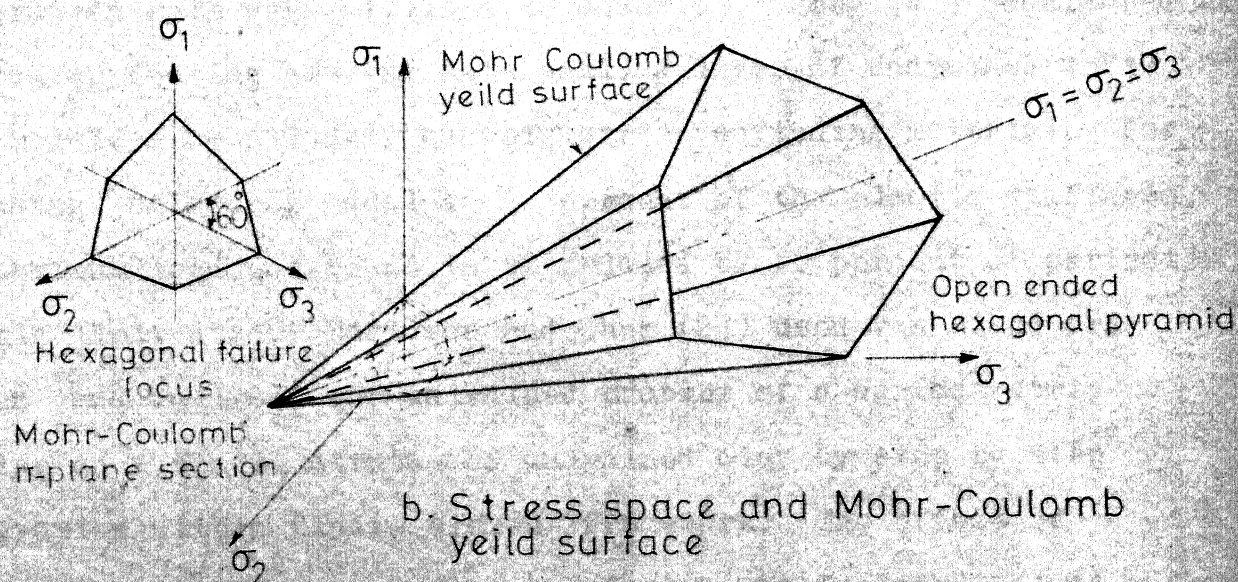


FIG. 21 ELASTIC PERFECTLY PLASTIC MODELS FOR NONFRICTIONAL SOIL BEHAVIOUR



a. Stress space and Drucker-Prager yield surface



b. Stress space and Mohr-Coulomb yield surface

FIG. 2.2 DRUCKER-PRAGER AND MOHR-COULOMB CRITERIA FOR FRICTIONAL SOIL BEHAVIOUR

shallow layer of an undrained clay using elastic perfectly plastic yielding according to Tresca criterion was given by Høegg et al. (43). Ang and Harper's (4) lumped parameter model was used for formulating the problem. Finite difference method was used for the analysis. The numerically determined limit load and exact limit loads were found to be identical. Valliappan (99) used finite element method with Von-Mises criterion to solve the undrained deformation problem of a strip on elasto-plastic medium. Fernandez and Christian (29) treated the strip footing bearing on undrained clay where both material and geometric nonlinearities were included in the formulation. A hyperbolic nonlinear elastic model and a perfectly plastic Tresca model were used to describe the clay. The finite element method and midpoint integration rule were utilised in solution. Høeg (41) considered a circular footing bearing on a shallow layer of undrained soft clay modelled as a linear elastic strain softening material. For softening stiffness equal to 20 percent of the elastic stiffness, the maximum load was found to be reduced by 40 percent of perfectly plastic limit load. Davidson and Chen (21) used Von-Mises criterion and analysed the undrained problem of a surface strip bearing on a finite stratum of undrained clay by step by step integration within finite element framework. The effect of large deformation on the response of clay was included. Load displacement curves, stress distributions, zones of yielding and velocity fields were presented.

One of the earliest applications of finite element method to elasto-plastic analysis of geomechanics problems was carried out by Reyes and Deere (75). Drucker-Prager criterion (27) suggested for modelling frictional behaviour of soils was used in the analysis of problems concerning stress concentration and displacements around an underground opening in a rock mass. A variable elasto-plastic matrix was used in the solution. Ziekiewicz et al. (108), Shieh and Sandhu (89), and Boonlualohr et al. (10) used the same model to simulate frictional behaviour of soils in analysing certain soil and rock mechanics problems. Hagmann (35) described the investigation of three material constitutive relations for frictional soils, i) an elasto-plastic Mohr-Coulomb material that obeys the laws of perfect plasticity (i.e. normality rule), ii) an elastic-plastic Mohr-Coulomb material having non-associated flow rule such that the material undergoes no plastic volumetric strain during yielding, iii) a strain hardening material similar in concept to those developed by Roscoe and his associates (76,77,78,79,86). For each of the models mentioned above incremental stress strain relations for plane strain case were derived and finite element load deformation behaviour under footings were investigated.

One of the main stumbling blocks of the classical plasticity theory lies in the universal assumption made based on Drucker's postulates (27) that the plastic behaviour is associated. With the Mohr-Coulomb type yield envelope to define the

limit between states of elasticity and continuing irreversible deformation, the associated behaviour gave dilation much in excess of observed behaviour. It became necessary, therefore, to extend plasticity approach to a non-associated form in which plastic potential and yield surfaces are defined separately (23). Zienkiewicz et al. (106) studied some typical problems of ideally plastic situations involving associated and non-associated laws and compared collapse loads in frictional materials.

In real soils the phenomenon of strain hardening or softening are present and limit collapse state is not directly approachable. For such soils partly or fully associated strain hardening plasticity models have been suggested and used with considerable success in defining deformation characteristics (25,47,71,84,91,92,107). For most of the formulations listed in references cited above critical state model is the basis (76,77,78,79,86).

Only very limited attempts were made in the elasto-plastic analysis of anchor problem. Muga (61) developed a numerical procedure based on discrete element model introduced by Ang and Harper (4) for analytical determination of breakout force of an embedded object in plane strain condition. The soil in this analysis is assumed to behave as a homogeneous elastic perfectly plastic solid following Von-Mises yield criterion. Davie and Sutherland (22) carried out an axisymmetric elasto-plastic iterative analysis employing Von-Mises criterion. The procedure

could predict general type of failure only, regardless of the depth of anchor. Full bonding at soil anchor interface was assumed. Rowe et al. (82) developed a sub-structure finite element approach to analyse the non-linear soil structure interaction problem and analysed the strip anchor problem using Von-Mises criterion. The load deflection behaviour of anchor was presented. Rowe and Davis (83) discussed the application of finite element method for prediction of collapse loads. The effect of convergence criterion and increment size on the collapse load were also discussed. Examples solved include the case of a deep rigid strip anchor also. Load deflection diagrams of smooth strip anchor and rough strip anchor at infinite depth based on elasto-plastic analysis using Von-Mises criterion and initial stress approach were presented.

2.2.3 Theoretical Approaches for the Computation of Ultimate Capacity of Anchors :

The analytical methods that are used for the calculation of ultimate capacity of horizontal strip anchor, vertical strip anchor and horizontal circular anchors are reviewed below. These methods present the ultimate capacity for design purposes.

a) Horizontal strip : Meyerhof and Adams (58) developed an approximate theory of uplift resistance for strip foundations based on observation and test data (Fig. 2.4g). They observed that at ultimate uplift load a soil mass having an approximately truncated pyramidal shape is lifted up, and for shallow footing

depths the failure surface reaches the ground surface. In the absence of a rigorous solution for stresses on failure surface the ultimate uplift capacity was calculated by the approximate relation using a vertical rupture surface as,

$$V_f = 2 CD + \gamma D^2 K_u \tan \phi + W_{sf} \quad (2.1)$$

where

V_f = gross ultimate uplift capacity of strip

C = cohesion

D = depth of strip below ground level

γ = unit weight of soil

K_u = nominal uplift coefficient of earth pressure on vertical plane through footing edge

ϕ = angle of internal friction

W_{sf} = weight of lifted soil mass and foundation.

K_u was found to generally vary between 0.7 to nearly unity, and for strips in granular materials, its value can be taken as 0.95 without much loss in accuracy. With increasing depth of footing the compressibility and deformation of the soil mass prevent the soil surface from reaching the ground surface. By limiting the vertical extent of the failure surface and using surcharge pressure above the failure surface as $p_o = \gamma(D-D')$, the total ultimate uplift load is obtained as,

$$V_f = 2 CD' + \gamma(2D-D') D' K_u \tan \phi + W_s \quad (2.2)$$

D' was determined from observed extent of the failure surface.

Limiting values of D'/B are given in Table 2.1 (58).

Table 2.1

Limiting values of D/B , beyond which no increase in uplift resistance is observed

ϕ in degrees	20	25	30	35	40	45	48
Limiting D/B	2.5	3	4	5	7	9	11

The upper limit of uplift resistance is limited to sum of bearing capacity of footing and skin friction of anchor shaft as per Meyerhof coefficients for ultimate bearing capacity of deep strip footings (55). The main contribution of this approach is the distinction made between shallow and deep anchor problems.

Vesic, et al. (102) solved the problem of expansion of cavities close to the surface of a semi-infinite rigid-plastic solid. The solution gave the ultimate radial pressure needed to breakout a cylindrical cavity of radius R , placed at a depth D below the surface of a rigid plastic solid. Vesic (101) modified the results for above problem for a long rectangular plate and presented the solution in the form of breakout factors.

$$p_u = CF_c + \gamma D F_q \quad (2.3)$$

where

p_u = intensity of ultimate uplift pressure

F_c, F_q = breakout factors for strip plate.

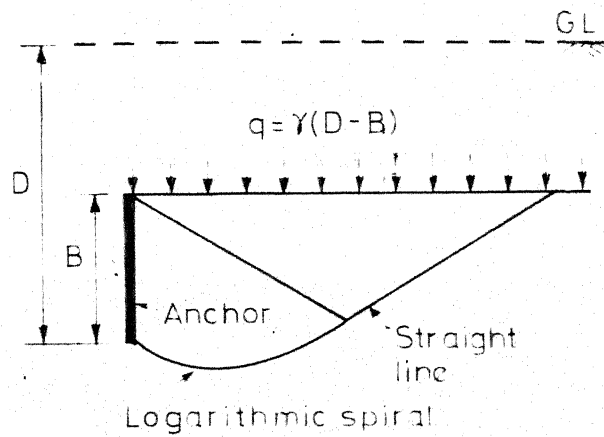
The above theory is valid only for shallow anchors.

Rowe and Davis (83) presented the lower and upper bound solution to the ultimate collapse load of strip anchor at infinite depth in a purely cohesive material. The well known Prandtl solution for a footing was used to obtain the lower bound load. The statically admissible limit load was obtained as 10.28 CB. The upper bound load calculated was 11.42 CB. The ultimate uplift load by Meyerhoff's solution (55) for ultimate bearing capacity of a deep footing in clay ranges from 8.28 CB to 8.85 CB.

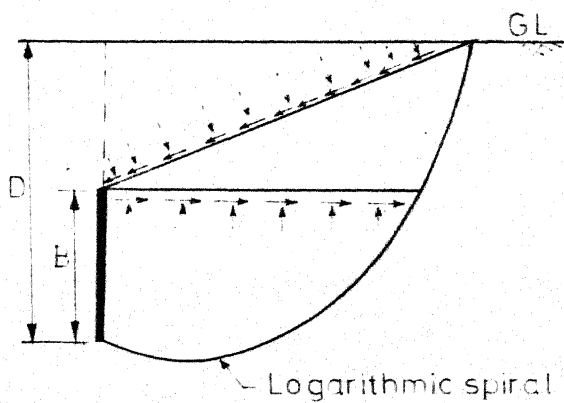
b) Vertical Strip : Hansen (38) considered the case of a deep anchor block of rectangular cross section pulled through a purely cohesive soil and obtained the upper bound limit load as 11.4 CB. This coincides with the upper bound load of Rowe and Davis (83) for a deep horizontal strip in clay. Hansen (37) presented a procedure for evaluating the capacity of vertical and inclined anchor slabs based on his method of calculation of earth pressure.

Neely et al. (64) analysed failure loads of vertical anchor plates in sand which derive their load bearing capacity from passive resistance of soil in front of plate. Theoretical ultimate resistance of anchor plates have been examined by both limit analysis and method of stress-characteristics in plasticity theory (Figs. 2.3a, 2.3b, 2.3c and 2.3d).

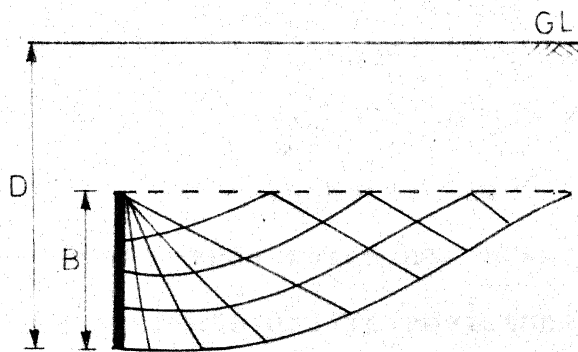
The simplest trial failure surface solution uses combination of logarithmic spiral and a plane surface inclined at an angle of



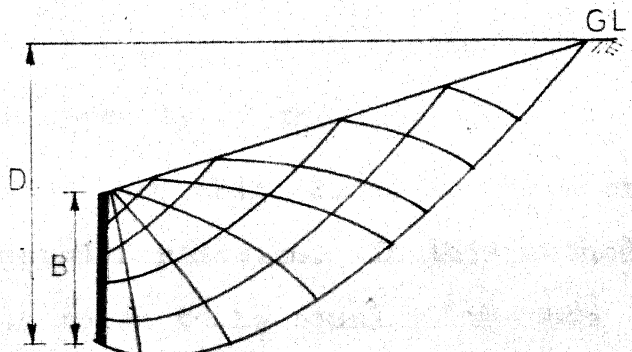
a. Surcharge method.
Limit analysis



b. Equivalent free surface method
Limit analysis



c. Surcharge method
Stress-characteristic
solution



d. Equivalent free surface method
Stress-characteristic
solution

FIG.2-3 LIMIT ANALYSIS AND STRESS CHARACTERISTIC
SOLUTION. VERTICAL STRIP ANCHOR

$(\pi/4 - \phi/2)$ to the horizontal, with the soil above the top of anchor plate being assumed to act as a simple surcharge. Contribution to the failure load due to surcharge and self weight were estimated separately. The shearing resistance of upper layers of soil was included in the calculation by making use of an equivalent free surface method proposed by Meyerhof (55). Trial failure surface methods have the advantage of simplicity but restrict the range of field and boundary conditions that can be examined. To overcome these difficulties the general numerical solution proposed by Sokolovskii (93) was used. Good agreement between limit analysis and stress-characteristic solutions were observed. Theoretical curves for the dimensionless parameter $P_u/\gamma B^2$ were given for various D/B ratios from which it was possible to estimate the capacity of vertical strip anchor. P_u is the ultimate capacity of the anchor.

c) Circular Anchor : Earth cone method (Fig. 2.4a) is the most common method which has been adopted for design. In this method the ultimate uplift resistance is taken to be equal to the sum of dead weight of footing and the soil mass contained in the truncated cone with the top of footing slab as base.

$$V_f = W_f + W_s \quad (2.4)$$

where,

$$W_f = W_b + V_s(\gamma_f - \gamma) \quad (2.5)$$

$$W_s = \gamma D \frac{\pi B^2}{4} \left[1 + \frac{4}{3} \frac{D^2}{B^2} \tan^2 \beta + \frac{2}{3} \frac{D}{B} \tan \beta \right] \quad (2.6)$$

in which,

W_f = effective weight of foundation

W_b = weight of the base slab

V_s = volume of the foundation stem

γ_f = unit weight of the foundation material

γ = unit weight of soil

β = semi-vertical angle of cone

Different codes and formulae specify different values of β for calculation. Indian Standard code of practice for the design and construction of transmission towers and poles (44) suggested β values to be 20° and 30° with a factor of safety equal to 1.0 for a footing with undercut and a factor of safety equal to 1.5 for a footing without undercut. β value equal to 20° was recommended for non-cohesive materials such as sands and gravelly soils. For a firm cohesive soil β value of 30° was recommended. It is generally observed that the earth cone method underestimates holding capacity at shallow depths and overestimates it at large depths.

Friction cylinder method (Fig. 2.4b) assumes that failure occurs along the surface of the cylinder of soil above anchor and the pullout load is equal to the weight of the soil and frictional resistance of soil mobilised along the surface of the cylinder.

Anchors may be buried at various depths of embedment. When an anchor is buried at a depth such that the depth of cover is the

limiting factor which controls the holding capacity, then it is referred to as shallow anchor. Anchors buried below the critical surface are referred to as deep embedment anchors. Balla(6) gave a useful relationship between anchor depth D and diameter B as $\lambda = D/B$. The recent approaches for the evaluation of the uplift capacity of anchors started with the work of Balla (6).

Balla's theory (6) was based on experimental observations of the breaking out earth body in model tests. Balla observed that the meridian section of the sliding surface starts vertically from upper plane of foundation slab, curves outwardly from axis and intersects the ground level at an angle approximately equal to $(\pi/4 - \phi/2)$ (Fig. 2.4c). To find the distribution of stresses on the slip surface he applied Kotter's equation and assumed that the distribution in axially symmetric situation is the same as in plane strain case. The final results of his computation were in the form,

$$P_u = \gamma D^3 [F_1(\phi, \lambda) + \frac{C}{\gamma D} F_2(\phi, \lambda) + F_3(\phi, \lambda)] \quad (2.7)$$

where F_1, F_2, F_3 are non-dimensional parameters which are functions of ϕ and λ and P_u is the ultimate uplift load of the anchor. The results of computation for D/B upto 4.0 were presented in graphical and tabular forms for the practical range of ϕ values.

Mariupol'skii (51) determined the shape of rupture surface for shallow anchors from laboratory experiments and developed a solution for the soil resistance to pullout (Fig. 2.4d). He

used the following assumptions : (i) the maximum shear stress due to vertical pullout force on anchor develops along the cylindrical surface 1234, around the anchor axis and with an increase in uplift force this shear stress increases, (ii) the earth column 1234, when moving upward holds adjacent rings of earth under the effect of friction and cohesive forces. This process leads to the development of tensile stresses under the effect of which failure is most probable as a certain volume of earth in the form of a cone with a curvi-linear generatrix is pulled out. Accordingly, the pullout resistance was given by,

$$P_u = \frac{\pi}{4} (B^2 - B_o^2) \gamma D \frac{1 - \frac{B_o}{B} + 2K' \tan \phi \frac{D}{B} + 4C \frac{D}{B}}{1 - \left(\frac{B_o}{B}\right)^2 - 2n \frac{D}{B}} \quad (2.7)$$

where

B_o = the diameter of anchor shaft

K' = coefficient of lateral earth pressure

n = empirical coefficient.

The empirical coefficient n , was determined from laboratory and field experiments and was approximately equal to 0.0025ϕ , where ϕ was in degrees. Since the value of n was determined for specific conditions of tests, its validity for use in other situations is doubtful. Arbitrary assumptions were made in analysing the stresses in the soil wedge above anchor.

Matsuo (52) proposed a method for the calculation of uplift capacity of anchors assuming the sliding surface cross-section

to be a combination of logarithmic spiral and straight line (Fig. 2.4e). The particular logarithmic spiral and tangent straight line giving the failure surface was determined by trial and error. For each trial sliding surface, the equilibrium of the soil included in the portion 'abcdfa' was considered. Matsuo (53) simplified the procedure by eliminating the trial and error method and assuming an average angle of θ_0 to be 60° (Fig. 2.4e). For this value of $\theta_0 = 60^\circ$, if the ultimate uplift capacity was presented in terms of non-dimensional factors proposed by Balla as functions of D/B and ϕ or in terms of break out factors proposed by Vesic et al. (102), the effort involved in final calculation would have been much less. Matsuo (53) finally proposed the expressions for ultimate uplift capacity in the following form after many simplifications,

$$V_f = W_f + \gamma B_2^3 K_1 + C B_2^2 K_2 \quad (2.8)$$

$B_2^3 K_1$ and $B_2^2 K_2$ were expressed as functions of ϕ , B , D/B and for different ranges of D/B , different expressions were given for their calculations.

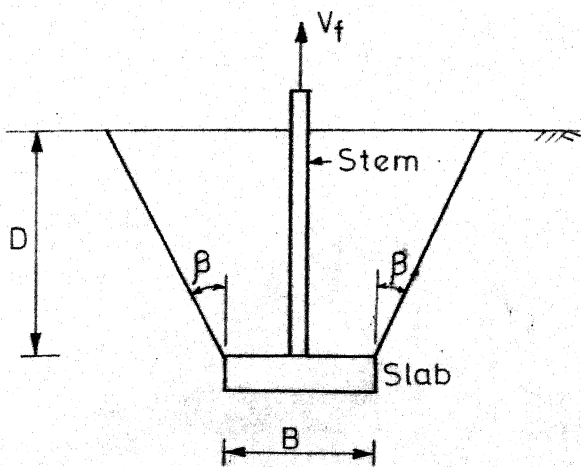
Meyerhof and Adams (58) extended their analysis developed for strip to circular anchor. They computed the shearing resistance from cohesion and passive earth pressure inclined at an angle δ on a vertical cylindrical surface through foundation edge (Fig. 2.4g). For shallow depths,

$$V_f = \pi C B D + s K_u (\pi/2) \gamma B D^2 \tan \phi + W_{sf} \quad (2.9)$$

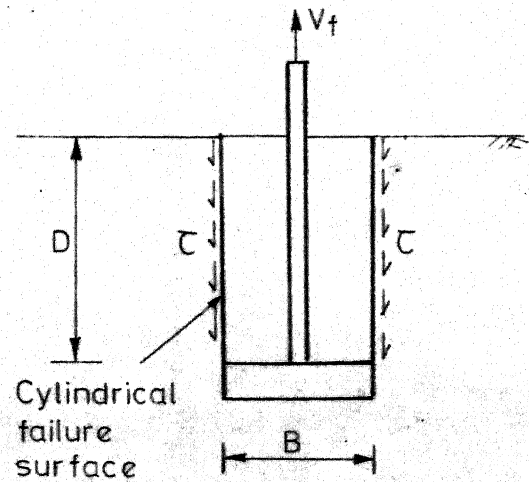
where s is shape factor governing passive earth pressure on a convex cylindrical wall from approximate earth pressure theories based on plane failure surfaces. They have presented in graphical form the value of earth pressure coefficient sK_u for shallow and deep anchors.

Vesic et al. (102) solved the problem of point charge expanding a spherical cavity close to the surface of a semi-infinite homogeneous isotropic solid. These solutions gave the ultimate radial pressure inside the spherical cavity of diameter B and depth D below the surface of the solid (Fig. 2.4f). The above solutions were reduced by Esquivel-Diaz (28) and Vesic (101) for a shallow embedded circular plate and presented as break out factors for circular plate for a range of ϕ values and D/B values upto 5.0.

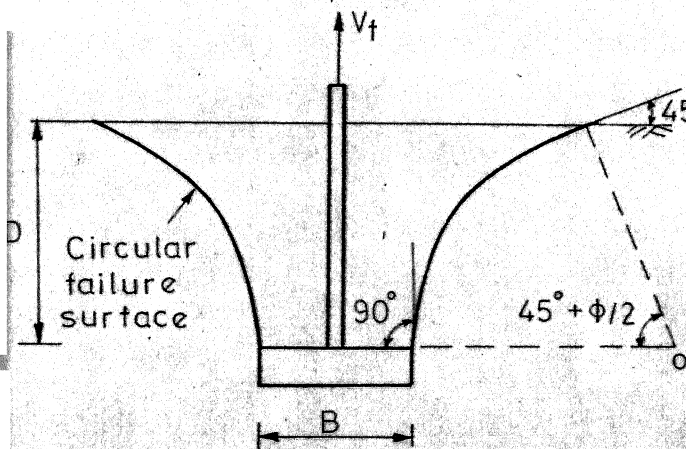
It was observed that behaviour of deeply embedded anchors differed from shallow embedded ones. Special theories were developed for calculating the break out resistance of deeply embedded anchors. Mariupol'skii (51) presented a solution of a deep circular anchor problem by assuming that the work required to displace an anchor should be equal to the work needed to expand a vertical cylindrical cavity of diameter B (Fig. 2.4h). In unsaturated soils which are not in a loose state, Mariupol'skii states that the deformation of the cavity walls under the anchor does not occur. As the anchor is withdrawn, the conical wedge formed immediately above the anchor plate moves apart and forces



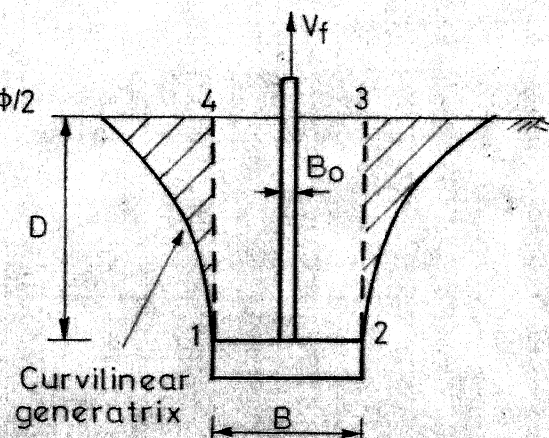
a. Earth cone method



b. Friction cylinder method

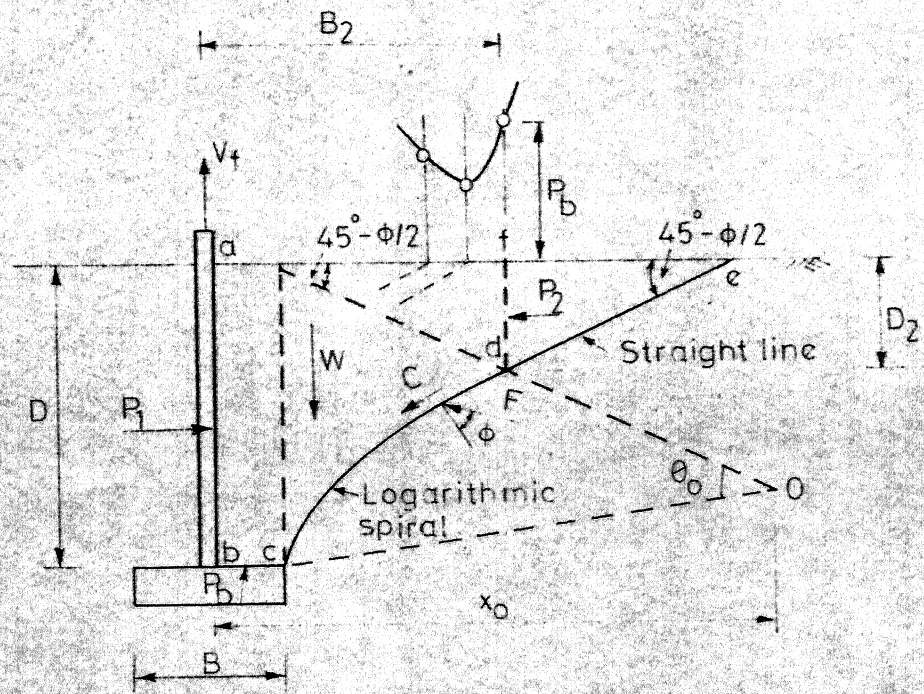


c. Balla's theory

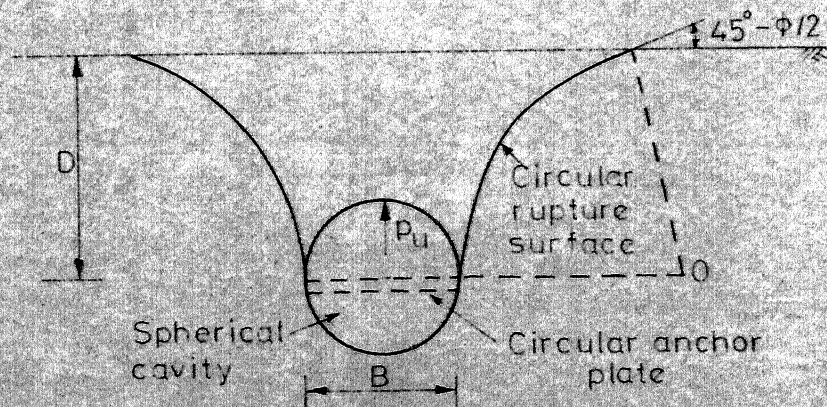


d. Mariupol'skii's theory

FIG.2-4 THEORETICAL METHODS FOR THE ESTIMATE OF UPLIFT CAPACITY-CIRCULAR ANCHOR

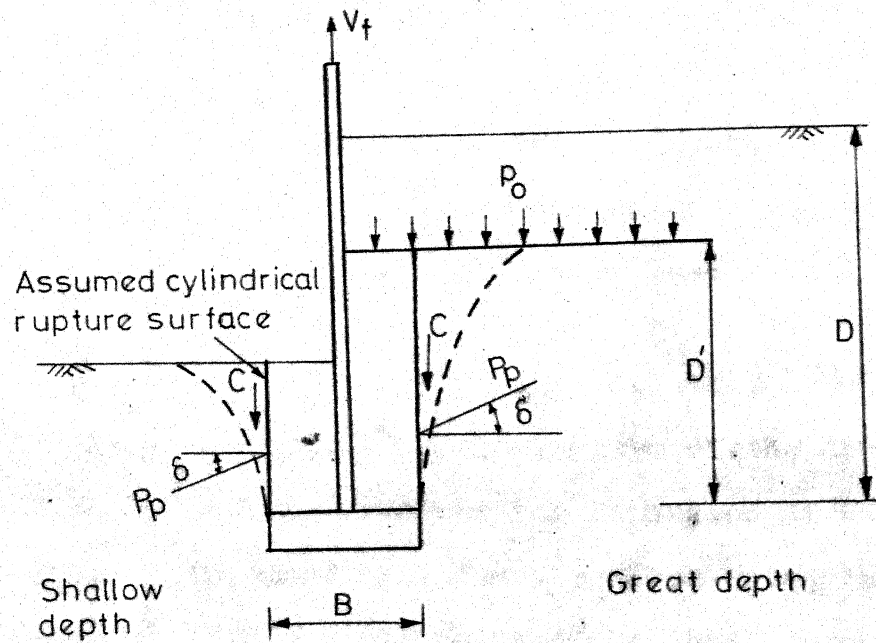


e. Matsou's theory

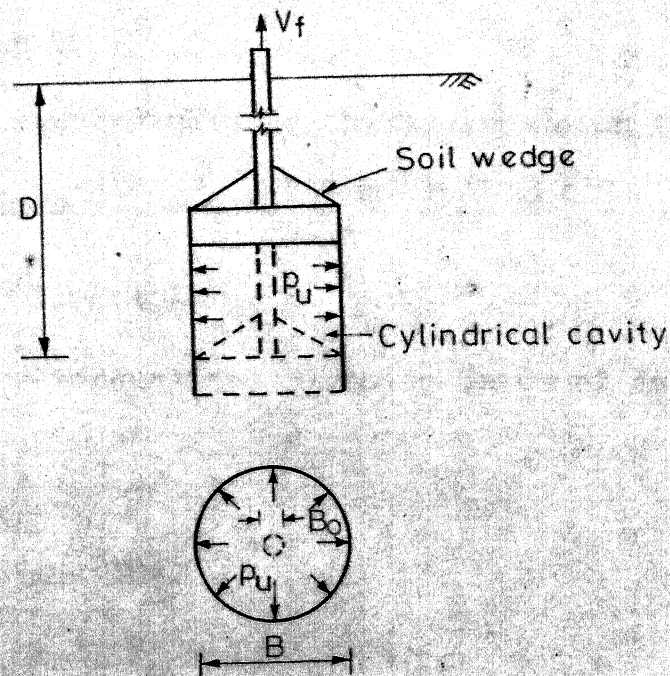


f. Vesic's theory from expansion of a spherical cavity near the surface

FIG.2-4 THEORETICAL METHODS FOR THE ESTIMATE OF UPLIFT CAPACITY-CIRCULAR ANCHOR



- g. Meyerhof and Adams theory
 Failure of soil above strip anchor
 Modified for circular anchor



- h. Failure mechanism for deep anchor
 proposed by Mariupol'skii

FIG.24 THEORETICAL METHODS FOR THE ESTIMATE OF
 UPLIFT CAPACITY-CIRCULAR ANCHOR

the soil lying above it to the sides, and the anchor practically begins to move at a constant load. He presented a solution which has been reduced into the following form by Vesic (101),

$$V_f = W_f + \pi B_o [D - B + B_o] f_o + \pi/4 \left[\frac{(B^2 - B_o^2)}{1 - 0.5 \tan \phi} \right] p_u \quad (2.10)$$

where f_o = unit skin resistance along the stem of the anchor of radius B_o , and p_u = ultimate pressure for expansion of a deep cylindrical cavity. Mariupol'skii found p_u from a lengthy trial and error procedure. Vesic (101) pointed out that p_u could be found directly from the results of the rigorous solution carried out by him on the expansion of cylindrical cavity in an infinite mass, given in the following form,

$$p_u = C F'_c + \gamma D F'_q \quad (2.11)$$

where F'_c and F'_q are cylindrical cavity expansion factors.

$$F'_q = (1 + \sin \phi) (I_r \sec \phi)^{\sin \phi / (1 + \sin \phi)} \quad (2.12)$$

$$F'_c = (F'_q - 1) \cot \phi \quad (2.13)$$

The quantity I_r represents the rigidity index of soil given by

$$I_r = \frac{G}{C + \gamma D \tan \phi} \quad (2.14)$$

where G = shear modulus.

For $\phi = 0$, $F'_c = 1$, $F'_q = \ln I_r + 1$.

The numerical values of F'_c and F'_q for different values of ϕ and I_r were tabulated. The above solutions were based on the assumption that there was no change in volume in the plastic zone

surrounding the cavity. To introduce the effect of volume change occurring in the zone as well, a reduced rigidity index based on an average volumetric strain was suggested.

$$\text{The reduced rigidity Index} = \frac{I_r}{1 + \frac{I_r}{\Delta \sec \phi}} = \xi'v I_r \quad (2.15)$$

Numerical values of $\xi'v$ (volume change factor) were computed and tabulated.

Meyerhof and Adams (58) extended their solution for shallow anchors to the case of deep embedment anchor. They limit the vertical extent of the cylindrical failure surface to a height D' above the anchor and add a surcharge pressure p_0 , as indicated in Fig. 2.4g. The equation for pull out resistance of a deep circular anchor was given by

$$V_f = \pi C B D' + \gamma (2D - D') D' s K_u \tan \phi + W_{sf} \quad (2.16)$$

Meyerhof and Adams (58) presented D' as a function of angle of internal friction and embedment ratio (Table 2.1). The upper limit of uplift resistance was limited to the sum of bearing capacity of footing and skin friction of the shaft as per Meyerhof (55) coefficients for ultimate bearing capacity of deep circular footings.

2.3 Experimental Investigations :

Many experimental investigations on anchor piles, flared out foundations and slab anchors were reported in literature. Only work on slab type of anchor is reviewed here. Some of the well documented test results are compared with theoretical predictions in Chapter 7.

Mors (60) and Turner (98) tested foundation for transmission towers and semi-empirical approaches to their design were suggested based on the results of the tests. Balla (6) determined the shape of the slip surfaces for shallow circular anchor plates of diameter 6 cms to 12 cms in dense sand. He observed that the shape of the rupture surface was circular and meets the ground surface at an angle of $(\pi/4 - \phi/2)$ (Fig. 2.4c). Reasonable agreement between theoretical results with results of model tests was observed. The field test results on uplift capacity of foundations from Brown-Boveri and Fielitz were also summarised by Balla and compared with his theory (6). Baker and Kondner (5) conducted laboratory tests on circular anchor plates in dense sand on four different diameters at D/B values ranging from 1 to 21. He confirmed Balla's major findings of shallow anchor behaviour in dense sand and observed that modes of failure for shallow ($\lambda < 6$) and deep ($\lambda > 6$) anchors were distinct and require separate analyses. Sutherland (95) conducted a comprehensive and well documented series of laboratory model tests on circular anchors in connection with the study of the problem of finding jack pressure in shaft raising operations in cohesionless soils. Loose sand ($\phi = 31^\circ$) and dense sand ($\phi = 45^\circ$) were used in this investigation and diameter of circular plates ranged from 3.81 cms ($1\frac{1}{2}$ ") to 15.24 cms (6"). D/B ratios investigated varied from 1 to 5. Sutherland observed that no single failure surface could be defined which would apply to all states of density of cohesionless soil. The results of tests were presented

as a plot of $p_u/\gamma D$ versus D/B (Fig. 2.5). He also presented the field test results of 2.39 m (94") diameter shaft raising operation in loose and dense sand. On the basis of his test results he concluded that no satisfactory theory was available in calculating uplift load. He commented that Balla's theory underestimated the uplift load in dense sand and overestimated the loads in loose sand. He argued that the experimental plot of $p_u/\gamma D$ versus D/B obtained by conducting tests on dimensionally similar models could be used in design.

Kananyan (46) conducted large scale tests on horizontal and inclined circular anchors. The pullout tests on horizontal anchors at shallow depths were conducted on anchor diameters 40,60,80,100 and 120 cms, all embedded at the same depth of 100 cms below ground level. Embedment ratio (D/B) ranged from 0.82 to 2.5. Inclined anchors, 80 cms diameter and embedded at 100 cms depth, with inclination of axis of load from vertical from 10° to 45° were tested. It was observed that the ultimate capacity of the anchor increased with angle of inclination.

At Duke University testing of model plates in loose and dense sand as well as soft and stiff clay were carried out (2,9,28) and the important results have been reproduced in Figs. 2.6 and 2.7. Esquivel-Diaz (28) conducted a series of laboratory tests on 7.62 cms (3") diameter anchor embedded in loose and dense sand. The embedment ratio (D/B) investigated ranges from 1.5 to 9.8. It was observed that the ultimate pullout resistance

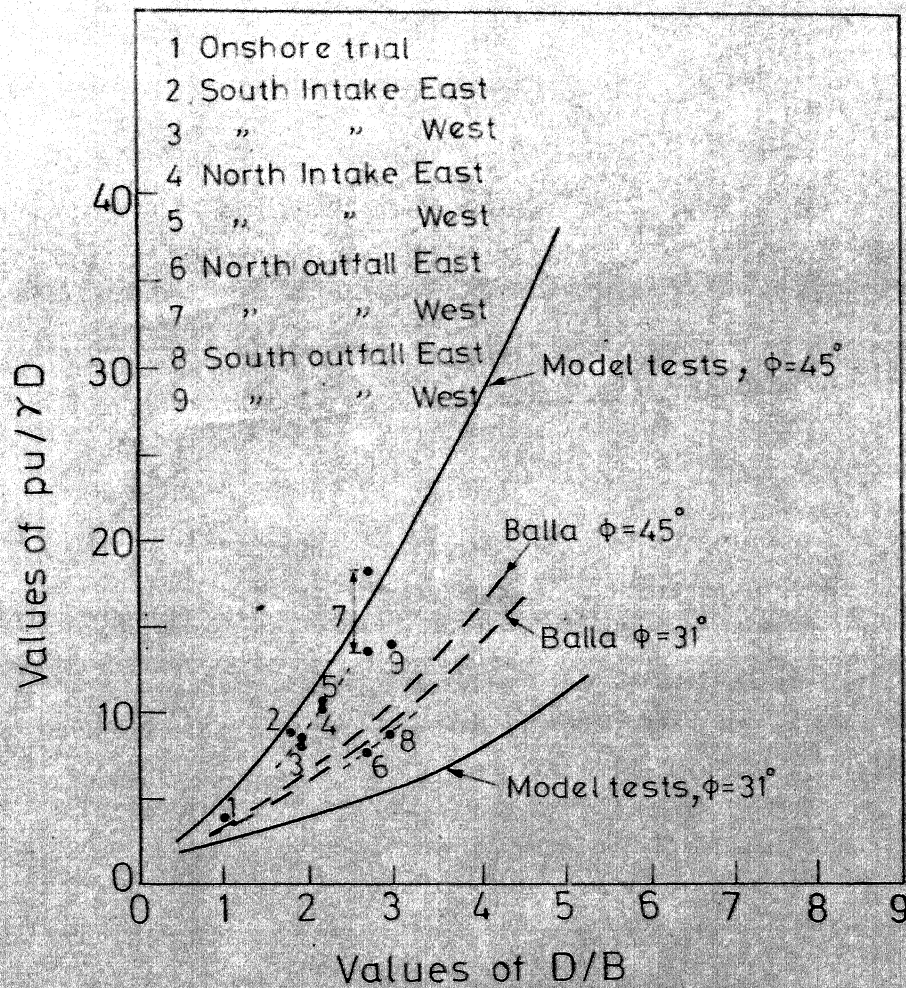


FIG.2.5 COMPARISON OF THEORETICAL, MODEL TEST AND SITE RESULTS
 (From Ref. 95)

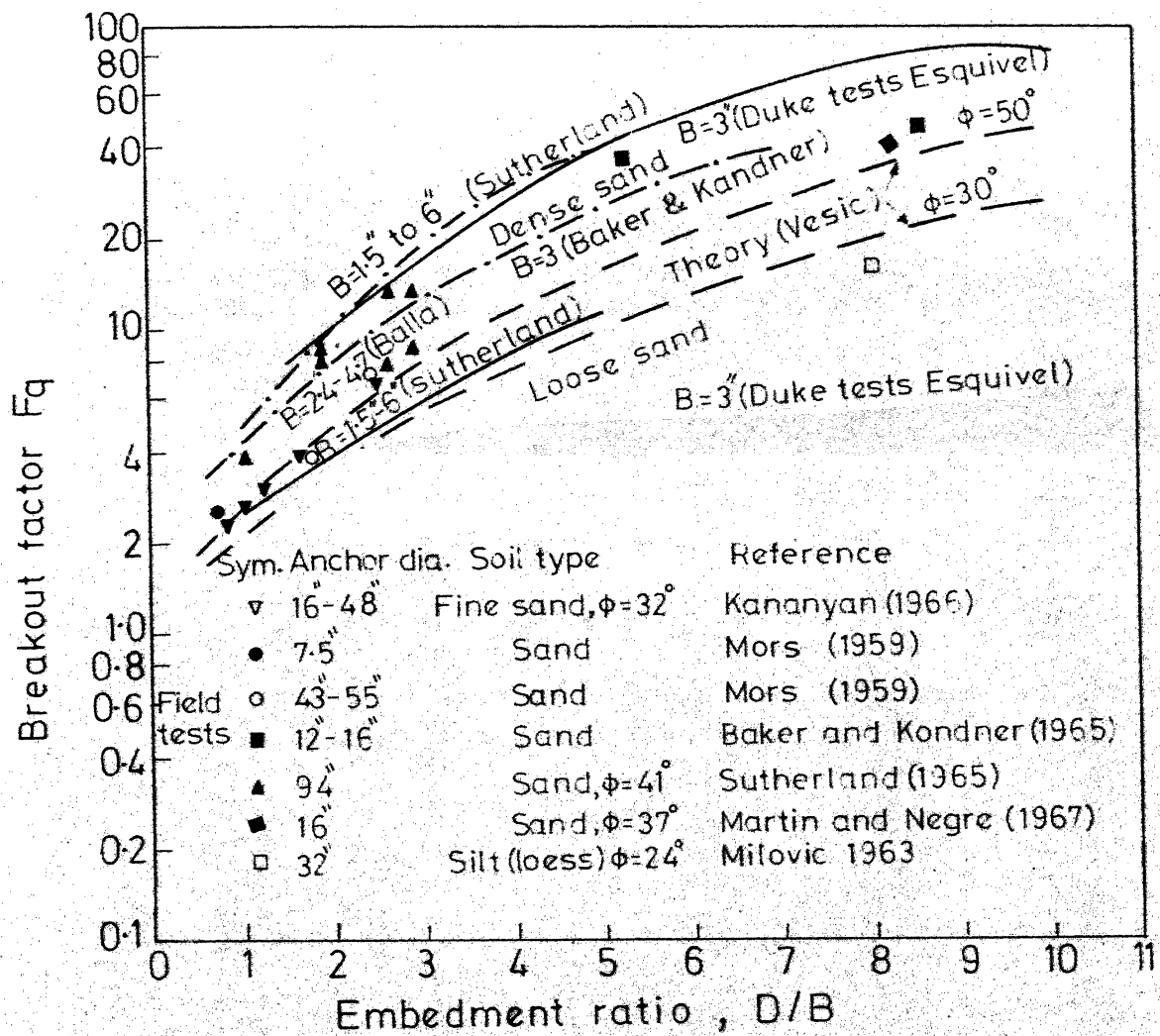


FIG. 2.6 BREAKOUT FACTOR F_q IN SANDS
(From Ref. 101)

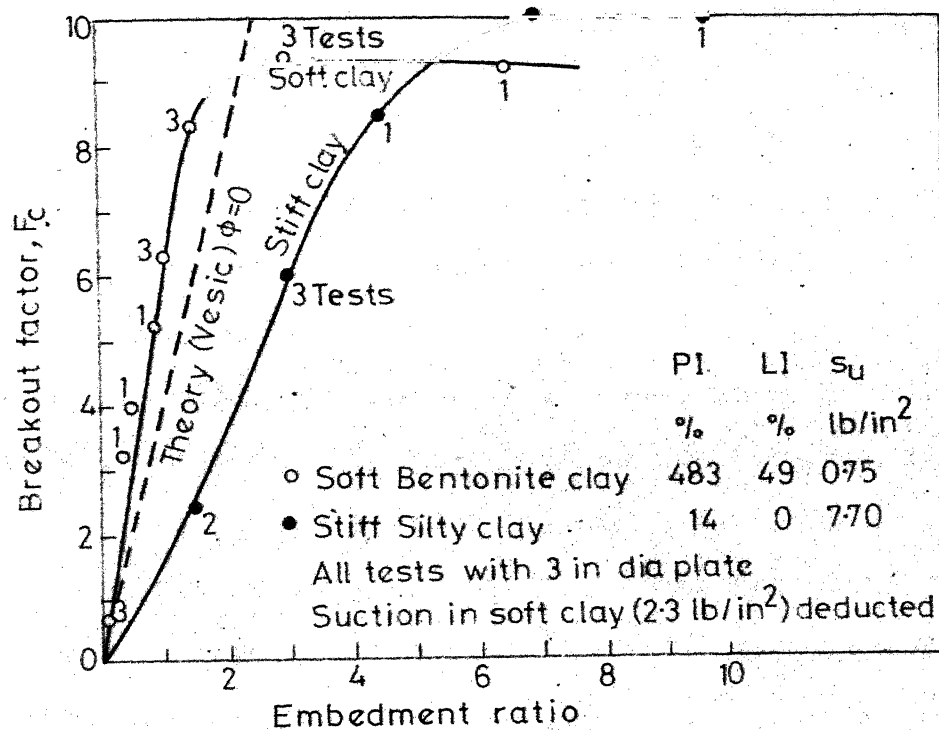


FIG. 2-7 BREAKOUT FACTOR F_c IN CLAYS
(From Ref. 101)

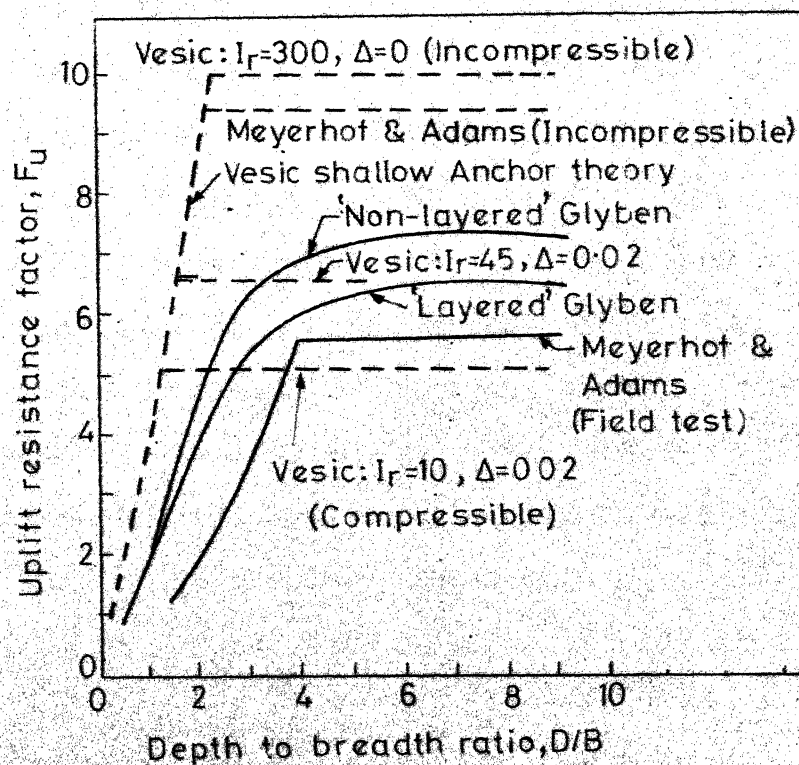


FIG. 2-8 COMPARISON OF THEORETICAL AND
TEST RESULTS
(From Ref. 22)

of anchor plates embedded in dense sand increased substantially with increase in depth of embedment whereas the ultimate pull-out resistance of an anchor plate buried in loose sand increased at a much smaller rate. A comparison with theory indicates that the pullout resistances obtained in dense sand are greater and in loose sand smaller than those determined from analytical results. The limiting depth beyond which there is no considerable increase in capacity is different for dense and loose states and this depth has been found to be smaller for loose state than in dense state.

Matsuo (52) conducted a comprehensive series of uplift tests on model footings, sizes of which ranged from 18 to 40 cms on sand and Kanto-Loam ($C - \phi$ soil). The shape of sliding surface was observed to be a combination of logarithmic spiral and a straight line (Fig. 2.4e). Effects of slab shape, taper angle of footing, underground water table, inclined loading and inclined ground surface on the uplift capacity were studied. Matsuo (53) also conducted large scale tests in sands and clays for low embedment ratios. Square slab footings of sizes 105 to 180 cms were tested which were initially embedded by different methods of excavation and compaction states. Adams and Hayes (1) conducted laboratory and field uplift capacity tests on shallow foundations in sand and clay. He found that the extent of stressed zone in loose sand was much less than in dense sand which accounted for large difference in capacity between loose and dense sand. He observed that the uplift capacity in clay

individual and group anchors. Meyerhof (56) has investigated uplift capacity of foundation under inclined loads. Das and Seeley (20) have reported model test results on square plates under inclined load in sand. Das (18) conducted model tests on square and rectangular models under vertical load in clay and experimental results were presented in the form of breakout factors. The variation of critical embedment ratio and breakout factors for shallow and deep foundation conditions have been analysed.

Davie and Sutherland (22) reported results of experimental investigation on circular anchors in purely cohesive soil. Size of anchor plates ranged from 2.5 cms to 20 cms. They concluded from test results that the uplift resistance predicted by theories for purely cohesive soil overestimate the ultimate uplift load. The model tests also indicated that failure mechanism depends on the embedment ratio. They summarised the results of tests as a plot of ultimate uplift capacity factor (F_u) versus embedment ratio (Fig. 2.8).

Mackenzie (48) performed small scale model tests with two plastic clays to obtain the capacity of anchor blocks subjected to horizontal loads. Neely et al. (64) conducted laboratory tests on vertical anchor plates in dry sand. The anchor plates were 5.1 cms high and widths ranged from 5.1 cms to 25.5 cms.

They have compared the results of tests with theoretical prediction of capacity and concluded that to obtain good agreement, it is necessary to use experimentally observed shape factors which appear to be independent of scale, together with values of ϕ which are scale dependent. Das (17) has conducted tests on vertical anchor plates in sand.

CHAPTER 3

ANALYTICAL MODEL, METHODS OF SOLUTION

3.1 Introduction :

This chapter briefly outlines the theory of finite element displacement formulation as applied to the solution of problems of statics. Displacement formulation of elements used in the analysis of anchor problem in plane strain and axisymmetric situations is described. In two dimensional plane strain case, the soil medium is represented by linear (four noded) and parabolic (eight noded) isoparametric elements. The beam bending element with restriction imposed on plane strain behaviour, used to simulate strip anchor structure in few cases of elastic analysis is given. The four noded and six noded interface elements that can be used to model the properties of the interface between the anchor and the soil are also derived. In axisymmetric analysis of circular anchor problem the four noded and eight noded axisymmetric isoparametric ring elements are used to model the soil continuum. The circular anchor is modelled by an axisymmetric thin plate bending element to study the effect of anchor rigidity on its elastic behaviour. Four noded and six noded axisymmetric interface elements that can model the interface and which can be used with four and eight noded axisymmetric continuum elements are derived.

The two dimensional and axisymmetric elastic analysis of the anchor problem is explained. The details of derivation of elasto-plastic incremental constitutive matrix and the 'initial stress' technique used for the elasto-plastic analysis of the anchor problem is discussed.

Kotter's equation which forms the basis of derivation of uplift capacity of horizontal anchors is derived for the special case of circular rupture surfaces (37).

3.2 Finite Element Method :

In many situations an adequate engineering model of the system is obtained by replacing the system by a finite number of well defined components. Such problems are called discrete problems. In contrast to this, are the continuous systems in which the formulation leads to differential equations or equivalent statements which imply an infinite number of elements (104). Even if the number of elements is very large the discrete problems can be solved readily now with the advent of digital computers. The various discretisation methods suggested from time to time to solve the realistic continuum problem both by engineers and mathematicians, all involve approximations which approach the true continuum solution as the number of discrete variables increase.

Finite element method (FEM) is now very well described in a number of books (7,24,104). However, it is briefly outlined

here to keep continuity of the discussion. FEM is a numerical discretisation procedure by the use of which a wide range of complex boundary value problems can be analysed. Most of the geotechnical engineering problems are associated with complex geometrical configurations, material constitutive relations and loading conditions. In interaction problems the finite rigidity of structure and special interface conditions complicates the problem further. Closed-form elastic solutions of these problems are not feasible generally. Finite element method as a numerical tool permits greater flexibility in tackling geotechnical problems. The method permits a realistic modelling of structure, soil and interface behaviour. Elastic, non-linear elastic and elasto-plastic constitutive relations can be implemented within finite element framework in a straight forward manner.

In finite element method, the region of interest is divided into a finite number of simply connected sub-domains or elements. An approximate functional value of the solution is assumed over the sub-domain so that the parameters, say u_i ($i = 1, \dots, n$), of the function become the unknowns of the problem.

3.2.1 Physical Interpretation :

The basic concept is derived from structural analysis. The main feature is that every structure may be approximated as a physical assemblage of individual structural components or finite elements. The elements are interconnected at a finite

UPUR
LIBRARY
70100

number of nodes and sometimes along the boundaries of the element. Assuming the approximate behaviour of individual element, the behaviour of the entire system can be analysed. After assembling the individual elements, the necessary boundary conditions are imposed with primary nodal values as unknowns. Solution of the resulting set of equations yields the system response.

Considering the nature of each individual component in an element, the relationship between the primary variable u^e and the forcing function Q^e , for a linear system can be written as (104),

$$Q_i^e = K_{ij}^e u_j^e + Q_{oi}^e \quad (3.1)$$

repetitive indices indicating summation.

Connection among elements can be established using,

- (a) one set of variables, u_j , for the assembled system, i.e. the condition of continuity

$$u_j = u_j^e \quad (3.2)$$

- (b) the equilibrium of the second set of variables Q_i^e , at each node and equating it to zero,

$$\sum_{e=1}^{NEL} Q_i^e = 0 \quad (3.3)$$

in which, NEL, is the number of elements considered.

Using eqns. (3.1) to (3.3), the resulting equations can be written as

$$[K] \{u\} + \{Q\} = 0 \quad (3.4)$$

in which

$$[K] = K_{ij} = \sum_{e=1}^{NEL} K_{ij}^e \quad (3.5)$$

and

$$\{Q\} = Q_{oi} = \sum_{e=1}^{NEL} Q_{oi}^e \quad (3.6)$$

3.2.2 Finite Element Displacement Formulation of an Elastic Continuum :

The special features of the problem are given below :

- (a) The continuum is separated by imaginary lines or surfaces into a number of 'finite elements'
- (b) The elements are assumed to be interconnected at a discrete number of nodal points situated on their boundaries. The nodal displacements will be the basic unknowns.
- (c) A set of functions is chosen to define uniquely the state of displacement within each finite element in terms of nodal displacements.
- (d) The displacement functions now define uniquely the state of strain within an element in terms of nodal displacements. These strains, together with any initial strains and constitutive properties of the material will define the state of stress throughout the element and hence along its boundaries.
- (e) A system of forces concentrated at the nodes and equilibrating the boundary stresses and any distributed load is determined.

Once this stage is reached, the solution procedure follows the standard discrete system pattern. The above procedure involve a series of approximations. Ensuring displacement compatibility between adjacent elements may not be possible always, though within each element it is obviously satisfied. Concentrating the equivalent forces at nodes, equilibrium conditions are satisfied in the overall sense only.

The displacements can be expressed as,

$$u = \sum N_i a_i^e = [N_i, N_j, \dots] \begin{Bmatrix} a_i \\ a_j \\ \vdots \end{Bmatrix}^e = N a^e \quad (3.7)$$

where

u = displacement at any point within an element

N = prescribed function of position called shape function

a^e = nodal displacement vector for a particular element.

The strain vector, ϵ , can be obtained with displacements known at all points within the element. Dropping subscript for element,

$$\epsilon = B a \quad (3.8)$$

For a linearly elastic constitutive law,

$$\sigma = D(\epsilon - \epsilon_0) + \sigma_0 \quad (3.9)$$

where

ϵ_0 = initial strain matrix

D = symmetric matrix of elastic constants

σ_0 = initial residual stresses.

$$q^e = \begin{Bmatrix} q_i^e \\ q_j^e \\ \vdots \\ \vdots \end{Bmatrix} = \text{nodal force vector which are statically equivalent to the boundary stresses and distributed loads on the element.}$$

To make the nodal forces statically equivalent to the actual boundary stresses, and distributed loads, the simplest procedure is to impose an arbitrary virtual displacement and to equate the external and internal work done by the various forces and stresses during that displacement (i.e.)

$$\delta a^{eT} q^e = \delta a^{eT} \left[\int_{V^e} B^T \sigma d(\text{vol}) - \int_{V^e} N^T b d(\text{vol}) - \int_{A^e} N^T \bar{t} d(\text{Area}) \right] \quad (3.10)$$

where

b = vector of body force components

\bar{t} = vector of traction components.

As this relation is valid for any value of virtual displacement,

$$q^e = \int_{V^e} B^T \sigma d(\text{vol}) - \int_{V^e} N^T b d(\text{vol}) - \int_{A^e} N^T \bar{t} d(\text{Area}) \quad (3.11)$$

$$q^e = K^e a^e + f^e \quad (3.12)$$

$$K^e = \int_{V^e} B^T D B d(\text{vol}) \quad (3.13a)$$

$$f^e = - \int_{V^e} N^T b d(\text{vol}) - \int_{A^e} N^T \bar{t} d(\text{Area}) - \int_{V^e} B^T D \epsilon_0 d(\text{vol}) + \int_{V^e} B^T \sigma_0 d(\text{vol}) \quad (3.13b)$$

External concentrated forces may exist at the nodes denoted by vector

$$r = \begin{Bmatrix} r_1 \\ r_2 \\ \vdots \\ r_n \end{Bmatrix} \quad (3.14)$$

Equation (3.7) can be interpreted as applying to the whole structure,

$$u = \bar{N} a \quad (3.15)$$

in which a is nodal displacement vector for all the nodal points. Similarly,

$$\varepsilon = \bar{B} a \quad (3.16)$$

Dropping the bar superscript,

$$\delta a^T r = \int_V \delta u^T b \, dV + \int_A \delta u^T \bar{t} \, dA - \int_V \delta \varepsilon^T \sigma \, dV \quad (3.17)$$

Substituting, eqns. (3.15), (3.8) and (3.9), once again a system of linear equations are obtained.

$$K a + f = r \quad (3.18)$$

$$K = \int_V B^T D B \, dV \quad (3.19a)$$

$$f = - \int_V N^T b \, dV - \int_A N^T \bar{t} \, dA - \int_V B^T D \varepsilon_0 \, dV + \int_V B^T \sigma_0 \, dV \quad (3.19b)$$

The integrals are taken over the whole volume V and over the whole area A on which the tractions are given.

$$K_{ij} = \int K_{ij}^e, \quad f_i = \int f_i^e \quad (3.20)$$

$$\int_V N^T b \, dV = \sum \int_{V_e} N^T b \, dV \quad (3.21a)$$

$$\int_V N^T \bar{t} \, dA = \sum \int_{A_e} N^T \bar{t} \, dA \quad (3.21b)$$

The same is true for other elements in the equation (3.19).

3.2.3 Convergence in Finite Element Method :

Since finite element method is an approximate numerical procedure for solution of field problems, like any other approximate numerical techniques, the question of convergence, rate of convergence and accuracy of the method are of great importance.

If the procedure in developing finite element method employing variational, residual or virtual work methods, the key equations involve integrals over the domain (and also in some cases over the boundary) as is seen from eqns. (3.19a) and (3.19b). If each of these integrals tends to its exact value as the element size decreases to zero the finite element method would yield a solution which correspondingly tends to the exact solution. Each integrand contains (a) nodal parameters and their derivatives, (b) material properties of the media, and (c) prescribed physical variables such as body forces. For convergence, the piecewise specified contributions of (a), (b) and (c) both within the elements and across inter-element boundaries must tend to their exact values as the element size tends to zero. Conditions imposed on (b) and (c) can be satisfied easily. Condition (a) becomes prime requirement for convergence. The convergence criterion in a displacement formulation can be stated

as follows (24) :

- (a) The displacement model must be continuous within the the elements and the displacements must be compatible between the adjacent elements.
- (b) The displacement model should include the rigid body displacements of the element.
- (c) The displacement model should include constant strain states of the element.

Element formulations which satisfy criterion (a) is called compatible or conforming and formulations which satisfy (b) and (c) are called complete.

3.3 Displacement Formulation of Elements Used :

3.3.1 Continuum Elements :

The unique description of the displacement within each element in terms of nodal values at boundary points or internal points of the element is the basic step in any displacement finite element formulation and can be expressed as

$$u = N a^e$$

where N is the shape function matrix.

If the shape function chosen to describe the element co-ordinates are identical to those used to prescribe function (displacement) variation, then the element is termed isoparametric. The basic procedure in the isoparametric finite element formulation is to express the element co-ordinates and element displacements in the

form of interpolation functions using natural co-ordinate system of the element. The fundamental property of the interpolation function N_i is that its value in the natural co-ordinate system is unity at node i and zero at all other nodes. The scheme given below follows general pattern of derivation suggested by Bathe and Wilson (7) and Zienkiewicz (104). For a two-dimensional element interpolation functions for four and eight noded cases are given below (Fig. 3.1 and Fig. 3.2).

4 noded element :

$$\begin{aligned}
 N_1 &= \frac{1}{4} (1 - s) (1 - t) \\
 N_2 &= \frac{1}{4} (1 + s) (1 - t) \\
 N_3 &= \frac{1}{4} (1 + s) (1 + t) \\
 N_4 &= \frac{1}{4} (1 - s) (1 + t)
 \end{aligned} \tag{3.22}$$

8 noded element :

$$\begin{aligned}
 N_1 &= \frac{1}{4} (1 - s) (1 - t) - \left(\frac{1}{2}\right) N_5 - \left(\frac{1}{2}\right) N_8 \\
 N_2 &= \frac{1}{4} (1 + s) (1 - t) - \left(\frac{1}{2}\right) N_5 - \left(\frac{1}{2}\right) N_6 \\
 N_3 &= \frac{1}{4} (1 + s) (1 + t) - \left(\frac{1}{2}\right) N_6 - \left(\frac{1}{2}\right) N_7 \\
 N_4 &= \frac{1}{4} (1 - s) (1 + t) - \left(\frac{1}{2}\right) N_7 - \left(\frac{1}{2}\right) N_8 \\
 N_5 &= \frac{1}{2} (1 - s^2) (1 - t) \\
 N_6 &= \frac{1}{2} (1 - t^2) (1 + s) \\
 N_7 &= \frac{1}{2} (1 - s^2) (1 + t) \\
 N_8 &= \frac{1}{2} (1 - t^2) (1 - s)
 \end{aligned} \tag{3.23}$$

a) Four Noded Isoparametric Quadrilateral Element for Two-Dimensional Plane Strain/Plane Stress Problems :

Since the number of natural co-ordinate variables is equal to the number of global variables the calculation of the element matrices can be carried out in the global co-ordinate system directly. For all continuum elements derived the local x, y and global X, Y are assumed to coincide and hence no transformation is needed. Four noded quadrilateral element has eight degrees of freedom as shown in Fig. 3.1a.

Cartesian co-ordinates x, y and natural co-ordinates s, t are related as follows :

$$x = N_1 x_1 + N_2 x_2 + N_3 x_3 + N_4 x_4 \quad (3.24a)$$

$$y = N_1 y_1 + N_2 y_2 + N_3 y_3 + N_4 y_4 \quad (3.24b)$$

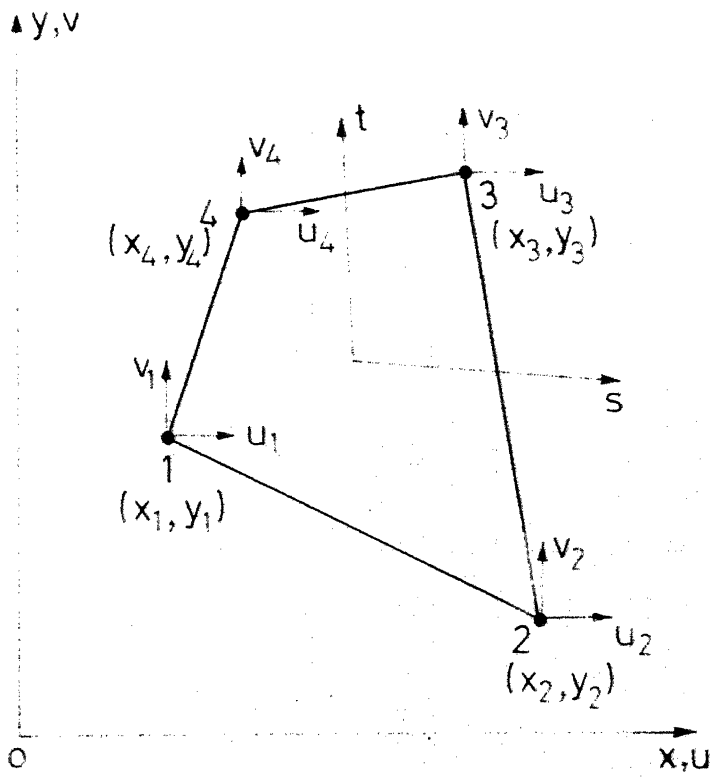
where N_1, N_2, N_3 and N_4 for a 4 noded element are given in eqn. (3.22). When natural co-ordinates are used, the displacement within the element expressed in terms of nodal values are :

$$u = N_1 u_1 + N_2 u_2 + N_3 u_3 + N_4 u_4 \quad (3.25a)$$

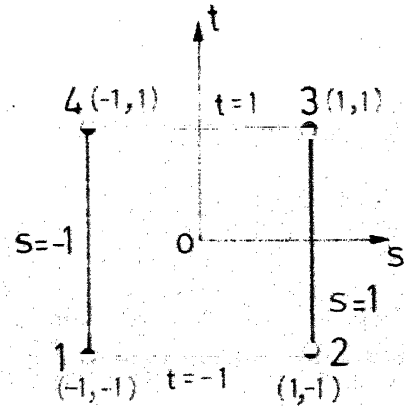
$$v = N_1 v_1 + N_2 v_2 + N_3 v_3 + N_4 v_4 \quad (3.25b)$$

Along the edge of the element the variation of displacement is linear.

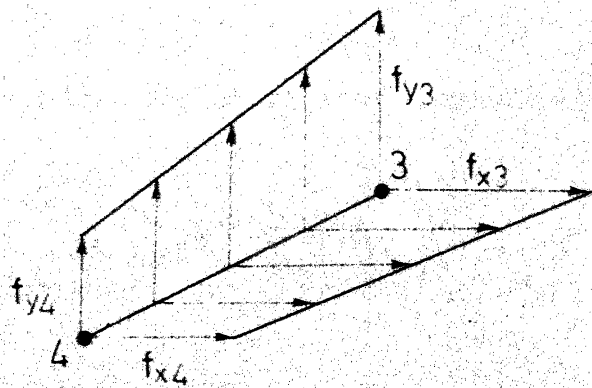
$$\begin{Bmatrix} u \\ v \end{Bmatrix} = \begin{bmatrix} N_1 & 0 & N_2 & 0 & N_3 & 0 & N_4 & 0 \\ 0 & N_1 & 0 & N_2 & 0 & N_3 & 0 & N_4 \end{bmatrix} \{ a \} \quad (3.26a)$$



a. Local co-ordinate system



b. Natural co-ordinate system



c. Linearly varying traction on edge 43

FIG-31 FOUR NODED LINEAR ISOPARAMETRIC QUADRILATERAL ELEMENT FOR TWO DIMENSIONAL ANALYSIS

$$\{u\} = [N] \{a\}$$

$$\{a\}^T = [u_1 \ v_1 \ u_2 \ v_2 \ u_3 \ v_3 \ u_4 \ v_4] \quad (3.26b)$$

Element strain vector for plane strain case is

$$\{\epsilon\}^T = [\epsilon_{xx} \ \epsilon_{yy} \ \gamma_{xy}] \quad (3.27a)$$

$$\epsilon_{xx} = \frac{\partial u}{\partial x}, \quad \epsilon_{yy} = \frac{\partial v}{\partial y}, \quad \gamma_{xy} = \frac{\partial v}{\partial x} + \frac{\partial u}{\partial y} \quad (3.27b)$$

Relationship between derivatives in the two co-ordinate systems is given by chain rule of partial differentiation as follows :

$$\frac{\partial}{\partial s} = \frac{\partial x}{\partial s} \frac{\partial}{\partial x} + \frac{\partial y}{\partial s} \frac{\partial}{\partial y}$$

$$\frac{\partial}{\partial t} = \frac{\partial x}{\partial t} \frac{\partial}{\partial x} + \frac{\partial y}{\partial t} \frac{\partial}{\partial y}$$

$$\begin{Bmatrix} \frac{\partial}{\partial s} \\ \frac{\partial}{\partial t} \end{Bmatrix} = \begin{bmatrix} \frac{\partial x}{\partial s} & \frac{\partial y}{\partial s} \\ \frac{\partial x}{\partial t} & \frac{\partial y}{\partial t} \end{bmatrix} \begin{Bmatrix} \frac{\partial}{\partial x} \\ \frac{\partial}{\partial y} \end{Bmatrix} = [J] \begin{Bmatrix} \frac{\partial}{\partial x} \\ \frac{\partial}{\partial y} \end{Bmatrix} \quad (3.28)$$

where $[J]$ is the Jacobian matrix of transformation. By inverting,

$$\begin{Bmatrix} \frac{\partial}{\partial x} \\ \frac{\partial}{\partial y} \end{Bmatrix} = [J]^{-1} \begin{Bmatrix} \frac{\partial}{\partial s} \\ \frac{\partial}{\partial t} \end{Bmatrix} = [J^*] \begin{Bmatrix} \frac{\partial}{\partial s} \\ \frac{\partial}{\partial t} \end{Bmatrix} \quad (3.29)$$

$$\begin{Bmatrix} \frac{\partial u}{\partial x} \\ \frac{\partial u}{\partial y} \\ \frac{\partial v}{\partial x} \\ \frac{\partial v}{\partial y} \end{Bmatrix} = \begin{bmatrix} J_{11}^* & J_{12}^* & 0 & 0 \\ J_{21}^* & J_{22}^* & 0 & 0 \\ 0 & 0 & J_{11}^* & J_{12}^* \\ 0 & 0 & J_{21}^* & J_{22}^* \end{bmatrix} \begin{Bmatrix} \frac{\partial u}{\partial s} \\ \frac{\partial u}{\partial t} \\ \frac{\partial v}{\partial s} \\ \frac{\partial v}{\partial t} \end{Bmatrix} \quad (3.30)$$

where J_{ij}^* are elements of matrix $[J]^{-1}$.

Substituting of eqn. (3.30) into eqn. (3.27) yields

$$\begin{Bmatrix} \epsilon_{xx} \\ \epsilon_{yy} \\ \gamma_{xy} \end{Bmatrix} = \begin{bmatrix} J_{11}^* & J_{12}^* & 0 & 0 \\ 0 & 0 & J_{21}^* & J_{22}^* \\ J_{21}^* & J_{22}^* & J_{11}^* & J_{12}^* \end{bmatrix} \begin{Bmatrix} \frac{\partial u}{\partial s} \\ \frac{\partial u}{\partial t} \\ \frac{\partial v}{\partial s} \\ \frac{\partial v}{\partial t} \end{Bmatrix} \quad (3.31)$$

$$\begin{Bmatrix} \frac{\partial u}{\partial s} \\ \frac{\partial u}{\partial t} \\ \frac{\partial v}{\partial s} \\ \frac{\partial v}{\partial t} \end{Bmatrix} = \begin{bmatrix} \frac{\partial N_1}{\partial s} & 0 & \frac{\partial N_2}{\partial s} & 0 & \frac{\partial N_3}{\partial s} & 0 & \frac{\partial N_4}{\partial s} & 0 \\ \frac{\partial N_1}{\partial t} & 0 & \frac{\partial N_2}{\partial t} & 0 & \frac{\partial N_3}{\partial t} & 0 & \frac{\partial N_4}{\partial t} & 0 \\ 0 & \frac{\partial N_1}{\partial s} & 0 & \frac{\partial N_2}{\partial s} & 0 & \frac{\partial N_3}{\partial s} & 0 & \frac{\partial N_4}{\partial s} \\ 0 & \frac{\partial N_1}{\partial t} & 0 & \frac{\partial N_2}{\partial t} & 0 & \frac{\partial N_3}{\partial t} & 0 & \frac{\partial N_4}{\partial t} \end{bmatrix} \begin{Bmatrix} u_1 \\ v_1 \\ u_2 \\ v_2 \\ u_3 \\ v_3 \\ u_4 \\ v_4 \end{Bmatrix} \quad (3.32)$$

$$\begin{Bmatrix} \frac{\partial u}{\partial x} \\ \frac{\partial v}{\partial y} \\ \frac{\partial v}{\partial x} + \frac{\partial u}{\partial y} \end{Bmatrix} = \begin{bmatrix} \frac{\partial N_1}{\partial x} & 0 & \frac{\partial N_2}{\partial x} & 0 & \frac{\partial N_3}{\partial x} & 0 & \frac{\partial N_4}{\partial x} & 0 \\ 0 & \frac{\partial N_1}{\partial y} & 0 & \frac{\partial N_2}{\partial y} & 0 & \frac{\partial N_3}{\partial y} & 0 & \frac{\partial N_4}{\partial y} \\ \frac{\partial N_1}{\partial y} & \frac{\partial N_1}{\partial x} & \frac{\partial N_2}{\partial y} & \frac{\partial N_2}{\partial x} & \frac{\partial N_3}{\partial y} & \frac{\partial N_3}{\partial x} & \frac{\partial N_4}{\partial y} & \frac{\partial N_4}{\partial x} \end{bmatrix} \begin{Bmatrix} u_1 \\ v_1 \\ u_2 \\ v_2 \\ u_3 \\ v_3 \\ u_4 \\ v_4 \end{Bmatrix} \quad (3.33)$$

Equation (3.33) can be identified as,

$\{\epsilon\} = [B] \{a\}$ where B is the strain displacement matrix.

The elasticity matrix for plane stress can be written as

$$[D] = \frac{E}{1-\nu^2} \begin{bmatrix} 1 & \nu & 0 \\ \nu & 1 & 0 \\ 0 & 0 & \frac{1-\nu}{2} \end{bmatrix} \quad (3.34a)$$

For plane strain the elasticity matrix can be written as

$$[D] = \frac{E}{(1+\nu)(1-2\nu)} \begin{bmatrix} (1-\nu) & \nu & 0 \\ 0 & 1-\nu & 0 \\ 0 & 0 & \frac{1-2\nu}{2} \end{bmatrix} \quad (3.34b)$$

The matrices to be evaluated are the stiffness matrix K , the body force vector, and the surface load vector for distributed loads at the boundary if there are no initial stresses and strains. The matrices in general are evaluated by numerical integration, using Gaussian quadrature formula. Economy in the matrix product requires special attention because many zeroes are present in matrices B and D . One of the methods to reduce the number of operations is to form explicitly the matrix triple product and use it directly to calculate stiffness matrix by numerical integration. If the thickness of the element is constant (for plane strain condition thickness is unity), the matrix K can be obtained as

$$[K] = t \sum_{i=1}^n \sum_{j=1}^n \alpha_i \alpha_j F_{ij} \quad (3.35a)$$

$$F_{ij} = B_{ij}^T D B_{ij} \det J_{ij} \quad (3.35b)$$

in which n is the number of integration points in each direction,

α_i, α_j are Gaussian quadrature weights.

F_{ij} are the function values to be evaluated at sampling points s_i, t_j .

For evaluation of stiffness matrix of the element 2x2 numerical integration is used. The function values are evaluated at 4 sampling points and summed up to get the stiffness matrix of the four noded element. Because the element stiffness matrix is symmetric, only one half would be formed and the other half formed by reflection. The body force vector, and the surface load vector due to distributed loads can also be evaluated by numerical integration, in general.

The surface load vector for a linearly varying traction acting on the element edge can be evaluated without resorting to numerical integration. For traction on boundary 43 shown in Fig. 3.1c, the consistent load vector evaluated by direct integration gives,

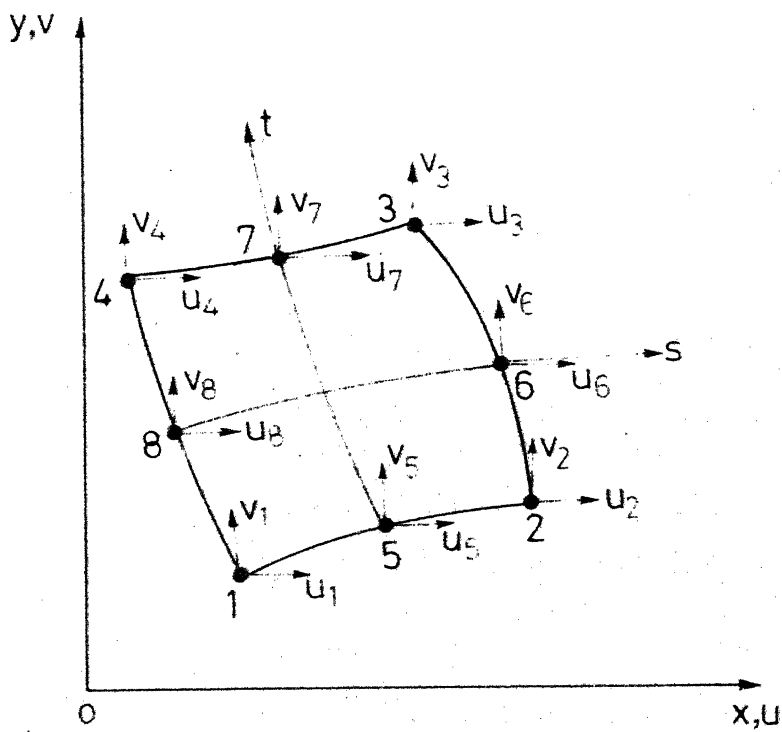
$$\begin{Bmatrix} R_{4x} \\ R_{4y} \\ R_{3x} \\ R_{3y} \end{Bmatrix} = \frac{tL}{6} \begin{Bmatrix} 2f_{x4} + f_{x3} \\ 2f_{y4} + f_{y3} \\ 2f_{x3} + f_{x4} \\ 2f_{y3} + f_{y5} \end{Bmatrix} \quad (3.36)$$

where t is the length of side 43.

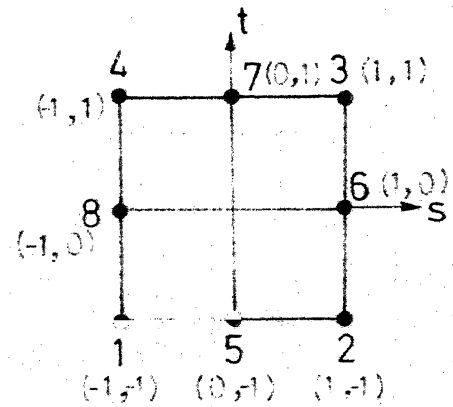
b) Eight Noded Isoparametric Curved Element for Two-Dimensional Plane Strain/Plane Stress Problems :

A quadratic variation of displacement and geometry are assumed for this element and it has 16 displacement degrees of freedom (Fig. 3.2).

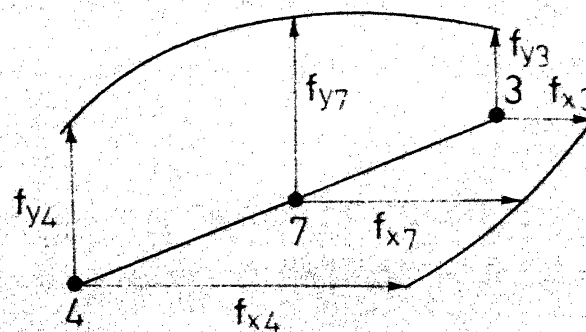
Cartesian co-ordinates x, y and natural co-ordinates s, t are



a. Local co-ordinate system



b. Natural co-ordinate system



c. Parabolic variation of surface fraction on straight edge 43

FIG-32 EIGHT NODED PARABOLIC ISOPARAMETRIC ELEMENT FOR TWO DIMENSIONAL ANALYSIS

related as follows :

$$x = N_1x_1 + N_2x_2 + N_3x_3 + N_4x_4 + N_5x_5 + N_6x_6 + N_7x_7 + N_8x_8 \quad (3.37a)$$

$$y = N_1y_1 + N_2y_2 + N_3y_3 + N_4y_4 + N_5y_5 + N_6y_6 + N_7y_7 + N_8y_8 \quad (3.37b)$$

where N_1 to N_8 are given in eqn. (3.23).

Similarly, the displacements expressed in terms of nodal values are :

$$u = N_1u_1 + N_2u_2 + N_3u_3 + N_4u_4 + N_5u_5 + N_6u_6 + N_7u_7 + N_8u_8 \quad (3.38a)$$

$$v = N_1v_1 + N_2v_2 + N_3v_3 + N_4v_4 + N_5v_5 + N_6v_6 + N_7v_7 + N_8v_8 \quad (3.38b)$$

The further steps in derivation of the strain-displacement matrix are the same as for the four noded elements. The B matrix will be the order of 3×16 . The stiffness matrix of the element is evaluated by 2×2 numerical integration using Gauss quadrature rules. Using symmetry conditions, one half is formed and other the other half formed by reflection. The body force vector and the surface load vector are also in general evaluated by numerical integration.

For a parabolic variation of traction acting over a straight edge of the boundary (Fig. 3.2c) the consistent load vector can be derived explicitly and is given below :

$$\begin{Bmatrix} R_{4x} \\ R_{4y} \\ R_{7x} \\ R_{7y} \\ R_{3x} \\ R_{3y} \end{Bmatrix} = \frac{tL}{30} \begin{Bmatrix} 4f_{x4} + 2f_{x7} - f_{x3} \\ 4f_{y4} + 2f_{y7} - f_{y3} \\ 2f_{x4} + 16f_{x7} + 2f_{x3} \\ 2f_{y4} + 16f_{y7} + 2f_{y3} \\ -f_{x4} + 2f_{x7} + 4f_{x3} \\ -f_{y4} + 2f_{y7} + 4f_{y3} \end{Bmatrix} \quad (3.39)$$

4 and 3 are corner nodes and 7 is mid-side node. L is the length of side of the element on which the traction is acting.

c) Four Noded Isoparametric Ring Element for Axisymmetric Problems :

Cartesian co-ordinates r, z and natural co-ordinates s, t are related as follows (Fig. 3.3b) :

$$r = N_1 r_1 + N_2 r_2 + N_3 r_3 + N_4 r_4 \quad (3.40a)$$

$$z = N_1 z_1 + N_2 z_2 + N_3 z_3 + N_4 z_4 \quad (3.40b)$$

where N_1, N_2, N_3 and N_4 are element shape functions given in eqn. (3.22).

The displacements within an element are expressed in terms of the nodal values as :

$$u = N_1 u_1 + N_2 u_2 + N_3 u_3 + N_4 u_4 \quad (3.41a)$$

$$w = N_1 w_1 + N_2 w_2 + N_3 w_3 + N_4 w_4 \quad (3.41b)$$

$$\{u\} = [N] \{a\}$$

$$\{a\}^T = [u_1 \ w_1 \ u_2 \ w_2 \ u_3 \ w_3 \ u_4 \ w_4]$$

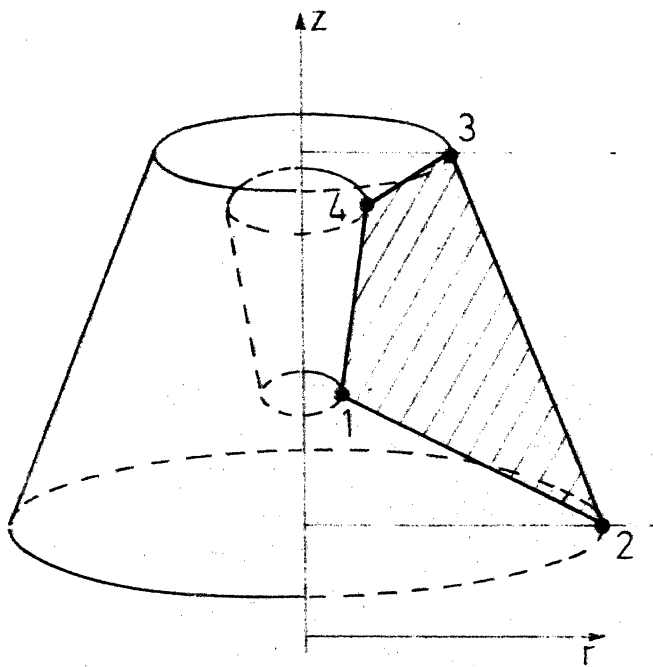
Element strain vector in axisymmetric case, ϵ can be written as,

$$\{\epsilon\}^T = [\epsilon_{rr} \ \epsilon_{\theta\theta} \ \epsilon_{zz} \ \gamma_{rz}] \quad (3.42a)$$

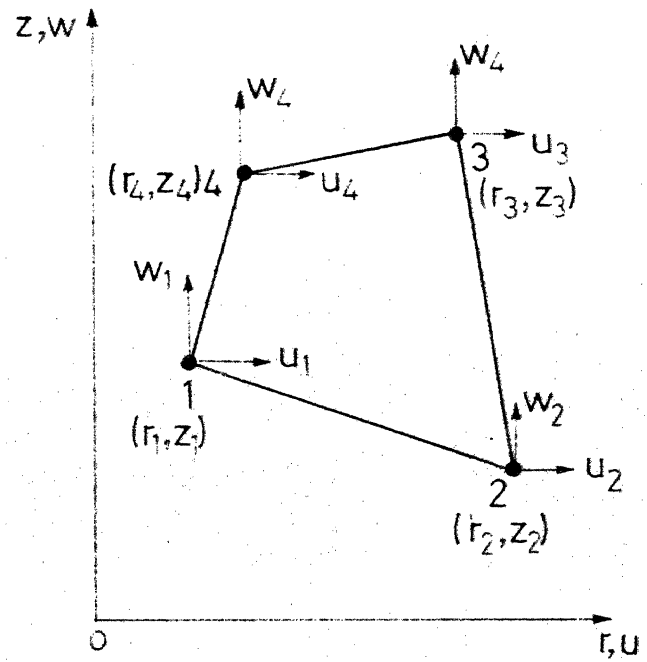
where

$$\epsilon_{rr} = \frac{\partial u}{\partial r}, \quad \epsilon_{\theta\theta} = \frac{u}{r}, \quad \epsilon_{zz} = \frac{\partial w}{\partial z}, \quad \gamma_{rz} = \frac{\partial w}{\partial r} + \frac{\partial u}{\partial z} \quad (3.42b)$$

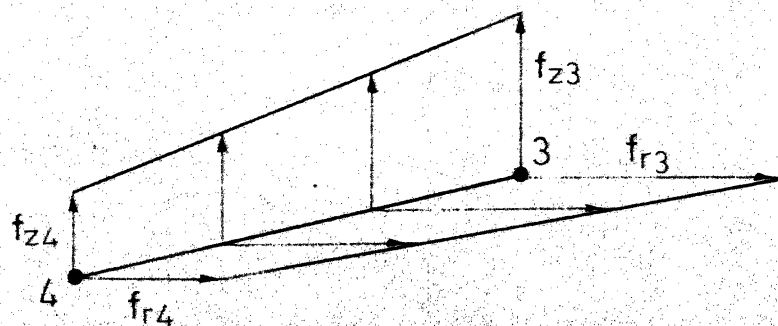
Following the same steps carried out in the derivation of 4 noded isoparametric two-dimensional quadrilateral element and noting



a. Element of an axisymmetric solid-element section



b. Ring element cross section



c. Linearly varying traction on edge 43.
(ring load)

FIG. 33 FOUR NODED ISOPARAMETRIC QUADRILATERAL RING ELEMENT FOR AXISYMMETRIC ANALYSIS

the difference in $\epsilon_{\theta\theta}$ only, the relation between the element strains and nodal displacements are :

$$\begin{Bmatrix} \frac{\partial u}{\partial r} \\ \frac{u}{r} \\ \frac{\partial w}{\partial z} \\ \frac{\partial w}{\partial r} + \frac{\partial u}{\partial z} \end{Bmatrix} = \begin{bmatrix} \frac{\partial N_1}{\partial r} & 0 & \frac{\partial N_2}{\partial r} & 0 & \frac{\partial N_3}{\partial r} & 0 & \frac{\partial N_4}{\partial r} & 0 \\ \frac{N_1}{r} & 0 & \frac{N_2}{r} & 0 & \frac{N_3}{r} & 0 & \frac{N_4}{r} & 0 \\ 0 & \frac{\partial N_1}{\partial z} & 0 & \frac{\partial N_2}{\partial z} & 0 & \frac{\partial N_3}{\partial z} & 0 & \frac{\partial N_4}{\partial z} \\ \frac{\partial N_1}{\partial z} & \frac{\partial N_1}{\partial r} & \frac{\partial N_2}{\partial z} & \frac{\partial N_2}{\partial r} & \frac{\partial N_3}{\partial z} & \frac{\partial N_3}{\partial r} & \frac{\partial N_4}{\partial z} & \frac{\partial N_4}{\partial r} \end{bmatrix} \begin{Bmatrix} u_1 \\ w_1 \\ u_2 \\ w_2 \\ u_3 \\ w_3 \\ u_4 \\ w_4 \end{Bmatrix} \quad (3.43)$$

Equation (3.43) can be identified as

$\{\epsilon\} = [B] \{a\}$ where B is the strain displacement matrix.

The strain displacement matrix is a 4x8 matrix.

The elasticity matrix for axisymmetric case can be written as,

$$\begin{Bmatrix} \sigma_{rr} \\ \sigma_{\theta\theta} \\ \sigma_{zz} \\ \tau_{rz} \end{Bmatrix} = \frac{E}{(1+\nu)(1-2\nu)} \begin{bmatrix} (1-\nu) & \nu & \nu & 0 \\ \nu & (1-\nu) & \nu & 0 \\ 0 & 0 & (1-\nu) & 0 \\ 0 & 0 & 0 & \frac{1-2\nu}{2} \end{bmatrix} \begin{Bmatrix} \epsilon_{rr} \\ \epsilon_{\theta\theta} \\ \epsilon_{zz} \\ \gamma_{rz} \end{Bmatrix} \quad (3.44)$$

Explicit expressions for matrix triple product $B^T D B$ are obtained and used directly to economise operations in forming stiffness matrix. The stiffness matrix is evaluated by numerical integration and can be obtained by,

$$[K] = 2\pi \sum_{i=1}^n \sum_{j=1}^n \alpha_i \alpha_j F_{ij} \quad (3.45a)$$

where

$$F_{ij} = B_{ij}^T D B_{ij} r_{ij} \det J_{ij} \quad (3.45b)$$

F_{ij} are function values evaluated at sampling points s_i, t_j .

For evaluation of stiffness matrix, 2x2 numerical integration using Gauss quadrature rules is carried out, i.e. the function values are evaluated at 4 points inside the element. One half of the stiffness matrix is formed by numerical integration but the other half is obtained by reflection because of symmetry. The body force vector and surface load vector due to distributed loads on element edges can also be evaluated by numerical integration.

The surface load vector for a linearly varying traction acting on the edge of the element can be evaluated without resorting to numerical integration. Referring to Fig. 3.3c, and noting that the load acts on side 43, the load vector can be expressed as

$$\begin{Bmatrix} R_{4r} \\ R_{4z} \\ R_{3r} \\ R_{3z} \end{Bmatrix} = \frac{\pi L}{6} \begin{Bmatrix} (3r_4 + r_3) f_{r4} + (r_4 + r_3) f_{r3} \\ (3r_4 + r_3) f_{z4} + (r_4 + r_3) f_{z3} \\ (r_4 + r_3) f_{r4} + (r_4 + 3r_3) f_{r3} \\ (r_4 + r_3) f_{z4} + (r_4 + 3r_3) f_{z3} \end{Bmatrix} \quad (3.46)$$

d) Eight Noded Isoparametric Ring Element for Axisymmetric Problems :

A quadratic variation of geometry in r, z plane and

displacements are assumed for this element which has 16 degrees of freedom (Fig. 3.4a).

r, z co-ordinates and s, t co-ordinates are related as follows :

$$r = N_1 r_1 + N_2 r_2 + N_3 r_3 + N_4 r_4 + N_5 r_5 + N_6 r_6 + N_7 r_7 + N_8 r_8 \quad (3.47a)$$

$$z = N_1 z_1 + N_2 z_2 + N_3 z_3 + N_4 z_4 + N_5 z_5 + N_6 z_6 + N_7 z_7 + N_8 z_8 \quad (3.47b)$$

where N_1 to N_8 are shape function for the nodal points in Fig. 3.4a and are given in eqn. (3.23).

Similarly, the displacements expressed in terms of nodal values are,

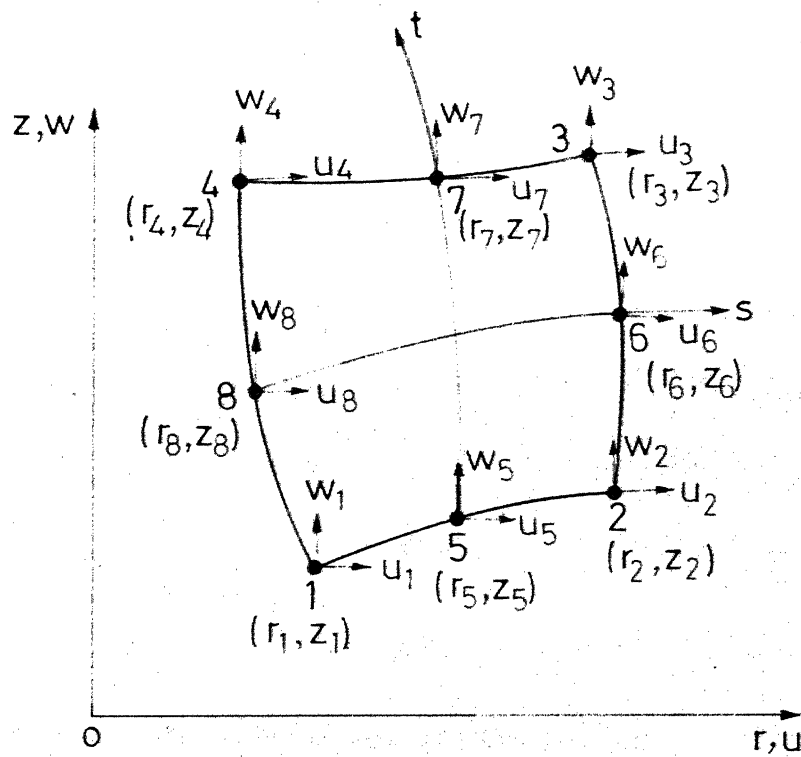
$$u = N_1 u_1 + N_2 u_2 + N_3 u_3 + N_4 u_4 + N_5 u_5 + N_6 u_6 + N_7 u_7 + N_8 u_8 \quad (3.47c)$$

$$w = N_1 w_1 + N_2 w_2 + N_3 w_3 + N_4 w_4 + N_5 w_5 + N_6 w_6 + N_7 w_7 + N_8 w_8 \quad (3.47d)$$

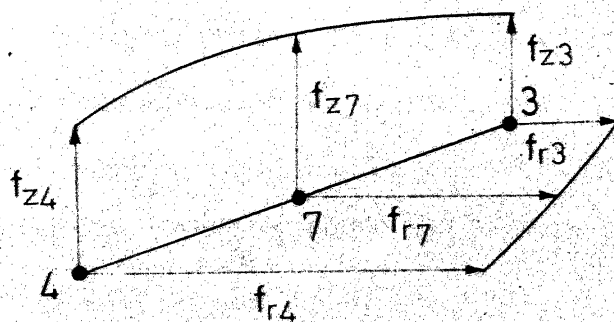
The further steps of derivation of the strain-displacement matrix follow the pattern given for the 4 noded element. The B matrix will be of the order of 4×16 .

Half of the stiffness matrix of the element is evaluated by 2×2 numerical integration using Gauss quadrature rules and the other half is formed by reflection because of symmetry. The body force vector and surface load vector due to distributed loads on the boundary are also evaluated by numerical integration.

For a parabolic variation of traction acting on a straight boundary edge, (Fig. 3.4b), the consistent load vector can be evaluated directly without resorting to numerical integration and



a. Ring element cross section



b. Parabolic variation of traction on a straight edge 43 (ring load)

FIG. 3-4 EIGHT NODDED ISOPARAMETRIC QUADRILATERAL RINGELEMENT FOR AXISYMMETRIC ANALYSIS

is given in eqn. (3.48). 4 and 3 are corner nodes and 7 is a midside node. The load vector can be obtained as

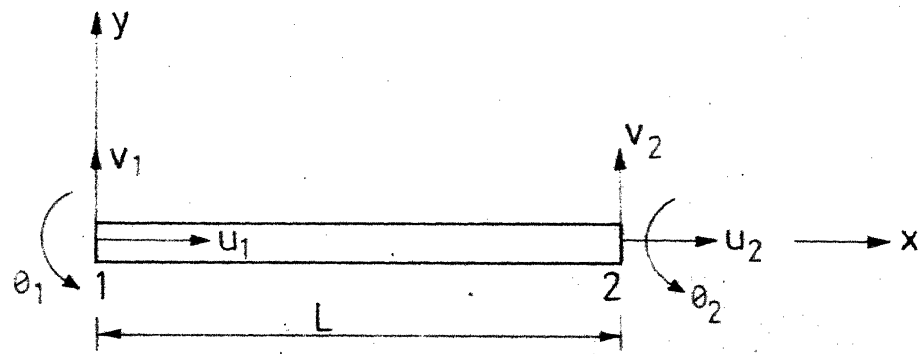
$$\begin{Bmatrix} R_{4r} \\ R_{4z} \\ R_{7r} \\ R_{7z} \\ R_{3r} \\ R_{3z} \end{Bmatrix} = \frac{\pi L}{60} \begin{Bmatrix} (14r_4 + 2r_3) f_{r4} + (8r_4) f_{r7} - (2r_4 + 2r_3) f_{r3} \\ (14r_4 + 2r_3) f_{z4} + (8r_4) f_{z7} - (2r_4 + 2r_3) f_{z3} \\ (8r_4) f_{r4} + (32r_4 + 32r_3) f_{r7} + 8r_3 f_{r3} \\ (8r_4) f_{z4} + (32r_4 + 32r_3) f_{z7} + 8r_3 f_{z3} \\ -(2r_4 + 2r_3) f_{r4} + (8r_3) f_{r7} + (2r_4 + 14r_3) f_{r3} \\ -(2r_4 + 2r_3) f_{z4} + (8r_3) f_{z7} + (2r_4 + 14r_3) f_{z3} \end{Bmatrix} \quad (3.48)$$

3.3.2 Structural Elements :

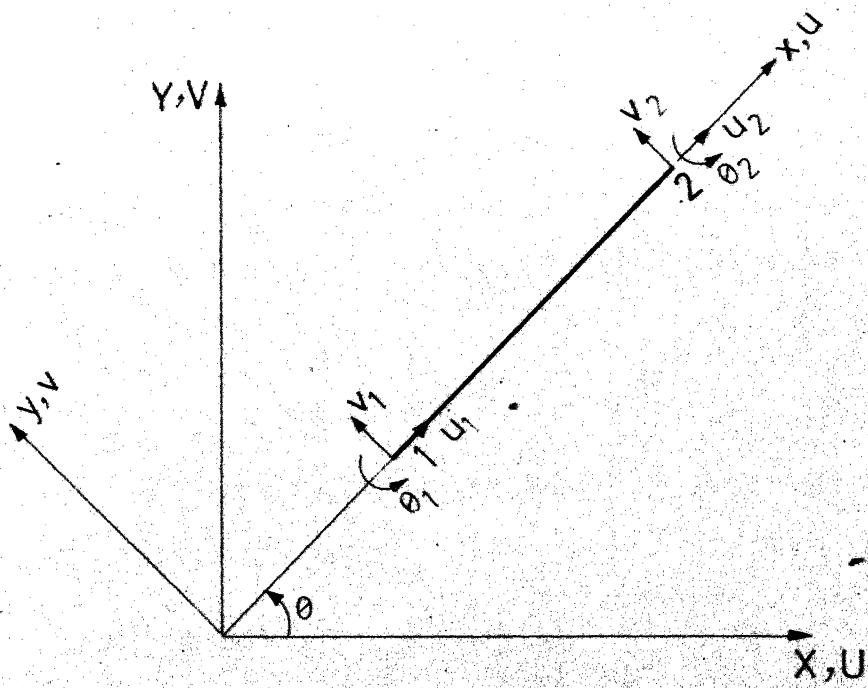
The beam-column element is used in a two-dimensional situation of plane strain to simulate strip anchor behaviour. The details of derivation of this element is given by Przemieniecki (73). The axisymmetric thin plate bending element is used to model the circular anchor to study the effect of structural rigidity of anchor on elastic behaviour. The element matrices were derived by Pardoen (67) and was used by Paramasivam (66) in the axisymmetric analysis of plates.

a) Beam-Column Element

Figure 3.5a shows the 6 degree of freedom element. The element is assumed to be prismatic and of unit width and constant properties along longitudinal beam axis. The stiffness matrix of this element, if placed in two dimensional plane strain situation can be expressed as,



a. Beam-column element, local co-ordinates



b. Element in global axes

FIG-3-5 BEAM-COLUMN ELEMENT USED FOR TWO DIMENSIONAL ANALYSIS

$$[K] = \frac{E}{1-\nu^2} \begin{bmatrix} -\frac{A}{L} & 0 & 0 & -\frac{A}{L} & 0 & 0 \\ & \frac{12I}{L^3} & \frac{6I}{L^2} & 0 & -\frac{12I}{L^3} & \frac{6I}{L^2} \\ & & \frac{4I}{L} & 0 & -\frac{6I}{L^2} & \frac{2I}{L} \\ & & & \frac{A}{L} & 0 & 0 \\ & & & & \frac{12I}{L^3} & -\frac{6I}{L^2} \\ & & & & & \frac{4I}{L} \end{bmatrix} \quad (3.49)$$

(Symmetrical)

where

A = area of cross-section of member

L = length of the member

I = moment of inertia of the cross-sectional area about axis of bending

$$\{a\}^T = [u_1 \ v_1 \ \theta_1 \ u_2 \ v_2 \ \theta_2] \quad (3.50)$$

The transformation matrix given below is used for co-ordinate transformation (Fig. 3.5b).

$$\begin{Bmatrix} u_1 \\ v_1 \\ \theta_1 \\ u_2 \\ v_2 \\ \theta_2 \end{Bmatrix} = \begin{bmatrix} \cos\theta & \sin\theta & 0 & 0 & 0 & 0 \\ \sin\theta & \cos\theta & 0 & 0 & 0 & 0 \\ 0 & 0 & 1 & 0 & 0 & 0 \\ 0 & 0 & 0 & \cos\theta & \sin\theta & 0 \\ 0 & 0 & 0 & -\sin\theta & \cos\theta & 0 \\ 0 & 0 & 0 & 0 & 0 & 1 \end{bmatrix} \begin{Bmatrix} U_1 \\ V_1 \\ \theta_1 \\ U_2 \\ V_2 \\ \theta_2 \end{Bmatrix} \quad (3.51)$$

b) Axisymmetric Thin Plate Bending Element :

Stiffness matrix and load vector for annular plate bending element and the central closure element needed for the analysis of circular plates are derived directly from the solution of basic differential equation for circular plates (66,67). Because of the elimination of the approximation involved in the assumed displacement function, this approach leads to the same solution for axisymmetric plate problems as obtained from classical thin plate theory.

Since the solutions from classical plate theory are used directly in the stiffness formulation a matching of co-ordinate system is needed. Since the plate and loading are axisymmetric it is enough if the diametrical section is considered.

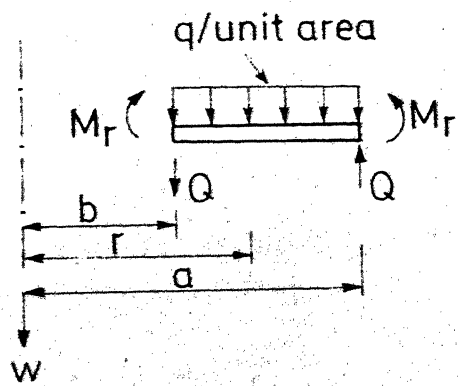
i) Annular Plate Element : The relationship between two displacements of the system for the annular plate element can be expressed by the following relations (Fig. 3.6a).

$$\begin{aligned}
 \delta_1 &= -(w)_{r=b} & F_1 &= -(Q)_{r=b} \\
 \delta_2 &= -\left(\frac{dw}{dr}\right)_{r=b} & F_2 &= -(M)_{r=b} \\
 \delta_3 &= -(w)_{r=a} & F_3 &= (Q)_{r=a} \\
 \delta_4 &= -\left(\frac{dw}{dr}\right)_{r=a} & F_4 &= (M)_{r=a}
 \end{aligned}
 \tag{3.52a} \tag{3.52b}$$

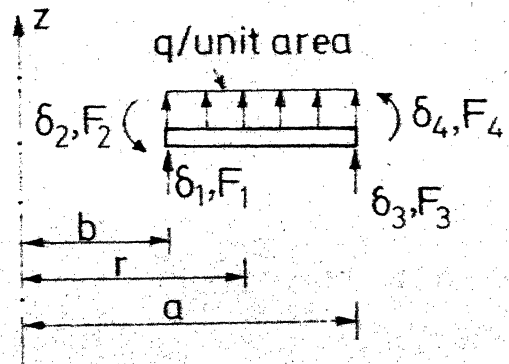
where F_1, F_3 are radial shear/unit circumference

F_2, F_4 are radial moments/unit circumference.

Considering the annular plate subjected to a distributed load

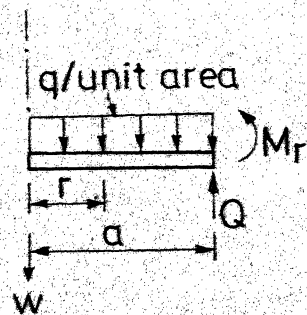


Classical theory

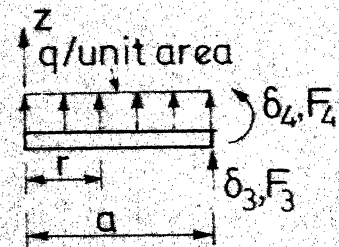


Finite element

a. Axisymmetric plate element



Classical theory



Finite element

b. Axisymmetric closure element

FIG. 3.6 CO-ORDINATE SYSTEMS, AXISYMMETRIC THIN PLATE ELEMENT

q /unit area, the radial shear at inner periphery being C_1 , shear at any radius r is given by the following expression (Fig. 3.6a),

$$Q = \frac{C_1 b}{r} + \frac{q}{2r} (r^2 - b^2) \quad (3.53)$$

The differential equation of bending of circular plate is given by (96)

$$\frac{d}{dr} \left[\frac{1}{r} \frac{d}{dr} \left(r \frac{dw}{dr} \right) \right] = \frac{Q}{D} \quad (3.54)$$

The solution for w can be written as,

$$w = \frac{C_1 b}{4D} r^2 (\log \frac{r}{a} - 1) - \frac{C_2 r^2}{4} - C_3 \log \frac{r}{a} + C_4 + \frac{q}{2D} \left[\frac{r^4}{32} - \frac{b^2 r^2}{4} (\log \frac{r}{a} - 1) \right] \quad (3.55)$$

Differentiating w ,

$$\frac{dw}{dr} = \frac{C_1 b}{4D} r (2 \log \frac{r}{a} - 1) - \frac{C_2 r}{2} - \frac{C_3}{r} + C_4(0) + \frac{q}{2D} \left[\frac{r^3}{8} - \frac{b^2 r}{4} (2 \log \frac{r}{a} - 1) \right] \quad (3.56)$$

$$\frac{d^2 w}{dr^2} = \frac{C_1 b}{4D} (2 \log \frac{r}{a} + 1) - \frac{C_2}{2} + \frac{C_3}{r^2} + C_4(0) + \frac{q}{2D} \left[\frac{3r^2}{8} - \frac{b^2}{4} (2 \log \frac{r}{a} + 1) \right] \quad (3.57)$$

Defining

$$\delta_1 = (-w)_{r=b}, \quad q = -q$$

$$\delta_1 = \frac{b^3}{4D} (1 - \log \frac{b}{a}) C_1 + \frac{b^2}{4} C_2 + \log \frac{b}{a} C_3 - C_4 - \frac{q}{2D} \left[\frac{b^4}{32} - \frac{b^4}{4} (\log \frac{b}{a} - 1) \right] \quad (3.58a)$$

$$\delta_2 = - \left(\frac{dw}{dr} \right)_{r=b}, \quad q = -q$$

$$\delta_2 = \frac{b^2}{4D} (1 - 2 \log \frac{b}{a}) c_1 + \frac{b}{2} c_2 + \frac{1}{b} c_3 + (0) c_4 - \frac{q}{2D} \left[\frac{b^3}{8} - \frac{b^3}{4} (2 \log \frac{b}{a} - 1) \right] \quad (3.58b)$$

$$\delta_3 = -(w)_{r=a}, \quad q = -q$$

$$\delta_3 = \frac{ba^2}{4D} c_1 + \frac{a^2}{4} c_2 + (0) c_3 - c_4 - \frac{q}{2D} \left(\frac{a^4}{32} + \frac{a^2 b^2}{4} \right) \quad (3.58c)$$

$$\delta_4 = - \left(\frac{dw}{dr} \right)_{r=a}, \quad q = -q$$

$$\delta_4 = \frac{ab}{4D} c_1 + \frac{a}{2} c_2 + \frac{1}{a} c_3 + (0) c_4 - \frac{q}{2D} \left(\frac{a^3}{8} + \frac{ab^2}{4} \right) \quad (3.58d)$$

The above can be written as

$$[R] \{C\} = \{\delta\} + \{e\} \quad (3.59a)$$

where

$$[R] = \begin{bmatrix} \frac{b^3}{4D} (1 - \log \frac{b}{a}) & \frac{b^2}{4} & \log \frac{b}{a} & -1 \\ \frac{b^2}{4D} (1 - 2 \log \frac{b}{a}) & \frac{b}{2} & \frac{1}{b} & 0 \\ \frac{a^2 b}{4D} & \frac{a^2}{4} & 0 & -1 \\ \frac{ab}{4D} & \frac{a}{2} & \frac{1}{a} & 0 \end{bmatrix} \quad (3.59b)$$

$$D = \frac{Et^3}{12(1-\nu^2)} \quad (3.59c)$$

where D = flexural rigidity of the plate

t = thickness of the plate.

$$\{C\}^T = [c_1 \quad c_2 \quad c_3 \quad c_4] \quad (3.59d)$$

$$\{\delta\}^T = [\delta_1 \quad \delta_2 \quad \delta_3 \quad \delta_4] \quad (3.59e)$$

$$\{e\} = \frac{q}{2D} \left\{ \begin{array}{l} \frac{b^4}{32} - \frac{b^4}{4} (\log \frac{b}{a} - 1) \\ \frac{b^3}{8} - \frac{b^3}{4} (2 \log \frac{b}{a} - 1) \\ \frac{a^4}{32} + \frac{a^2 b^2}{4} \\ \frac{a^3}{8} + \frac{a b^2}{4} \end{array} \right\} \quad (3.59f)$$

From eqn. (3.59a),

$$\{C\} = [R]^{-1} (\{\delta\} + \{e\}) \quad (3.60)$$

The equivalent load vector for the element can be obtained as negative of the fixed end forces for the element. For fixed end condition, denoting the constant vector by $\{C^0\}$

$$\{C^0\} = [R]^{-1} \{e\} \quad (3.61)$$

For nodal loads only

$$\{C\} = [R]^{-1} \{\delta\} \quad (3.62)$$

The expressions for Q_r , M_r , M_t in classical plate theory are,

$$Q_r = \frac{C_1 b}{r} + \frac{q}{2r} (r^2 - b^2) \quad (3.63)$$

$$M_r = -D \left(\frac{d^2 w}{dr^2} + \frac{\nu}{r} \frac{dw}{dr} \right) \quad (3.64)$$

$$M_t = -D \left(\frac{1}{r} \frac{dw}{dr} + \nu \frac{d^2 w}{dr^2} \right) \quad (3.65)$$

Substitution of eqn. (3.56) and eqn. (3.57) into eqn. (3.64) yields

$$M_r = -\frac{b}{4} \left[2 \log \frac{r}{a} (1+\nu) + (1-\nu) \right] C_1 + \frac{D}{2} (1+\nu) C_2 - \frac{D}{r^2} (1-\nu) C_3 - \frac{q}{2} \left[\frac{r^2}{8} (3+\nu) - \frac{b^2}{2} \log \frac{r}{a} (1+\nu) - \frac{b^2}{4} (1-\nu) \right] \quad (3.66)$$

Substitution of eqns. (3.63) and (3.66) into eqn. (3.52b) yields

$$F_1 = -C_1 \quad (3.67a)$$

$$F_2 = \frac{b}{4} [2(1+v) \log \frac{b}{a} + (1-v)] C_1 - \frac{D}{2} (1+v) C_2 + \frac{D}{b^2} (1-v) C_3 - \frac{q}{2} \left[\frac{b^2}{8} (3+v) - \frac{b^2}{2} \log \frac{b}{a} (1+v) - \frac{b^2}{4} (1-v) \right] \quad (3.67b)$$

$$F_3 = \frac{b}{a} C_1 - \frac{q}{2a} (a^2 - b^2) \quad (3.67c)$$

$$F_4 = -\frac{b}{4} (1-v) C_1 + \frac{D}{2} (1+v) C_2 - \frac{D}{a^2} (1-v) C_3 + \frac{q}{2} \left[\frac{a^2}{8} (3+v) - \frac{b^2}{4} (1-v) \right] \quad (3.67d)$$

The above eqns. (3.67a) to (3.67d) can be written as

$$[S] \{C\} = \{F\} + \{g\} \quad (3.68a)$$

where

$$\{F\}^T = [F_1 \ F_2 \ F_3 \ F_4] \quad (3.68b)$$

$$[S] = \begin{bmatrix} -1 & 0 & 0 & 0 \\ \frac{b}{4} [2(1+v) \log \frac{b}{a} + (1-v)] & -\frac{D}{2}(1+v) & \frac{D}{b^2}(1-v) & 0 \\ \frac{b}{a} & 0 & 0 & 0 \\ -\frac{b}{4}(1-v) & \frac{D}{2}(1+v) - \frac{D}{a^2}(1-v) & 0 & 0 \end{bmatrix} \quad (3.68c)$$

$$g = \begin{Bmatrix} 0 \\ + \frac{qb^2}{16} (1+3v) + \frac{qb^2}{4} (1+v) \log \frac{b}{a} \\ + \frac{q}{2a} (a^2 - b^2) \\ - \frac{qa^2}{16} (3+v) + \frac{qb^2}{8} (1-v) \end{Bmatrix} \quad (3.68d)$$

For nodal forces only eqn. (3.68a) takes the form

$$[S] \{C\} = \{F\} \quad (3.69)$$

But $\{F\}$ can be expressed as

$$\{F\} = [K] \{\delta\} \quad (3.70)$$

Substituting eqn. (3.60) into eqn. (3.69) the resulting expressions are

$$[S] [R]^{-1} \{\delta\} = [F] \quad (3.71)$$

And from eqn. (3.70)

$$[K] = [S][R]^{-1} \quad (3.72)$$

Equivalent nodal forces due to distributed loads is $-\{F_o\}$ where $\{F_o\}$ is given by

$$\{F_o\} = [K] \{e\} - \{g\} \quad (3.73)$$

Once the nodal displacements are calculated the internal forces can be calculated from

$$\{C\} = [R]^{-1} (\{\delta\} + \{e\})$$

$$[F] = [S] \{C\} - \{g\} \quad (3.74)$$

$(M_t)_{r=b}$ and $(M_t)_{r=a}$ can be separately calculated from substituting the necessary values in eqn. (3.65). If this element is combined with 4 noded axisymmetric ring element, the stiffness matrix and equivalent load vector are to be properly adjusted to get the equivalent quantities for an annular ring element.

ii) Closure Element :

Referring to Fig. 3.6b, the relation between the classical and

$$\{g\} = \begin{Bmatrix} q\pi a^2 \\ -q \frac{\pi a^3}{8} (3+\nu) \end{Bmatrix} \quad (3.81)$$

$$[K] = \begin{bmatrix} 0 & 0 \\ 0 & 2\pi D(1+\nu) \end{bmatrix} \quad (3.82)$$

Equivalent load vector, F can be written as,

$$\{F\} = \begin{Bmatrix} F_3 \\ F_4 \end{Bmatrix} = \begin{Bmatrix} \pi q a^2 \\ -\frac{\pi q a^3}{4} \end{Bmatrix} \quad (3.83)$$

Once the value of $\{\delta\}$ are found, $\{C\}$ can be worked out and internal forces can be calculated using the relation

$$\{F\} = [S] \{C\} - \{g\}$$

3.3.3 Interface Elements :

Discontinuities embedded in a continuous system result mainly from rock joints, faults and interfaces. The physical behaviour of such systems are characterised by slip and debonding along the discontinuity. The term debonding describes the separation of the two blocks of continuum adjacent to the joint surface which were initially in contact. The term slip defines the relative motion along the joint surface.

Goodman et al. (34) developed a simple rectangular two-dimensional joint element with eight degrees of freedom. Zienkiewicz et al. (105) advocated the use of curved isoparametric joint elements with simple non-linear material properties for shear and normal stresses assuming uniform strain in the

thickness direction in connection with analysis of jointed rock systems. Mahtab and Goodman (49) presented the derivation and use of an eight noded joint element which can be used with eight noded three dimensional brick element. Varma et al. (100) derived the stiffness matrix for a four noded axisymmetric joint element. Sharma et al. (88), Buragohain and Shah (12) formulated the method to calculate the six noded curved interface elements. Buragohain and Shah (12) also indicated the method of derivation for a six noded curved axisymmetric isoparametric element which can be used with eight noded axisymmetric continuum element. Ghamboussi et al. (33) derived the four noded element with relative displacement coding. Schafer (85) developed straight bond elements with linear and parabolic variation of slip.

In the following paragraphs the derivation of the four noded interface element which can be used in two dimensional plane strain case is given. The results of the stiffness matrices for six noded interface elements with linear geometry and parabolic variations in displacement, four noded axisymmetric interface element, eight noded axisymmetric interface element with straight geometry and parabolic displacement variation are also included. Six noded elements can be used with straight edged eight noded elements.

a) Four Noded Interface Element for Plane Strain : This element can be combined with a four noded linear quadrilateral

element to simulate interface behaviour. The interface elements is shown in Fig. 3.7b.

The strain vector for a joint element is defined by the relative displacements of the two walls as measured at the joint centre. The relative displacements at a and b are given by

$$\Delta a = \begin{Bmatrix} \Delta u_a \\ \Delta v_a \end{Bmatrix} = \begin{Bmatrix} u_4 - u_1 \\ v_4 - v_1 \end{Bmatrix} = \begin{bmatrix} -1 & 0 & 1 & 0 \\ 0 & -1 & 0 & 1 \end{bmatrix} \begin{Bmatrix} u_1 \\ v_1 \\ u_4 \\ v_4 \end{Bmatrix} \quad (3.84a)$$

$$\Delta b = \begin{Bmatrix} \Delta u_b \\ \Delta v_b \end{Bmatrix} = \begin{Bmatrix} u_3 - u_2 \\ v_3 - v_2 \end{Bmatrix} = \begin{bmatrix} -1 & 0 & 1 & 0 \\ 0 & -1 & 0 & 1 \end{bmatrix} \begin{Bmatrix} u_2 \\ v_2 \\ u_3 \\ v_3 \end{Bmatrix} \quad (3.83b)$$

$$\begin{Bmatrix} \Delta u_a \\ \Delta v_a \\ \Delta u_b \\ \Delta v_b \end{Bmatrix} = \begin{bmatrix} -1 & 0 & 0 & 0 & 0 & 0 & 1 & 0 \\ 0 & -1 & 0 & 0 & 0 & 0 & 0 & 1 \\ 0 & 0 & -1 & 0 & 1 & 0 & 0 & 0 \\ 0 & 0 & 0 & -1 & 0 & 1 & 0 & 0 \end{bmatrix} \begin{Bmatrix} u_1 \\ v_1 \\ u_2 \\ v_2 \\ u_3 \\ v_3 \\ u_4 \\ v_4 \end{Bmatrix} \quad (3.85)$$

The above equation can be recognised as,

$$\{\Delta\} = [T] \{a\} \quad (3.86)$$

$$\Delta u = N_a \Delta u_a + N_b \Delta u_b \quad (3.87a)$$

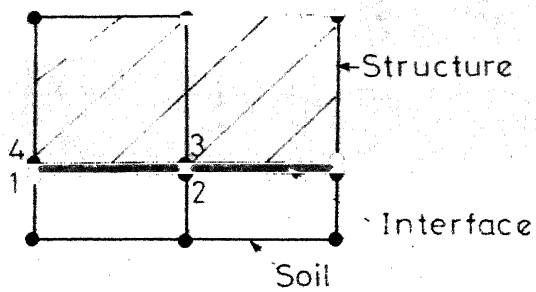
$$\Delta v = N_a \Delta v_a + N_b \Delta v_b \quad (3.87b)$$

$$\text{where } N_a = \frac{1}{2} (1-s) \quad (3.87c)$$

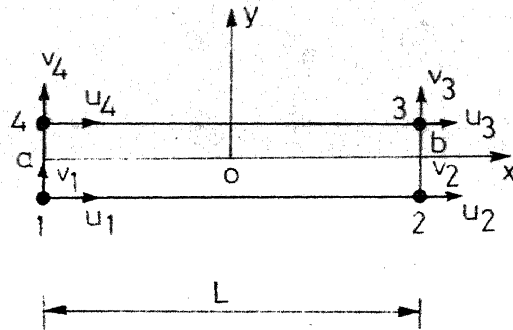
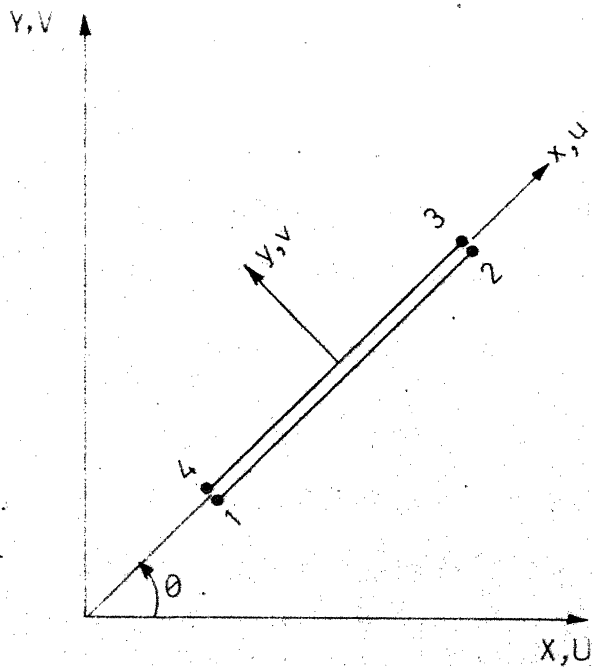
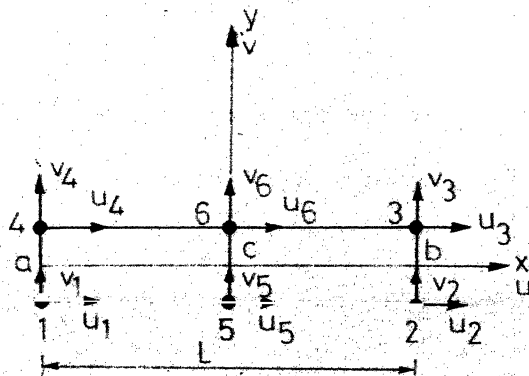
$$N_b = \frac{1}{2} (1+s) \quad (3.87d)$$

i.e.

$$\begin{Bmatrix} \Delta u \\ \Delta v \end{Bmatrix} = \begin{bmatrix} N_a & 0 & N_b & 0 \\ 0 & N_a & 0 & N_b \end{bmatrix} [T] \{a\} \quad (3.87e)$$



a. Soil-structure interface

b. Finite element representation,
local co-ordinates
4 noded elementc. Element in global
co-ordinate systemd. Finite element representation
local co-ordinates
6 noded elementFIG.3-7 FOUR NODED AND SIX NODED INTERFACE ELEMENTS
FOR TWO DIMENSIONAL ANALYSIS

$$\begin{Bmatrix} \Delta u \\ \Delta v \end{Bmatrix} = \begin{bmatrix} -N_a & 0 & -N_b & 0 & N_b & 0 & N_a & 0 \\ 0 & -N_a & 0 & -N_b & 0 & N_b & 0 & N_a \end{bmatrix} \{a\} \quad (3.87f)$$

Symbolically, eqn. (3.87f) can be expressed as

$$\{u\} = [B] \{a\} \quad (3.87g)$$

where $\{u\}$ is the relative displacement vector.

Defining

$$\{P\} = \begin{Bmatrix} P_s \\ P_n \end{Bmatrix} \quad (3.88a)$$

where $\{P\}$ = vector of forces/unit length along the joint element.

Vector $\{P\}$ may be expressed as the product of unit joint stiffness matrix and relative displacements as

$$\{P\} = [D] \{u\} \quad (3.88b)$$

where $[D]$ is a diagonal material property matrix, expressing the joint stiffness/unit length in the normal and tangential direction and can be written as

$$[D] = \begin{bmatrix} K_s & 0 \\ 0 & K_n \end{bmatrix} \quad (3.88c)$$

In eqn. (3.88c), K_s , K_n are shearing and normal material properties at interface.

The stiffness matrix of the interface element of length can be written as

$$[K] = \frac{L}{2} \int_{-1}^{+1} B^T D B \, ds \quad (3.89a)$$

Carrying out the integration, the stiffness matrix of the element in local co-ordinates is obtained as

$$[K] = \frac{L}{6} \begin{bmatrix} 2K_s & 0 & K_s & 0 & -K_s & 0 & -2K_s & 0 \\ & 2K_n & 0 & K_n & 0 & -K_n & 0 & -2K_n \\ & & 2K_s & 0 & -2K_s & 0 & -K_s & 0 \\ & & & 2K_n & 0 & -2K_n & 0 & -K_n \\ & & & & 2K_s & 0 & K_s & 0 \\ & & & & & 2K_n & 0 & K_n \\ & & & & & & 2K_s & 0 \\ & & & & & & & 2K_n \end{bmatrix} \quad (3.89b)$$

(Symmetrical)

If the local co-ordinates (x,y) and the global co-ordinates (X,Y) do not coincide transformation is needed before assembly (Fig. 3.7c). Once the nodal displacements are found out nodal force values can be worked out at element level from,

$$\{F\} = [K] \{a\} \quad (3.90)$$

where F is the nodal force vector.

b) Six Noded Interface Element for Plane Strain : This element has a straight geometry and quadratic variation of displacement. This element can be used with straight edged 8 noded quadrilateral element to simulate interface behaviour. (Fig. 3.7d). The relative displacements in u,v directions at a,b and c can be expressed as,

$$\Delta a = \begin{Bmatrix} \Delta u_a \\ \Delta v_a \end{Bmatrix} = \begin{Bmatrix} u_4 - u_1 \\ v_4 - v_1 \end{Bmatrix} \quad (3.91a)$$

$$\Delta b = \begin{Bmatrix} \Delta u_b \\ \Delta v_b \end{Bmatrix} = \begin{Bmatrix} u_3 - u_2 \\ v_3 - v_2 \end{Bmatrix} \quad (3.91b)$$

$$\Delta c = \begin{Bmatrix} \Delta u_c \\ \Delta v_c \end{Bmatrix} = \begin{Bmatrix} u_6 - u_5 \\ v_6 - v_5 \end{Bmatrix} \quad (3.91c)$$

$$\{\Delta\} = [T] \{a\} \quad (3.92a)$$

where

$$\{\Delta\}^T = [\Delta u_a \quad \Delta v_a \quad \Delta u_b \quad \Delta v_b \quad \Delta u_c \quad \Delta v_c] \quad (3.92b)$$

$$\{a\}^T = [\Delta u_1 \quad v_1 \quad u_2 \quad v_2 \quad u_3 \quad v_3 \quad u_4 \quad v_4 \quad u_5 \quad v_5 \quad u_6 \quad v_6] \quad (3.92c)$$

$$\Delta u = N_a \Delta u_a + N_b \Delta u_b + N_c \Delta u_c \quad (3.93a)$$

$$\Delta v = N_a \Delta v_a + N_b \Delta v_b + N_c \Delta v_c \quad (3.93b)$$

$$\text{where } N_a = \frac{1}{2} s(s - 1) \quad (3.93c)$$

$$N_b = \frac{1}{2} s(s + 1) \quad (3.93d)$$

$$N_c = (1 - s^2) \quad (3.93e)$$

Following the same steps as for 4 noded element in developing matrix B and carrying out the necessary integration, the 12x12 stiffness matrix is obtained as given in eqn. (3.94).

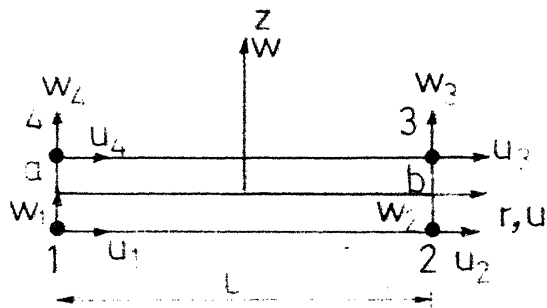
c) Four Noded Axisymmetric Interface Ring Element : This element has 8 degrees of freedom and can be combined with the 4 noded isoparametric axisymmetric ring element (Fig. 3.8a). The relative displacement vector at a and b are given by,

(3.94)

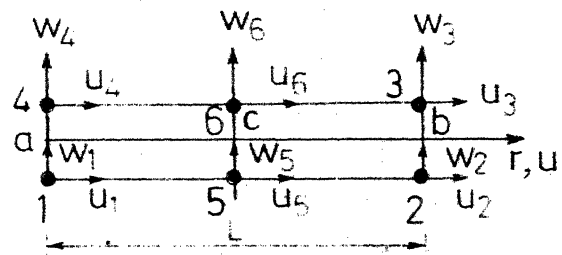
$$[K] = \frac{1}{30}$$

(Symmetrical)

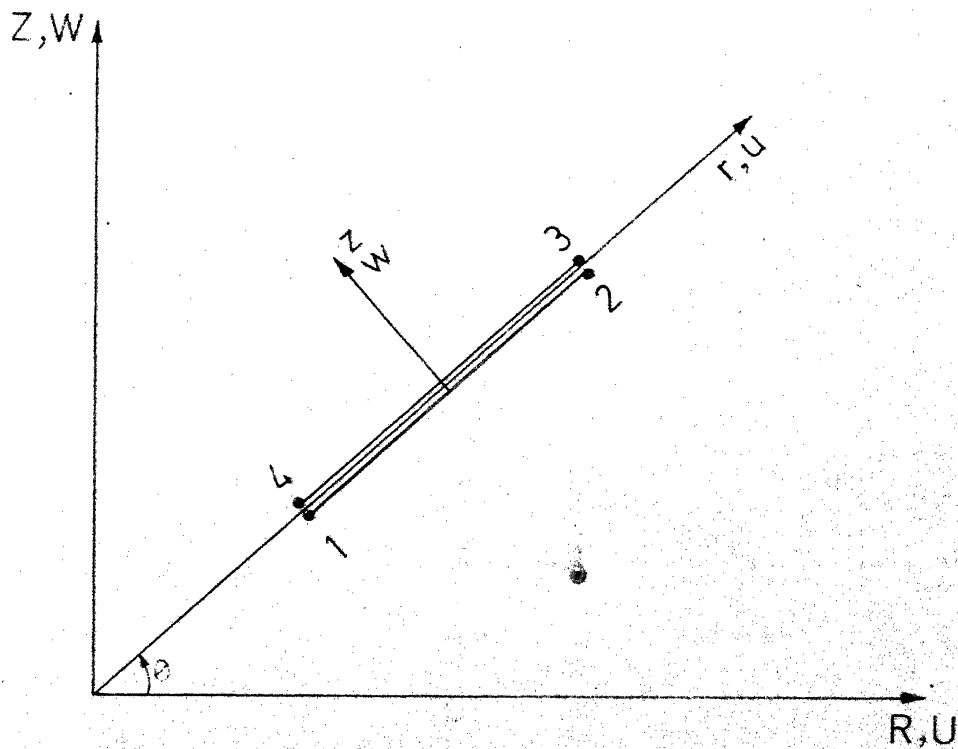
$$\begin{bmatrix} 4K_s & 0 & -K_s & 0 & K_s & 0 & -4K_s & 0 & 2K_s & 0 & -2K_s & 0 \\ 0 & 4K_n & 0 & -K_n & 0 & K_n & 0 & -4K_n & 0 & 2K_n & 0 & -2K_n \\ 4K_n & 0 & 0 & -K_n & 0 & K_n & 0 & -4K_n & 0 & 2K_n & 0 & -2K_n \\ 0 & -K_n & 0 & 4K_n & 0 & -4K_n & 0 & K_n & 0 & -2K_n & 0 & 2K_n \\ K_s & 0 & -4K_s & 0 & 4K_s & 0 & -K_s & 0 & -2K_s & 0 & 2K_s & 0 \\ 0 & 4K_n & 0 & -4K_n & 0 & 4K_n & 0 & -K_n & 0 & -2K_n & 0 & 2K_n \\ -4K_s & 0 & 4K_s & 0 & -K_s & 0 & 4K_s & 0 & -2K_s & 0 & 2K_s & 0 \\ 0 & -4K_n & 0 & 4K_n & 0 & -4K_n & 0 & K_n & 0 & -2K_n & 0 & 2K_n \\ 2K_s & 0 & -2K_s & 0 & -2K_s & 0 & 16K_s & 0 & 16K_s & 0 & -16K_s & 0 \\ 0 & 2K_n & 0 & -2K_n & 0 & -2K_n & 0 & 4K_n & 0 & -2K_n & 0 & 2K_n \\ -2K_s & 0 & 16K_s & 0 & 16K_s & 0 & -16K_s & 0 & 16K_s & 0 & -16K_s & 0 \\ 0 & -16K_n & 0 & 16K_n & 0 & 16K_n & 0 & -16K_n & 0 & 16K_n & 0 & -16K_n \\ 16K_n & 0 & 16K_n & 0 & 16K_n & 0 & 16K_n & 0 & 16K_n & 0 & 16K_n & 0 \end{bmatrix}$$



a. 4 Noded axisymmetric ring element,
Local co-ordinates



b. 6 Noded axisymmetric ring element,
Local co-ordinates



c. 4 Noded element in global co-ordinate system

FIG.38 FOUR NODED AND SIX NODED INTERFACE RING ELEMENTS FOR AXISYMMETRIC ANALYSIS

$$\Delta a = \begin{Bmatrix} \Delta u_a \\ \Delta w_a \end{Bmatrix} = \begin{Bmatrix} u_4 - u_1 \\ w_4 - w_1 \end{Bmatrix} = \begin{bmatrix} -1 & 0 & 1 & 0 \\ 0 & -1 & 0 & 1 \end{bmatrix} \begin{Bmatrix} u_1 \\ w_1 \\ u_2 \\ w_2 \end{Bmatrix} \quad (3.95a)$$

$$\Delta b = \begin{Bmatrix} u_b \\ v_b \end{Bmatrix} = \begin{Bmatrix} u_3 - u_2 \\ w_3 - w_2 \end{Bmatrix} = \begin{bmatrix} -1 & 0 & 1 & 0 \\ 0 & -1 & 0 & 1 \end{bmatrix} \begin{Bmatrix} u_1 \\ w_1 \\ u_2 \\ w_2 \end{Bmatrix} \quad (3.95b)$$

$$\begin{Bmatrix} \Delta u_a \\ \Delta w_a \\ \Delta u_b \\ \Delta w_b \end{Bmatrix} = \begin{bmatrix} -1 & 0 & 0 & 0 & 0 & 0 & 1 & 0 \\ 0 & -1 & 0 & 0 & 0 & 0 & 0 & 1 \\ 0 & 0 & -1 & 0 & 1 & 0 & 0 & 0 \\ 0 & 0 & 0 & -1 & 0 & 1 & 0 & 0 \end{bmatrix} \begin{Bmatrix} u_1 \\ w_1 \\ u_2 \\ w_2 \\ u_3 \\ w_3 \\ u_4 \\ w_4 \end{Bmatrix} \quad (3.95c)$$

which can be recognised as,

$$\{\Delta\} = [T] \{a\} \quad (3.96)$$

where

$$\{a\}^T = [u_1 \ w_1 \ u_2 \ w_2 \ u_3 \ w_3 \ u_4 \ w_4] \quad (3.96b)$$

$$\begin{Bmatrix} \Delta u \\ \Delta w \end{Bmatrix} = \begin{bmatrix} -N_a & 0 & -N_b & 0 & N_b & 0 & N_a & 0 \\ 0 & -N_a & 0 & -N_b & 0 & N_b & 0 & N_a \end{bmatrix} \{a\} \quad (3.97a)$$

where

$$N_a = \frac{1}{2}(1 - s) \quad (3.97b)$$

$$N_b = \frac{1}{2}(1 + s) \quad (3.97c)$$

$$[K] = 2\pi \frac{L}{2} \int B^T D B r \, ds \quad (3.98a)$$

$$\text{where } r = N_a r_1 + N_b r_2$$

By substituting for r from eqn. (3.98b) and carrying out the integration, stiffness matrix K is obtained as given in eqn. (3.98c).

$$[K] = \frac{\pi L}{6} \begin{bmatrix} K_s C_1 & 0 & K_s C_2 & 0 & -K_s C_2 & 0 & -K_s C_1 & 0 \\ & K_n C_1 & 0 & K_n C_2 & 0 & -K_n C_2 & 0 & -K_n C_1 \\ & & K_s C_3 & 0 & -K_s C_3 & 0 & -K_s C_2 & 0 \\ & & & K_n C_3 & 0 & -K_n C_3 & 0 & -K_n C_2 \\ & & & & K_s C_3 & 0 & K_s C_2 & 0 \\ & & & & & K_n C_3 & 0 & K_n C_2 \\ & & & & & & K_s C_1 & 0 \\ & & & & & & & K_n C_1 \end{bmatrix}$$

(Symmetrical)

(3.98c)

where

$$C_1 = (3r_1 + r_2) ; C_2 = (r_1 + r_2) \text{ and } C_3 = (r_1 + 3r_2).$$

d) Six Noded Axisymmetric Interface Ring Element : The element has a straight geometry and quadratic variation of displacement. This element can be used with straight edged 8 noded quadrilateral ring element to model interface behaviour. The element has 12 degrees of freedom (Fig. 3.8b). The relative displacements in u and w direction at a, b and c are :

$$\Delta a = \begin{Bmatrix} \Delta u_a \\ \Delta w_a \end{Bmatrix} = \begin{Bmatrix} u_4 - u_1 \\ w_4 - w_1 \end{Bmatrix} \quad (3.99a)$$

$$\Delta b = \begin{Bmatrix} \Delta u_b \\ \Delta w_b \end{Bmatrix} = \begin{Bmatrix} u_3 - u_2 \\ w_3 - w_2 \end{Bmatrix} \quad (3.99b)$$

$$\Delta c = \begin{Bmatrix} \Delta u_c \\ \Delta w_c \end{Bmatrix} = \begin{Bmatrix} u_6 - u_5 \\ w_6 - w_5 \end{Bmatrix} \quad (3.99c)$$

$$\{\Delta\} = [T] \{a\} \quad (3.100a)$$

$$\text{where } \{\Delta\}^T = [u_a \quad w_a \quad u_b \quad w_b \quad u_c \quad w_c] \quad (3.100b)$$

$$\{a\}^T = [u_1 \quad w_1 \quad u_2 \quad w_2 \quad u_3 \quad w_3 \quad u_4 \quad w_4 \quad u_5 \quad w_5 \quad u_6 \quad w_6] \quad (3.100c)$$

$$\Delta u = N_a \Delta u_a + N_b \Delta u_b + N_c \Delta u_c \quad (3.101a)$$

$$\Delta w = N_a \Delta w_a + N_b \Delta w_b + N_c \Delta w_c \quad (3.101b)$$

$$N_a = \frac{1}{2} s(s - 1) \quad (3.101c)$$

$$N_b = \frac{1}{2} s(s + 1) \quad (3.101d)$$

$$N_c = (1 - s^2) \quad (3.101e)$$

$$[K] = 2\pi \frac{L}{2} B \{B^T D B r ds \quad (3.102a)$$

$$\text{where } r = N_a r_1 + N_b r_2 \quad (3.102b)$$

By substituting r from eqn. (3.102b) and carrying out the integration, the stiffness matrix in local co-ordinates is obtained as given in eqn. (3.102c).

3.4 Elasto-Plastic Analysis :

The differences in elastic and plastic behaviour under uniaxial stress is clearly brought out in Fig. 3.9. In non-linear elastic formulations, the stress can be expressed as a function of strain as $\sigma = \sigma(\epsilon)$. The main difference of plasticity formulation from non-linear elastic formulation is, such an explicit relationship is not available. Although the stresses at any level of strain have to lie on or within the current yield surface, the exact value of each component cannot be determined. The common computational approaches used with incremental theory

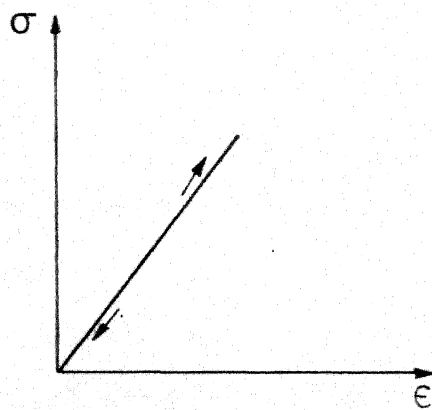
$$[K] = \frac{\pi L}{30}$$

$$\begin{bmatrix} K_s B_4 & 0 & -K_s B_3 & 0 & K_s B_3 & 0 & -K_s B_4 & 0 & K_s B_1 & 0 & -K_s B_1 & 0 \\ K_n B_4 & K_n B_4 & 0 & -K_n B_3 & 0 & K_n B_3 & 0 & -K_n B_4 & 0 & K_n B_1 & 0 & -K_n B_1 \\ K_s B_5 & 0 & -K_s B_5 & 0 & K_s B_5 & 0 & K_s B_3 & 0 & K_s B_2 & 0 & -K_s B_2 & 0 \\ K_n B_5 & K_n B_5 & 0 & -K_n B_5 & 0 & K_n B_3 & 0 & K_n B_3 & 0 & K_n B_2 & 0 & -K_n B_2 \\ K_s B_5 & 0 & K_s B_5 & 0 & -K_s B_3 & 0 & -K_s B_3 & 0 & -K_s B_2 & 0 & K_s B_2 & 0 \\ K_n B_5 & 0 & K_n B_5 & 0 & -K_n B_3 & 0 & -K_n B_3 & 0 & -K_n B_2 & 0 & K_n B_2 & 0 \\ K_s B_4 & 0 & K_s B_4 & 0 & -K_s B_1 & 0 & -K_s B_1 & 0 & K_s B_1 & 0 & K_n B_1 & 0 \\ K_n B_4 & K_n B_4 & 0 & K_n B_4 & 0 & K_n B_4 & 0 & K_n B_4 & 0 & K_n B_1 & 0 & K_n B_1 \\ K_s B_6 & 0 & -K_s B_6 & 0 & K_s B_6 & 0 & K_s B_6 & 0 & -K_s B_6 & 0 & -K_s B_6 & 0 \\ K_n B_6 & 0 & K_n B_6 & 0 & K_n B_6 & 0 & K_n B_6 & 0 & K_n B_6 & 0 & K_n B_6 & 0 \end{bmatrix} \quad (3.102c)$$

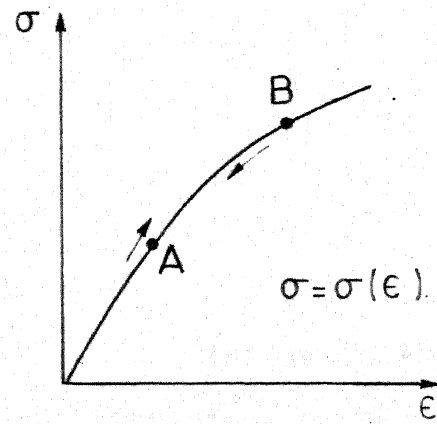
Symmetrical

where $B_1 = 4r_1$; $B_2 = 4r_2$; $B_3 = (r_1 + r_2)$; $B_4 = (7r_1 + r_2)$; $B_5 = (r_1 + 7r_2)$ and

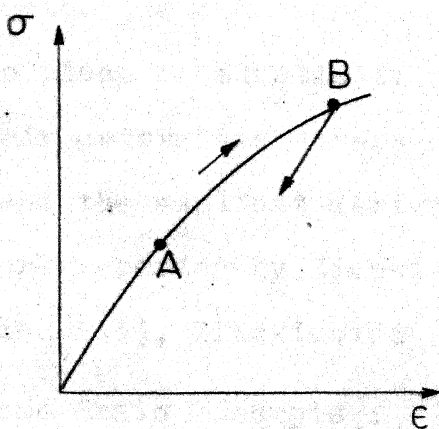
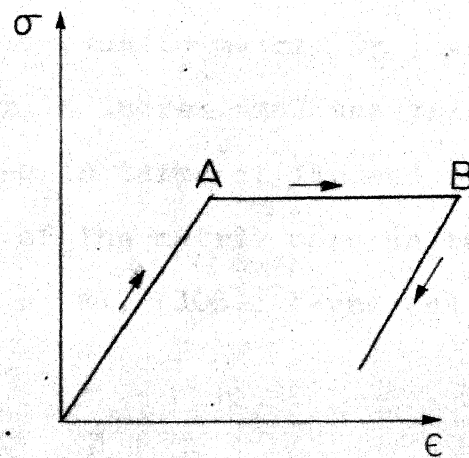
$$B_6 = 16(r_1 + r_2).$$



a. Linear elastic



b. Non-linear elastic

c. Strain hardening
plasticity

d. Ideal plasticity

FIG-3-9 UNIAXIAL BEHAVIOUR

of plasticity in finite element method are : (i) incremental tangent stiffness approach, (ii)'initial strain'method, and (iii)'initial stress'method (24,94). In the first method the change of material constitutive matrix forming element stiffness, assembling and inverting an overall stiffness matrix for each step of analysis is to be carried out. In 'initial strain' and the 'initial stress' approaches, in all iterations a simple resolution of constant linear elastic problem is carried out. The 'initial stress' method is suitable for solution of ideal plasticity or for strain hardening formulations.

The important part of plasticity formulations in finite element method is obtaining an elasto-plastic matrix D_{ep}^* , which takes the place of elasticity matrix in incremental analysis. This matrix determines stress changes in terms of imposed strain changes and the explicit derivation of the matrix used is based on the work reported by Zienkiewicz et al. (108), Nayak and Zienkiewicz (63), Zienkiewicz (104).

3.4.1 Some Basic Concepts :

a) Yield Surface : Yielding can occur only if stresses σ , satisfy the general yield criterion,

$$F(\sigma, \kappa) = 0 \quad (3.103)$$

where κ is a hardening parameter. This yield condition can be visualised as a surface in n-dimensional stress space with the position of the surface dependent on the current value of .

The equation $F = 0$ represents a closed surface in the stress space. The yielding is characterised as follows :

$F < 0$, no change in plastic deformation occurs,

$F = 0$, change in plastic deformation takes place.

For the case of perfectly plastic material, the yield function depends solely on the state of stress. For two-dimensional case the meaning of eqn. (3.103) can be visualised by Fig. 3.10a. For a stress point moving from B to C and D to E the behaviour is elastic, whereas it is plastic for a stress point remaining at A or moving from A to F.

b) Flow Rule (Normality Principle) : If $d\varepsilon_p$ denotes the increment of plastic strain, then

$$d\varepsilon_p = \lambda \frac{\partial F}{\partial \sigma} \quad (3.104a)$$

or for any component, n

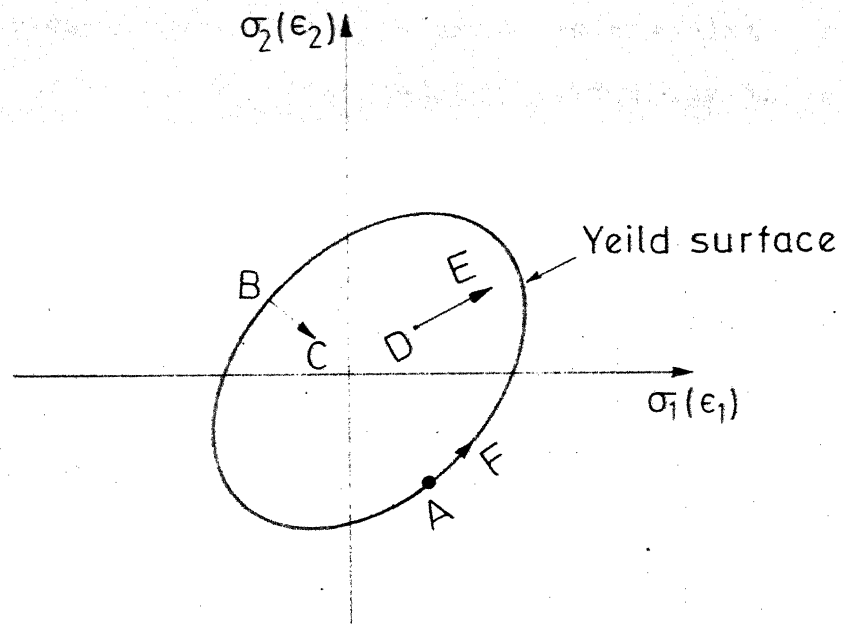
$$d\varepsilon_{n,p} = \lambda \frac{\partial F}{\partial \sigma_n} \quad (3.104b)$$

where λ is a proportionality constant. The above relation can be interpreted as requiring normality of plastic strain increment vector to the yield surface in the space of n stress dimensions. A reduction of restriction of the above rule can be made by specifying the plastic potential.

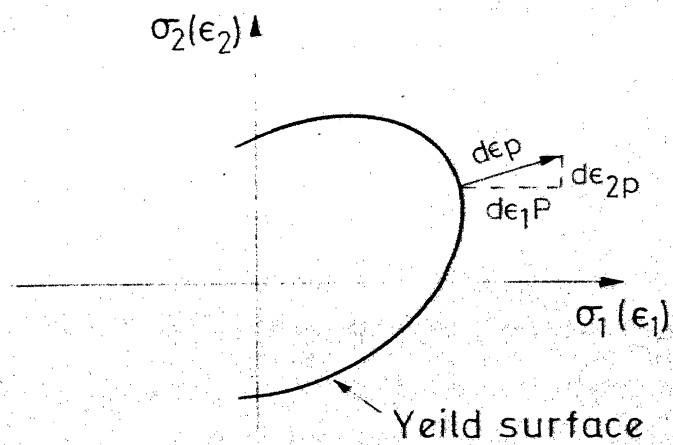
$$Q = Q(\sigma, \kappa) \quad (3.105)$$

If $d\varepsilon_p$ denotes the increment of plastic strain,

$$d\varepsilon_p = \lambda \frac{\partial Q}{\partial \sigma} \quad (3.106)$$



a. Yield surface



b. Normality principle in two dimensions

FIG. 3.10 YIELD SURFACE AND NORMALITY CONCEPT

The particular case where $Q = F$ is known as associated plasticity. When this relation is not satisfied, the plasticity is termed non-associated.

3.4.2 Derivation of Elasto-Plastic Matrix :

Changes in strain due to an infinitesimal increment of stress can be separated as elastic and plastic i.e.

$$d\epsilon = d\epsilon_e + d\epsilon_p \quad (3.107a)$$

$$d\epsilon = D^{-1} d\sigma + \frac{\partial Q}{\partial \sigma} \lambda \quad (3.107b)$$

When plastic yielding occurs, the stresses on the yield surface are given by $F(\sigma, \kappa) = 0$. Differentiating F ,

$$dF = \frac{\partial F}{\partial \sigma_1} d\sigma_1 + \frac{\partial F}{\partial \sigma_2} d\sigma_2 + \dots + \frac{\partial F}{\partial \kappa} d\kappa = 0 \quad (3.108)$$

$$\left\{ \frac{\partial F}{\partial \sigma} \right\}^T d\sigma - A \lambda = 0 \quad (3.109a)$$

where

$$A = - \frac{\partial F}{\partial \kappa} d\kappa \quad \frac{1}{\lambda} \quad (3.109b)$$

Equations (3.107b) and (3.109a) can be written in a single symmetric matrix form as

$$\begin{Bmatrix} d\epsilon \\ 0 \end{Bmatrix} = \begin{bmatrix} D^{-1} & \frac{\partial Q}{\partial \sigma} \\ \left(\frac{\partial F}{\partial \sigma} \right)^T & -A \end{bmatrix} \begin{Bmatrix} d\sigma \\ \lambda \end{Bmatrix} \quad (3.110)$$

The indeterminate constant λ can be eliminated, taking care not to multiply or divide by A . The explicit expression for elasto-plastic matrix is,

$$\{d\sigma\} = [D_{ep}^*] \{d\epsilon\} \quad (3.111a)$$

where

$$[D_{ep}^*] = [D] - [D] \left\{ \frac{\partial Q}{\partial \sigma} \right\} \left\{ \frac{\partial F}{\partial \sigma} \right\}^T [D] [A + \left\{ \frac{\partial F}{\partial \sigma} \right\}^T [D] \left\{ \frac{\partial Q}{\partial \sigma} \right\}]^{-1} \quad (3.111b)$$

The above matrix is symmetric only when the plasticity is associated. The derivation of elasto-plastic matrix for ideal plasticity from Von-Mises criterion is straight forward for three-dimensional case with the use of the above equation. For the three dimensional case,

$$\{d\sigma\}^T = [d\sigma_{xx} \ d\sigma_{yy} \ d\sigma_{zz} \ d\tau_{xy} \ d\tau_{yz} \ d\tau_{zx}] \quad (3.112a)$$

$$\{d\epsilon\}^T = [d\epsilon_{xx} \ d\epsilon_{yy} \ d\epsilon_{zz} \ d\gamma_{xy} \ d\gamma_{yz} \ d\gamma_{zx}] \quad (3.112b)$$

Special forms of elasto-plastic matrix needed for axisymmetric, plane stress or plane strain cases can be derived by following the procedure suggested by Zienkiewicz et al. (108). For axisymmetric case,

$$\{d\sigma\}^T = [d\sigma_{rr} \ d\sigma_{\theta\theta} \ d\sigma_{zz} \ d\tau_{rz}] \quad (3.113a)$$

$$\{d\epsilon\}^T = [d\epsilon_{rr} \ d\epsilon_{\theta\theta} \ d\epsilon_{zz} \ d\gamma_{rz}] \quad (3.113b)$$

and for plane strain :

$$\{d\sigma\}^T = [d\sigma_{xx} \ d\sigma_{yy} \ d\sigma_{zz} \ d\tau_{xy}] \quad (3.114a)$$

$$\{d\epsilon\}^T = [d\epsilon_{xx} \ d\epsilon_{yy} \ 0 \ d\gamma_{xy}] \quad (3.114b)$$

The explicit form of the elasto-plastic matrices for Von-Mises criterion using eqn. (3.111b) are derived for three-dimensional, axisymmetric and plane strain cases. They are given in eqns. (3.115), (3.116) and (3.117) respectively.

$$\begin{bmatrix}
 (1-\nu) - Ms_x^2 & \nu - Ms_x s_y & \nu - Ms_x s_z & -Ms_x \tau_{xy} & -Ms_x \tau_{yz} & -Ms_x \tau_{zx} \\
 (1-\nu) - Ms_y^2 & (1-\nu) - Ms_y^2 & \nu - Ms_y s_z & -Ms_y \tau_{xy} & -Ms_y \tau_{yz} & -Ms_y \tau_{zx} \\
 (1-\nu) - Ms_z^2 & (1-\nu) - Ms_z^2 & (1-\nu) - Ms_z^2 & -Ms_z \tau_{xy} & -Ms_z \tau_{yz} & -Ms_z \tau_{zx} \\
 \frac{1-2\nu}{2} - M\tau_{xy}^2 & \frac{1-2\nu}{2} - M\tau_{xy}^2 & \frac{1-2\nu}{2} - M\tau_{xy}^2 & -M\tau_{xy} \tau_{yz} & -M\tau_{xy} \tau_{zx} & -M\tau_{xy} \tau_{zx} \\
 \frac{1-2\nu}{2} - M\tau_{yz}^2 & \frac{1-2\nu}{2} - M\tau_{yz}^2 & \frac{1-2\nu}{2} - M\tau_{yz}^2 & -M\tau_{yz} \tau_{zx} & -M\tau_{yz} \tau_{zx} & -M\tau_{yz} \tau_{zx} \\
 \frac{1-2\nu}{2} - M\tau_{zx}^2 & \frac{1-2\nu}{2} - M\tau_{zx}^2 & \frac{1-2\nu}{2} - M\tau_{zx}^2 & -M\tau_{zx} \tau_{xy} & -M\tau_{zx} \tau_{yz} & -M\tau_{zx} \tau_{yz}
 \end{bmatrix}$$

$$D_{ep}^* = \frac{E}{(1+\nu)(1-2\nu)}$$

(Symmetrical)

$$\text{where } M = \frac{1-2\nu}{2\sigma}$$

(3.115)

$$[D_{ep}^*] = \frac{E}{(1+\nu)(1-2\nu)} \quad (3.116)$$

$$\text{where } M = \frac{1-2\nu}{2\sigma}$$

$$s_r = \sigma_r - \sigma_m, \quad s_\theta = \sigma_\theta - \sigma_m, \quad s_z = \sigma_z - \sigma_m$$

$$\begin{bmatrix} (1-\nu) - Ms_r & \nu - Ms_r s_\theta & \nu - Ms_z r \\ (1-\nu) - Ms_\theta^2 & \nu - Ms_\theta s_z & \nu - Ms_z s_r \\ \text{(Symmetrical)} & (1-\nu) - Ms_z^2 & \nu - Ms_z s_r \end{bmatrix} \begin{bmatrix} -Ms_r \tau_{rz} \\ -Ms_\theta \tau_{rz} \\ -Ms_z \tau_{rz} \\ \frac{1-2\nu}{2} - M\tau_{rz}^2 \end{bmatrix}$$

$$\begin{bmatrix} (1-\nu) - \frac{s_r^2(1-2\nu)}{L_0} & -\frac{(1-2\nu)s_r s_\theta}{L_0} & -\frac{\tau_{xy} s_x(1-2\nu)}{L_0} \\ \frac{s_\theta^2(1-2\nu)}{L_0} & (1-\nu) - \frac{s_\theta^2(1-2\nu)}{L_0} & -\frac{\tau_{xy} s_y(1-2\nu)}{L_0} \\ \text{(Symmetrical)} & (1-\nu) - \frac{s_z^2(1-2\nu)}{L_0} & -\frac{(\frac{1-2\nu}{2}) - \frac{\tau_{xy}^2(1-2\nu)}{L_0}}{L_0} \end{bmatrix} \quad (3.117)$$

$$[D_{ep}^*] = \frac{E}{(1+\nu)(1-2\nu)}$$

$$\text{where } L_0 = s_x^2 + s_y^2 + 2\tau_{xy}^2 - s_z^2(1+2\nu)$$

1
}

For Von-Mises criterion, the derivation of D_{ep}^* from eqn. (3.111b) is straight forward. But the invariants suggested and the method followed below are more elegant (62) for use when yield criteria such as Tresca, Mohr-Coulomb, Drucker-Prager are used. If the yield surface and the material are isotropic, it is convenient to express yield surface in terms of three stress invariants, $\sigma_m, \bar{\sigma}, \theta$.

$$\sigma_m = J_1/3 = \frac{\sigma_x + \sigma_y + \sigma_z}{3} \quad (3.118a)$$

$$\bar{\sigma} = J_2^{1/2} = \left[\frac{1}{2} (s_x^2 + s_y^2 + s_z^2) + \tau_{xy}^2 + \tau_{yz}^2 + \tau_{zx}^2 \right]^{1/2} \quad (3.118b)$$

$$\theta = \frac{1}{3} \sin^{-1} \left[-\frac{3\sqrt{3}}{2} \frac{J_3}{\bar{\sigma}^3} \right] \text{ with } -\frac{\pi}{6} < \theta < \frac{\pi}{6} \quad (3.118c)$$

where

$$J_3 = s_x s_y s_z + 2 \tau_{xy} \tau_{yz} \tau_{zx} - s_x \tau_{yz}^2 - s_y \tau_{zx}^2 - s_z \tau_{xy}^2$$

$$s_x = \sigma_x - \sigma_m, \quad s_y = \sigma_y - \sigma_m, \quad s_z = \sigma_z - \sigma_m$$

In terms of the invariants specified above the yield conditions can be expressed as given by :

a) Von-Mises :

$$F = \sqrt{3} \bar{\sigma} - \sigma_{yield} = 0 \quad (3.119)$$

$$\sigma_{yield} = \text{uniaxial yield stress}$$

b) Tresca :

$$F = 2\bar{\sigma} \cos\theta - \sigma_{yield} = 0 \quad (3.120)$$

c) Mohr-Coulomb :

$$F = \sigma_m \sin\phi + \bar{\sigma} \cos\theta - \frac{\bar{\sigma}}{\sqrt{3}} \sin\phi \sin\theta - C \cos\phi = 0 \quad (3.120)$$

d) Drucker-Prager :

$$F = 3\alpha' \sigma_m + \bar{\sigma} - K_1 = 0 \quad (3.122a)$$

$$\alpha' = \frac{2 \sin \phi}{\sqrt{3}(3 - \sin \phi)} \quad (3.122b)$$

$$K_1 = \frac{6 C \cos \phi}{\sqrt{3}(3 - \sin \phi)} \quad (3.122c)$$

For definition of the gradient vectors $\frac{\partial F}{\partial \sigma}$ or $\frac{\partial Q}{\partial \sigma}$ the above form is more convenient.

$$\left\{ \frac{\partial F}{\partial \sigma} \right\} = \{ a \} \quad (3.123a)$$

$$\{ a \}^T = \left[\frac{\partial F}{\partial \sigma_x} \frac{\partial F}{\partial \sigma_y} \frac{\partial F}{\partial \sigma_z} \frac{\partial F}{\partial \tau_{xy}} \frac{\partial F}{\partial \tau_{yz}} \frac{\partial F}{\partial \tau_{zx}} \right] \quad (3.123b)$$

$$\left\{ \frac{\partial F}{\partial \sigma} \right\} = C_1 \left\{ \frac{\partial \sigma_m}{\partial \sigma} \right\} + C_2 \left\{ \frac{\partial \bar{\sigma}}{\partial \sigma} \right\} + C_3 \left\{ \frac{\partial J_3}{\partial \sigma} \right\} \quad (3.124a)$$

$$\left\{ \frac{\partial \sigma_m}{\partial \sigma} \right\}^T = \frac{1}{3} [1 \ 1 \ 1 \ 0 \ 0 \ 0] \quad (3.124b)$$

$$\left\{ \frac{\partial \bar{\sigma}}{\partial \sigma} \right\}^T = \frac{1}{2 \bar{\sigma}} [s_x \ s_y \ s_z \ 2\tau_{xy} \ 2\tau_{yz} \ 2\tau_{zx}] \quad (3.124c)$$

$$\left\{ \frac{\partial J_3}{\partial \sigma} \right\}^T = [a'_3]^T + \frac{1}{3} \bar{\sigma}^2 [1 \ 1 \ 1 \ 0 \ 0 \ 0] \quad (3.124d)$$

$$\begin{aligned} \{ a'_3 \} = & [(s_y s_z - \tau_{yz}^2) (s_x s_z - \tau_{zx}^2) (s_x s_y - \tau_{xy}^2) \\ & 2(\tau_{yz} \tau_{zx} - s_z \tau_{xy}) 2(\tau_{zx} \tau_{xy} - s_x \tau_{yz}) \\ & 2(\tau_{xy} \tau_{yz} - s_y \tau_{zx})] \end{aligned} \quad (3.124e)$$

C_1, C_2 and C_3 for different yield criteria are given in Table 3.1.

Table 3.1

Invariant Derivatives for Various Yield Conditions

Yield criterion	C_1	C_2	C_3
Von-Mises	0	$\sqrt{3}$	0
Tresca	0	$2 \cos\theta(1+\tan\theta \tan 3\theta)$	$\frac{\sqrt{3}}{2} \frac{\sin\theta}{\cos 3\theta}$
Mohr-Coulomb	$\sin\phi$	$\cos\theta[1+\tan\theta \tan 3\theta + \frac{\sin\phi}{\sqrt{3}}(\tan 3\theta - \tan\theta)]$	$\frac{\sqrt{3}\sin\theta + \cos\theta \sin\phi}{(2\cos^2\theta \cos 3\theta)}$
Drucker-Prager	$3\alpha'$	1.0	0

For many potential or yield surfaces, the vectors $\frac{\partial F}{\partial \sigma}$, $\frac{\partial Q}{\partial \sigma}$ are not uniquely defined at certain stress combinations arising out of corners. The direction of straining at the corners, is indeterminate. In practice it is very rare that difficulties with singularities will arise. To overcome this difficulty in numerical work a check can be introduced using the magnitude of θ , to find whether the stress state is within a prescribed vicinity of a singularity. If the state of stress is within such a limit then $\frac{\partial F}{\partial \sigma}$ or $\frac{\partial Q}{\partial \sigma}$ are evaluated on either side of the singularity and an average value is assumed. The procedure corresponds to a rounding off of singularity corners.

The above general procedure can be used to obtain the elasto-plastic matrix for axisymmetric, plane stress or plane strain cases with proper modifications and selection of necessary stress and strain vectors.

3.4.3 The 'Initial Stress' Computational Method :

In the 'initial stress' method, the solution of the non-linear problem is approached in a series of approximations. During a load increment, a purely elastic problem is solved, determining an increment of strain $\{\Delta\epsilon'\}$ and stress $\{\Delta\sigma'\}$ at every point of the continuum. For the increment of strain found from the analysis, the stress increment in general will not be correct. If $\{\Delta\sigma\}$ is the true increment of stress possible for the given strain then the situation can only be maintained by a set of body forces, equilibrating the initial stress system given by $\{\Delta\sigma'\} - \{\Delta\sigma\}$. At the second stage of the computation, this body force system can be removed by allowing the structure, (with unchanged elastic properties) to deform further. An additional set of strain and corresponding stress increments are caused. Once again these are likely to exceed those permissible by the non-linear relationship and the redistribution of equilibrating body forces has to be repeated. If the process converges then within an increment the full non-linear compatibility and equilibrium conditions will be satisfied. In each cycle, since the same elastic problem is being solved only partial inversion of the elastic equations is needed.

For the elasto-plastic situation, the steps during a typical load increment can be summarised as follows (108) :

1. Increment of load is applied. Elastic increments of

strain $\{\Delta \epsilon'\}_1$ and elastic increments of stress $\{\Delta \sigma'\}_1$ which corresponds are found.

2. $\{\Delta \sigma'\}_1$ is added to stresses existing at start of increment, $\{\sigma_0\}$, to obtain $\{\sigma'\}$. Check whether $F\{\sigma'\} < 0$. If the condition is satisfied only elastic strain changes occur and the process is stopped. If the condition is not satisfied proceed to next step.

3. If $F\{\sigma'\} \geq 0$ and if $F\{\sigma_0\} = 0$ (the element has yielded at start of increment), $\{\Delta \sigma\}_1$ is found by $\{\Delta \sigma_1\} = [\text{Dep}]^* \{\Delta \epsilon\}_1$ where $[\text{Dep}]^*$ is computed using $\{\sigma'\}$. Stresses which are to be supported by body forces are evaluated.

$$\{\Delta \sigma''\}_1 = \{\Delta \sigma'\}_1 - \{\Delta \sigma\}_1 \quad (3.125)$$

Current stress is stored

$$\{\sigma\} = \{\sigma'\} - \{\Delta \sigma''\}_1 \quad (3.126)$$

Current strain is stored

$$\{\epsilon\} = \{\epsilon'\} + \Delta \{\epsilon'\}_1 \quad (3.127)$$

4. If $F\{\sigma\} > 0$, but $F\{\sigma_0\} < 0$, the intermediate stress value is found at which yield begins and the increment in stress is computed by the relation, $\{\Delta \sigma_1\} = [\text{Dep}]^* \{\Delta \epsilon'\}_1$ starting from that point. Then proceed as in step 3.

5. Nodal forces are computed corresponding to the equilibrating body forces. These are given by,

$$\{P\}_1^e = \int [B]^T \{\Delta \sigma''\}_1 d(\text{vol}) \quad (3.128)$$

6. The problem is resolved using original elastic properties and the load system P to find $\{\Delta \sigma\}_2$ and $\{\Delta \epsilon\}_2$.

7. Current values are found.

8. Steps 2 to 6 are repeated.

The cycling can be stopped when the appropriate convergence criterion specified is satisfied.

3.4.4 Convergence Criteria and Increment Size :

The adoption of an incremental plasticity theory and iterative solution technique, such as used in 'initial stress' method leads to errors due to size of increment and finite values of criteria for convergence specified. These errors influence the numerical limit loads found and also will influence the load deflection curve obtained in an elasto-plastic analysis in particular.

Convergence criteria specified in a solution, indicate whether the non-linear equations describing the behaviour of the material when subjected to an increment of load have been solved with sufficient accuracy. This is achieved by comparing the change in some aspect of the solution between iterations and terminating the procedure once this change has become sufficiently small. The convergence criterion imposed in this work is on the absolute maximum magnitude of load correction vector calculated by eqn. (3.128).

3.5 Kotter's Equation for Circular Rupture Surface (37) :

Referring to Fig. 3.11a and from considering equilibrium of forces in r and θ direction,

$$\frac{\partial \sigma_r}{\partial r} + \frac{1}{r} \frac{\partial \tau_{r\theta}}{\partial \theta} + \frac{\sigma_r - \sigma_\theta}{r} + \gamma \cos \theta = 0 \quad (3.129)$$

$$\frac{1}{r} \frac{\partial \sigma_\theta}{\partial \theta} + \frac{\partial \tau_{r\theta}}{\partial r} + \frac{2\tau_{r\theta}}{r} - \gamma \sin \theta = 0 \quad (3.130)$$

Investigating the stresses on the rupture circle with its centre in the pole of the co-ordinate system and inserting the stresses σ_r and $\tau_{r\theta}$ in Coulomb's Law, $\tau = C + \sigma \tan \phi$ can be written as,

$$\tau_{r\theta} - \sigma_r \tan \phi \leq C \quad (3.131)$$

The function indicated on the left hand side of eqn. (3.131) must have a constant value in the rupture line proper and as regards its variation in radial direction, it must either be constant (zone rupture) or attain a maximum value at rupture line, (line rupture). In both cases,

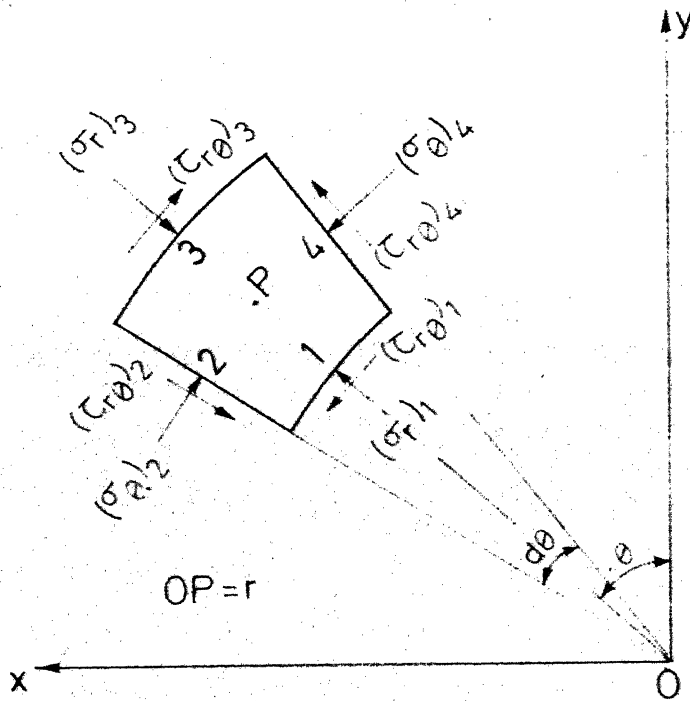
$$\frac{\partial(\tau_{r\theta} - \sigma_r \tan \phi)}{\partial r} = 0 \quad (3.132a)$$

$$\frac{\partial(\tau_{r\theta} - \sigma_r \tan \phi)}{\partial \theta} = 0 \quad (3.132b)$$

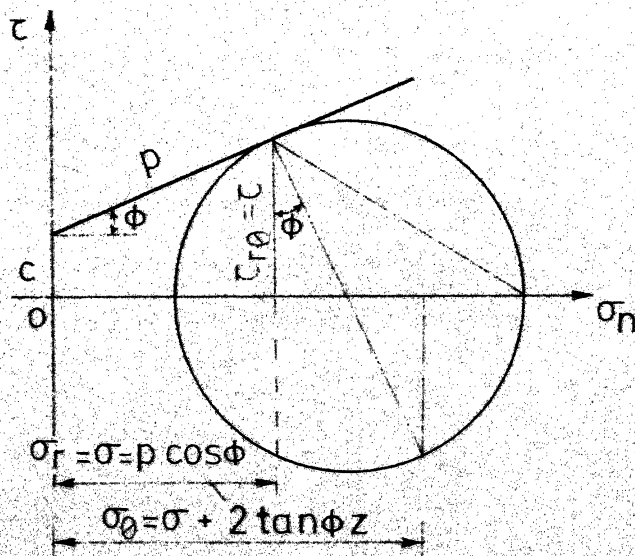
Multiplying eqn. (3.129) by $\tan \phi$ and subtracting from eqn. (3.130) and simplifying results

$$\frac{\partial(\sigma_\theta - \tau_{r\theta} \tan \phi)}{\partial \theta} + \tan \phi (\sigma_\theta - \sigma_r) + 2\tau_{r\theta} - \frac{r\gamma \sin(\theta + \phi)}{\cos \phi} = 0 \quad (3.133)$$

Omitting the subscripts on rupture line proper for σ and τ , other stress, σ_θ is obtained from Mohr's circle (Fig. 3.11b) as



a. Infinitesimal soil element on rupture circle



b. Mohr's circle of stress

FIG-3-11 CIRCULAR RUPTURE SURFACE

$$\sigma_{\theta} = \sigma + 2\tau \tan \phi \quad (3.134)$$

Using eqns. (3.132a) and (3.134) to eliminate normal stress from eqn. (3.133), the differential equation in terms of τ is obtained as

$$\frac{d\tau}{d\theta} + 2\tau \tan \phi - r\gamma \sin(\theta + \phi) \sin \phi = 0 \quad (3.135)$$

The above is known as Kotter's equation which gives the variation of shear stress (τ) on the rupture line.

The above equation can also be written in terms of cohesion C and angle of internal friction ϕ , by making use of the following substitution for τ :

$$\tau = C + p \sin \phi . \quad (3.136)$$

The resulting form of equation in p is,

$$\frac{dp}{d\theta} + 2p \tan \phi - r\gamma \sin(\theta + \phi) + 2C \sec \phi = 0 \quad (3.137)$$

The above equation is valid for the position of origin and angles θ assumed as shown in Fig. 3.11a.

CHAPTER 4

HORIZONTAL STRIP ANCHORS

4.1 Introduction :

Geometric configuration of some three-dimensional problems make their treatment as plane problems possible under certain circumstances. Continuous footings, retaining walls and embankments are cases wherein, because one geometric dimension is very large in comparison to the other two, the analysis is done as a two-dimensional plane strain case instead of the three-dimensional case. In the case of rectangular plate anchor where the length of the anchor is large compared to breadth and thickness an analysis carried out as a plane strain case is usually justified.

The present chapter deals with elastic and elasto-plastic analysis of horizontal strip anchors by finite element method. An idealised model of a foundation subjected to vertical uplift load can be visualised by applying a load of uniform intensity inside the medium (Fig. 4.1a). This presupposes that the anchor is thin and perfectly flexible and does not have any property different from the medium within which it is buried. This case can be named as a flexible anchor subjected to a uniform intensity of load. The anchor can be modelled also as perfectly rigid one. A perfectly rigid anchor when subjected to vertical uplift load will undergo uniform vertical

displacement. This is modelled in displacement finite element method by specifying known equal displacement at nodal points corresponding to anchor position and obtaining nodal loads from the stresses that result (Fig. 4.1b). Here again the anchor is assumed to be infinitely thin and perfectly rigid. A strip anchor can also be modelled by the same continuum elements (Fig. 4.1c) used to discretise the soil medium within which it is embedded. Anchor width, thickness and material properties of anchor can be assigned in an elastic analysis of the problem. The anchor plate can be simulated by beam bending elements (Fig. 4.1d). The beam-column element is a line element but the structural properties of the anchor can be put in and the effect of these on anchor response can be studied. Bending moments are obtained directly from analysis. The above idealisations have been used in modelling foundations by finite element method. Under the application of small loads, it is usually assumed that a full bonding of anchor bottom and soil exists. Since the interface separation is one very important parameter which can affect the anchor displacement and pattern of stress distribution throughout the continuum, results are also obtained assuming full separation at the bottom of anchor. This is a limiting case, which may not represent the true situation for very low loads especially under deep embedment.

The elastic response of a flexible strip subjected to uniform pressure and embedded inside a medium of limited depth has

been studied for different depth of embedment ratios and Poisson's ratios and also for two different layer depths. The response of rigid anchor subjected to uplift load is also analysed. For specific embedment and layer depth, a typical case has been selected ($H/B = 2.0$, $D/B = 1.0$) for studying the behaviour of anchor simulated by beam-column elements and continuum elements. A comparison of the anchor response from the above studies has been presented.

For elastic-plastic undrained analysis, Von-Mises model has been used mainly. Tresca model has been used in limited computer runs for making comparisons. Some of the important aspects like effect of structural rigidity of anchor, interface breakaway, magnitude of incremental load, convergence criterion, mesh refinement etc. on the response and limit load has been investigated. The Mohr-Coulomb associated perfectly plastic model is used to simulate frictional behaviour of soil. Effects of variation of angle of internal friction, interface breakaway, initial stresses etc. on limit load are investigated.

4.2 Finite Element Model :

4.2.1 Elastic Analysis :

The discretisation of the soil mass for analysis is done by four noded linear isoparametric elements which have eight degrees of freedom. The finite element meshes used are shown in Figs. 4.2 and 4.3. The number of nodal points is 630 and

number of elements 580 for the mesh used for the case where there are no joint elements, i.e. there is no separation at the interface. The number of nodal points is 641 and number of elements 590 where interface elements are used to simulate the breakaway. Because of the symmetry of loading and boundary conditions only half portion of the soil medium is discretised in the analysis. The bottom of the continuum has been assumed as a rough rigid boundary and the side boundaries as smooth rigid ones (Figs. 4.2 and 4.3). The width of the anchor (B) is fixed as 100 cms. Depending on the H/B ratios used, the soil layer depth is 200 cms for $H/B = 2$ and 400 cms for $H/B = 4.0$. The distance of the side boundary is fixed at 400 cms from centre line as indicated in the Fig. 4.2.

The modelling of full separation beneath the anchor is done by providing four noded interface elements with very low values of normal and shear stiffness. The elastic analysis of horizontal strip is carried out for full bonding and full separation for the following four cases.

- a. Flexible strip subjected to uniform pressure : This case is analysed by applying the intensity of uniform pressure at the level where the flexible strip is supposed to be placed (Fig. 4.1a).
- b. Rigid strip : A rigid strip embedded inside the soil is simulated by applying known uniform vertical displacement at the node level where the strip is placed (Fig. 4.1b). The nodal forces equivalent to this known specified displacements are calculated

from the stresses surrounding the nodes. The strip is considered to be infinitely thin when compared to the soil elements (Fig. 4.1b).

c. Strip of finite rigidity continuum elements : The thickness of the anchor considered is 20 cms (Fig. 4.1c). 20 elements are used to discretise the anchor. The relative stiffness of anchor for the analysis is specified by Borowicka (69) as

$$K_r = \frac{1}{6} \frac{(1 - \nu^2)}{(1 - \nu_p^2)} \frac{E_p}{E} \left(\frac{2t}{B}\right)^3 \quad (4.1)$$

where

E, ν = elastic moduli of soil

E_p, ν_p = elastic moduli of strip

t = thickness of strip

B = width of strip

The analysis is carried out for $\nu = 0.3$ and 0.49 . The ν_p value of anchor plate material is fixed at 0.3 . The cases of anchor subjected to (i) uniform uplift pressure on the surface and (ii) a concentrated central uplift load are analysed. The relative stiffness is changed by changing E_p value and a range of K_r varying from 0.01 to 100 is used in the study of response.

d. Strip of finite rigidity, beam-column elements : The beam column element is a line element. It is placed inside the continuum with necessary changes in stiffness to simulate the anchor in plane strain. The relative stiffness of anchor for the analysis is specified by eqn. (4.1). 10 beam-column elements are used

to simulate the strip anchor structure. The analysis is carried out for $\nu = 0.3$ and $\nu = 0.49$. The ν_p value of the anchor material is taken as 0.3. Both uniform intensity of load as well as concentrated central loads are considered for the analysis. The range of relative stiffness values from 0.01 to 100 are selected for the response study.

The cases (a), (b) and (c) above are analysed by using the computer program 'ISOPIN' developed. The general features and capabilities of the computer program are given in Appendix A. For analysis of case (d) where a beam-column element is implemented, a computer program 'ISOBMJ' is developed. This program is a modification of the 'ISOPIN' to take into account the beam-column element also, with necessary changes in routines. These computer programs are developed at IIT Kanpur, Computer Centre, in DEC-1090 system.

4.2.2 Elasto-Plastic Analysis :

The discretisation of the soil medium and anchor for analysis is done by eight noded parabolic isoparametric elements. These elements have sixteen degrees of freedom. The ~~three~~ finite element meshes used for the full anchor bonding cases are shown in Figs. 4.30a, 4.30c and 4.30 d. The number of nodal points are 251, 147, 79 and number of elements 72, 40 and 20 respectively for Mesh-1, Mesh-3 and Mesh-4. The Mesh-2, incorporating interface elements, has 256 nodes and 74 elements as shown in Fig. 4.30b. The breadth of the anchor is fixed as 100 cms and

thickness 25 cms. The relative stiffness is calculated by using eqn. (4.1). 6 noded joint elements are used to simulate interface separation. Because of symmetry only half the problem geometry is discretised. The depth of the layer considered is 200 cms and the distance of lateral boundary from anchor centre line limited to 400 cms.

The load is applied as a concentrated upward load at anchor centre. Relative stiffness value equal to 10 is fixed for studying effect of various other parameters. In carrying out the elasto-plastic analysis the 'initial stress' approach is used. This is an incremental iterative approach. In such a procedure the number of increments in which the total load is applied and the number of iterations carried out within an increment to satisfy the convergence criteria are both important.

The elasto-plastic analysis is carried out in approximately 20 to 25 increments. The convergence criterion specified for the analysis is on the absolute maximum magnitude of the residual load vector. Maximum number of iterations within an increment is specified as 200. The convergence criterion on residual load vector is taken as 1 percent of the load applied in an increment. If the number of iteration needed to satisfy convergence requirements is greater than 200, it is deemed that the ultimate load is reached.

(C_u) equal to 20 KN/m^2 . The ratio E_u/C_u is thus fixed at 500. The modulus of elasticity of the foundation is fixed, depending upon the relative stiffness values. For the assumed dimensions of the anchor, and Poisson's ratio equal to 0.3 used for the analysis, the modulus of elasticity of the anchor material for $K_r = 10$, works out to be $5.675 \times 10^6 \text{ KN/m}^2$. A very high value of K_r is not used because of the possibility of the resulting system of equations getting ill-conditioned, because of this. $K_r = 100$ is used for comparison of response and ultimate load obtained with $K_r = 10$. The cohesion (C_u) for foundation material is specified such that there is no yielding of the foundation material under the applied loading and it remains elastic throughout.

Von-Mises criterion is used to model the undrained behaviour and Tresca model is only used for comparisons in specific cases.

Since both Von-Mises and Tresca criteria are independent of the mean stress (σ_m), neither the load at first yield nor the collapse load will be effected if initial vertical stresses are assigned values corresponding to the weight of the material and lateral stresses are set equal to the vertical stress assuming coefficient of lateral pressure (K_0) is equal to unity. Weight of material will affect the yield, deformation response or ultimate load only if the lateral earth pressure coefficient is different from one. To study the effect of initial stresses, the coefficient of lateral earth pressure has been chosen as 0.5.

Drained Analysis : The model used is associated Mohr-Coulomb criterion. This model is specified by modulus of elasticity, (E), Poisson's ratio (ν), cohesion (c) and angle of internal friction (ϕ). For this analysis, materials which are purely frictional are considered by setting the value of cohesion equal to zero. It is generally observed that the associated Mohr-Coulomb model and associated flow rule, gives unrealistically large plastic volume increases. Since the main objective of the study is the prediction of ultimate uplift load, the use of this model is justified. The analysis is carried out by specifying drained modulus value (E) of the soil to be $2 \times 10^5 \text{ KN/m}^2$ and Poisson's ratio equal to 0.3. The modulus of elasticity of the foundation material for a relative stiffness value equal to 10 and Poisson's ratio equal to 0.3 works out to $9.60 \times 10^7 \text{ KN/m}^2$. The material parameters C , ϕ assigned to the foundation material are such that the anchor remains elastic in all load increments and only the soil elements yield. The same value of E is kept even when the response due to different values of ϕ are found, so as to enable comparison of ultimate load variation due to a variation in value of ϕ , easier and straightforward. The yield criterion for frictional material depend on the mean stress (σ_m) and hence the weight of the material will effect the yield and ultimate load. The density of the material is assumed to be 16 KN/m^3 . In calculating lateral stress, the coefficient of lateral earth pressure K_0 is fixed as 1.0 in all the runs except

where the effect of K_0 on yield and uplift load are studied.

Computer Programs : Two computer programs ELPLP1, ELPLP2 are developed in DEC-1090 system for general finite element elasto-plastic analysis of plane strain problem, using 'initial stress' technique. Explicit expressions are available for elasto-plastic matrix for Von-Mises criterion. ELPLP1 carries out the elasto-plastic incremental analysis using Von-Mises model. ELPLP2 can take the Tresca or Mohr-Coulomb models for the analysis. The general features and capabilities of ELPLP1 are given in Appendix B. ELPLP2 forms the elasto-plastic matrix by the general method outlined in Sec. 3.4.

Testing of Programs : As a check on the elasto-plastic formulation, numerical methods adopted and the computer programs developed, a thick walled cylinder of internal radius 'a' and external radius '2a' was analysed. (Fig. 4.29). The cylinder was subjected to an internal pressure p and zero external pressure. This problem has been selected because an analytical solution for the entire elastic and elasto-plastic range for this simple case is available (39,40) for Von-Mises and Tresca criteria. Program ELPLP1 is used to solve the problem using Von-Mises model and Program ELPLP2 is used to solve the problem using Tresca model. The cylinder is analysed for the following parameters :

$$E = 6.09 \times 10^4 \text{ N/cm}^2, \nu = 0.3, C = 6.09 \text{ N/cm}^2, a = 2.54 \text{ cms.}$$

The elastic horizontal displacement of A, (u_A), internal pressure needed to cause first yield, the internal pressure needed to make all the sampling points to yield are checked with the results available (39,40). The elasto-plastic displacement response obtained using the two criteria are given in Fig. 4.29, as a plot of p/C versus $2 G u_A/Ca$, where G is the shear modulus. The limit pressure and the load displacement curve using finite element elasto-plastic analysis are very close to results from analytical solution of the above problem.

4.3 Results and Discussions :

4.3.1 Elastic Analysis :

a. Flexible Anchor : A flexible anchor subjected to uniform upward pressure is simulated as shown in Fig. 4.1a. For a flexible anchor embedded inside an elastic layer of limited depth, finite element elastic analyses are carried out for $H/B = 2.0$ and $H/B = 4.0$. The embedment ratios (D/B) considered are 0.5, 1.0, 1.5 and 1.0, 2.0, 3.0 for $H/B = 2.0$ and $H/B = 4.0$ respectively. Results are obtained for Poisson's ratio equal to 0.2, 0.3, 0.4 and 0.49. When uplift load is applied, if full bonding between anchor and soil below the anchor at the level of applied load is assumed, it is known as the full bonding case. If there is break-away at the level of application of load by formation of a slit, the case is named as full separation case. These are the two extreme situations studied. For a flexible anchor under a small load full bonding may be a more reasonable assumption.

Table 4.1 summarises the results of analysis for displacements for full bonding case. For particular value of H/B , D/B and ν , the table presents the influence factors for vertical displacement at centre of anchor, at edge of anchor and at the surface directly over the centre of anchor. Poisson's ratio and depth of embedment of anchor has considerable influence on the vertical displacement of anchor. The vertical displacement decreases with increase in Poisson's ratio from 0.2 to 0.49. With increase in embedment of anchor the vertical displacement of anchor decreases. Comparing the results for $H/B = 2.0$ and $H/B = 4.0$ for D/B ratio equal to 1.0, the vertical deflection is considerably more for $H/B = 4.0$ than for $H/B = 2.0$. This brings out the fact that the depth of the elastic layer below the anchor has considerable influence on vertical deflections, for the H/B ratios considered.

The variation of vertical displacement along the centre line for $D/B = 0.5, 1.0$ and 1.5 is shown in Figs. 4.4, 4.5 and 4.6. The vertical displacement is maximum at anchor level. The variation of vertical displacement for $\nu = 0.2, 0.3, 0.4$, and 0.49 is shown in the above figures. They show the same general trends for $D/B = 0.5, 1.0$ and 1.5 .

The results of analysis of flexible anchor subjected to uniformly distributed uplift load under full separation are summarised in Table 4.2. Figures 4.7, 4.8 and 4.9 show the variation of the vertical displacement along the centre line for

Table 4.1

Influence factors for vertical displacement of flexible strip, uniformly distributed uplift load

Full bonding
a. $H/B = 2.0$

$$\rho = \frac{pB}{E} I$$

v	I_c			I_e			I_{cs}		
D/B 0.5	1.0	1.5	0.5	1.0	1.5	0.5	1.0	1.5	
0.2	0.837	0.575	0.341	0.595	0.394	0.206	0.781	0.446	0.197
0.3	0.780	0.531	0.305	0.537	0.352	0.177	0.721	0.407	0.174
0.4	0.666	0.439	0.234	0.430	0.270	0.123	0.618	0.337	0.133
0.49	0.444	0.255	0.092	0.242	0.123	0.032	0.440	0.220	0.066

b. $H/B = 4.0$

v	I _c			I _e			I _{cs}		
	D/B 1.0	2.0	3.0	1.0	2.0	3.0	1.0	2.0	3.0
0.2	1.033	0.749	0.503	0.827	0.567	0.338	0.875	0.470	0.204
0.3	0.976	0.706	0.466	0.767	0.523	0.303	0.811	0.428	0.181
0.4	0.848	0.606	0.384	0.643	0.430	0.232	0.691	0.351	0.138
0.49	0.569	0.379	0.187	0.400	0.242	0.090	0.480	0.213	0.063

I_c - Influence factor for vertical deflection at the centre of strip

I_e - Influence factor for vertical deflection at the edge of strip

I_{cs} - Influence factor for vertical deflection at the surface above centre.

Table 4.2

Influence factors for vertical displacement of flexible
strip uniformly distributed uplift load

Full separation

$$\rho = \frac{pB}{E} I.$$

a. $H/B = 2.0$

v	I _c			I _e			I _{cs}			
	D/B	0.5	1.0	1.5	0.5	1.0	1.5	0.5	1.0	1.5
0.2	3.321	1.811	1.370	1.565	0.948	0.659	0.030	1.306	0.734	
0.3	3.178	1.728	1.309	1.496	0.907	0.633	2.871	1.234	0.691	
0.4	2.894	1.574	1.197	1.351	0.812	0.570	2.615	1.112	0.620	
0.49	2.057	1.196	0.925	0.857	0.528	0.363	1.832	0.832	0.455	

b. $H/B = 4.0$

v	I _c			I _e			I _{cs}			
	D/B	1.0	2.0	3.0	1.0	2.0	3.0	1.0	2.0	3.0
0.2	2.140	1.523	1.263	1.279	0.862	0.635	1.631	0.802	0.438	
0.3	2.041	1.451	1.207	1.222	0.822	0.609	1.538	0.749	0.409	
0.4	1.846	1.306	1.096	1.086	0.725	0.543	1.368	0.652	0.357	
0.49	1.347	0.946	0.815	0.714	0.455	0.344	0.984	0.434	0.240	

I_c - Influence factor for vertical deflection at the centre of strip

I_e - Influence factor for vertical deflection at the edge of strip

I_{cs} - Influence factor for vertical deflection at the surface above centre.

$H/B = 2.0$ and D/B ratios equal to 0.5, 1.0 and 1.5 respectively. It is seen that the vertical displacement of the points below the slit are of negligible magnitude. The dependence of the vertical displacement on Poisson's ratio and embedment depth is evident from the influence values given. Comparing the displacement influence values in $H/B = 2.0$, $H/B = 4.0$ for $D/B = 1.0$, it is seen that the vertical central displacement is more for $H/B = 4.0$. But the increase in displacement is smaller, as compared to the full bonding case. Interface breakaway is an important factor which effects the vertical displacement of anchor.

The vertical stress variation along the centre line with depth is shown in Fig. 4.10 for full bonding case. The stresses in elements nearest to the centre line are used as σ_y along the axis. The applied loading of uniform intensity is shared by the elements above and below the line of load application. The elements above the anchor level are in compression and those below are subjected to tension. The elements below the anchor are stressed more than the elements above the anchor. The non-dimensional stress ratio σ_y/p is approximately 0.15 to 0.25 only for the elements directly above the anchor for the D/B ratios investigated, $D/B = 0.5$, 1.0 and 1.5.

The variation of vertical stress with depth along anchor axis is shown in Fig. 4.11 for full separation case for D/B ratios equal to 0.5, 1.0 and 1.5. The pattern of variation of σ_y

is considerably altered by the loss of adhesion below the anchor. The value of σ_y/p in the elements directly above the anchor is near to unity and in the elements directly below the anchor, the value of σ_y/p is negligibly small. The pattern of stress transfer above and below the anchor for the cases of full bonding and full separation are very much different.

The variation of the vertical contact stress in soil elements above and below the level of application of load along anchor length is shown in Figs. 4.12 and 4.13 for $\nu = 0.3$ and 0.49 respectively. The stresses marked above the horizontal axis are compressive and those marked below are tensile. The pattern of distribution of σ_y/p for full bonding does not seem to be effected by the Poisson's ratio. For full separation case, there is difference in variation of vertical stress in soil between $\nu = 0.3$ and $\nu = 0.49$ towards the edge of the anchor. The same trends in variation of σ_y is observed for cases when $D/B = 0.5$ and $D/B = 1.5$ were investigated, although they are not plotted in the figure.

b. Rigid Anchor : The influence coefficients for vertical displacement for a rigid strip for full bonding and separation are tabulated in Table 4.3 and Table 4.4. The vertical displacement at the centre of anchor and at the surface of the layer above the centre for $H/B = 2.0$ and $\nu = 0.2, 0.3, 0.4, 0.49$ are presented for $D/B = 0.5, 1.0$ and 1.5 . The vertical displacement of anchor decreases with increase in Poisson's ratio and as the embedment

Table 4.3

Influence factors for vertical displacement of rigid strip

Full bonding

H/B = 2.0

$$\rho = \frac{p_{av} B}{E} I$$

v	I _c			I _{cs}			I _{c(av)}		
	D/B	0.5	1.0	1.5	0.5	1.0	1.5	0.5	1.0
0.2	0.733	0.505	0.292	0.725	0.439	0.197	0.716	0.485	0.274
0.3	0.673	0.460	0.260	0.663	0.398	0.174	0.659	0.441	0.241
0.4	0.560	0.371	0.196	0.557	0.327	0.132	0.548	0.354	0.179
0.49	0.349	0.198	0.071	0.377	0.209	0.066	0.343	0.189	0.062

Table 4.4

Influence factors for vertical displacement of rigid strip

Full separation

H/B = 2.0

$$\rho = \frac{p_{av} B}{E} I$$

v	I _c			I _{cs}			I _{c(av)}		
	D/B	0.5	1.0	1.5	0.5	1.0	1.5	0.5	1.0
0.2	2.016	1.345	1.005	2.026	1.138	0.654	2.443	1.380	1.015
0.3	1.921	1.283	0.962	1.897	1.074	0.616	2.337	1.318	0.971
0.4	1.745	1.163	0.877	1.740	0.969	0.553	2.123	1.193	0.884
0.49	1.479	0.959	0.711	1.494	0.831	0.454	1.457	1.026	0.644

I_c - Influence factor for vertical deflection at the centre of strip

I_{cs} - Influence factor for vertical deflection at the surface above the centre

I_{c(av)} - Influence factor calculated from flexible anchor analysis as (I_c + I_e)/2.

ratio of anchor increases. The variation of vertical displacement with depth is shown in Figs. 4.4, 4.5, 4.6, 4.7, 4.8 and 4.9 for $\nu = 0.3$ and $\nu = 0.49$. Table 4.3 and Table 4.4 also gives the influence factor $I_{c(av)}$ which are the values calculated from flexible strip analysis, averaging the influence factors for centre and edge of anchor. For full bonding, this approximation gives influence factors and hence displacement prediction without appreciable error, but numerically smaller than those obtained for rigid strip.

The variation of vertical stress in the elements above and below the rigid anchor for full bonding and full separation are shown in Figs. 4.12 and 4.13 for $\nu = 0.3$ and 0.49 respectively. For full bonding case and full separation case the vertical stress above the rigid anchor is compressive and that below the anchor tensile. For full bonding case, the vertical stress increases towards the edge of the anchor. For full separation at level of anchor from soil below it, the trend of variation of σ_y/p is remarkably changed, the compressive stress increasing towards the edge of the anchor. The value of σ_y/p approaches close to $2.5 P/B$ compared to a value of about $0.30 P/B$ near the axis of the anchor.

c. Anchor of Finite Stiffness, Continuum Element : For relative stiffness (K_r) values ranging from 0.01 to 100 , the results for vertical displacement at centre of anchor and maximum differential vertical displacement of anchor are presented in Table 4.5.

Table 4.5

Influence factors for vertical displacement of strip anchor - continuum element
and beam column element anchor discretisation

$\rho = (\bar{p}B/E); \quad \bar{p} = p \text{ for udl}$

$H/B = 2.0$

$\bar{p} = P/B \text{ for conc. load}$

$D/B = 1.0$

K_r	ν	Load: udl		Load: udl		Load: conc.		Load: conc.	
		I_c	I_d	Full separation	Full bonding	I_c	I_d	Full separation	Full bonding
0.01	$\nu = 0.3$	0.5359*	0.1829	1.4490	0.6375	1.4111	1.1416	2.6033	1.8299
	$\nu_p = 0.3$	0.5310**	0.1706	1.6549	0.7166	0.8945	0.6349	2.4072	1.5842
0.10	-do-	0.4333	0.1124	1.2290	0.4189	0.6962	0.4379	1.6527	0.8626
		0.5160	0.1335	1.4326	0.4336	0.7016	0.4276	1.7940	0.9014
1.00	-do-	0.3837	0.0470	0.9507	0.1285	0.4459	0.1350	1.0471	0.2313
		0.4667	0.0417	1.1809	0.0930	0.5176	0.1292	1.2549	0.1924
10.00	-do-	0.3580	0.0070	0.8456	0.0164	0.3663	0.0192	0.8573	0.0289
		0.4367	0.0050	1.0767	0.0101	0.4429	0.0161	1.0849	0.0213
100.00	-do-	0.3533	0.0007	0.8288	0.0025	0.3542	0.0020	0.8294	0.0030
		0.3649	0.0005	0.6229	0.0006	0.3656	0.0017	0.5237	0.0018

contd....

K_r	ν	Load : udl		Load: udl		Load : conc.		Load : conc.	
		Full bonding	I_d	Full separation	I_d	Full bonding	I_d	Full separation	I_d
		I_c		I_c		I_c		I_c	
0.01	$\nu = 0.49$	0.3196*	0.1612	1.1241	0.5750	0.9648	0.8818	2.0288	1.5101
	$\nu_p = 0.30$	0.2504**	0.1279	1.2527	0.6505	0.5068	0.4549	1.7662	1.2700
0.10	-do-	0.2184	0.0977	0.9369	0.3737	0.4435	0.3825	1.3054	0.7549
		0.2299	0.1029	1.0791	0.4330	0.3676	0.3126	1.3265	0.7912
1.00	-do-	0.1662	0.0403	0.6862	0.1153	0.2192	0.1162	0.7595	0.1909
		0.1884	0.0361	0.8030	0.0983	0.2296	0.1047	0.8520	0.1847
10.00	-do-	0.1442	0.0059	0.5877	0.0148	0.1492	0.0162	0.5979	0.0253
		0.1698	0.0050	0.7382	0.0113	0.1752	0.0139	0.7450	0.0212
100.00	-do-	0.1388	0.0007	0.5732	0.0016	0.1395	0.0016	0.5742	0.0026
		0.1516	0.0005	0.5629	0.0010	0.1522	0.0014	0.5620	0.0020

I_c - Influence factor for vertical displacement at centre of anchor

I_d - Influence factor for differential displacement between centre and edge

* Corresponds to continuum element discretisation of anchor

** Corresponds to beam-column element discretisation of anchor

The Poisson's ratio of the soil medium considered are 0.3 and 0.49. Cases of uniform intensity of upward load on the anchor and a concentrated uplift load at the centre of the anchor are considered. Full bonding and full separation between anchor and underlying soil beneath are analysed as two extreme cases. Figs. 4.14 and 4.15 show the variation of central vertical displacement of anchor and Figs. 4.16 and 4.17 show the variation of maximum differential vertical displacement for K_r varying from 0.01 to 100. Results of displacement influence factors obtained for central vertical displacement of flexible anchor and rigid anchor are also shown for comparison. The E_p/E values for $K_r = 0.01$ corresponds to 0.9375 and 1.123 respectively for $\nu = 0.3$ and 0.49. Because of this reason I_c value using continuum element discretisation of anchor is slightly higher than for the flexible anchor for $\nu = 0.3$. For $\nu = 0.49$, because $\nu_p = 0.3$, the displacement for $K_r = 0.01$ is higher than the case of a flexible anchor. For $\nu = 0.3$, I_c varies from 0.54 to 0.35 for variation of $K_r = 0.01$ to $K_r = 100$ for full bonding case and under a uniform uplift load, whereas for the same variation of K_r , I_c varies from 1.41 to 0.35 for a concentrated central load. When loads are concentrated, I_c is more affected by K_r variation in lower ranges of K_r . But these lower ranges of K_r may not be of practical importance. Variation of I_c for values of $K_r = 10.0$ to 100.0 is very small for the two Poisson's ratios investigated. This is true for full bonding as well as full separation cases. In this range of K_r , the mode of application of the load, namely,

uniformly distributed or centrally concentrated, do not effect the I_c values. For all practical purposes $K_r = 10$ represents a rigid anchor as increase in stiffness to $K_r = 100$ effects the central deflection and the maximum differential deflection values only nominally. In a displacement finite element analysis, values of K_r higher than 100 may not be advisable, especially for cases of ν nearer to 0.5 as it may result in build up of round-off errors and complete breakdown of solution by ill-conditioning of the resulting set of equations. Hence, it is not advisable nor essential to use K_r values greater than 100 to obtain displacement influence values for a rigid anchor. Even if, the actual E_p/E ratios are higher, it is better to limit them from the view point of accuracy of solution.

Maximum differential displacement of the anchor also depends on the type of loading as well as the Poisson's ratio values. For $K_r = 0.01$ and full bonding case the I_d values obtained are close to those of the flexible anchor. For $K_r = 10$, the difference in I_d values due to difference in Poisson's ratio and the type of loading is negligible. For the case of full separation because the breakaway takes place at the bottom level of anchor, the displacement obtained for this case is less than the corresponding case of a flexible anchor where the separation takes place at the level of the anchor itself.

Rigid anchor displacements are also shown in Figs. 4.14 and 4.15. It is observed that the displacement influence factors I_c

obtained for rigid anchor idealisation gives values higher than those corresponding to $K_r = 100$, in all the cases considered. It appears from this that specification of equal nodal displacement to simulate rigid anchor behaviour gives values of vertical displacement influence coefficients higher than values when simulating the anchor by its actual dimensions using continuum elements.

Figures 4.18 and 4.19 show the variation of vertical contact stress above and below the anchor for $\nu = 0.3$ and 0.49 respectively. Results for two representative values of $K_r = 0.01$ and $K_r = 10$ are only plotted. For the case of full bonding, variation of σ_y due to K_r can be observed from the diagram. For the case of full separation from soil elements below, the change in relative stiffness (K_r) from 0.01 to 10.0 effects σ_y/p variation more. For $K_r = 10$, the plot of σ_y/p with X/B due to a uniformly distributed and concentrated load almost coincides.

d. Anchor of Finite Stiffness, Beam-Column Element : Table 4.5 summarises the results for vertical displacement at centre of anchor and maximum differential vertical displacement of anchor for variation of relative stiffness from $K_r = 0.01$ to 100 . Full bonding of anchor with underlying soil and full breakaway are considered for two cases of uplift loads, namely, uniformly distributed and concentrated. The variation of central vertical displacement of anchor with K_r is plotted in Figs. 4.20 and 4.21 and the variation of maximum differential displacement in

Figs. 4.22 and 4.23. For $K_r = 0.01$ and full bonding, the results for flexible anchor and the beam-column element discretisation do not show any appreciable difference. The type of loading, namely, uniform or concentrated do not have any appreciable influence on I_c and I_d beyond $K_r = 10$. The I_c value decreases from $K_r = 10$ to 100, more than what is observed for the continuum element. If for $K_r = 10$, the continuum element and beam-column element discretisations are compared, it can be observed that I_c values for the latter are more in all the cases. For $K_r = 100$, the vertical displacement of continuum element is less than for the beam-column element for full bonding case. The rigid anchor simulation gives I_c values consistently greater than those for $K_r = 10$. This clearly shows that the response predicted by beam element does not approach the rigid anchor, simulated by specifying equal nodal displacements (Fig. 4.1b). The use of the structural element like beam column element for anchor makes the system more stiff. The value of central deflection of anchor obtained is less than that predicted by a simulation of rigid anchor for cases of prescribed relative stiffness values greater than 10 for beam-column element.

The variation of vertical stress above and below the anchor for $\nu = 0.3$ and 0.49 are shown in Figs. 4.24 and 4.25 respectively. $K_r = 0.01$ and $K_r = 10$ are only considered. K_r values affect the variation of σ_y/p for the case of full bonding. But K_r values affect the variation of σ_y/p considerably more in the

case of full separation. The edge stresses are more in this case than the corresponding values for the continuum element, for full separation case. For $K_r = 10$, practically there is no difference in variation of σ_y/p for uniform or concentrated loads for $\nu = 0.3$. For $\nu = 0.49$, soil stresses near the edge of anchor are more and the plot σ_y/p versus X/B shows some variation between uniform and concentrated load cases. For case of full bonding and $K_r = 10$, there is practically very little variation in σ_y/p due to the load being uniformly distributed or concentrated.

The variation of bending moment along the length of anchor is shown in Figs. 4.26, 4.27 and 4.28. In Fig. 4.26, the variation of bending moment along the length of anchor due to a uniform load is shown as a plot of non-dimensional ratios M/pB^2 versus X/B for $K_r = 0.01, 0.1, 1.0$ and 10.0 . The bending moment is maximum in the centre of the anchor for $K_r \geq 0.1$. The bending moment increases with K_r . For $K_r = 1$ and $K_r = 10$, the magnitude of maximum bending moment for $\nu = 0.49$ is greater than for $\nu = 0.3$. Comparing the cases of full bonding and full separation of anchor from underlying soil, it is noted that the maximum bending moment for the full separation case is higher. For $K_r = 10$, $\nu = 0.3$, the ratio of the maximum bending moments for full separation and full bonding cases can be seen to be around 2.0. Fig. 4.28, shows the variation of bending moment along the length of the anchor due to a concentrated central load and uniform load

for $K_r = 10$. The maximum bending moments due to concentrated central loads on anchor are more than the uniformly distributed uplift load acting on the anchor. The maximum bending moment in the full separation case is more than the corresponding case for full bending.

4.3.2 Elasto-Plastic Analysis :

a. Undrained Analysis : The results of the undrained analysis of horizontal strip anchor are presented in Table 4.6 for full bonding and full separation of anchor and underlying soil.

The soil models used for the undrained analysis are Von-Mises and Tresca. In the case of undrained analysis because $\phi = 0$, the Mohr-Coulomb model reduces to the Tresca model. The material is assumed to be perfectly plastic. If the coefficient of lateral earth pressure at rest (K_0) is assumed as equal to unity then the initial stresses due to weight of the material will not effect the elasto-plastic response. The criterion of yielding is not effected by an increase in volumetric stress. So, if K_0 is set equal to unity, the analysis with stresses due to weight of material and with initial stresses assumed equal to zero will produce the same response and the numerical limit load on the anchor. The effect of initial stresses will be felt only if K_0 is not equal to unity.

Relative stiffness values equal to 1,10 and 100 are used with Von-Mises criterion (R.No. 1, R.No.2 and R.No.3 in Table 4.6).

Table 4.6

Elasto-plastic undrained analysis - horizontal strip anchor

R.No.	Model	Mesh	Properties	Conv. crit. (%)	K _r	K _o	No.of incr.	F _y (KN/m)	F _u (KN/m)	CPU time in DEC-1090 (mts)
1	Von-Mises	1	Full bonding E=104 KN/m ² G=20 KN/m ² ν=0.48	1	1	1.0	25	110	250	12.45
2	-do-	1		1	10	1.0	25	110	250	12.42
3	-do-	1		1	100	1.0	24	110	240	12.03
4	-do-	1		1	10	0.5	24	110	240	11.87
5	-do-	3		1	10	1.0	25	140	250	6.15
6	-do-	4		1	10	1.0	28	150	280	2.05
7	-do-	1		0.1	10	1.0	23	110	230	11.37
8	-do-	1		1	10	1.0	13	120	260	8.67
9	-do-	1		1	10	1.0	6	120	240	5.37
10	Tresca	1		1	10	1.0	23	90	230	14.20
11	-do-	1		1	10	0.5	23	100	230	13.38

contd....

R.No.	Model	Mesh	Properties	Conv. crit. (%)	K _r	K _o	No.of incr.	P _y (KN/m)(KN/m)	P _u (KN/m)	CPU time in DEC-1090 (mts.)
12	Von-Mises	2	Full separation E=10 ⁴ KN/m ² C=20 KN/m ² v=0.48	1	1	1.0	23	25	57.5	9.75
13	-do-	2		1	10	1.0	23	22.5	57.5	10.13
14	-do-	2		1	100	1.0	23	22.5	57.5	9.96
15	-do-	2		1	10	0.5	22	22.5	55.0	9.08
16	Tresca	2		1	10	1.0	20	20.0	50.0	10.33
17	-do-	2		1	10	0.5	20	20.0	50.0	9.76

From the values reported in Table 4.6, it can be seen that the load at which the first point starts yielding is equal to 110 KN/m for all the three K_r values considered for analysis. For $K_r = 1$ and $K_r = 10$, the ultimate uplift loads obtained are the same and equal to 250 KN/m. For $K_r = 100$, the ultimate uplift load is obtained as 240 KN/m which is 4 percent lower when compared to $K_r = 10$. Fig. 4.31 shows the load displacement response of strip anchor for $K_r = 1$, $K_r = 10$ and $K_r = 100$. The plot is made between the non-dimensional ratios P/CB versus δ_c/B , where δ_c is the vertical displacement at centre of anchor. The response curve shows a straight line segment and a non-linear segment which eventually becomes asymptotic with the x-axis at collapse. From the diagram, it can be seen for $K_r = 1.0$ and 10, the initial elastic response and the non-linear deformation response are different. But at ultimate stages the two curves merge and the limit load obtained is the same for $K_r = 1.0$ and 10.0. It can also be observed from the diagram that the curves for $K_r = 10.0$ and 100.0 are close except at the final stages. Although, the deformation response of anchor is effected by change in relative stiffness from $K_r = 1.0$ to 100.0, the load at which the yielding of element starts and the limit load of anchor are not significantly affected by this variation. Hence, $K_r = 10.0$ is chosen for all subsequent analyses.

Table 4.7 summarises the load displacement results of the R.No. 2, with $K_r = 10.0$ using Von-Mises criteria. The load is

Table 4.7

Elasto-plastic undrained analysis - horizontal strip

Von-Mises criterion

$$\begin{aligned}
 E &= 1 \times 10^4 \text{ KN/m}^2 & K_r &= 10.0 \\
 C &= 20 \text{ KN/m}^2 & K_o &= 1.0 & \text{Full bonding} \\
 \nu &= 0.48
 \end{aligned}$$

Load (KN/m)	δ_c (m)	Number of iterations
10	0.1677×10^{-3}	1
100	0.1677×10^{-2}	1
110	0.1852×10^{-2}	4
120	0.2028×10^{-2}	4
130	0.2211×10^{-2}	4
140	0.2414×10^{-2}	7
150	0.2660×10^{-2}	8
160	0.2986×10^{-2}	12
170	0.3407×10^{-2}	18
180	0.3867×10^{-2}	19
190	0.4438×10^{-2}	27
200	0.5121×10^{-2}	31
210	0.5988×10^{-2}	43
220	0.7167×10^{-2}	62
230	0.9511×10^{-2}	84
240	1.0550×10^{-2}	170
250	2.3000×10^{-2}	200

applied in 25 equal increments. The load, vertical displacement at centre of anchor and the number of iterations for satisfying the convergence criterion for residual load vector are also given for every increment. Upto a load of 100 KN/m, one iteration is needed because all the elements are elastic. The load at which the first point yields is 110 KN/m and as the load level increases more and more points yield and the number of iterations needed to satisfy convergence criterion also increases. The load at which the solution fails to converge even after executing the specified maximum number of iterations is taken as the numerical limit load of the strip anchor which turned out to be 250 KN/m. In an incremental iterative technique like 'initial stress' method, used for the solution of the non-linear problem here, the limit load will be effected by the maximum number of iterations allowed within an increment. Referring to Table 4.7, if the maximum number of iterations were fixed at 50, the time for solution and hence, cost of analysis will be less but the limit load would have been 220 KN/m. This is less than 12 percent of the value reported with number of iterations fixed at an upper limit of 200. It can not be stated, whether a higher limit of iterations than 200 will increase the limit load at all. If 250 KN/m is the true limit load then more number of iterations may make the cost of analysis higher but may not refine the load. Hence, both cost of analysis and accuracy of the solution needed are to be considered in fixing the maximum number of iterations in elasto-plastic analysis by 'initial stress' technique. One iteration more means a

resolution in solution and all the necessary steps involved for this in elasto-plastic analysis.

For R.Nc.2, specified in Table 4.6, the spread of yielded points with load is given in Fig. 4.34. Due to the uplift load, the vertical stress below the anchor is tensile and above the anchor is compressive. Moreover, the magnitude of the tensile vertical stress developed is more in the elements below the anchor. The points below the anchor and at the sides yield first as is seen from Fig. 4.34a. At $P = 160 \text{ KN/m}$, more points in elements below the anchor reach plastic state. Fig. 4.34f shows the points which have yielded at failure load equal to 250 KN/m . From an observation, it can be made out that more points below the anchor have reached the plastic state than points above the anchor.

The velocity field at limit load is shown in Fig. 4.36. Because of the perfect bonding below the anchor, it is evident that the elements below the anchor also participate in deformation and a general mechanism like the Prandtl mechanism may form if the depth of layer below anchor is more than what is used in the present analysis. All the approximate shallow anchor theories base their calculation on the resistance of soil above anchor. If full bonding is assumed the elements below the anchor as well become important and the response of anchor and spread of yield zone are affected considerably.

If $K_0 = 1$ is used, it is equivalent to presence of zero initial stresses as far as response obtained by Von-Mises and Tresca models are concerned, because an increase in volumetric stress does not affect the yield. If the coefficient of lateral earth pressure is set equal to a value not equal to unity, there will be initial deviatoric stresses due to the weight of the material. Also, the elements at a greater depth from top will be stressed more than elements near the surface. To study the effect of initial stresses, $K_0 = 0.5$ is used with $\gamma = 16 \text{ KN/m}^3$. It is seen that using Von-Mises model, the load at which the first point yields is unaffected by the initial stresses. It is also seen that the ultimate uplift load obtained was reduced by 4 percent when compared to the case where the initial stresses due to weight of the material were zero.

To study the effect of mesh refinement Mesh-1, Mesh-3 and Mesh-4 given in Figs. 4.30a, 4.30c and 4.30d are used. For $K_r = 10$ and full bonding case the comparison is made using Von-Mises model. For Mesh-1, Mesh-2 and Mesh-3, the number of nodal points are 251, 147, 79 and number of elements are 72, 40 and 20 respectively. When Mesh-3 is used for the analysis which is cruder than Mesh-1, it is seen that the load at which the first yield takes place is increased to 140 KN/m from 110 KN/m for Mesh-1. The numerically obtained limit uplift load is unaltered. For Mesh-4, which is the crudest one the load at first yield as well as the uplift load obtained are greater than

obtained using Mesh-1. The increase in uplift load is about 12 percent more than that from using Mesh-1. Hence, fixing up an optimum mesh for the given problem for obtaining correct limit loads are extremely important in elasto-plastic analysis. The limit load obtained with a finer mesh usually is less than using a coarser mesh.

Convergence criterion used is based on the maximum value of the residual load vector. The criterion is fixed as 1 percent of the load applied in one increment. If the maximum residual load vector is below this limit then it is deemed that the solution has converged and next increment of load is applied. Specification of a stricter criterion will necessitate more iterations within an increment to satisfy the criterion for convergence. Because the failure is specified by maximum number of iterations allowed within a load increment, specification of a strict criterion for convergence may indicate a numerical limit load which is less. It may be seen from Table 4.6 (R.No.6) that a criterion of $\frac{1}{1000}$ (0.1 percent), reduces the limit load to 230 KN/m which is 8 percent less than the load for a criterion of $1/100$ (1 percent). More number of iterations within an increment and the lower limit load are possible results of a strict convergence criterion.

For the computer run shown in Table 4.6 (R.No.2), the load increment is set equal to 10 KN/m. To study the effect of load increment on the response, two cases were studied in which the

increment of load in each step is increased to 20 KN/m and 40 KN/m respectively in R.No. 8 and R.No.9. Fig. 4.32, also shows the points on the load deformation curve due to these two cases investigated. It is seen that the points lie on the curve obtained for R.No.2 with load increment fixed at 10 KN/m. The ultimate uplift loads obtained are 260 KN/m and 240 KN/m respectively and are not very different from the loads obtained for the case where an increment of 10 KN/m is used and the total load to reach ultimate load is applied in 25 equal increments. Using 'initial stress' method with sufficient number of iterations allowed within an increment the displacement response and limit load are not significantly effected by applying the total load in smaller number of increments.

Figure 4.32 shows the load displacement graph for Von-Mises and Tresca criteria for R.No.2 and R.No.10 in Table 4.6. It is seen that the deformation response above elastic state, the curve for Tresca model falls below that of Von-Mises model. It is also seen that the load at which the first point yields and the failure load are smaller than those for Von-Mises criterion. The limit load obtained is 230 KN/m which is 8 percent less than the load obtained by using Von-Mises model. It is also seen that the initial stresses developed due to weight of the material with $K_0 = 0.5$ do not effect the failure load of the strip anchor when Tresca criterion is used for elasto-plastic analysis.

Mesh-2 is used for finite element analysis of problem with full separation at the anchor bottom due to uplift load. It is clear that the three relative stiffnesses used namely $K_r = 1.0$, $K_r = 10$ and $K_r = 100.0$ do not effect the limit loads obtained. The limit load obtained is only 23 percent of the load for the case of full bonding. The load at which the first point yields is only 1/5 of the corresponding full bonding case. Fig. 4.33, shows the load deformation response of the strip anchor for $K_r = 1$, 10 and 100. Although the response at lower levels for $K_r = 1.0$ and $K_r = 10$ are not the same the response at limit state for all the three relative stiffness values approaches same curve separation of the anchor from the underlying soil effects the response, load at first yield and also the failure load obtained, significantly. For the value of $K_0 = 0.5$, it is seen that due to presence of initial stress in soil due to the weight, the uplift load is slightly reduced use of Tresca criterion results in loads which are smaller than those obtained by using Von-Mises, for full separation case also.

The spread of zone of yield with the increase in load for the case of full separation is shown in Fig. 4.35. It is seen that when compared to full bonding case, the points which reach plastic state are above the anchor and on the sides. The spread of yield zones is not considerable and it appears, from this figure and also from Fig. 4.37 in which the velocity field at

failure is given, that the yielding and uplift are localized. The elements which are away from the anchor on the sides, the displacements are also small. The circular rupture surface for $\phi = 0$, assumed for calculations in Strip Theory-1 and Strip Theory-2 presented in Chapter.7 is also shown in Fig. 4.37.

It is useful to compare the magnitude of ultimate uplift load obtained from the elasto-plastic analysis of strip plate anchor with the values of loads from other approximate theories. The strip anchor theories presented in Chapter 7 are used for this purpose. For the $\phi = 0$ case and $D/B = 1.0$, the following table summarises the results.

Table 4.8
Results from Strip Anchor Theories

	F_c	F_q	BCF_c (KN/m)	$P_u = B(C F_c + \gamma D F_q)$ (KN/m)
ST-1	2.00	1.26	40.0	60.2
ST-2, Vesic(101)	1.61	1.00	32.2	48.2
Meyerhoff and Adams (58)	2.00	1.00	40.0	56.0

The limit load obtained by elasto-plastic analysis using Von-Mises criterion and Tresca criterion are 250 KN/m and 230 KN/m for full bonding case and 57.5 KN/m and 50 KN/m for full separation case. In the derivation of all the theories

mentioned in Table 4.8, it is assumed that the resistance of soil above the anchor along an assumed rupture surface and the weight of soil enclosed within the wedge contributes to breakout resistance. The full bonding case gives very high load when compared to the loads obtained from approximate theories.

If $K_0 = 1$, the same uplift load will be obtained whether the weight of the material is considered or not in both Von-Mises and Tresca criteria. Hence, if it is assumed that the uplift resistance using these models is only due to cohesion then the magnitude of 57.5 KN/m obtained is higher than 'BC F_c ' contribution given in Table 4.8. It can be concluded that a full bonding case does not represent a realistic interface condition at collapse and the results of collapse loads obtained are very high in comparison to the approximate anchor theories. The collapse load obtained from assuming a full breakaway of anchor gives a collapse load nearer in magnitude to those obtained from shallow strip anchor theories but their magnitudes are still more than those predicted by these theories.

b. Drained Analysis : Mohr-Coulomb perfectly plastic model is used in this analysis. The results of the different cases investigated are given in Table 4.9. The yield criterion depends on the magnitude of the normal stress and a density value equal to 16 KN/m^3 is used in the analysis. K_0 equal to 1.0 is used except in two cases where the effect of change of K_0 on response is studied. A relative stiffness value of 10.0 is used throughout the analysis.

Table 4.9

Elasto-plastic drained analysis - horizontal strip anchor, Mohr-Coulomb Model

R.No.	Mesh	Properties	Conv. crit. (%)	K _r	K _o	No.of incr.	P _y (KN/m)	P _u (KN/m)	CFU time in DEC-1090 (mts)
1	1	Full bonding $\tau = 2 \times 10^5 \text{ KN/m}^2$ $\nu = 0.3$, $\gamma = 16 \text{ KN/m}^3$ $C = 0, \phi = 30^\circ$	1	10	1.0	18	6	36	18.78
2	1		1	10	0.5	18	2	36	14.53
3	3		1	10	1.0	18	6	36	5.43
4	4		1	10	1.0	17	10	34	11.03
5	1		0.1	10	1.0	14	6	28	8.62
6	1		0.01	10	1.0	14	6	28	8.80
7	1		1	10	1.0	9	8	36	11.53
8	1		1	10	1.0	5	8	40	7.40
9	1	Full separation $C=0, \phi=30^\circ$	1	10	1.0	15	2	15	14.10
10	1	$C=0, \phi=40^\circ$	1	10	1.0	18	2	18	24.37
11	1	$C=0, \phi=45^\circ$	1	10	1.0	20	2	20	24.27
12	1	$C=0, \phi=30^\circ$	1	10	0.5	12	1	12	20.20
13	1	$C=20 \text{ KN/m}^2, \phi=30^\circ$	1	10	1.0	30	24	60	24.10

Figure 4.38, shows the load displacement of the strip anchor, with material properties as specified and $C = 0$, $\phi = 30^\circ$, for full bonding and full separation. The vertical deformation of centre of anchor for full bonding does not deviate from the straight line even upto an applied load of 26 KN/m. After this load is reached the deformations increase suddenly and failure indicated at a load of 36 KN/m. The load at first yield is 6 KN/m and the ratio of limit load/yield load for Mohr-Coulomb criterion is 6 where as for the undrained models for $\phi = 0$ case, the ratio is about 2.2. The ultimate uplift load obtained with full separation below the anchor is only 15 KN/m. The load deformation response of the anchor for this case is also shown in Fig. 4.37.

The spread of yield zone with increase in load for the case of full bonding is shown in Fig. 4.39. The points near the surface and directly above the anchor yield first as shown for $P = 20$ KN/m and $P = 24$ KN/m. The points in elements below the anchor and sides also yield with increase in load. The points that have reached plastic state under the final load of 36 KN/m are shown in Fig. 4.39f. Fig. 4.40 shows the spread of points which are yielded for full separation case. Because of the fact that elements above the anchor are stressed more, even at a load of 2 KN/m the first yield starts. The first points which yield, are the ones near the surface where the normal stresses due to weight of the material is the least. At load of 10 KN/m,

the points at the side of the anchor also start yielding. Fig. 4.40f shows the points yielded at limit load of 15 KN/m. Fig. 4.41 shows the velocity field for limit load of 15 KN/m for the case of full separation below the anchor. It is seen that the mechanism of failure is localised with participation of points directly above the anchor. In the same figure, the circular rupture surface assumed in strip anchor theories, ST-1 and ST-2 (Vesic) are also given.

A comparison of the two cases (R.No.1 and R.No.9 in Table 4.9) shows the load at which first point yields, the load deformation response of anchor and the limit load are significantly affected by the interface separation below the anchor.

Results obtained using Mesh-3 and Mesh-4 are given in R.No.3 and R.No.4 in Table 4.9. Using Mesh-3, it is seen that the load at first yield and the ultimate uplift load are unaffected when compared with results of Mesh-1. Using Mesh-4, it is seen that P_{yield} is higher and the ultimate uplift load on anchor is about 6 percent less when compared to results from Mesh-1. For the specific geometry and ϕ values the mesh refinement does not appear to significantly effect the ultimate load.

A convergence criterion of 1/100 on the residual load vector is used for R.No.1. A stricter criterion of 1/1000 and 1/10000 are used in R.No.5 and 6. It is seen that the specification of a stricter criterion of 1/1000 brings the ultimate

uplift load to 28 KN/m, about 17 percent less than the load with a criterion of $1/100$. When the criterion is fixed at $1/10000$ the limit load remains at 28 KN/m.

The load per increment applied for R.No.1 is 2 KN/m. The effect of an increased increment of load is seen in R.No.7 and 8. In R.No.7 the applied load per increment is 4 KN/m and in R.No.8, 8 KN/m. The yield load is slightly increased in both these runs but the ultimate uplift loads are unaffected with an increment of 4 KN/m. Since in R.No.8, each load step is 8 KN/m, the load obtained is 40 KN/m instead of 36 KN/m because the load steps are not fine enough. Using 'initial stress' technique with sufficient number of iterations within an increment it can generally be observed that the limit load is not significantly affected by the number of increments in which the load is applied. A first approximation to the limit load can always be achieved by employing a larger load in each increment. The result obtained can be refined further by going in for smaller load increments.

R.No.9, 10 and 11 show the results for full separation case with $C=0$ and $\phi=30^\circ, 40^\circ$ and 45° respectively. It can be seen that the yield load is not affected by the increase in angle of internal friction but there is an increase in numerical limit load on the anchor from 15 KN/m for $\phi = 30^\circ$ to 20 KN/m for $\phi = 45^\circ$. Table 4.10, gives the results of $\phi = 30^\circ$, $\phi = 40^\circ$ and $\phi = 45^\circ$ using Strip Theory-1 (ST-1), Strip Theory-2,

Vesic (101) and Meyerhof and Adams's theories (58). All these approximate theories take into account the weight of the soil wedge and the resistance of the soil developed along the rupture surface against uplift as contributing to limit load.

Table 4.10

Comparison of uplift load

	Uplift Load (KN/m)			
	ST-1	ST-2 Vesic (101)	Meyerhof and Adams(58)	Elasto-plastic analysis(full separation)
1. $C=0$, $\phi=30^\circ$	28.3	23.5	24.8	15.0
2. $C=0$, $\phi=40^\circ$	29.6	25.2	28.8	18.0
3. $C=0$, $\phi=45^\circ$	29.8	25.9	31.2	20.0
4. $C=20\text{KN/m}^2$ $\phi=30^\circ$	60.9	55.1	64.8	60.0

It may also be observed that the weight of the material contributes to a major part of soil resistance in all the above theories. It is seen that the limit loads obtained from the elasto-plastic analysis is less than the values obtained from the other simplified theories for $C = 0$. Analysis is also carried out for a C, ϕ soil and Table 4.10 also gives the ultimate uplift capacity from the different theories and elasto-plastic analysis. It is seen that the results from ST-2 (Vesic)

gives breakout load less than obtained from elasto-plastic analysis but the results from ST-1 and Meyerhoff and Adams's theories are greater.

4.4 Conclusions :

From the finite element elastic and elasto-plastic analysis of the strip anchor problem carried out, the following inferences are made.

For shallow flexible anchors subject to vertical uniform load the Poisson's ratio of the soil medium and the embedment ratio of anchor effect the vertical elastic deformation of anchor. The central vertical displacement of anchor decreases with an increase in Poisson's ratio from 0.2 to 0.49. For a particular layer depth of material the vertical displacement of anchor decreases as embedment ratio increases. The anchor break-away from soil below it significantly effects the deformation response and the stress distribution within the soil medium in which it is embedded. The simulation of rigid anchor by specification of equal displacements at nodal points where anchor is acting shows results which also follow the above trends. The vertical contact stress distribution above anchor in the case of anchor separation shows a variation similar to that obtained below a rigid surface footing.

Shallow anchor discretisation by continuum element shows that the relative stiffness (K_p) of anchor affects the displacement response subjected to uniform and central concentrated

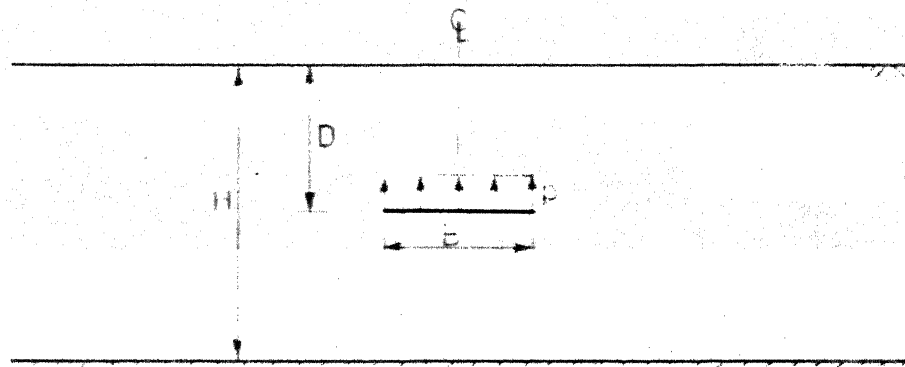
Elasto-plastic undrained progressive deformation analysis upto collapse can be carried out by Von-Mises or Tresca plasticity models. The 'initial stress' technique used for non-linear incremental analysis is found to be a satisfactory method.

The maximum number of iterations allowed within a load increment and the convergence criterion to be satisfied are important aspects in the non-linear analysis and a proper choice of these has direct bearing on the limit loads obtained from analysis as well as the cost of computer solution. With 'initial stress' technique even smaller number of load increments will give points on the load deformation curve. To obtain a smooth response variation and more refined limit load smaller increments of load have to be applied. The Tresca model gives the deformation response curve for anchor which falls below that obtained using Von-Mises model. The load at which first point reaches plastic state and the collapse loads obtained are also smaller than obtained using Von-Mises model.

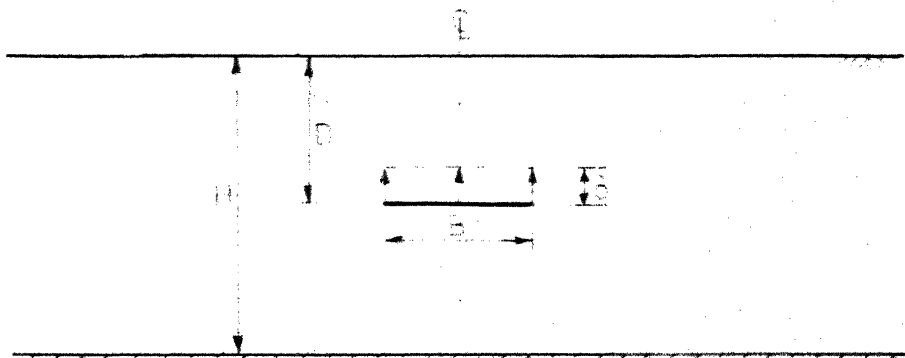
The deformation response, the load at first yield and the numerical limit load from elasto-plastic analysis using Von-Mises and Tresca criteria are effected considerably by anchor break-away at base. The full bonding situation, gives higher collapse loads for the elasto-plastic analysis when compared to the conventional strip anchor theories. With anchor breakaway the limit loads obtained are nearer to the results from strip anchor theories and the plastic zone obtained is localised to points

above the anchor. This is very well expected, since in all the theories the resistance from the soil above the anchor only brings the resistance against uplift.

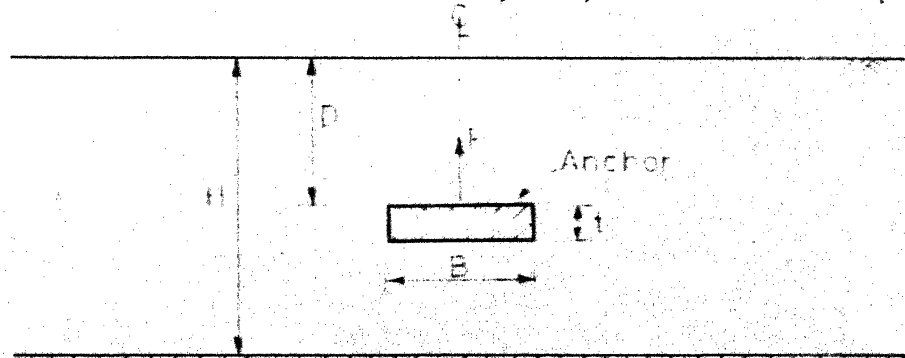
The progressive deformation behaviour of anchor upto collapse embedded in a frictional soil can be traced by finite element elasto-plastic non-linear analysis using associated Mohr-Coulomb criterion. The elements near the surface of the soil layer reaches plastic state first. The ratio of P_u/P_y is large for this criterion indicating onset of plastic state even at small loads. The full bonding below anchor gives collapse loads higher than predicted by shallow anchor theories. For full anchor breakaway the loads are smaller in comparison with the conventional theories for all the cases of ϕ values investigated. The anchor capacity increases with increase in angle of internal friction of soil. The limit loads obtained for C, ϕ soil in elasto-plastic analysis using Mohr-Coulomb model is in agreement and is within the range of values predicted by shallow strip anchor theories.



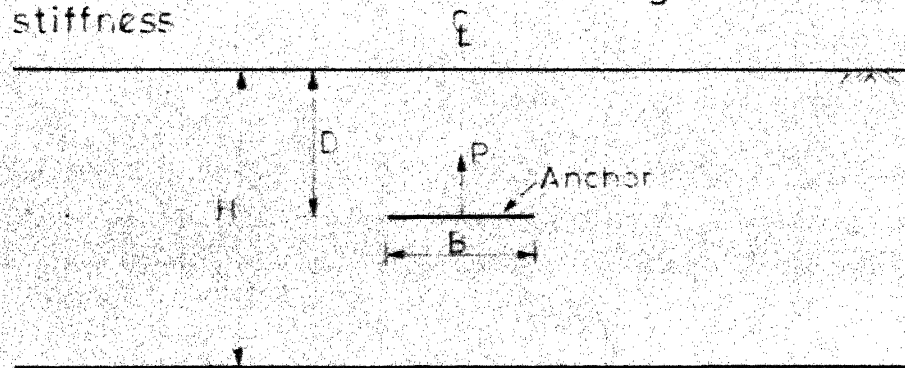
a. Flexible strip, uniform uplift pressure



b. Rigid strip simulation by imposed nodal displacement



c. Continuum element for simulating anchor of finite stiffness



d. Beam-column element for simulating anchor of finite stiffness

FIG. 4-1 SIMULATION OF ANCHOR BEHAVIOUR

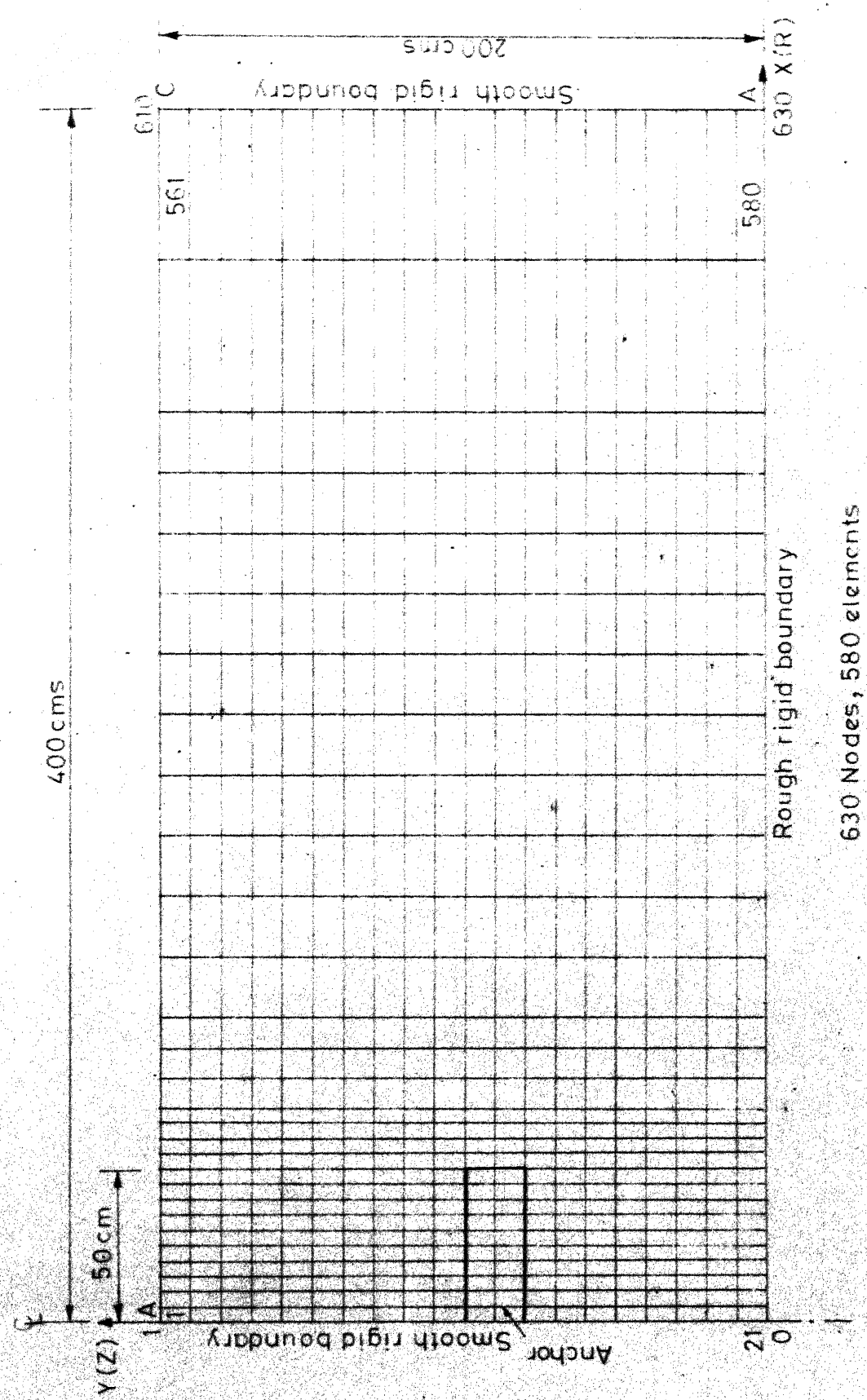


FIG.4.2 DISCRETISED MODEL OF SOIL LAYER OF FINITE DEPTH UNDERLAIN BY ROUGH RIGID BASE, MESH FOR ELASTIC ANALYSIS, FULL BONDING CASE

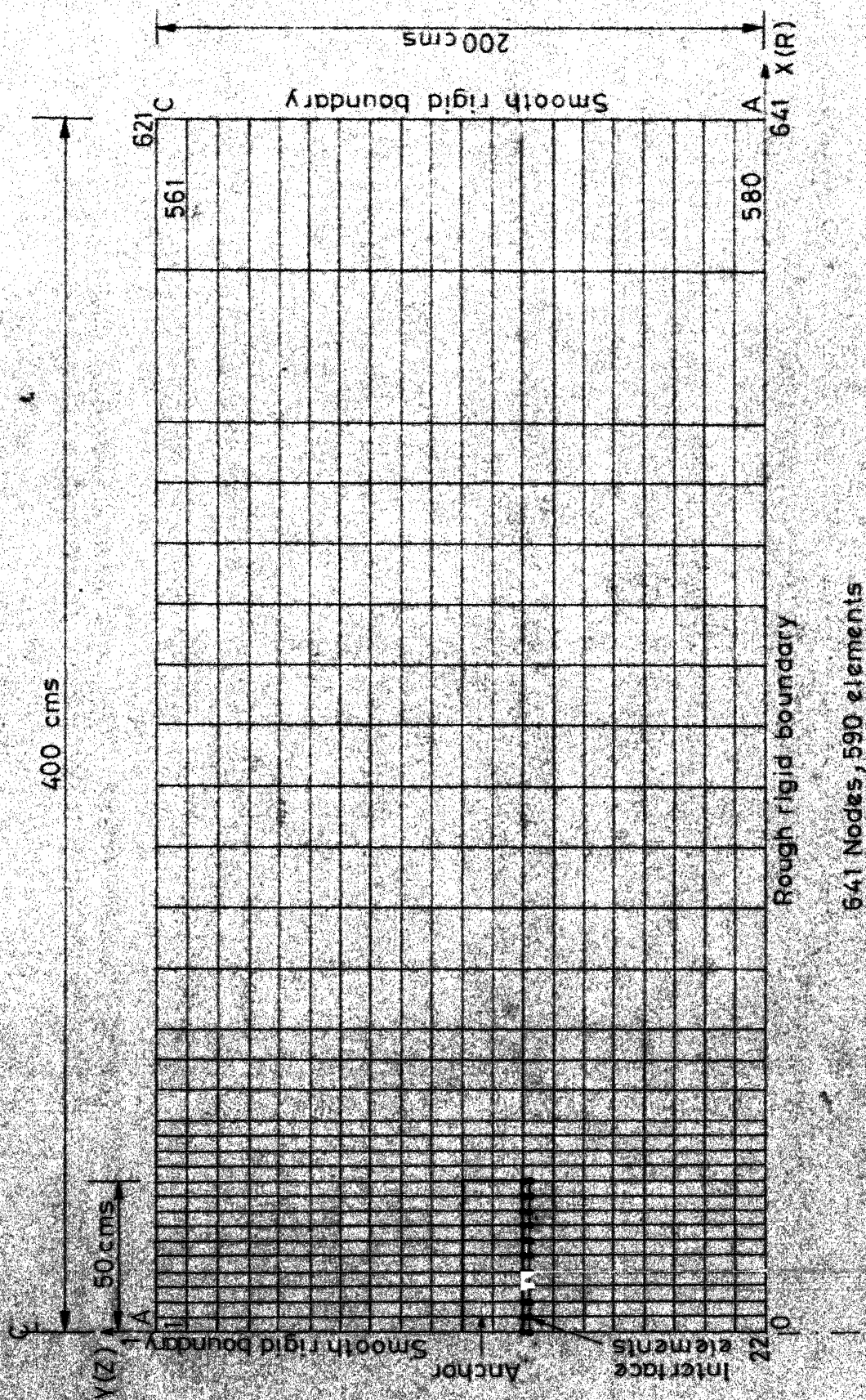


FIG. 4.3 DISCRETISED MODEL OF SOIL LAYER OF FINITE DEPTH UNDERLAIN BY ROUGH RIGID BASE, MESH FOR ELASTIC ANALYSIS, FULL SEPARATION

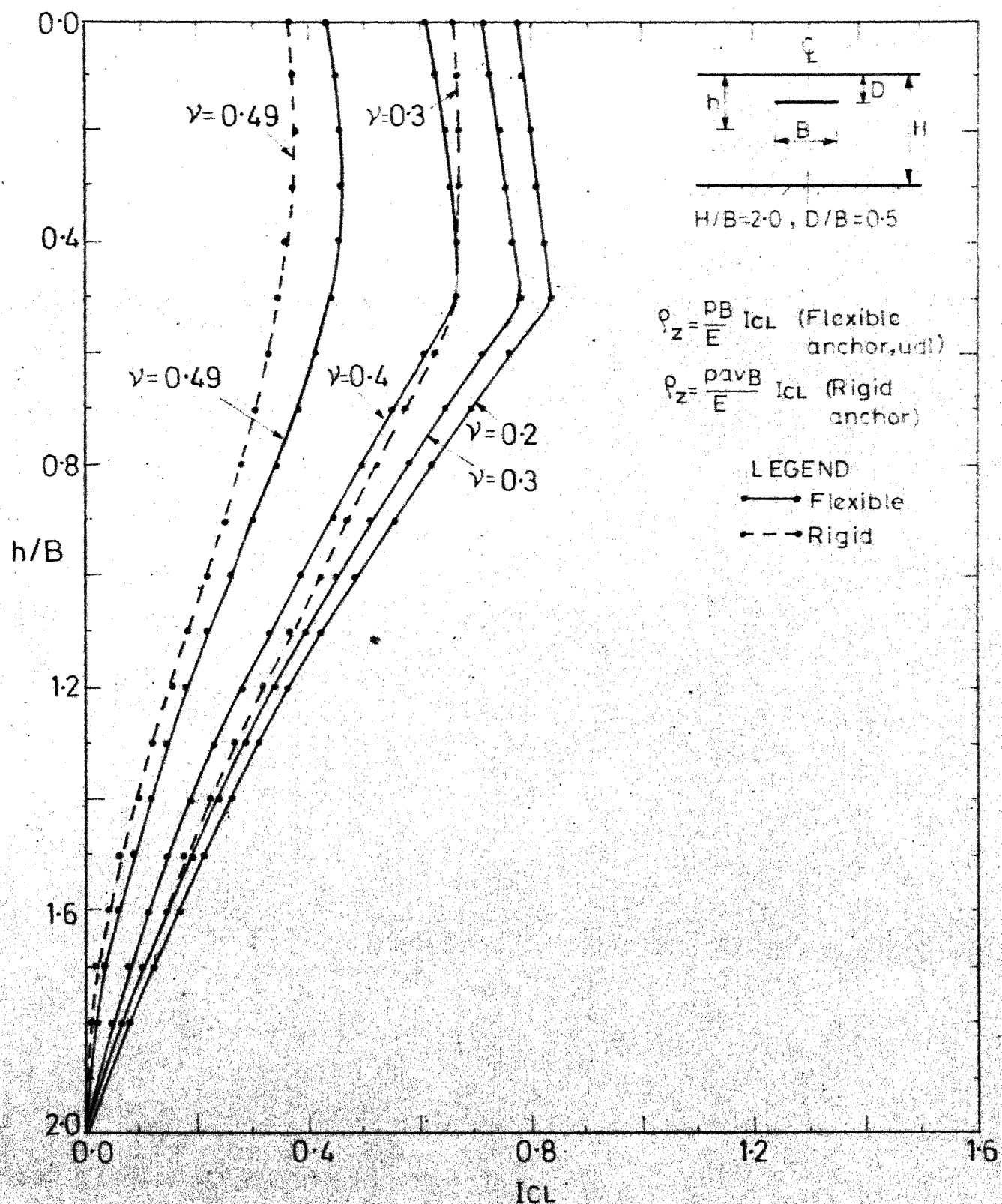


FIG. 4.4 VARIATION OF VERTICAL DISPLACEMENT WITH DEPTH
(HORIZONTAL STRIP, FULL BONDING, $H/B=2.0$, $D/B=0.5$)

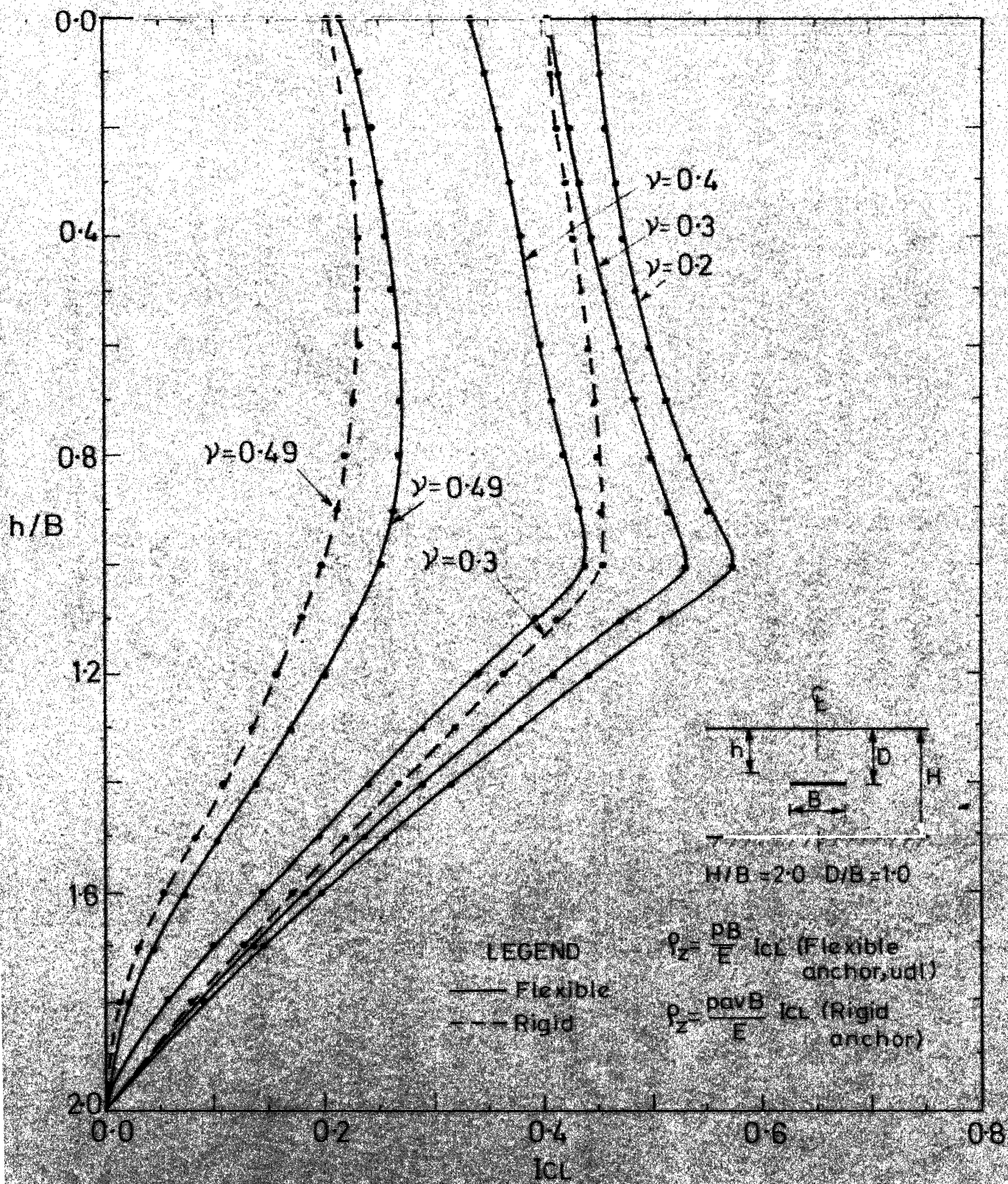


FIG. 4.5 VARIATION OF VERTICAL DISPLACEMENT WITH DEPTH
 (HORIZONTAL STRIP, FULL BONDING, $H/B = 2.0$, $D/B = 1.0$)

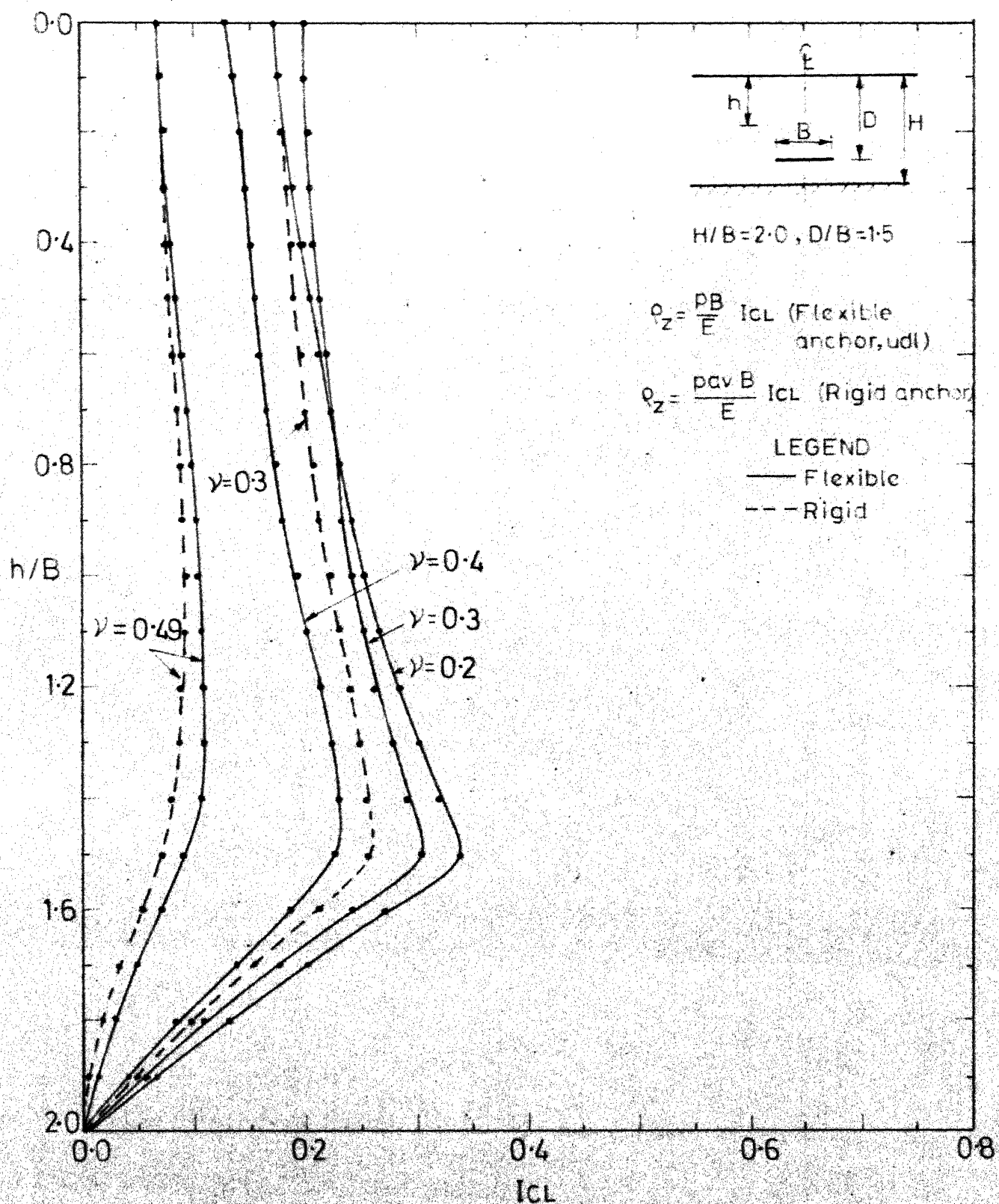


FIG-4-6 VARIATION OF VERTICAL DISPLACEMENT WITH DEPTH
(HORIZONTAL STRIP, FULL BONDING, $H/B=2.0, D/B=1.5$)

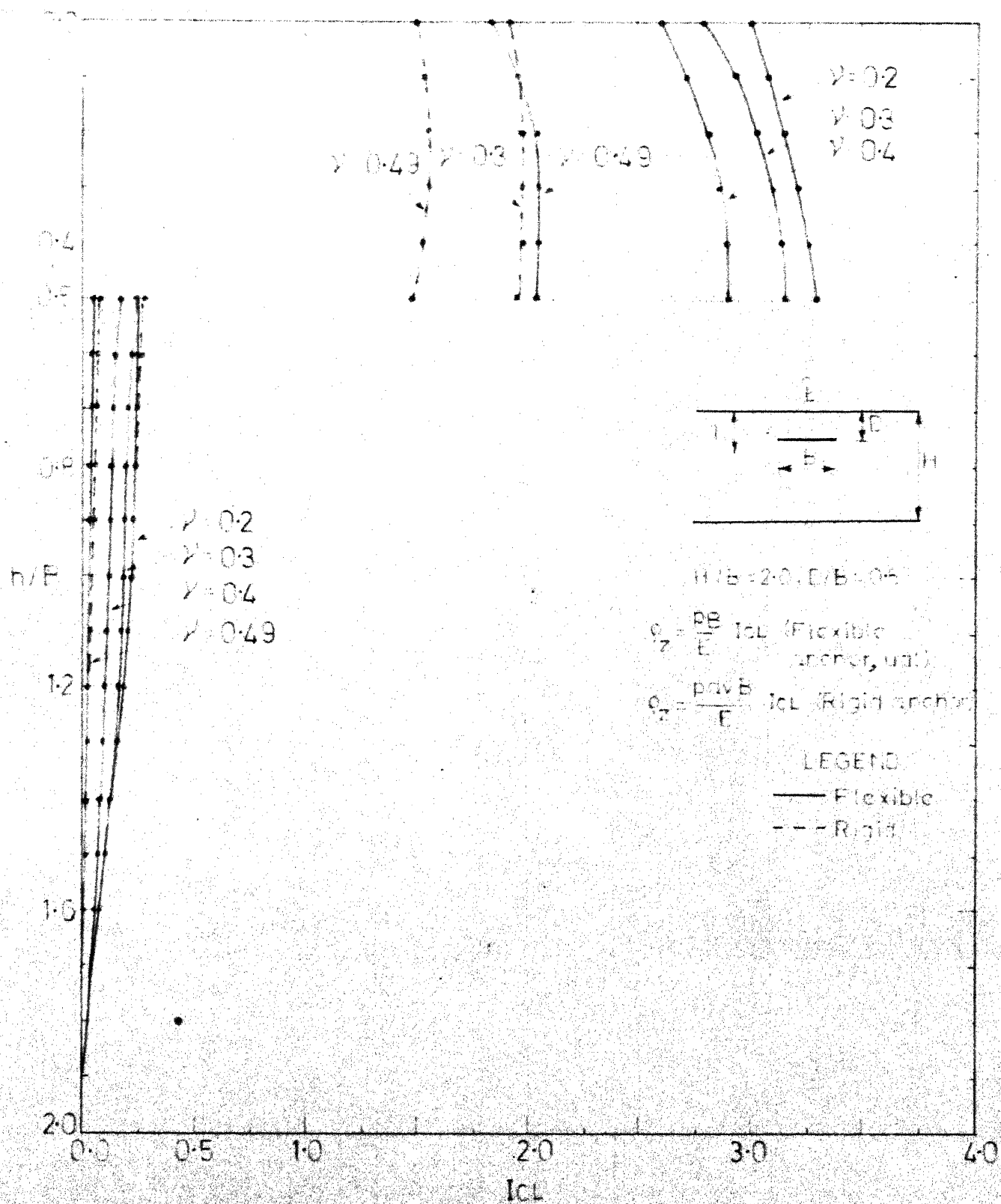


FIG. 4.7 VARIATION OF VERTICAL DISPLACEMENT WITH DEPTH (HORIZONTAL STRIP, FULL SEPARATION, $H/B=2.0$, $D/B=0.5$)

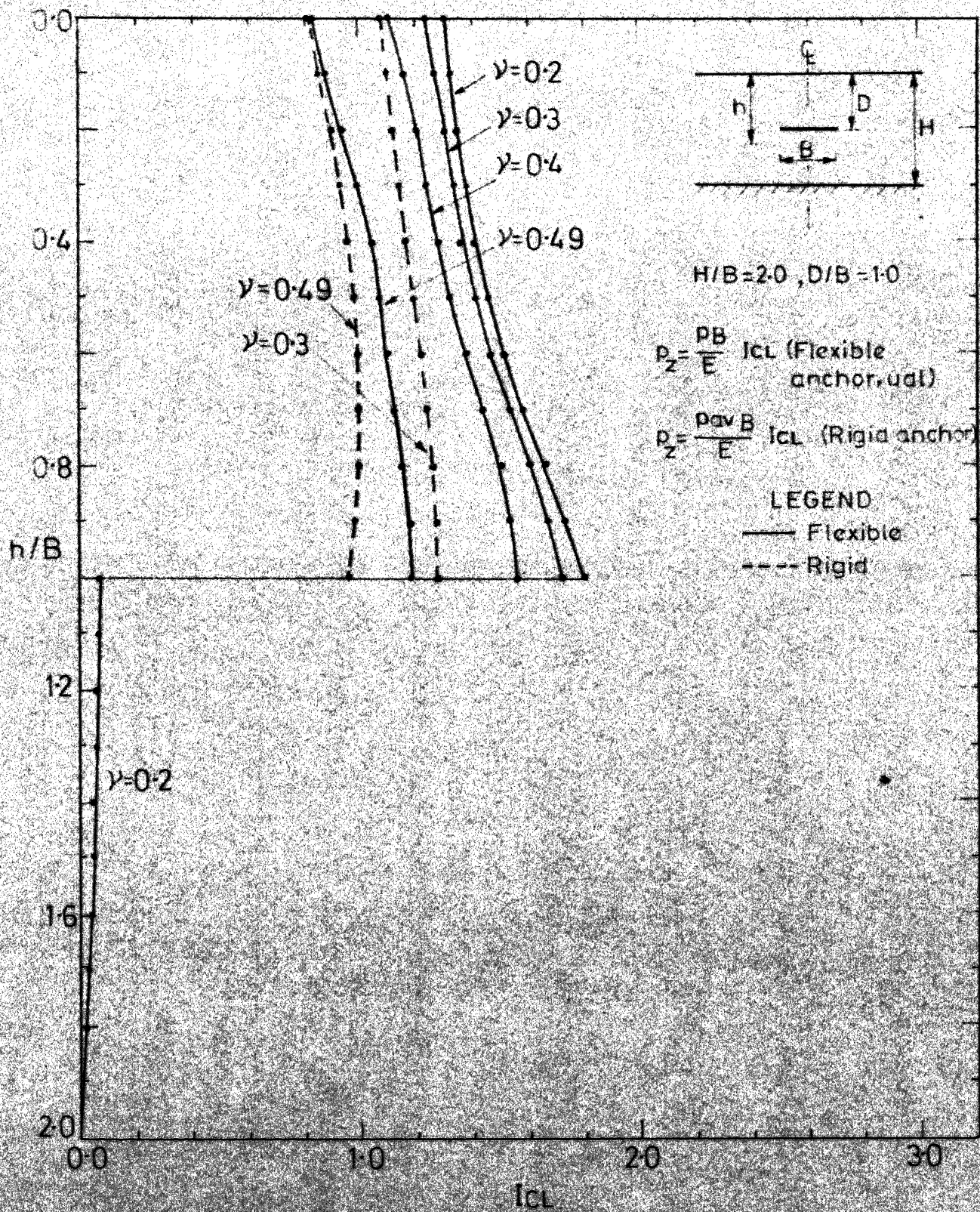


FIG. 4.8 VARIATION OF VERTICAL DISPLACEMENT WITH DEPTH
 (HORIZONTAL STRIP, FULL SEPARATION, $H/B=2.0$, $D/B=1.0$)

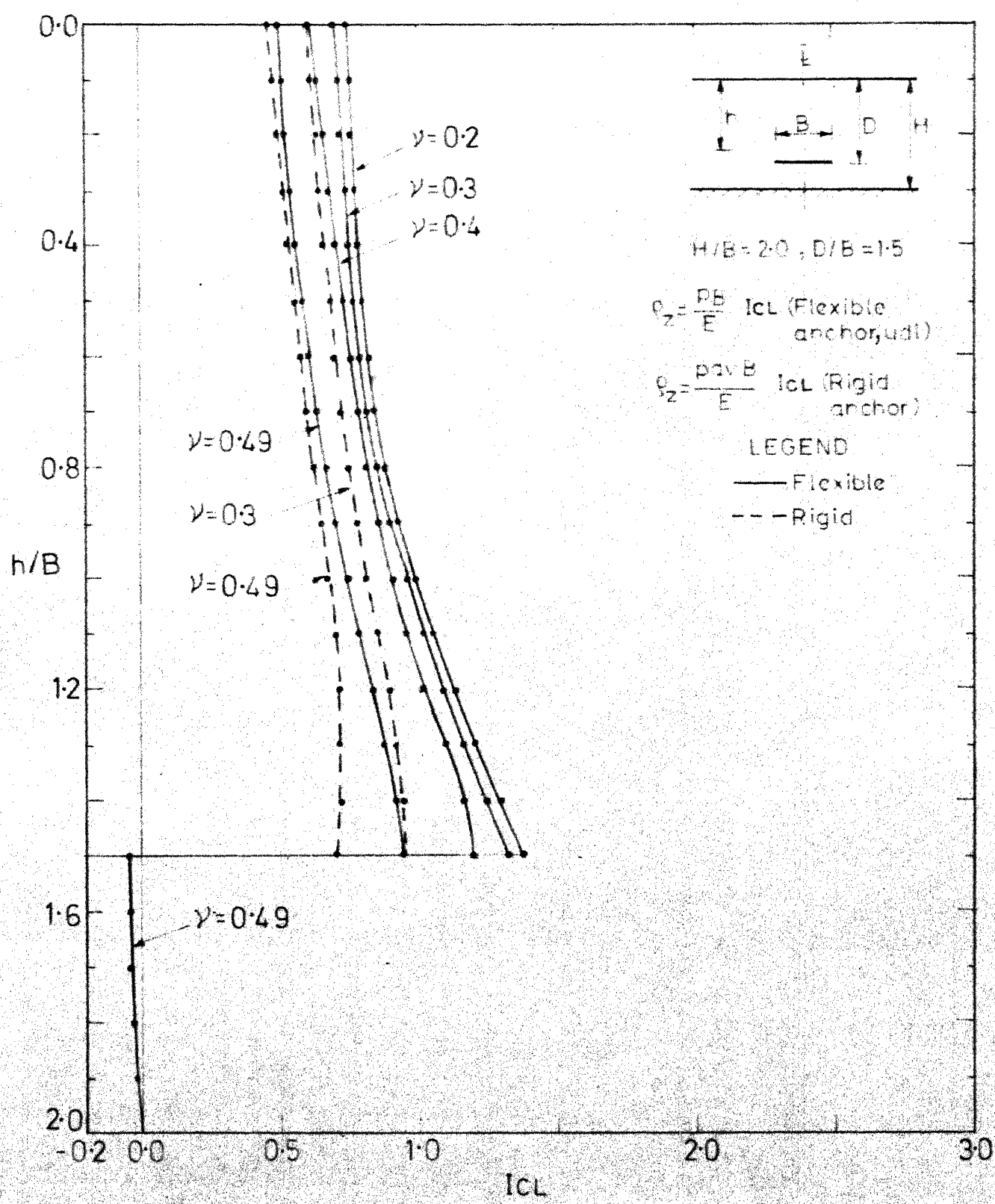


FIG-4-9 VARIATION OF VERTICAL DISPLACEMENT WITH DEPTH (HORIZONTAL STRIP, FULL SEPARATION, $H/B=2.0, D/B=1.5$)

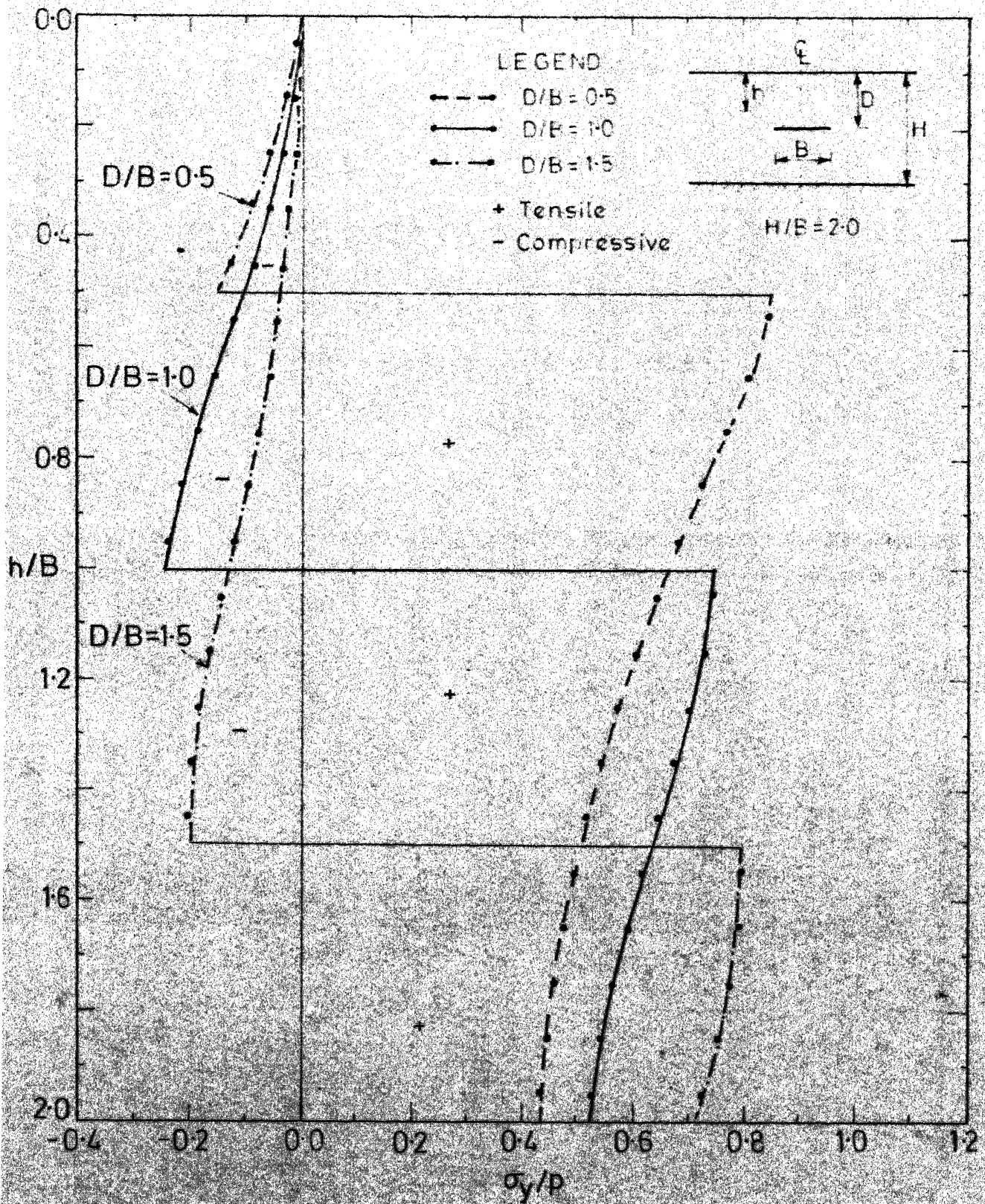


FIG. 4.10 VARIATION OF σ_y WITH DEPTH ALONG CENTRE LINE
(FLEXIBLE HORIZONTAL STRIP, FULL BONDING,
UDL, $\nu = 0.3$)

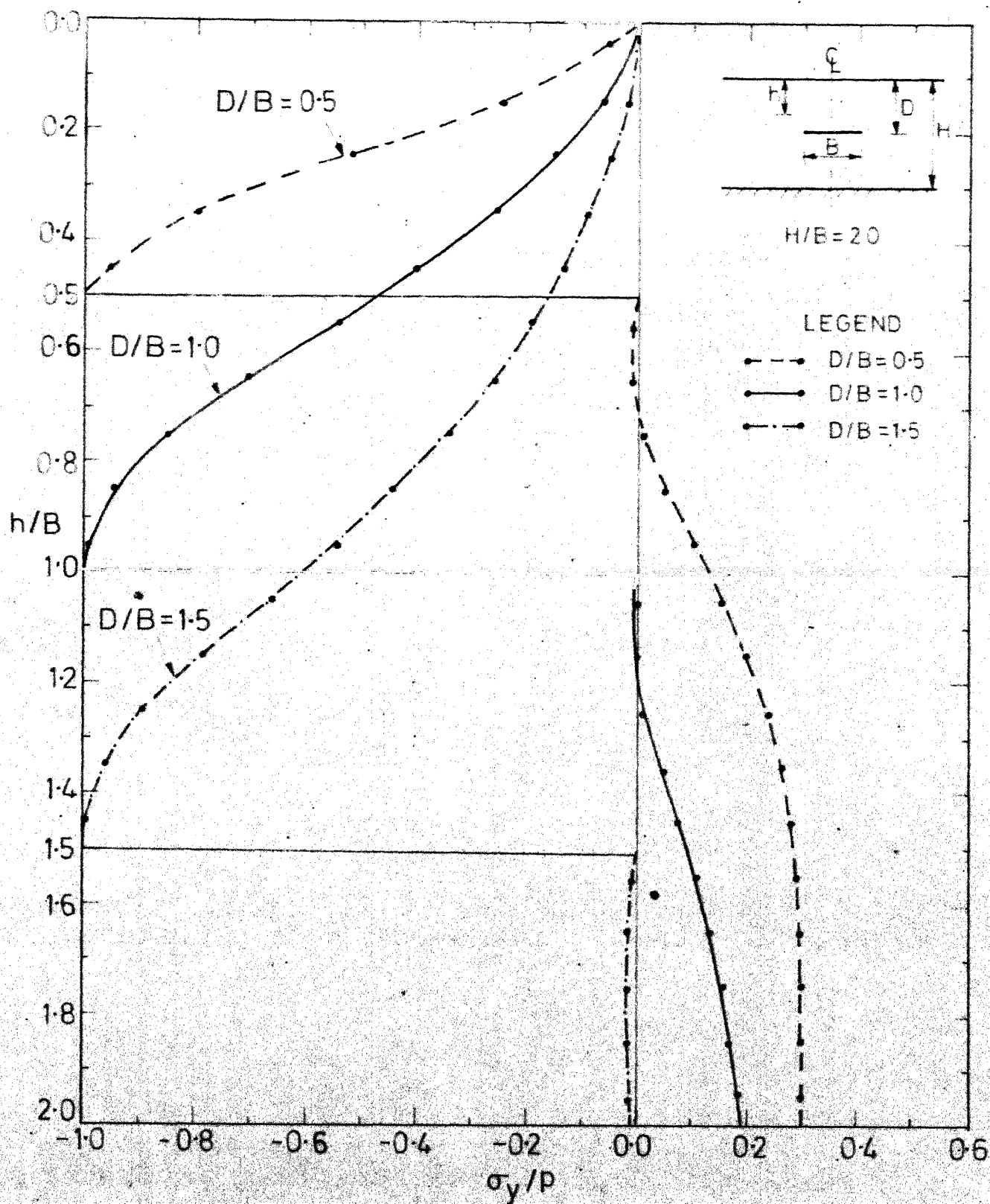


FIG.4.11 VARIATION OF σ_y WITH DEPTH ALONG CENTRE LINE
(FLEXIBLE HORIZONTAL STRIP, FULL SEPARATION,
UDL, $\nu=0.3$)

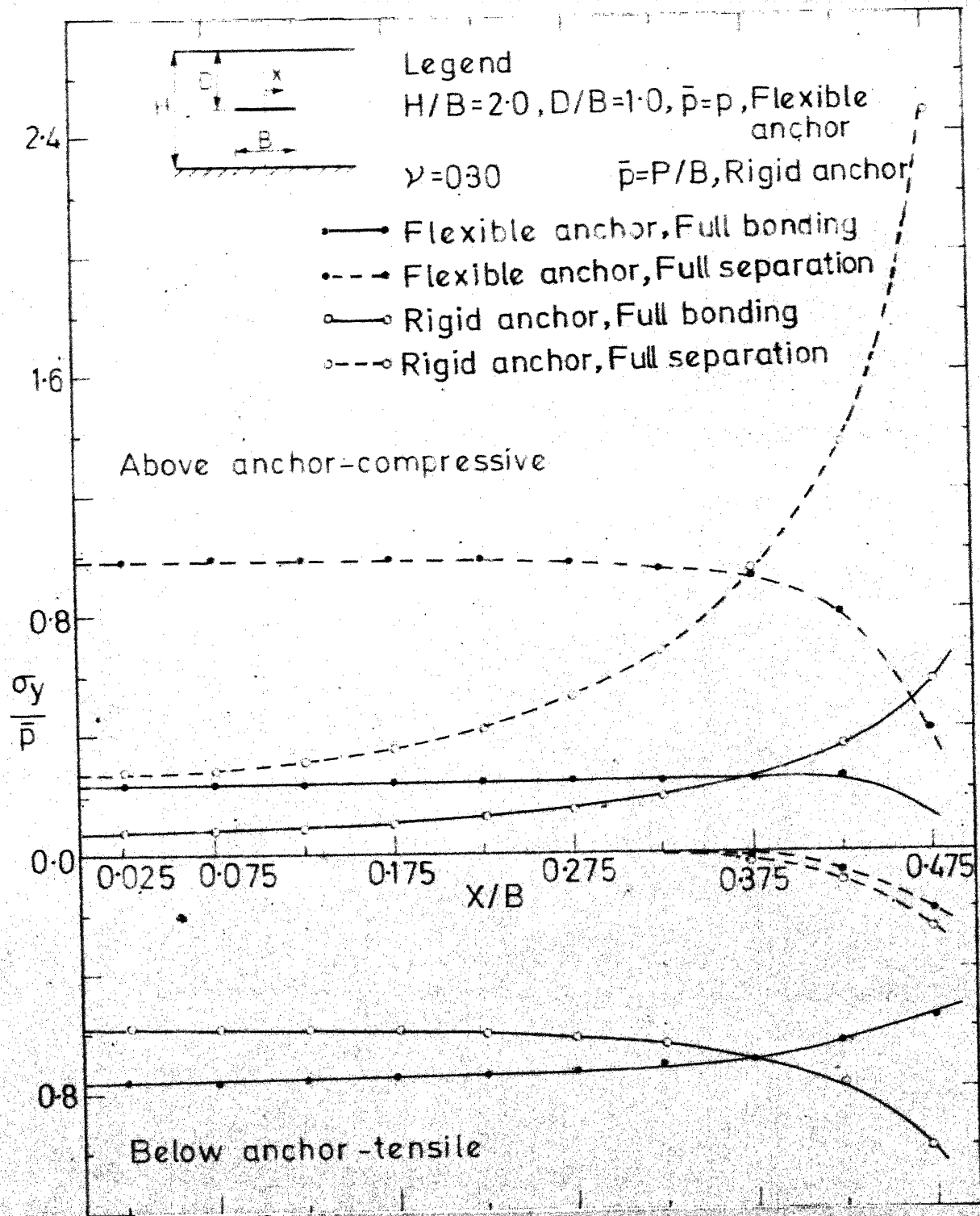


FIG. 4.12 VARIATION OF VERTICAL CONTACT STRESS
(HORIZONTAL STRIP, FLEXIBLE & RIGID ANCHORS,
 $\gamma = 0.3$)

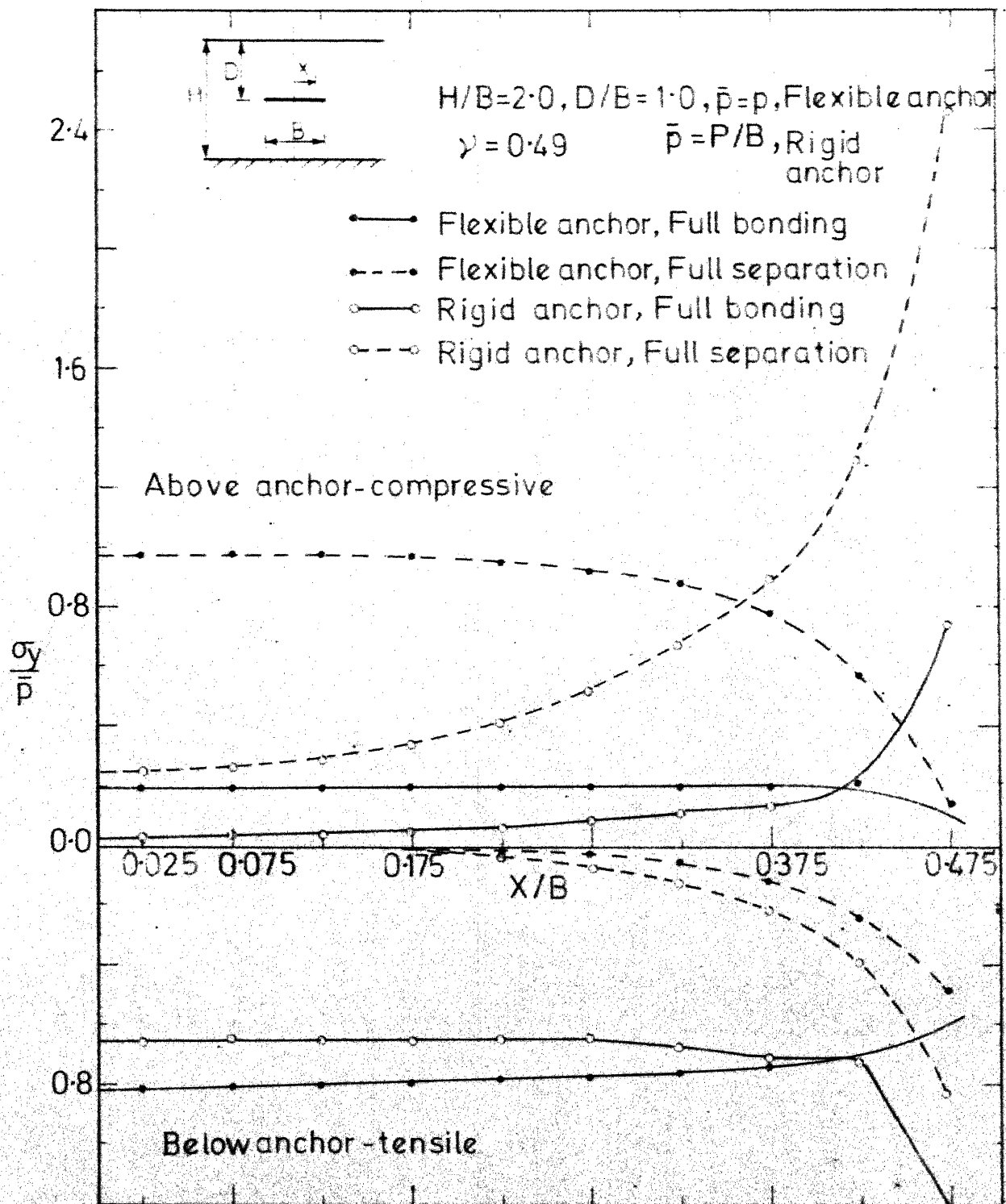


FIG. 4-13 VARIATION OF VERTICAL CONTACT STRESS (HORIZONTAL STRIP, FLEXIBLE & RIGID ANCHORS, $\nu=0.49$)

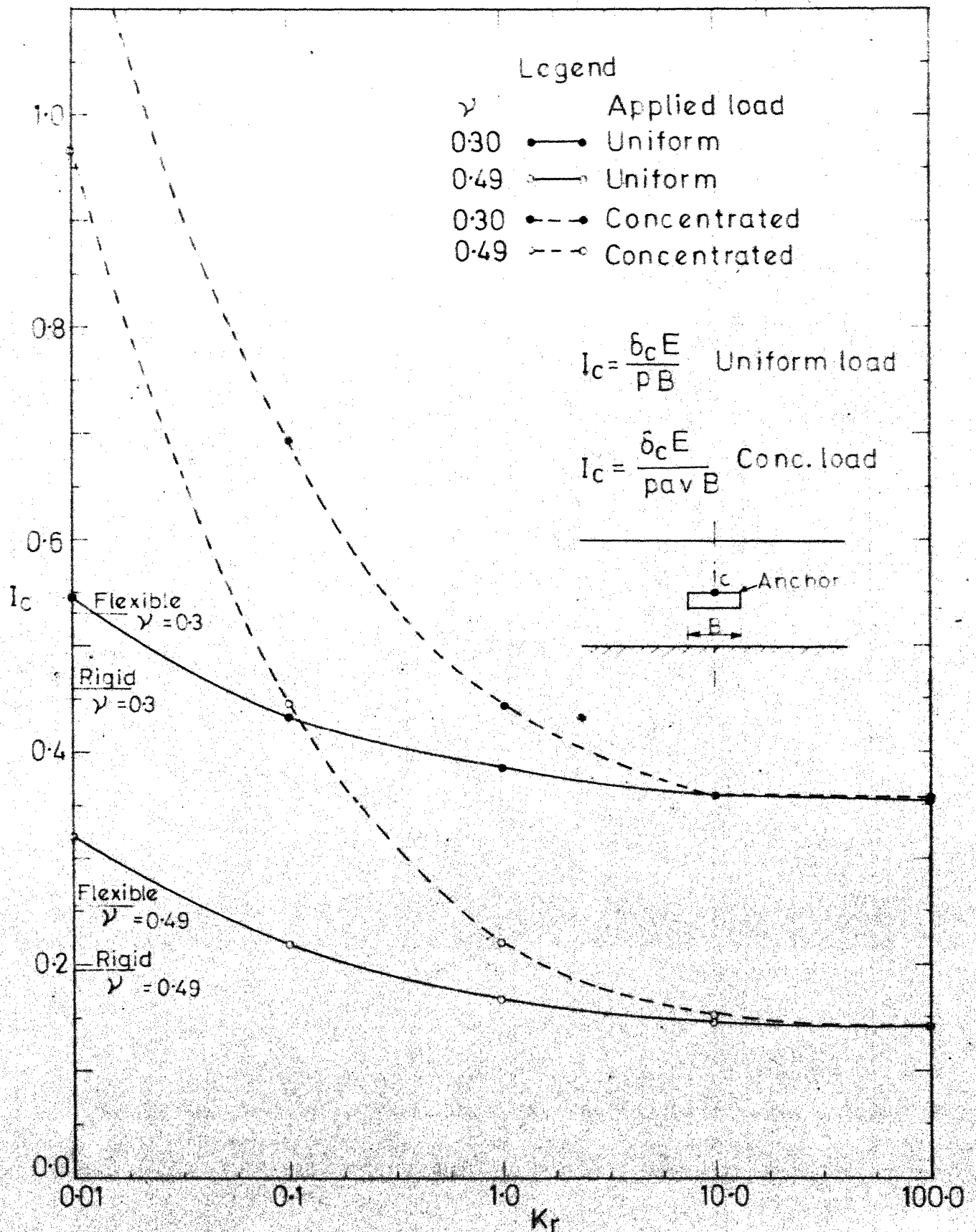


FIG. 4.14 VARIATION OF CENTRAL VERTICAL DISPLACEMENT OF ANCHOR WITH RELATIVE STIFFNESS (FULL BONDING, CONTINUUM ELEMENT)

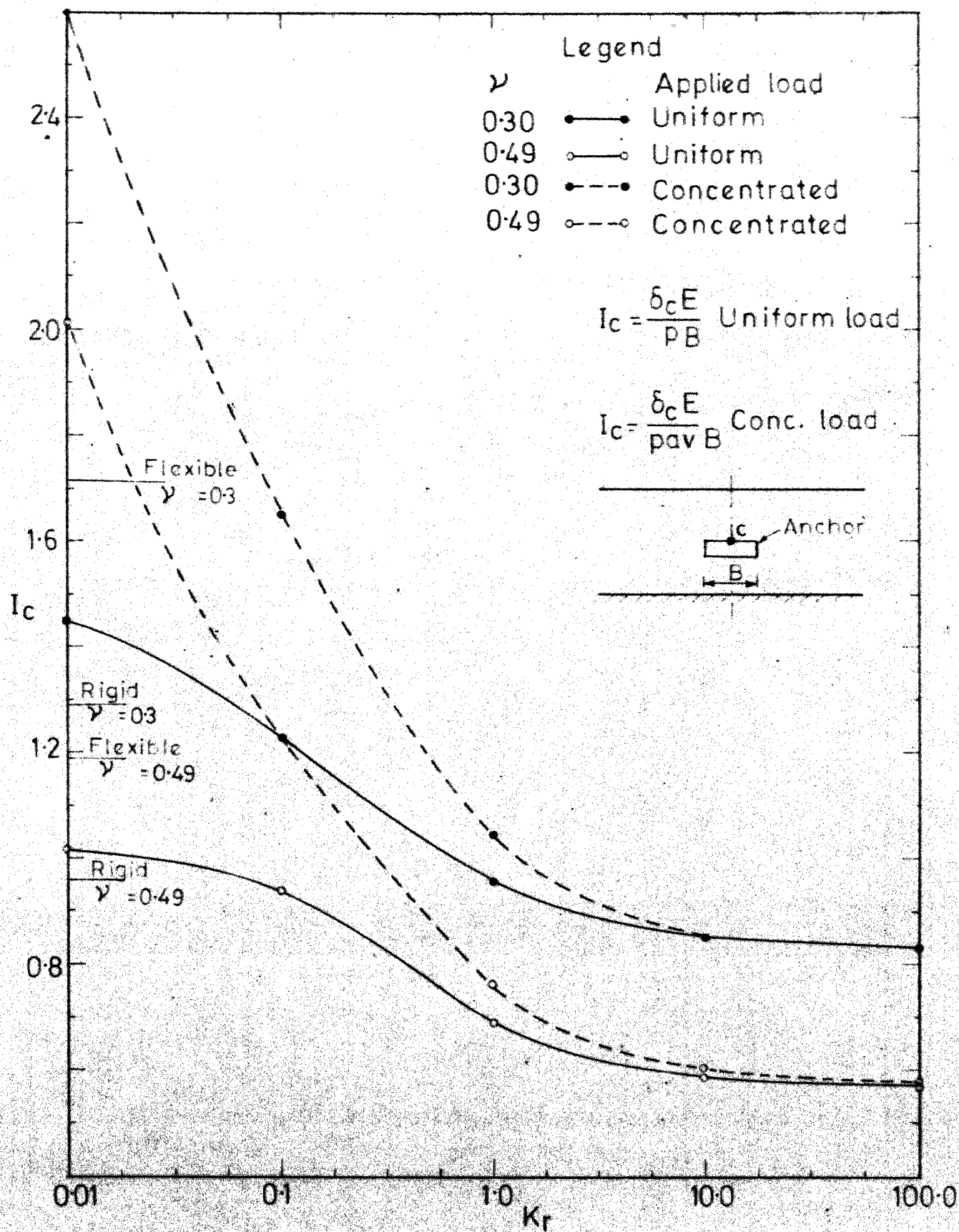


FIG. 4.15 VARIATION OF CENTRAL VERTICAL DISPLACEMENT OF ANCHOR WITH RELATIVE STIFFNESS (FULL SEPARATION, CONTINUUM ELEMENT)

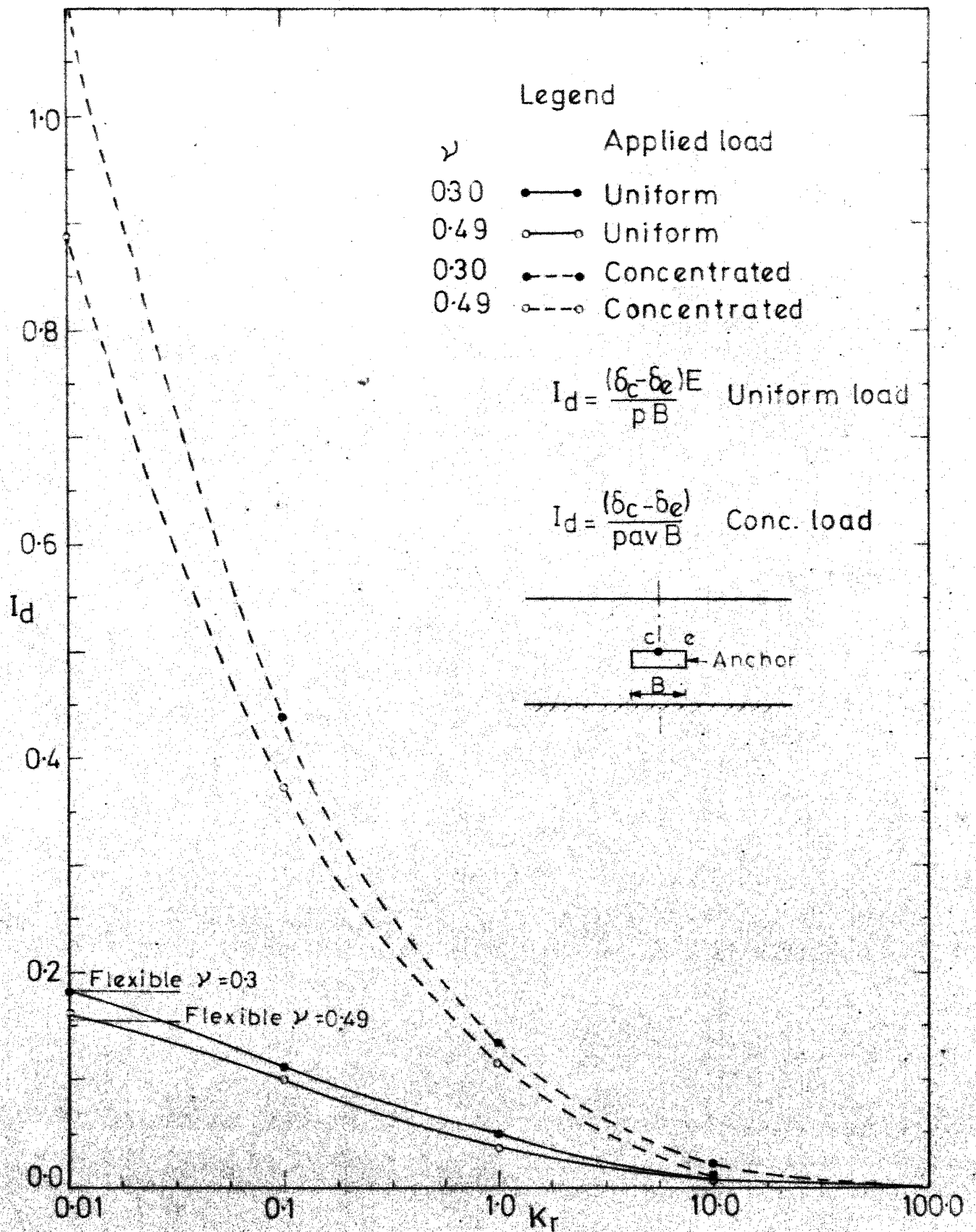


FIG. 4.16 VARIATION OF MAXIMUM DIFFERENTIAL DISPLACEMENT OF ANCHOR WITH RELATIVE STIFFNESS (FULL BONDING, CONTINUUM ELEMENT).

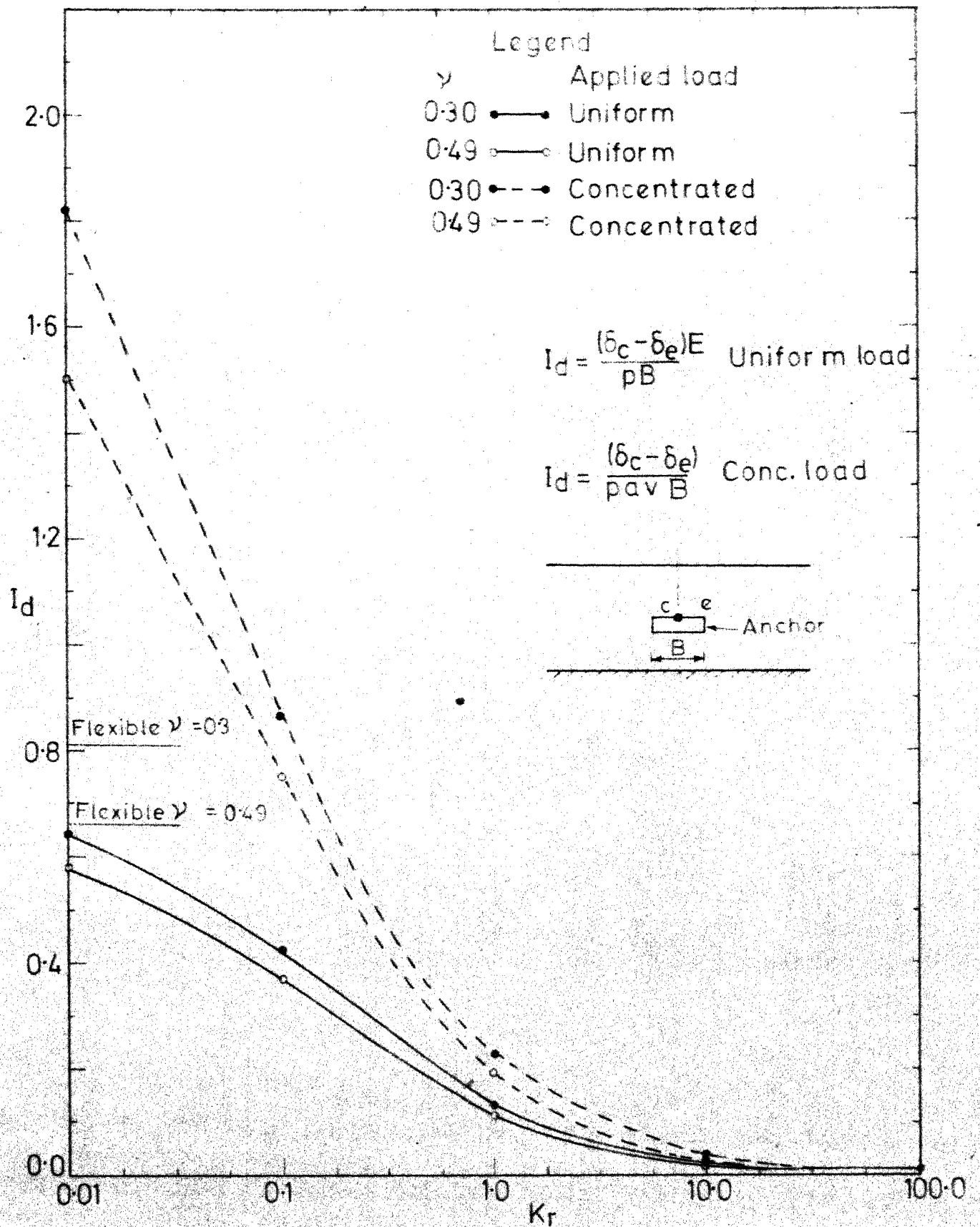


FIG. 4.17 VARIATION OF MAXIMUM DIFFERENTIAL DISPLACEMENT OF ANCHOR WITH RELATIVE STIFFNESS (FULL SEPARATION, CONTINUUM ELEMENT)

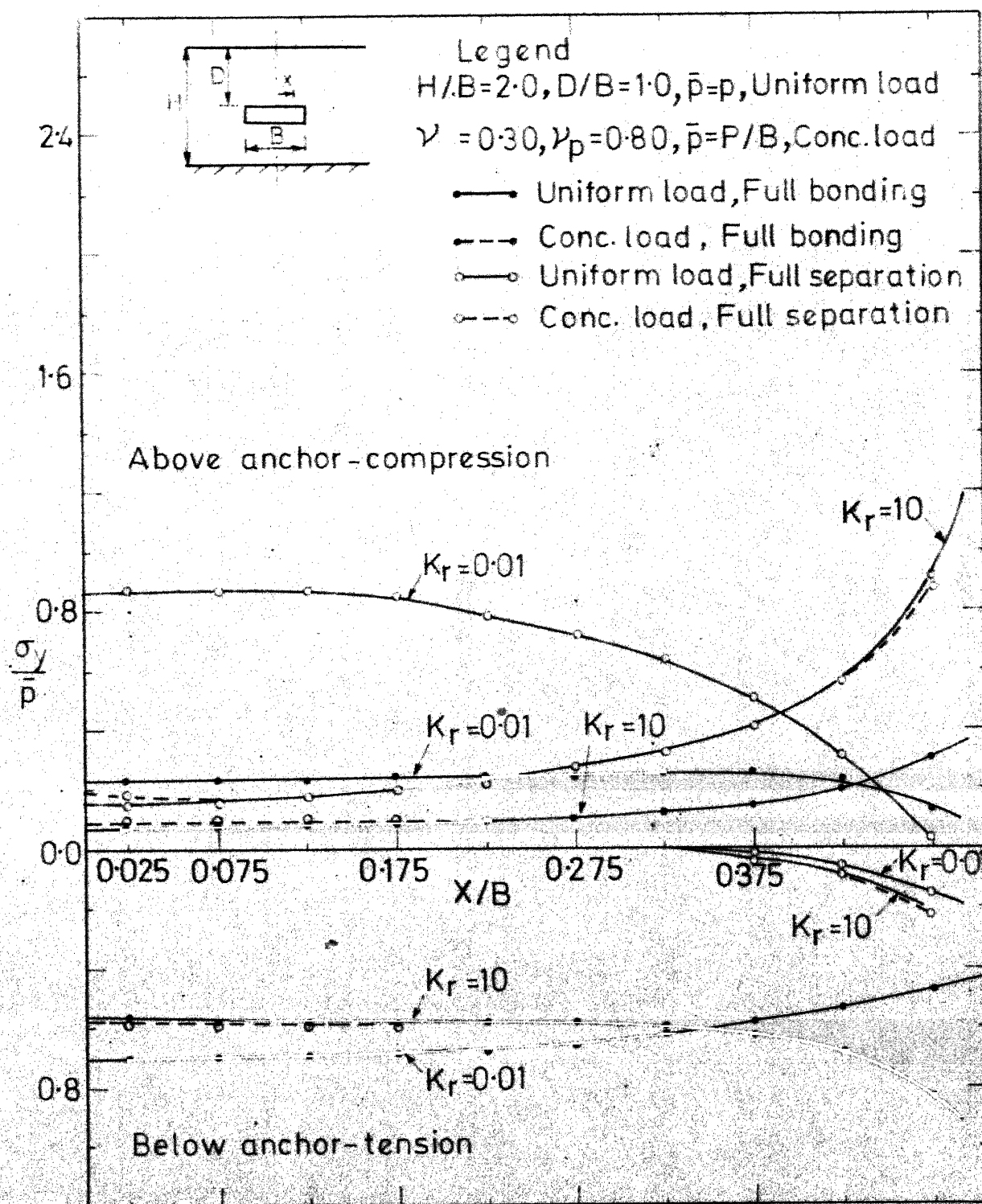


FIG. 4.18 VARIATION OF VERTICAL CONTACT STRESS DISTRIBUTION (HORIZONTAL STRIP, CONTINUUM ELEMENT, FULL BONDING, FULL SEPARATION, $\nu = 0.30$)

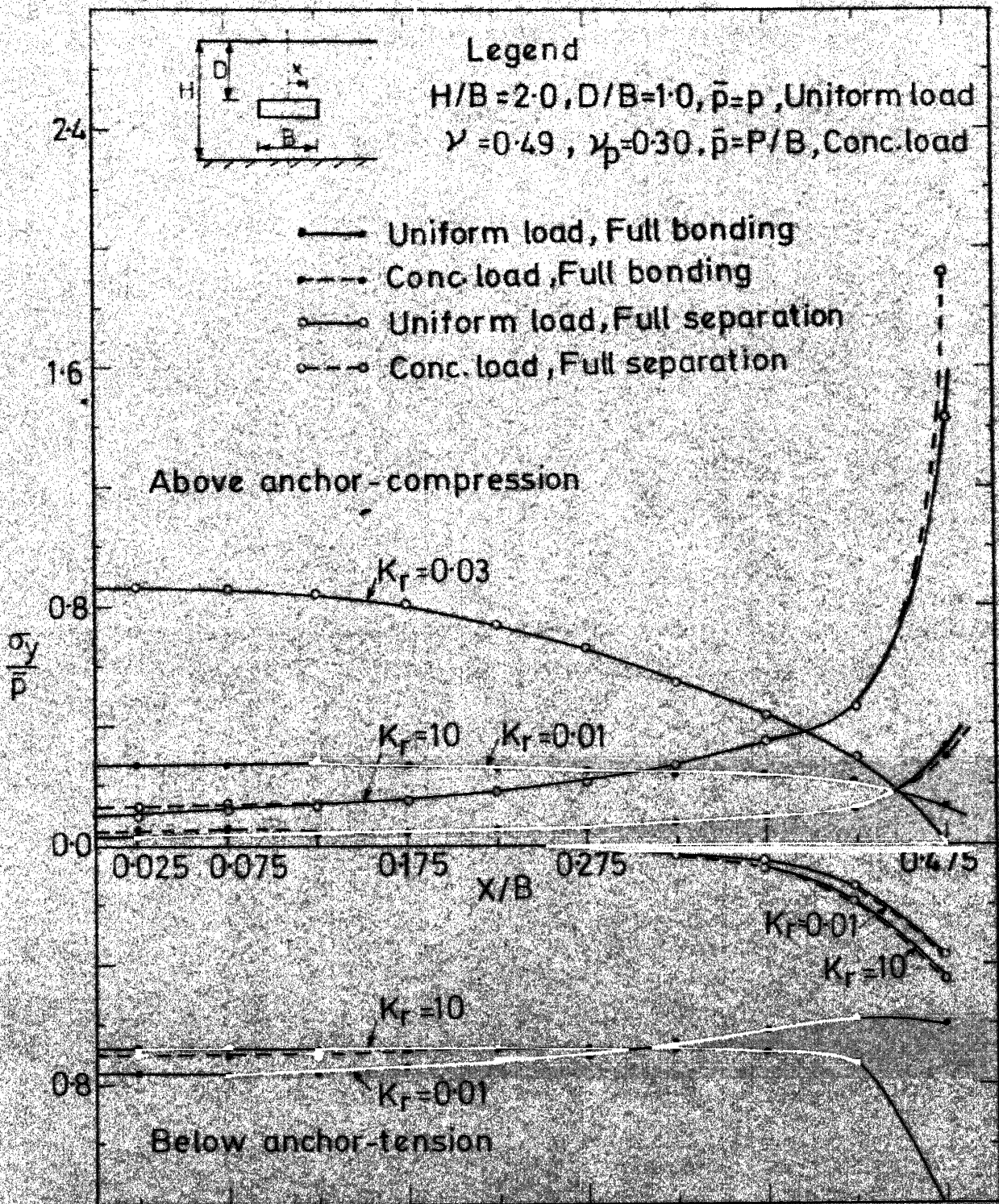


FIG. 4.19 VARIATION OF VERTICAL CONTACT STRESS DISTRIBUTION (HORIZONTAL STRIP, CONTINUUM ELEMENT, FULL BONDING, FULL SEPARATION, $\nu = 0.49$)

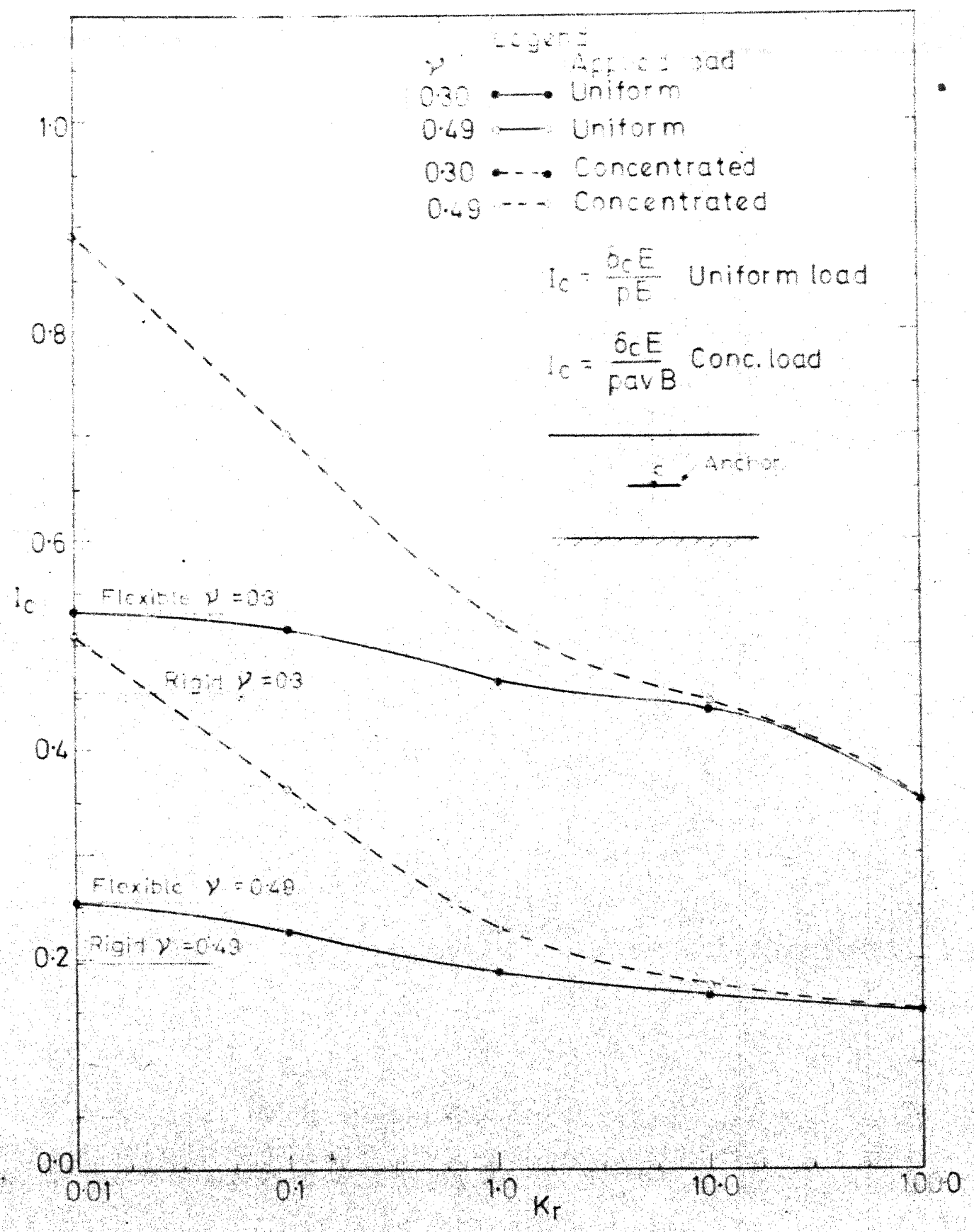


FIG. 420 VARIATION OF CENTRAL VERTICAL DISPLACEMENT OF ANCHOR WITH RELATIVE STIFFNESS (FULL BONDING, BEAM-COLUMN ELEMENT)

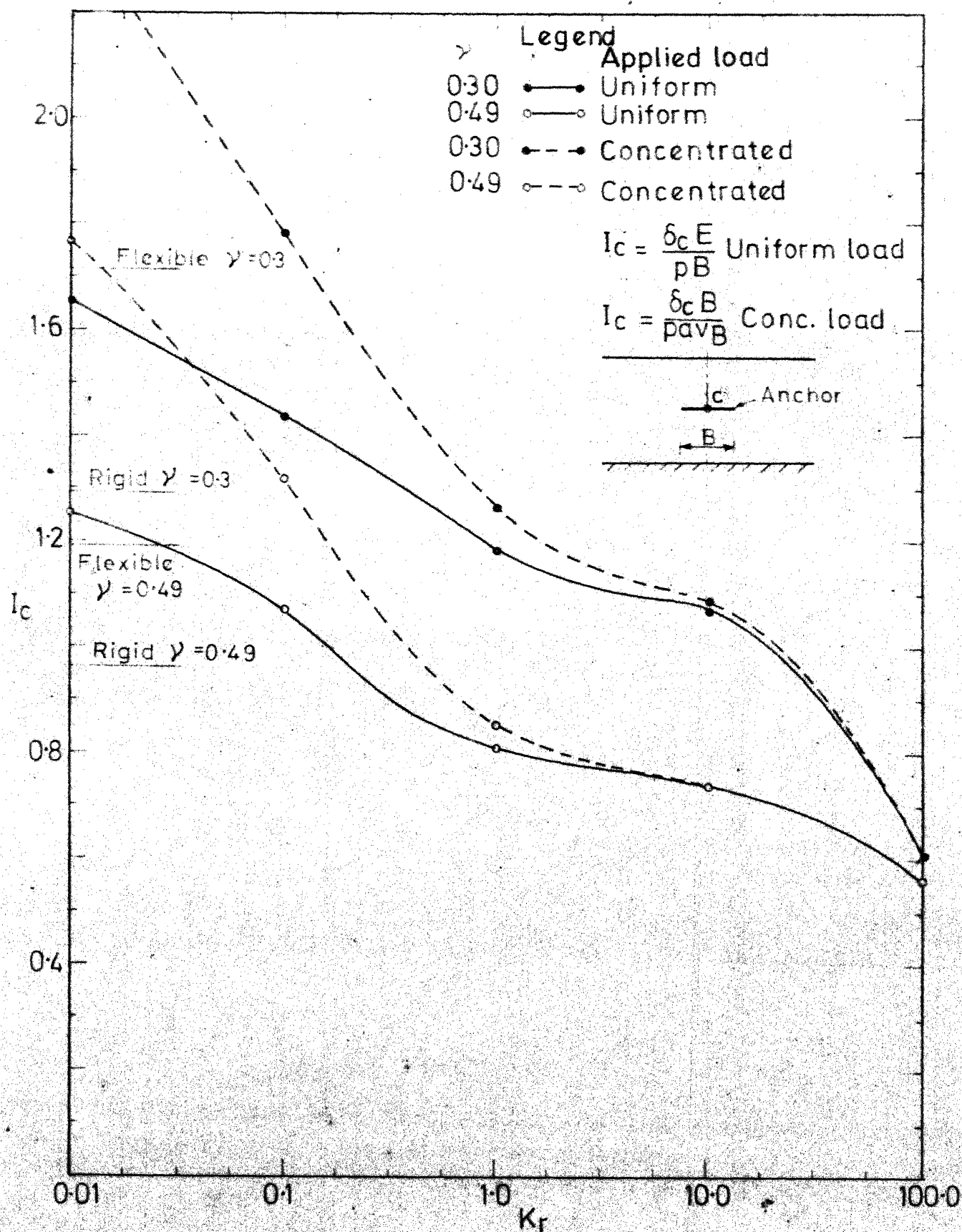


FIG.4.21 VARIATION OF CENTRAL VERTICAL DISPLACEMENT OF ANCHOR WITH RELATIVE STIFFNESS (FULL SEPARATION, BEAM-COLUMN ELEMENT)

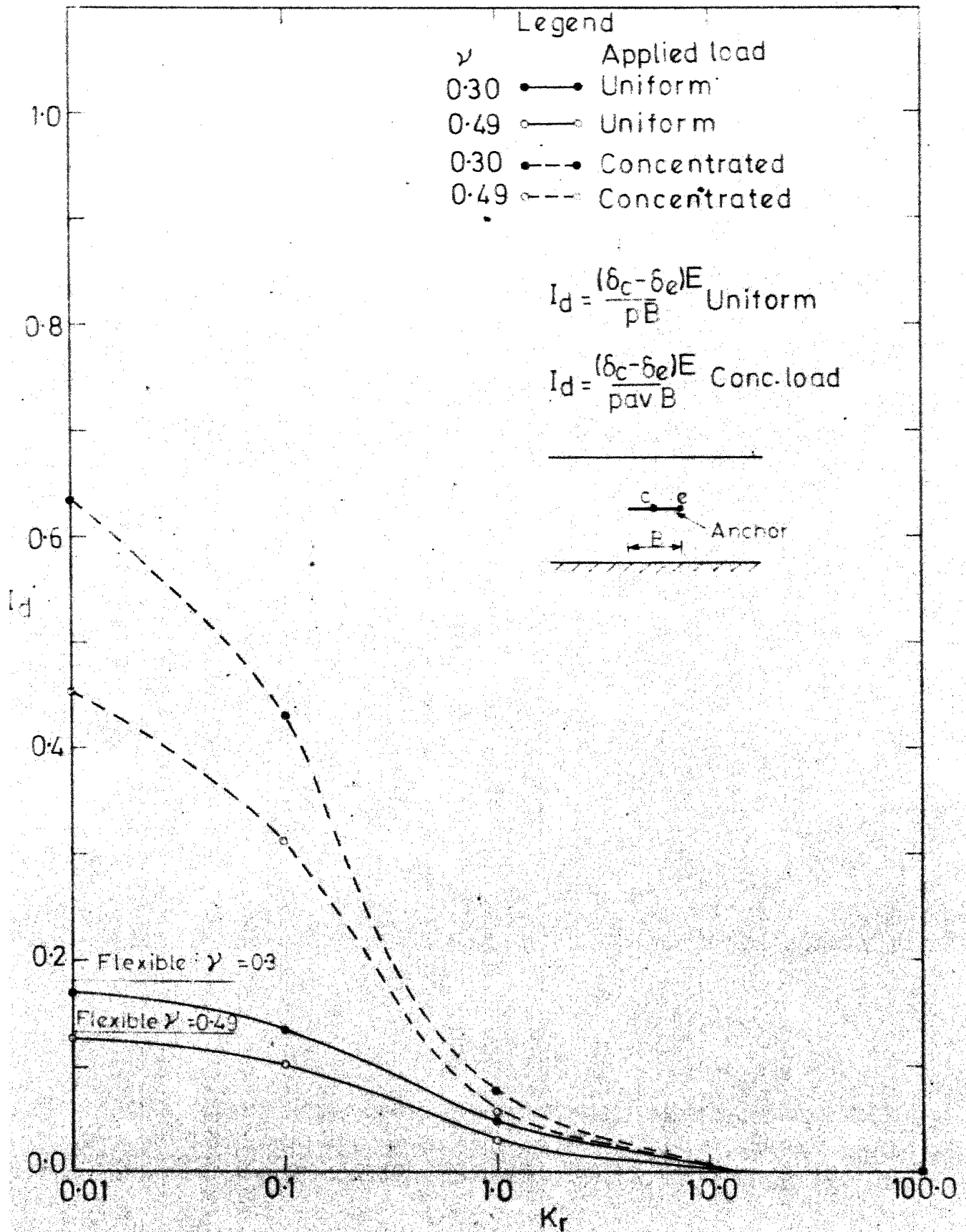


FIG. 4.22 VARIATION OF MAXIMUM DIFFERENTIAL DISPLACEMENT OF ANCHOR WITH RELATIVE STIFFNESS (FULL BONDING, BEAM-COLUMN ELEMENT)

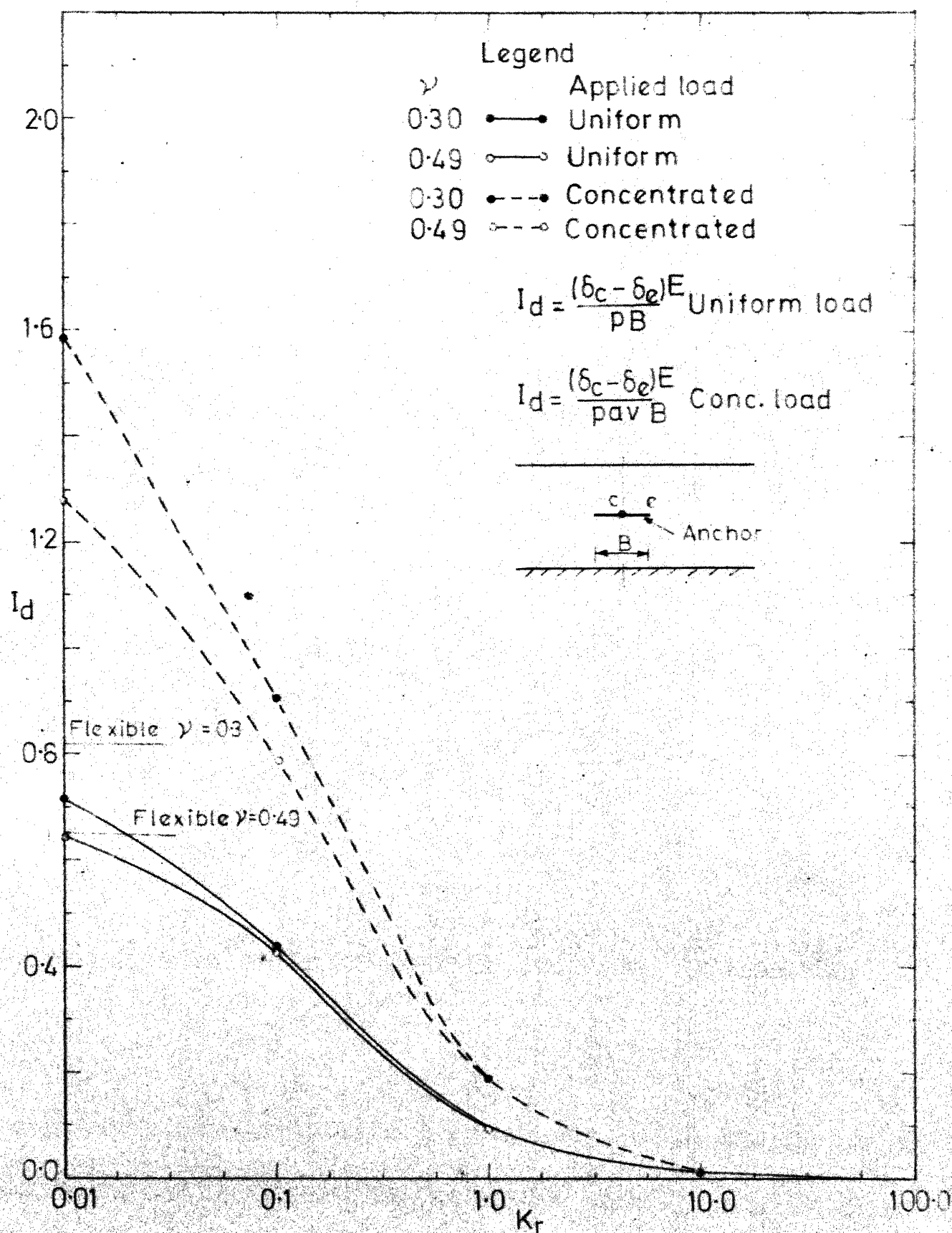


FIG. 4.23 VARIATION MAXIMUM DIFFERENTIAL DISPLACEMENT OF ANCHOR WITH RELATIVE STIFFNESS (FULL SEPARATION, BEAM-COLUMN ELEMENT)

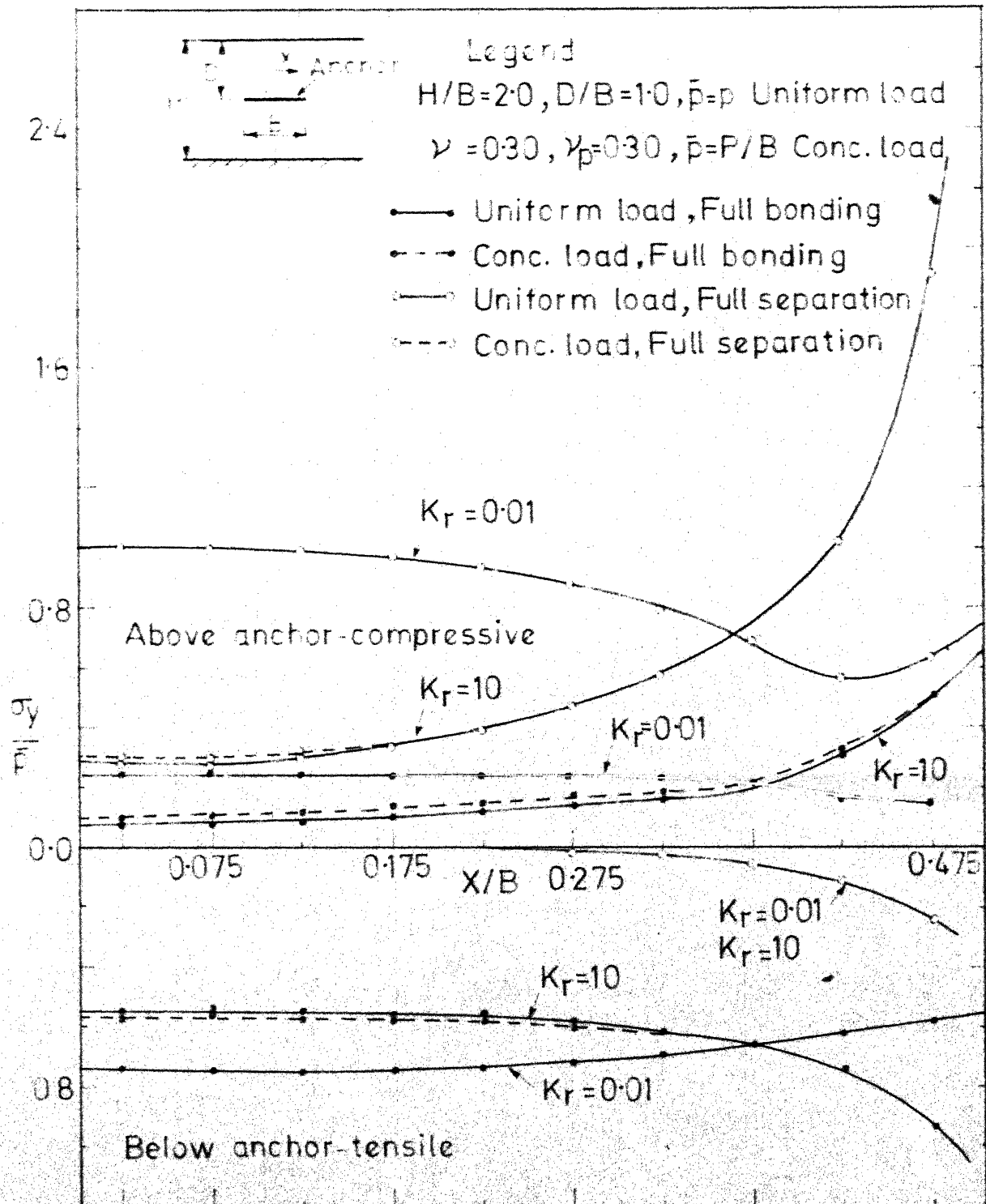


FIG.4.24 VARIATION OF VERTICAL CONTACT STRESS
(HORIZONTAL STRIP, BEAM COLUMN ELEMENT,
FULL BONDING, FULL SEPARATION, $\nu=0.3$)

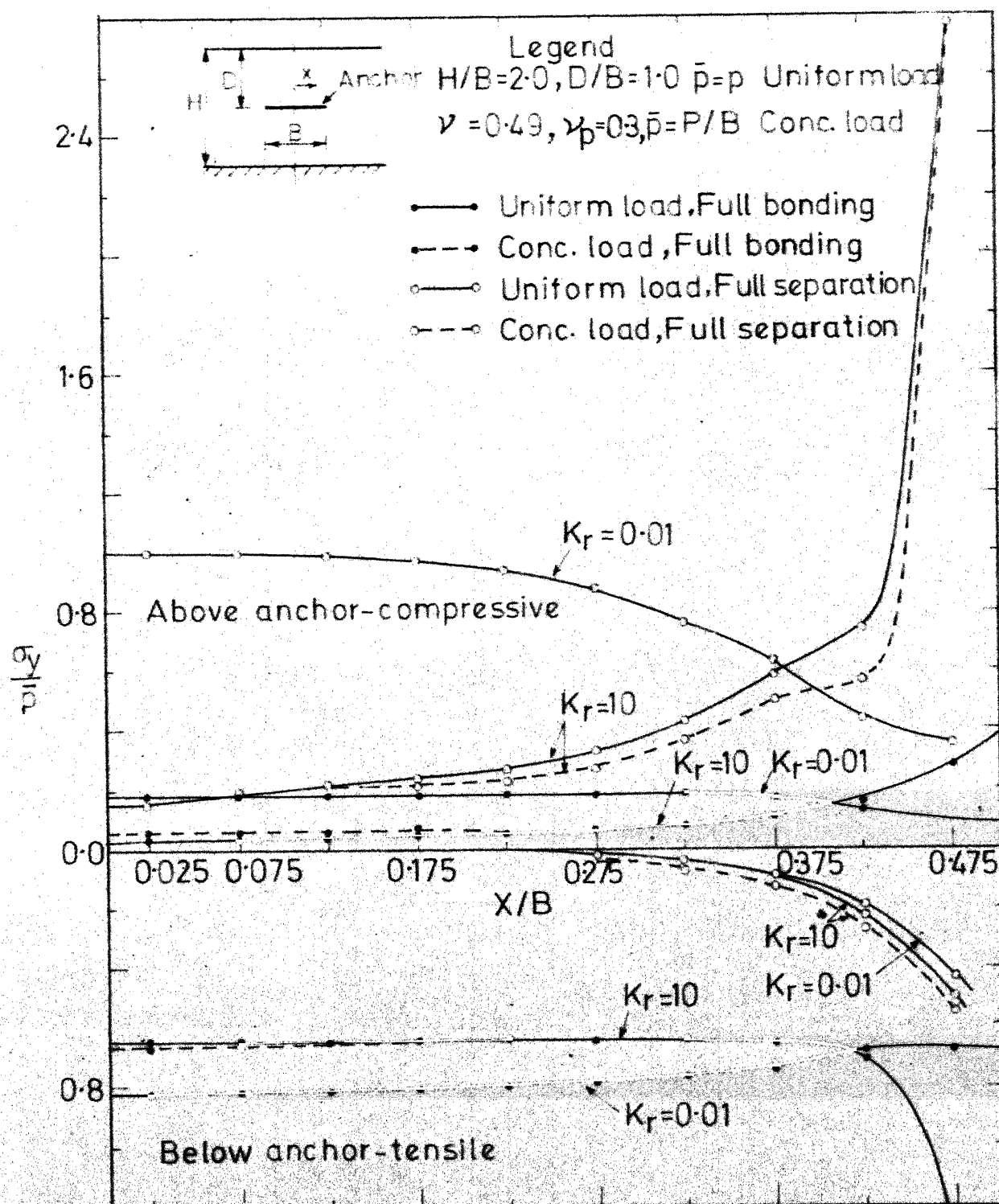


FIG-4.25 VARIATION OF VERTICAL CONTACT STRESS
 (HORIZONTAL STRIP, BEAM COLUMN ELEMENT,
 FULL BONDING, FULL SEPARATION, $\nu=0.49$)

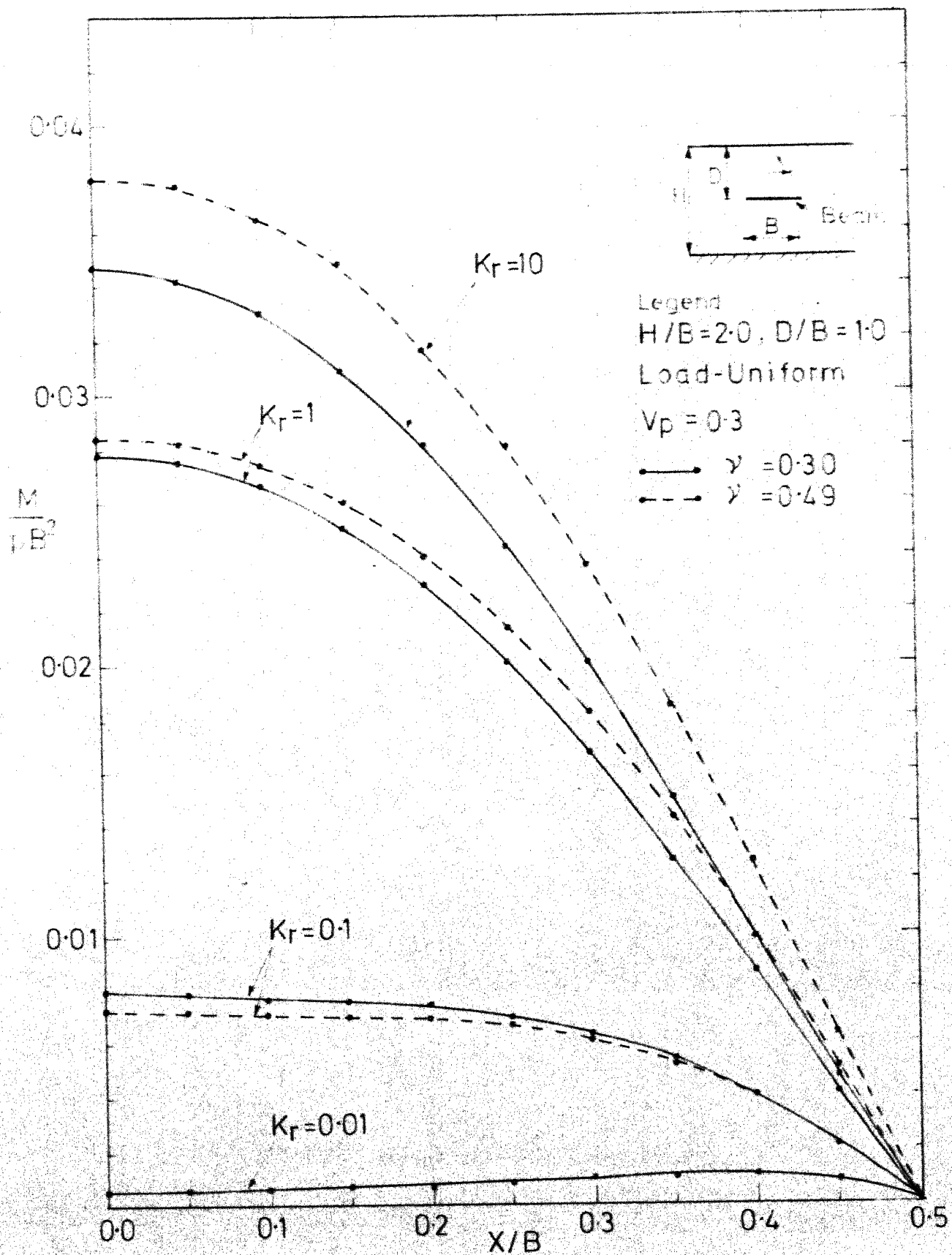


FIG.4.26 BENDING MOMENT DISTRIBUTION (HORIZONTAL STRIP, BEAM-COLUMN ELEMENT, UNIFORM LOAD, FULL BONDING)

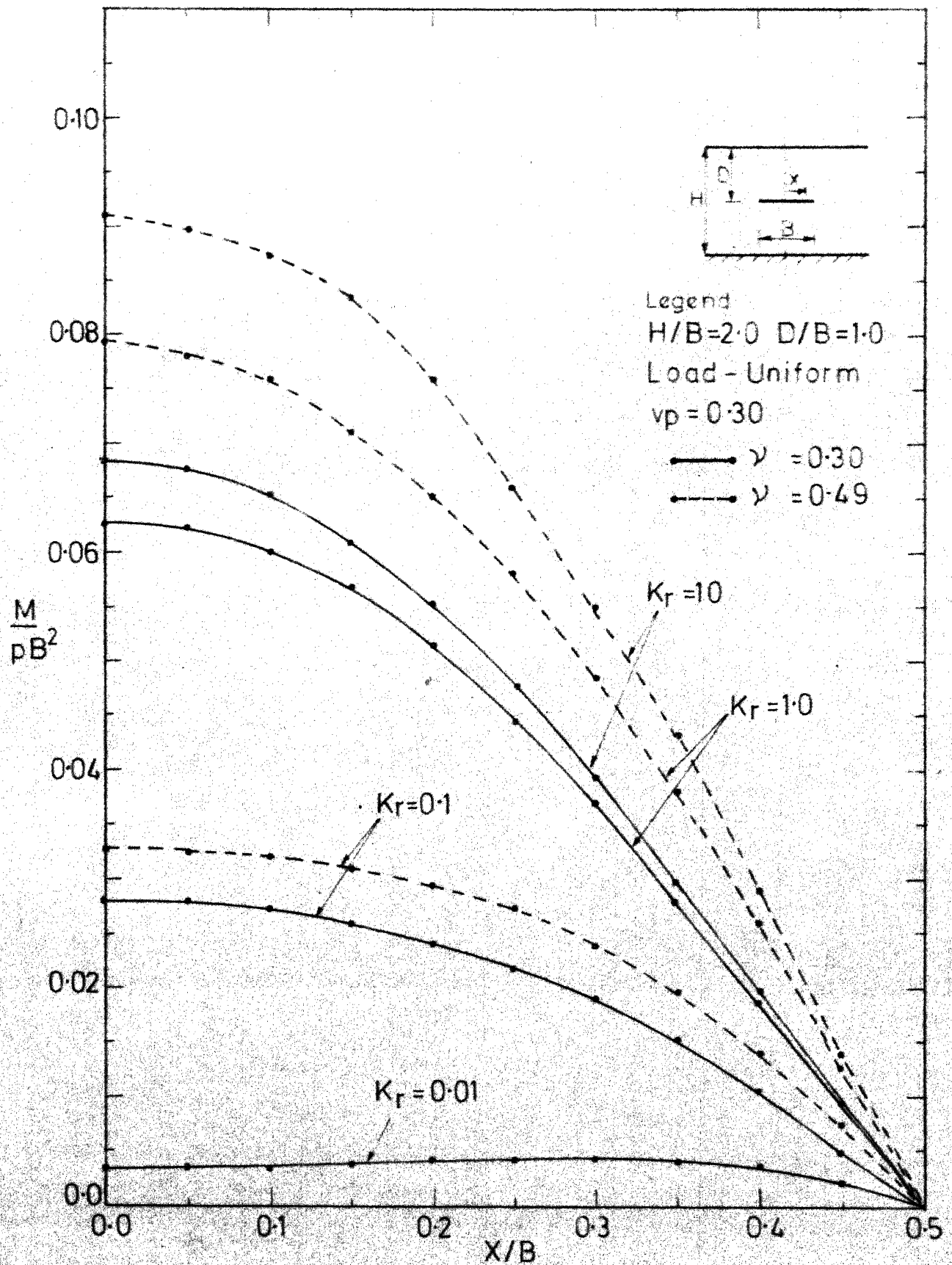


FIG.4.27 BENDING MOMENT DISTRIBUTION (HORIZONTAL STRIP, BEAM-COLUMN ELEMENT, UNIFORM LOAD, FULL SEPARATION)

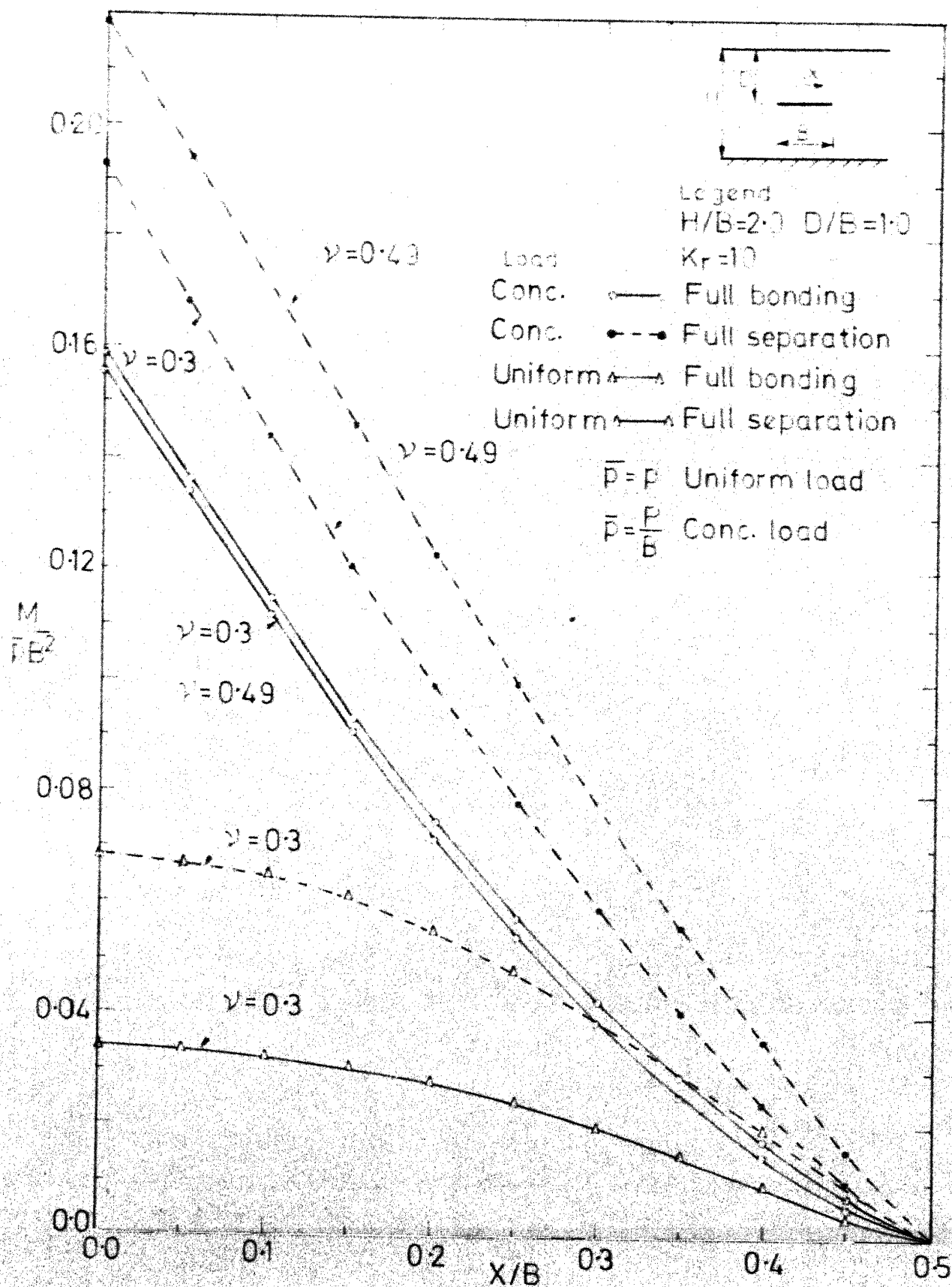


FIG. 4.28 BENDING MOMENT DISTRIBUTION DUE TO CONC. & UNIFORM LOAD ON ANCHOR (HORIZONTAL STRIP, BEAM-COLUMN ELEMENT)

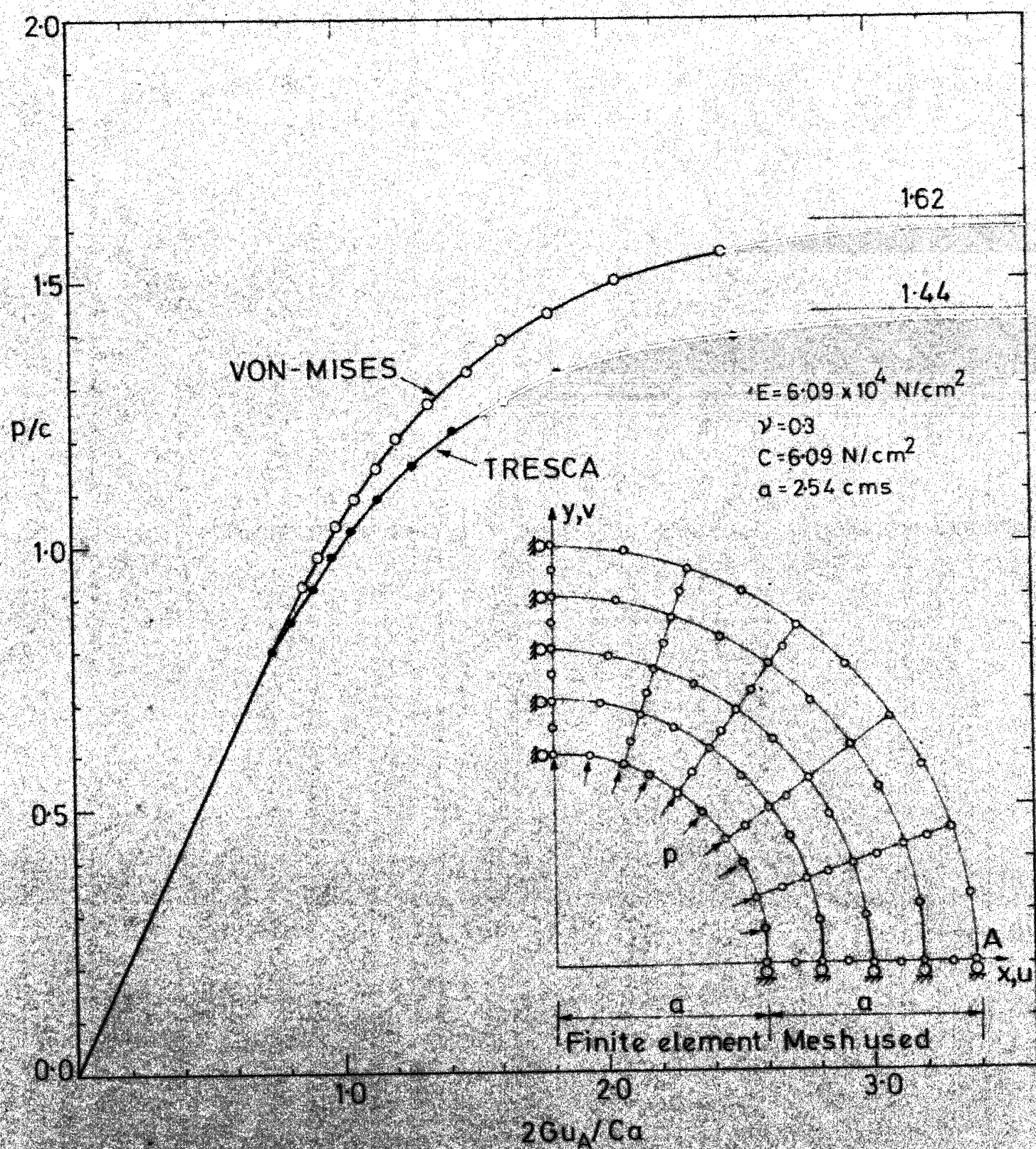
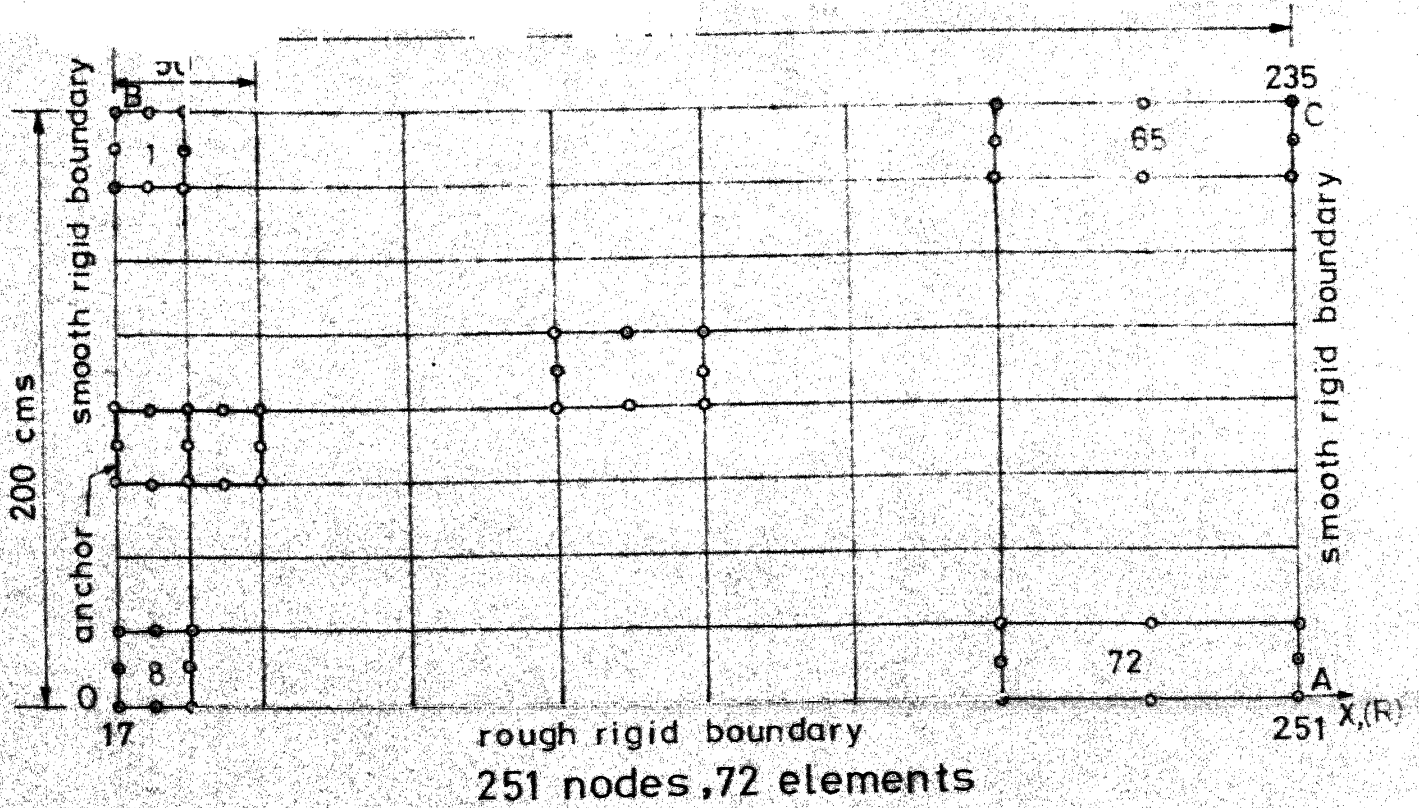
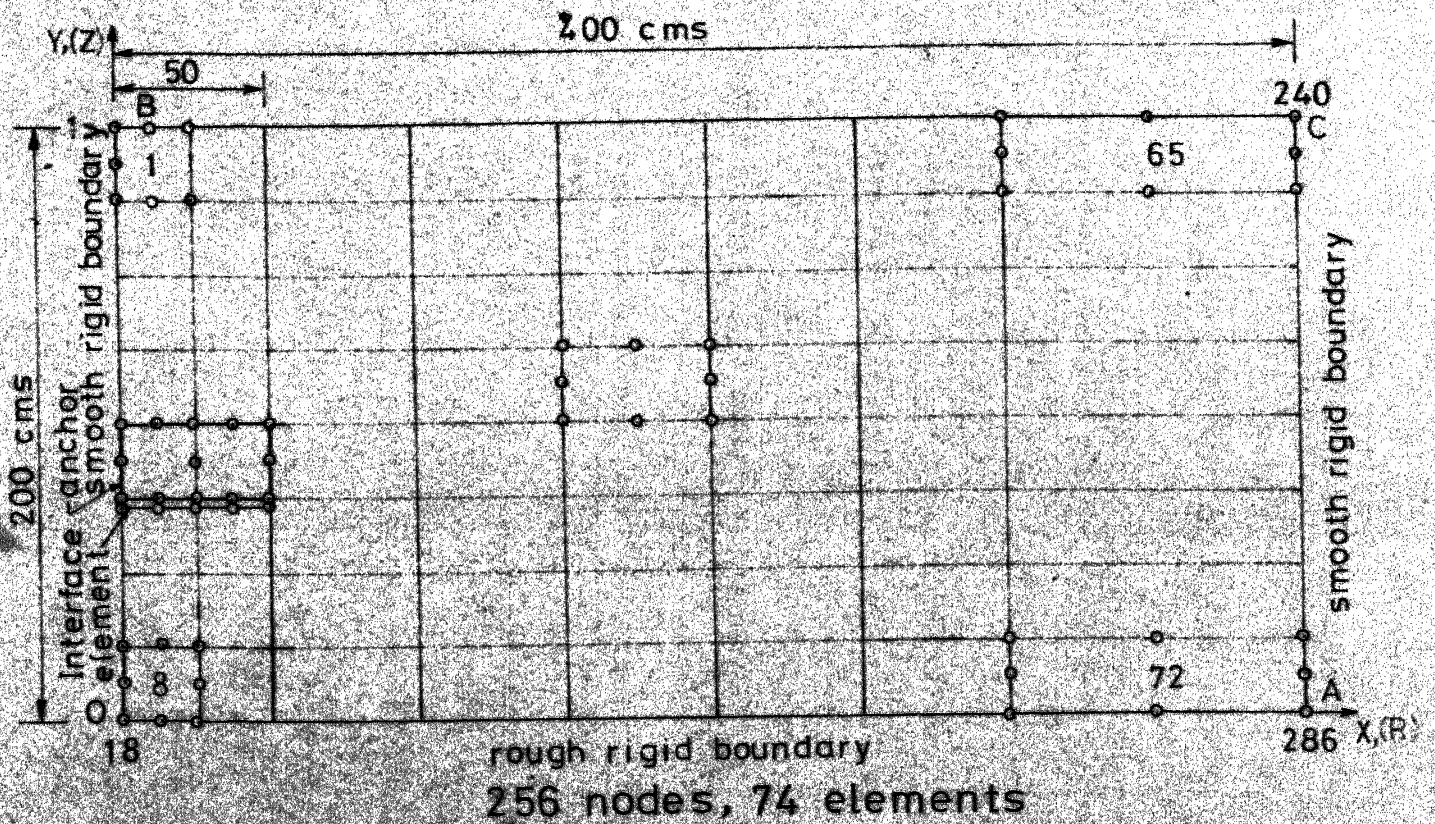


FIG. 4.29 ELASTO PLASTIC DISPLACEMENT RESPONSE OF THICK WALLED CYLINDER, VON-MISES & TRESCA CRITERIA

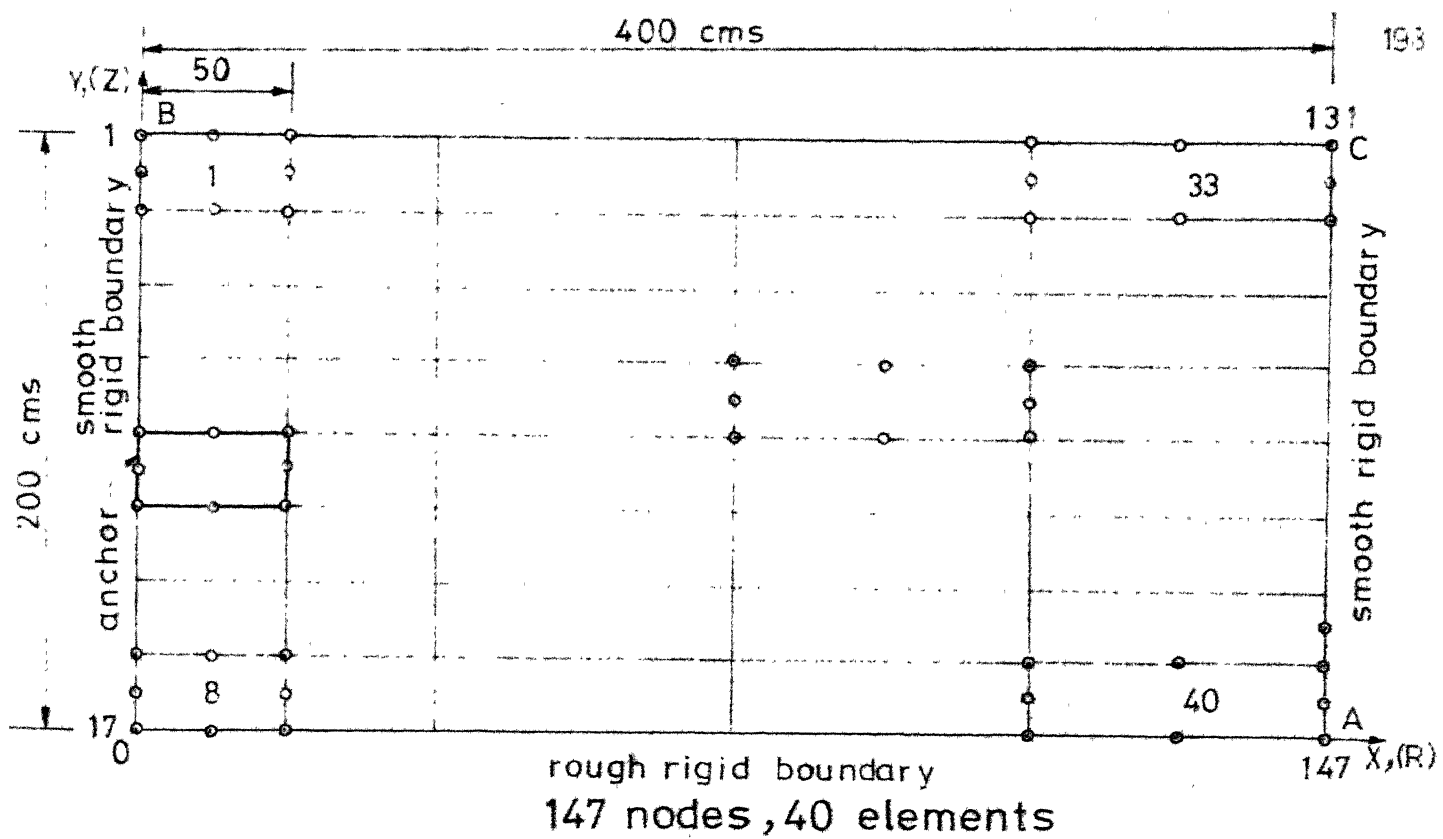


a. Mesh-1, for full bonding below anchor

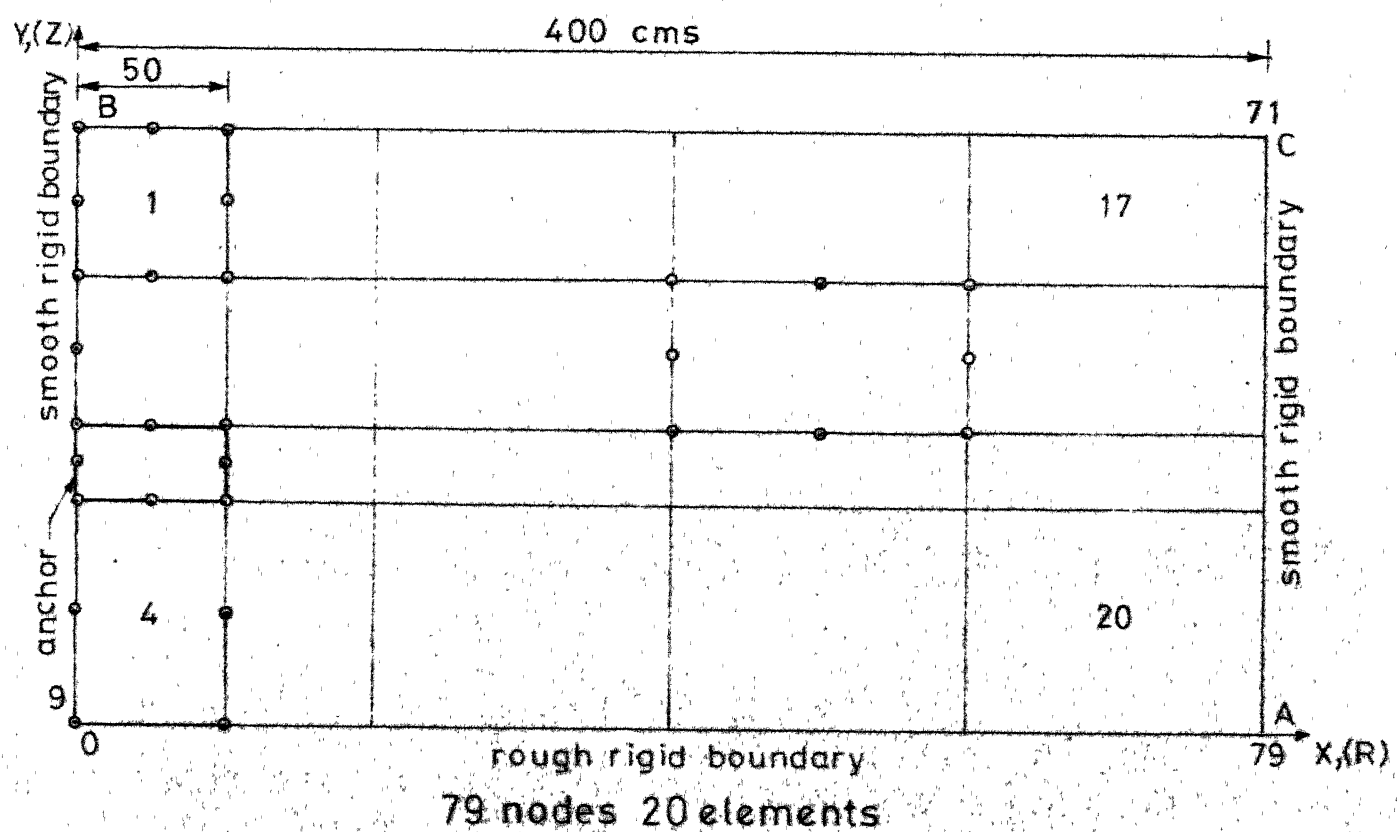


b. Mesh-2, full separation below anchor

FIG. 430 DISCRETISED MODEL OF SOIL LAYER OF FINITE DEPTH UNDERLAIN BY ROUGH RIGID BASE, ELASTO-PLASTIC ANALYSIS



c. Mesh-3, for full bonding below anchor



d. Mesh-4, for full bonding below anchor

FIG. 4.30. DISCRETISED MODEL OF SOIL LAYER OF FINITE DEPTH UNDER LAI BY ROUGH RIGID BASE, ELASTO-PLASTIC ANALYSIS

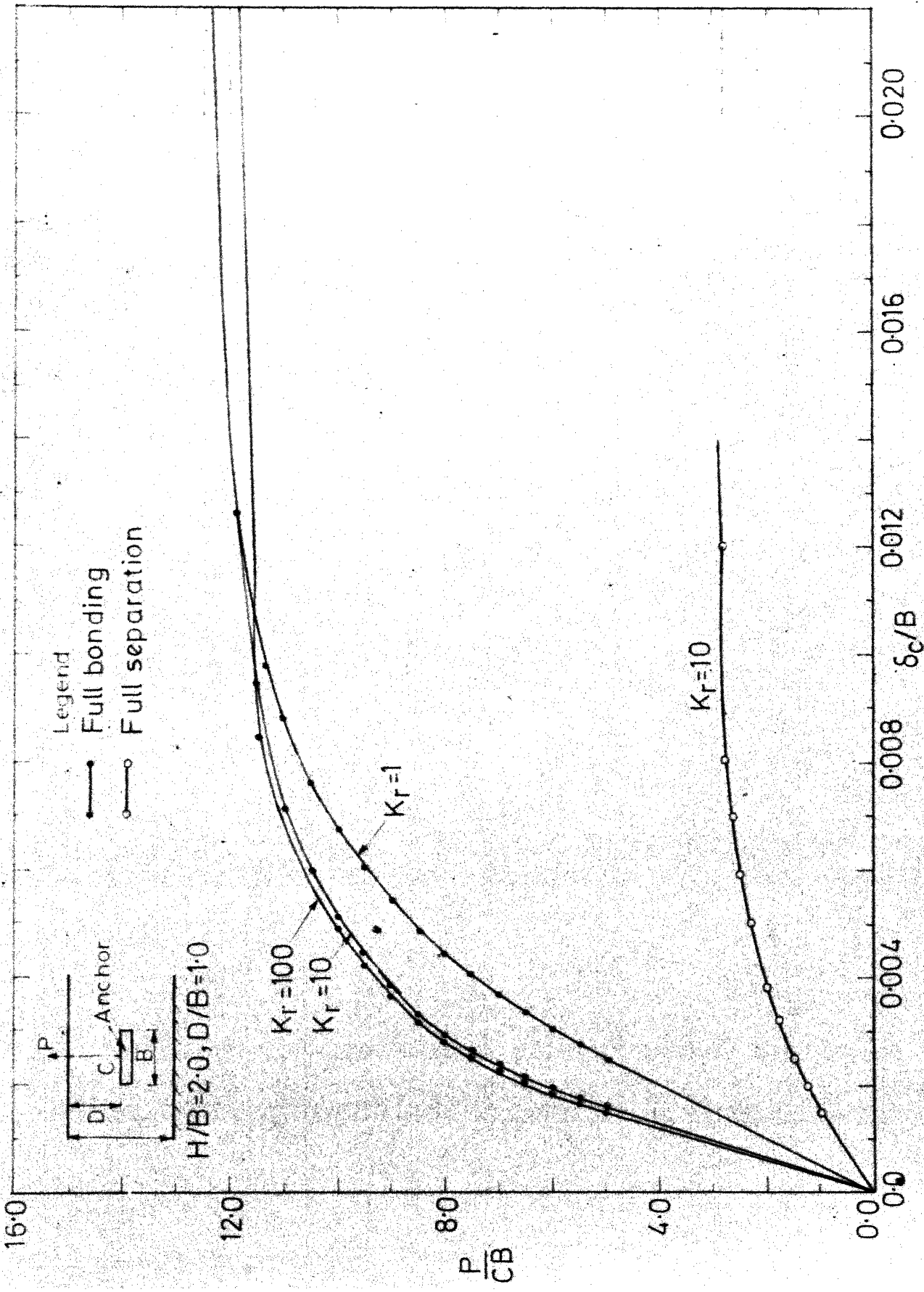


FIG. 4.31 LOAD DISPLACEMENT RESPONSE, HORIZONTAL STRIP ANCHOR, VON-MISES MODEL

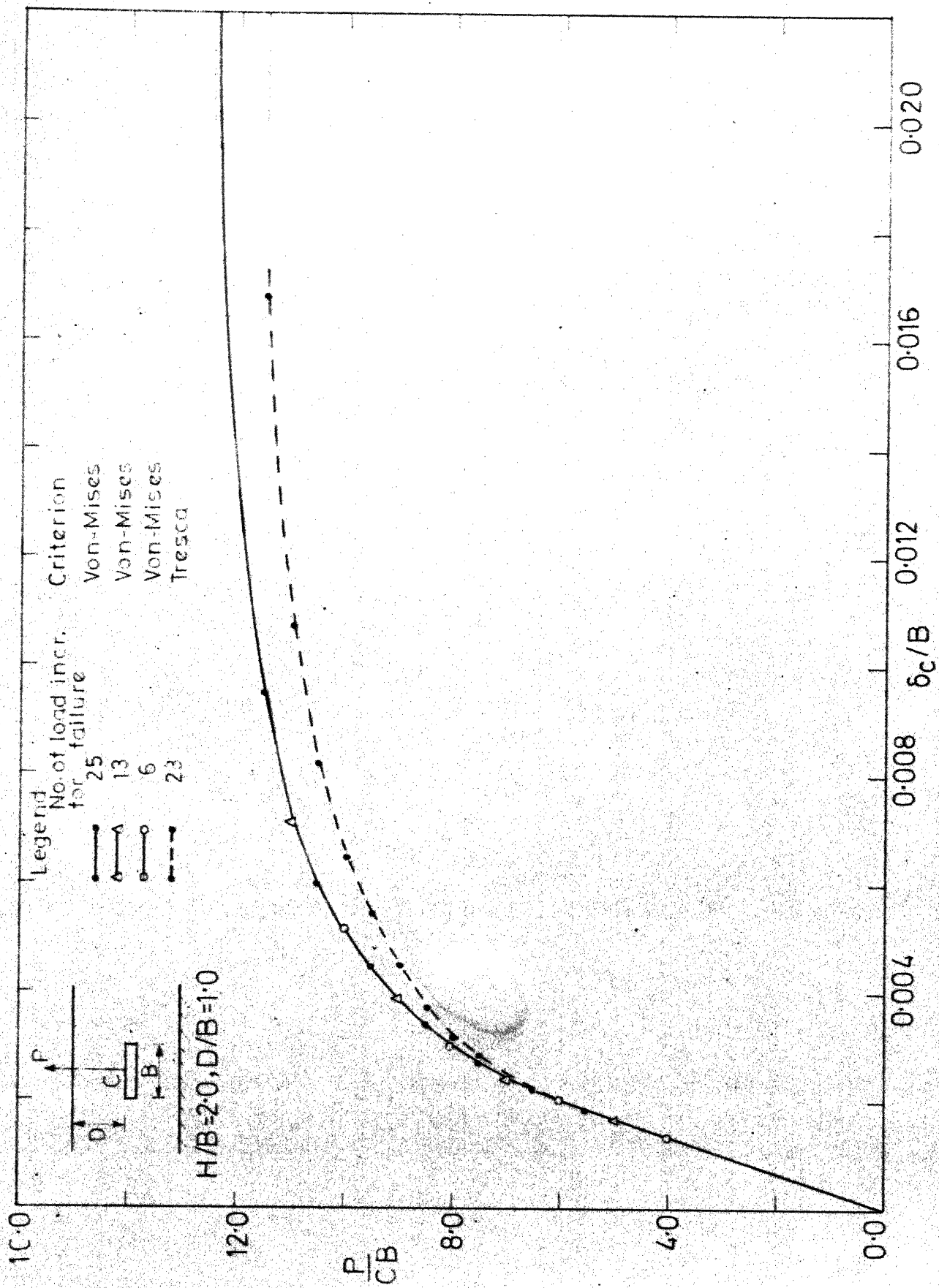


FIG. 432 LOAD DISPLACEMENT RESPONSE, HORIZONTAL STRIP ANCHOR, VON-MISES AND TRESCA MODELS

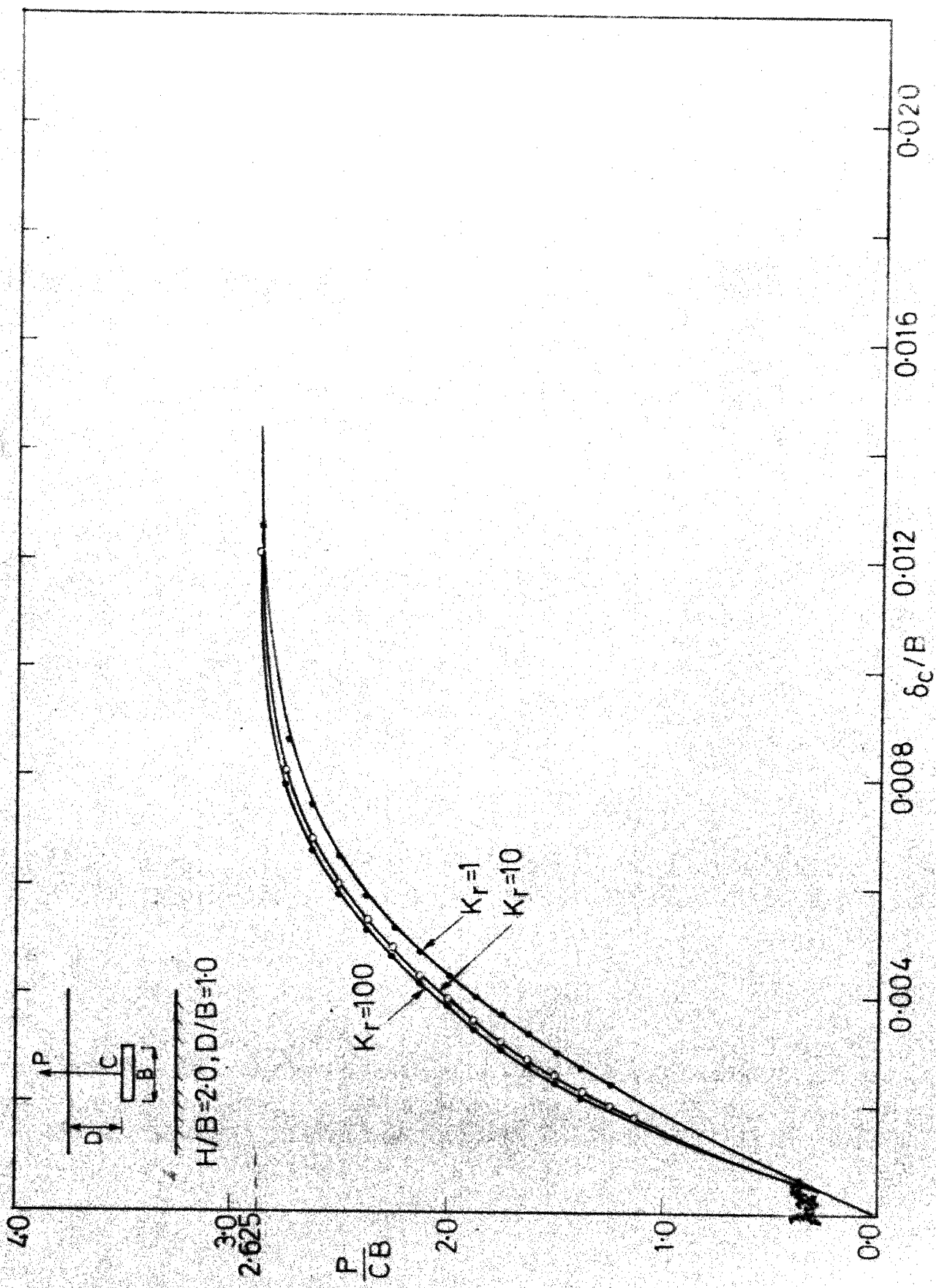


FIG. 4.33 LOAD DISPLACEMENT RESPONSE, HORIZONTAL STRIP ANCHOR: $K_r = 1, 10, 100$
FULL SEPARATION, VON-MISES MODEL

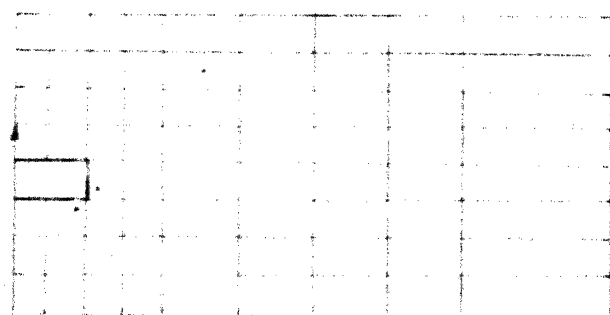
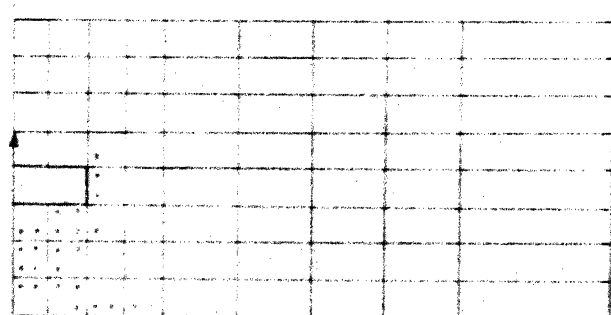
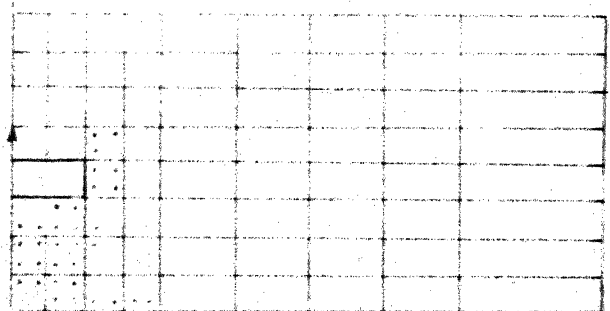
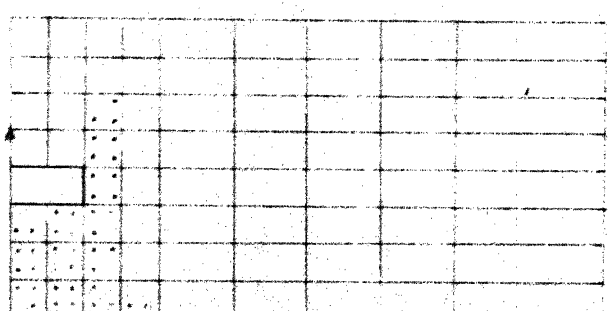
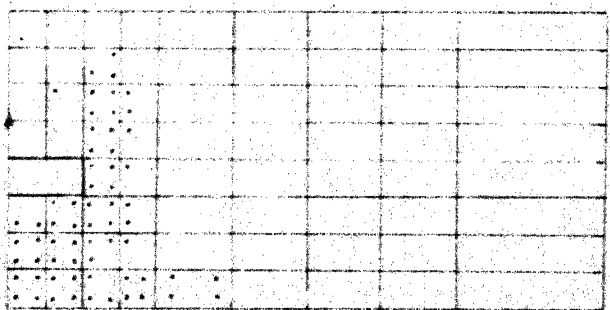
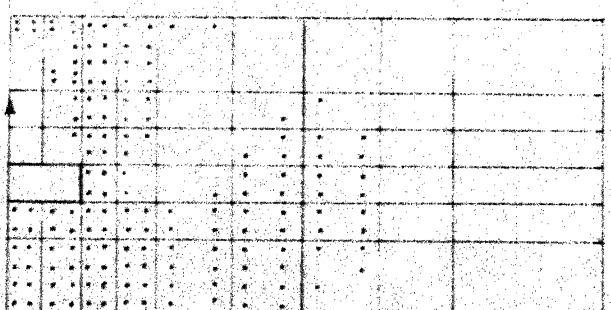
a. $P = 120 \text{ kN/m}$ b. $P = 160 \text{ kN/m}$ c. $P = 180 \text{ kN/m}$ d. $P = 200 \text{ kN/m}$ e. $P = 220 \text{ kN/m}$ f. $P = 250 \text{ kN/m}$

FIG. 4.34 SPREAD OF PLASTIC ZONE, HORIZONTAL STRIP ANCHOR, VON-MISES MODEL, FULL BONDING

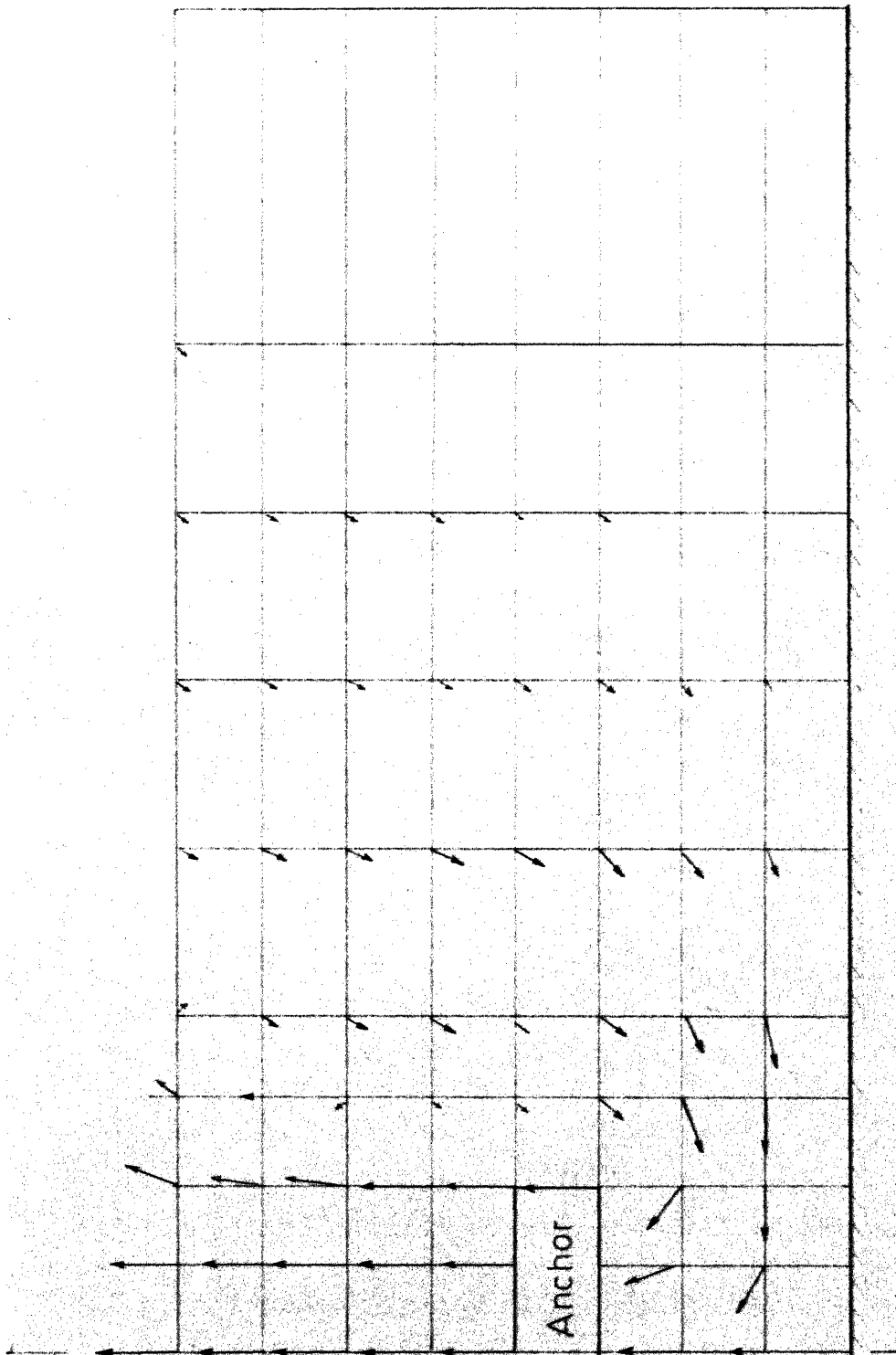


FIG. 4.36 VELOCITY FIELD AT LIMIT LOAD, VON-MISES CRITERION,
FULL BONDING

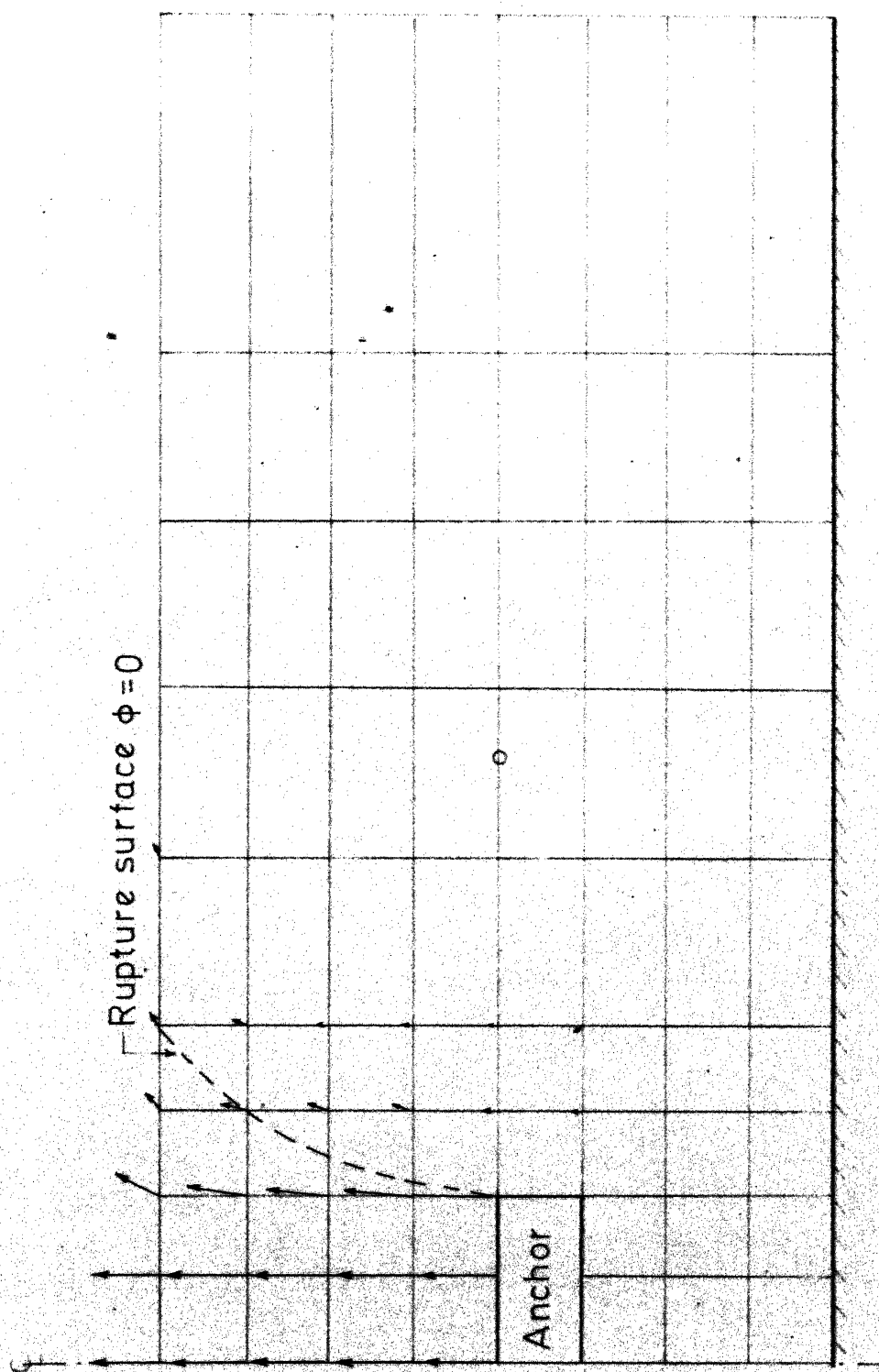


FIG. 4.37 VELOCITY FIELD AT NUMERICAL LIMIT LOAD, VON-MISES CRITERION, FULL SEPARATION

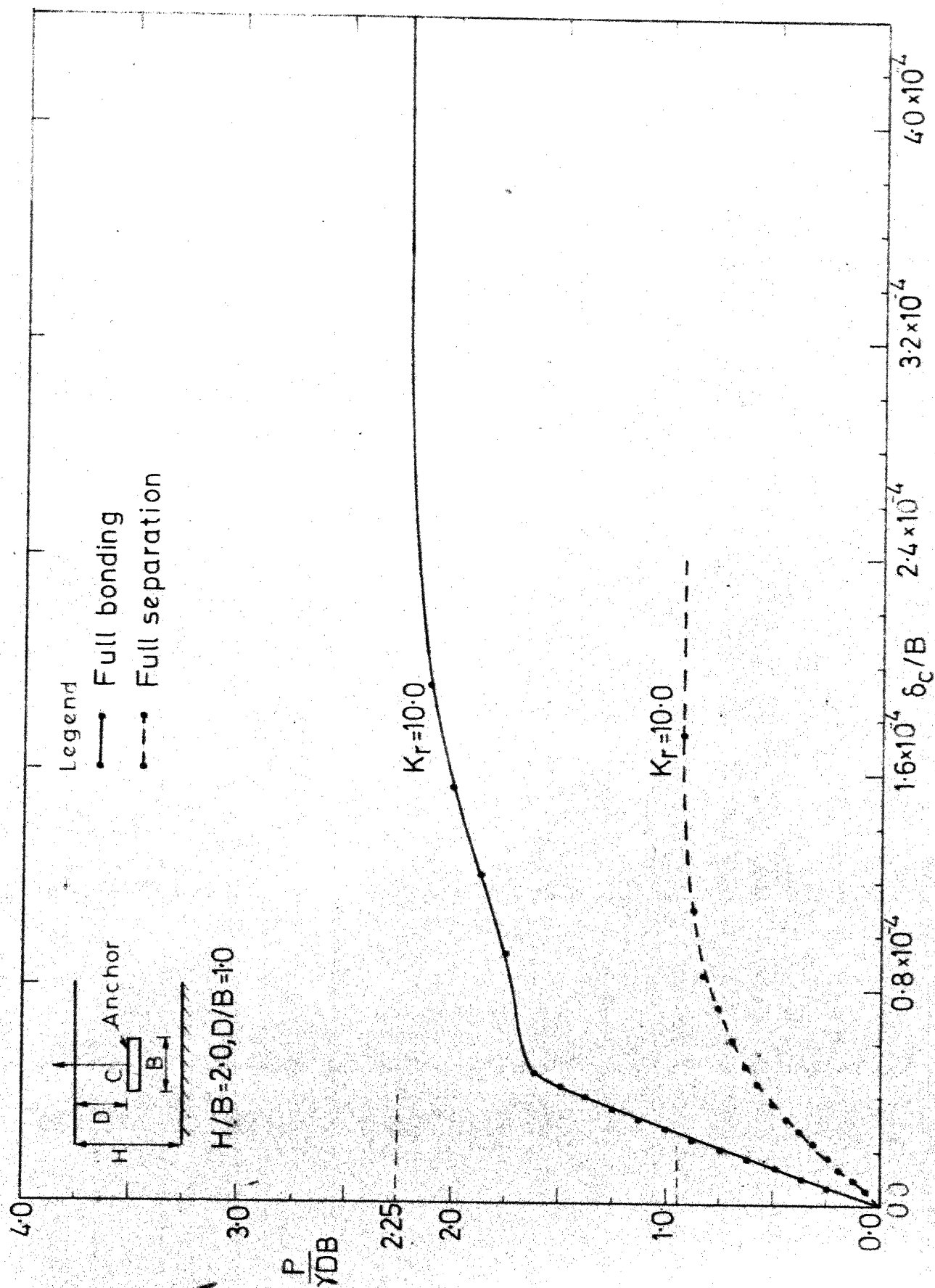


FIG. 4.38 LOAD DISPLACEMENT RESPONSE, HORIZONTAL STRIP, MOHR-COULOMB MODEL

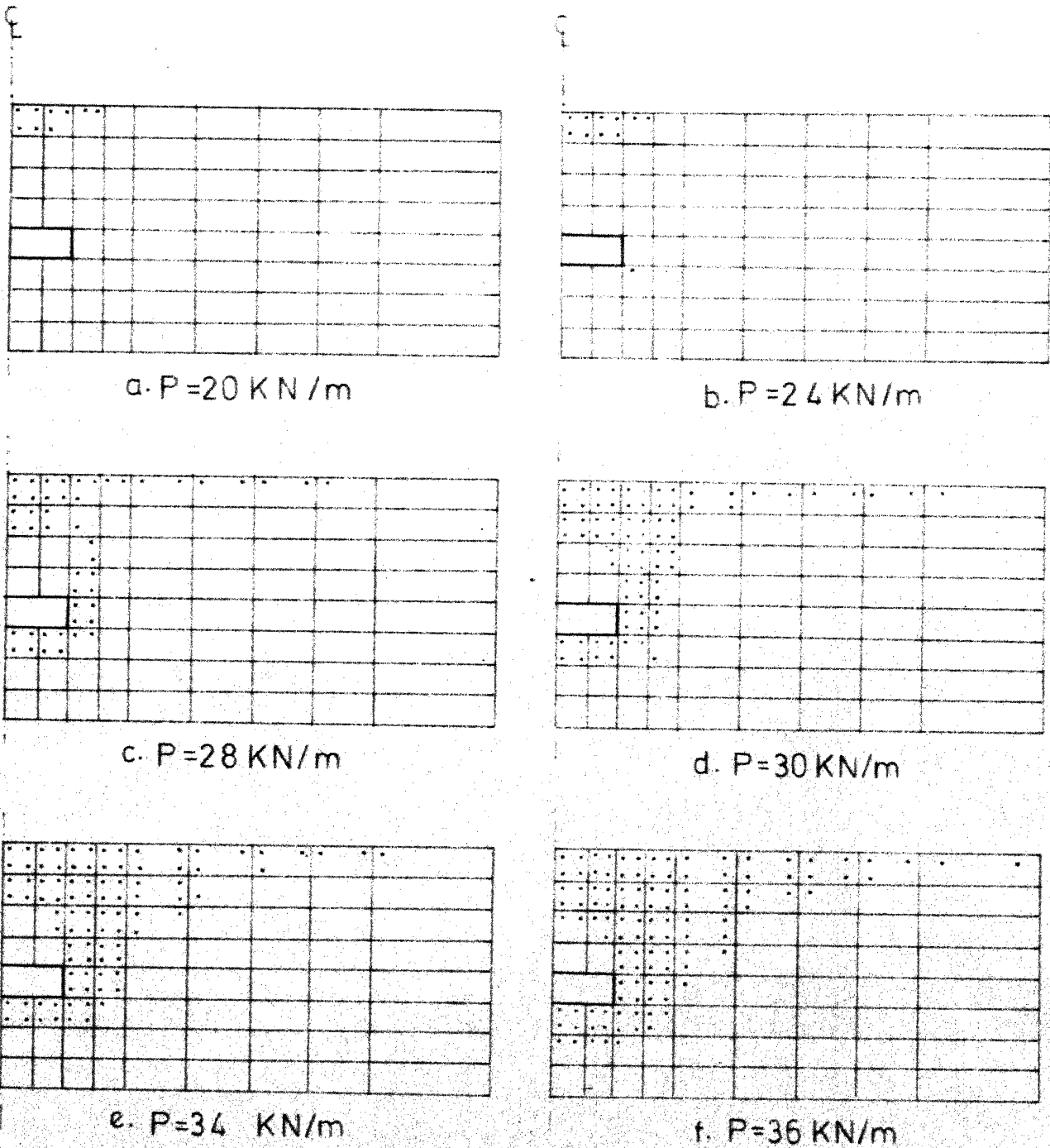


FIG. 4.39 SPREAD OF PLASTIC ZONE, HORIZONTAL STRIP, MOHR-COULOMB MODEL, FULL BONDING

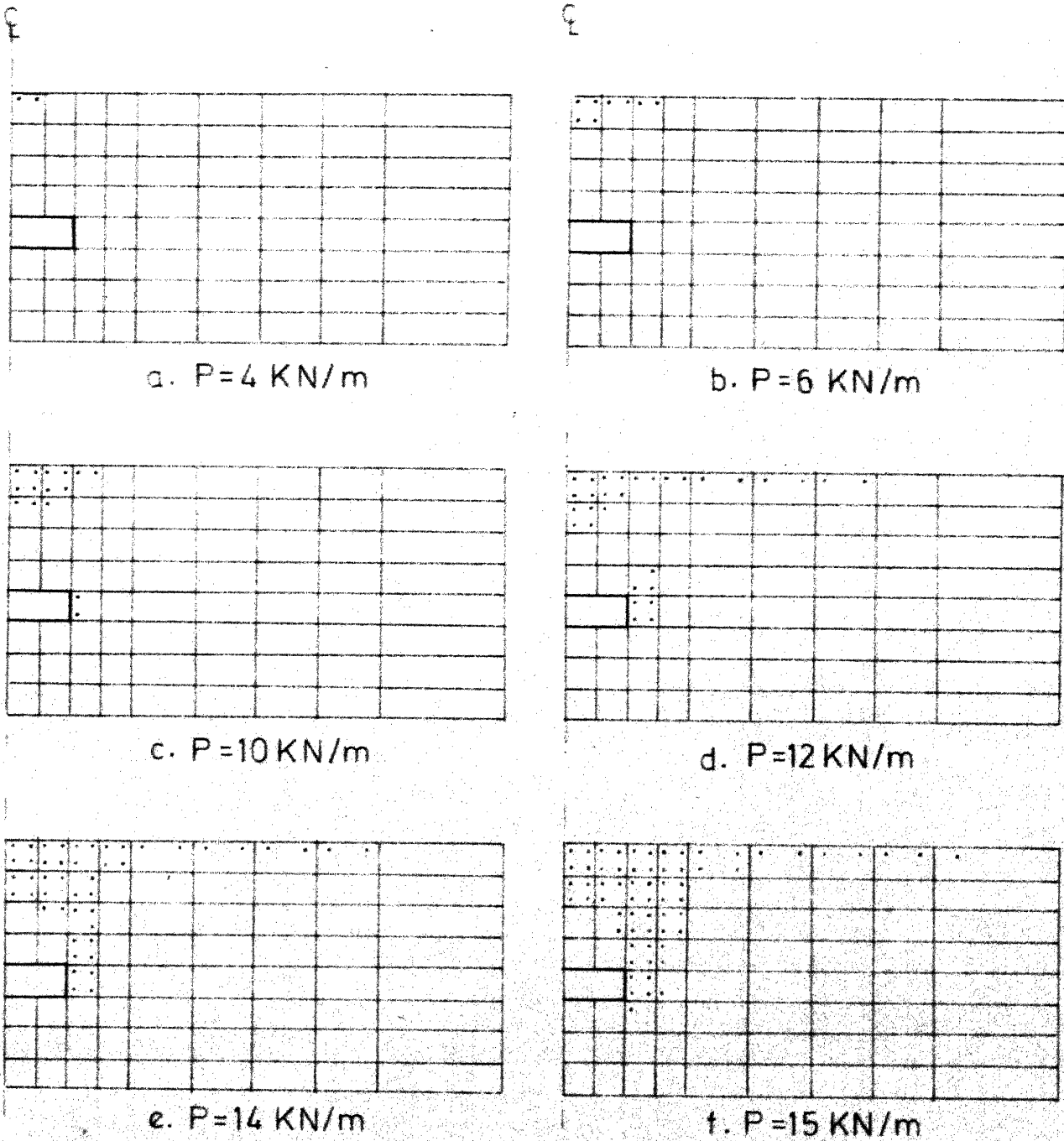


FIG. 4.40 SPREAD OF PLASTIC ZONE, HORIZONTAL STRIP, MOHR-COULOMB MODEL, FULL SEPARATION

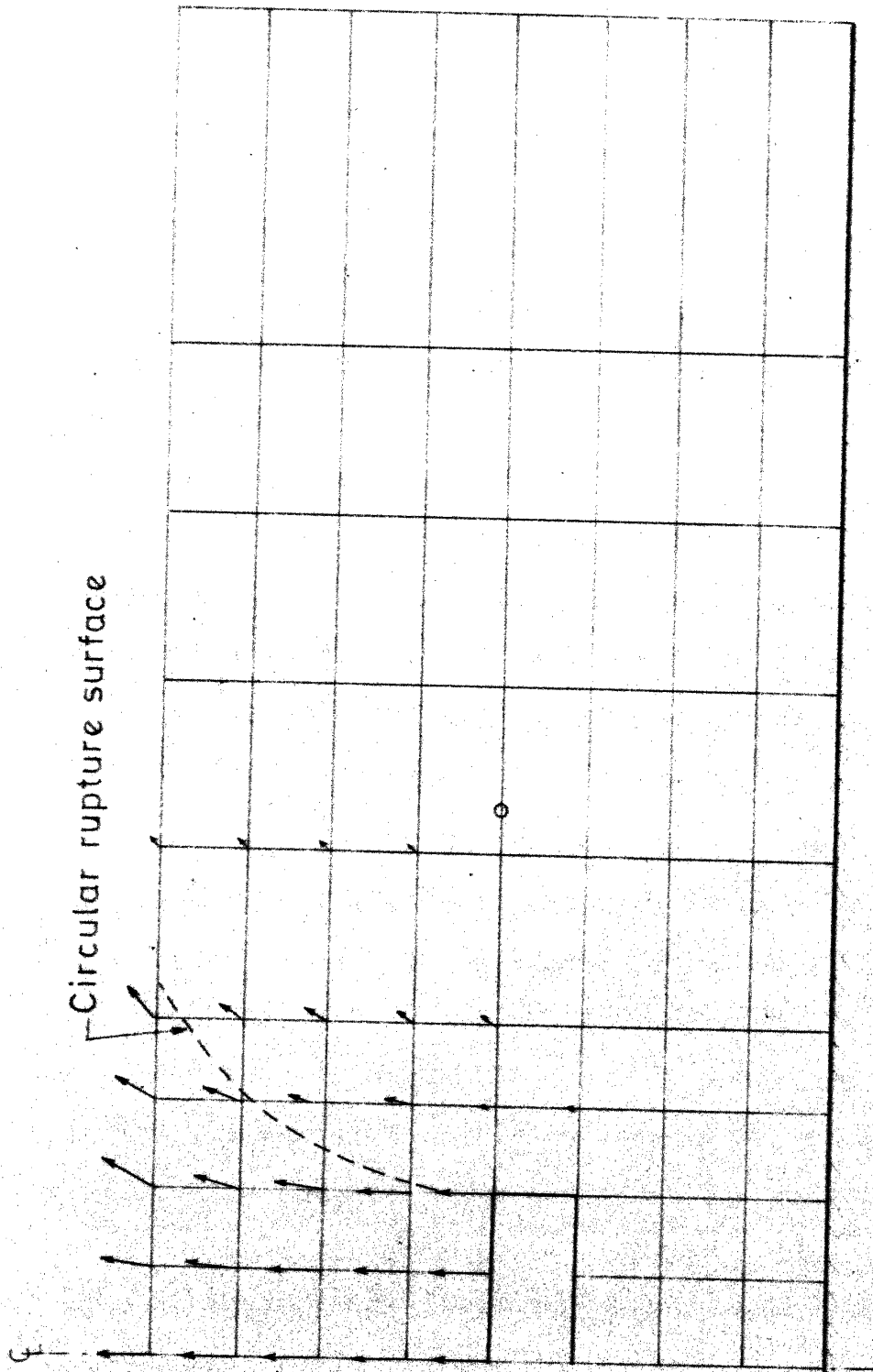


FIG.4.41 VELOCITY FIELD AT LIMIT LOAD, MOHR-COULOMB MODEL,
FULL SEPARATION, $\phi=30^\circ$, $c=0$

CHAPTER 5

VERTICAL STRIP ANCHORS

5.1 Introduction :

Vertical anchor plates (Fig. 1.1b) are used for transferring loads to the surrounding soil. Depending on the soil conditions and the loads to be carried by them, these may be made from driven steel sheet piling or using cast in situ concrete. Vertical anchors are commonly used as anchorage system for sheet pile walls and at bends in pressure pipe lines. Compared to the theoretical and experimental work done in the area of horizontal anchor subjected to vertical uplift load, the problem of vertical anchor subjected to horizontal load has received little attention from research workers. The problem needs thorough investigation since inadequate anchorage systems have been one of the main causes of failure of sheet pile walls.

The present chapter deals with the elasto-plastic undrained analysis of shallow vertical strip plate anchors, subjected to horizontal loads. The geometry of the strip plate is such that the problem can be solved as a plane-strain one. The constitutive relation used to simulate undrained behaviour of the saturated cohesive material is based on Von-Mises perfectly plastic model. For limited computer runs the perfectly plastic Tresca model is also employed for comparison purposes. Some of the few important aspects like anchor stiffness, anchor embedment, initial stresses, convergence criterion and effect of separation of anchor from soil

behind it, on response and limit load are studied.

The computer programs developed for elasto-plastic plane strain problem can use any of the classical plasticity models like Von-Mises, Tresca or Mohr-Coulomb. The undrained behaviour only is studied here, because of limitations of time. Moreover, the limited attention given to the vertical anchor problem by research workers also prompted this attempt on solution of some aspects of the problem.

5.2 Elasto-Plastic Analysis :

The discretisation of the soil layer and the vertical anchor embedded in it is carried out using eight noded parabolic isoparametric elements. The finite element meshes used for carrying out the analysis are given in Fig. 5.1. The soil layer depth is fixed as 200 cms and the bottom boundary is assumed to be a rough rigid one. Smooth rigid lateral boundaries are fixed at 600 cms from the centre line of anchor. The dimension of the vertical anchor used for analysis is 50 cms deep and 10 cms thick. Mesh-1 (Fig. 5.1a) has 313 nodal points and 90 elements. Mesh-3 (Fig. 5.1c) is coarser than Mesh-1 and has 193 nodes and 54 elements. Mesh-2 (Fig. 5.1b), incorporates six noded joint elements to simulate separation behind the anchor and has 318 nodal points and 92 elements. The anchor dimension chosen is such that, the H/B ratio works out to be 4.

The relative stiffness (K_r) of the anchor for carrying out the analysis as specified by Borowicka (69) is,

$$K_r = \frac{1}{6} \frac{(1 - \nu^2)}{(1 - \nu_p^2)} \frac{E_p}{E} \left(\frac{2t}{B}\right)^3 \quad (5.1)$$

The undrained analysis is carried out by specifying $\nu = 0.48$. The Poisson's ratio of the anchor material is fixed as, $\nu_p = 0.3$. A relative stiffness (K_r) value equal to 10 is chosen in all the computer runs where the effects of parameters other than relative stiffness are investigated. The load on the vertical anchor is applied as a concentrated load in the horizontal direction at the centre of the anchor.

'Initial stress' technique is used for the incremental elasto-plastic undrained progressive deformation analysis. The stiffness matrix of the element is formed by 2x2 numerical integration using Gaussian quadrature formula. Strains are calculated at the same four integration points from the calculated nodal displacements. Hence for each element, at four sampling points the stress state is checked to verify whether the material is in the elastic or the plastic states.

The undrained modulus specified is equal to $1 \times 10^4 \text{ KN/m}^2$ and undrained shear strength is fixed as 20 KN/m^2 . The ratio of E_u/C_u works out to be 500. For the anchor dimensions given and Poisson's ratio of anchor material equal to 0.3, if relative stiffness (K_r) is fixed at 10, the modulus of elasticity of anchor material by eqn. (5.1) works out to be $1.109 \times 10^6 \text{ KN/m}^2$. Choosing a very high value of relative stiffness (K_r), with

Poisson's ratio for soil chosen as 0.48, brings in the possibility of ill-conditioning in the system of equations to be solved. $K_r = 50$ is used only in one run where the effect of stiffness of anchor on deformation response and limit load are studied.

Von-Mises criterion and Tresca criterion do not depend on the first invariant of stress, σ_m . So, if the initial stresses due to weight of the material are isotropic, they will not affect the yield nor the ultimate load. If, $K_0 = 1$ is specified, the undrained behaviour is unaffected by the soil weight. The effect of initial stresses due to gravitational forces on the response and limit load are studied by specifying $K_0 = 0.5$.

The embedment ratio of the anchor selected is limited to $D/B = 1.0, 1.5$ and 2.0 , practically in the shallow anchor range. Computer Programs : Programs ELPLP1 and ELPLP2 are developed in DEC-1090 system for general finite element elasto-plastic analysis of the plane strain problem. Both the programs solve the non-linear problem by 'initial stress' technique. ELPLP1 is based on the Von-Mises model and ELPLP2 on Tresca and Mohr-Coulomb models. The general features and capabilities of ELPLP1 are given in Appendix B.

5.3 Results and Discussions :

The results of the undrained analysis of vertical strip anchor are presented in Table 5.1 for full bonding and full

Table 5.1

Elasto-plastic undrained analysis - vertical
strip anchor

R.No.	Model	D/B	Mesh	Properties	Conv. crit. (%)	K _r	K _o	No. of incr.	P _y (KN/m)	P _u (KN/m)	CPU time in DEC-1090(mts)
1	Von-Mises	1.5	1	Full bonding E=10 ⁴ KN/m ² C=20 KN/m ² ν= 0.48	1	1.0	1.0	19	55	95	9.45
2	-do-	1.5	1		1	10.0	1.0	19	55	95	9.32
3	-do-	1.5	1		1	50.0	1.0	19	50	95	9.58
4	-do-	1.0	1		1	10.0	1.0	15	50	75	7.09
5	-do-	2.0	1		1	10.0	1.0	24	65	120	9.53
6	-do-	1.5	1		1	10.0	0.5	19	55	95	11.53
7	-do-	1.5	1		1	10.0	1.0	10	60	100	7.03
8	-do-	1.5	1		1	10.0	1.0	5	60	100	5.27
9	-do-	1.5	1		0.1	10.0	1.0	19	55	95	13.87
10	-do-	1.5	1		0.01	10.0	1.0	18	55	90	12.04
11	-do-	1.5	3		1	10.0	1.0	21	60	105	16.81

contd..

R.No.	Model	D/B	Mesh	Properties	Conv. crit. (%)	K _r	K _o	No.of incr.	P _y (KN/m)	P _u (KN/m)	CFU time in DEC- 1090(mts)
12	Tresca	1.0	1		1	10.0	1.0	13	45	65	7.49
13	-do-	1.5	1		1	10.0	1.0	17	50	85	9.48
14	-do-	2.0	1		1	10.0	1.0	21	60	105	10.75
15	-do-	1.5	1		1	10.0	0.5	17	45	85	9.54
16	Von-Mises	1.0	2	Full separation	1	10.0	1.0	36	23	36	14.02
17	-do-	1.5	2		1	10.0	1.0	27	24	54	13.52
18	-do-	2.0	2		1	10.0	1.0	34	24	68	14.18
19	-do-	1.5	2		1	10.0	0.5	27	22	54	14.12
20	Tresca	1.5	2		1	10.0	1.0	24	20	48	18.61
21	-do-	1.5	2		1	10.0	0.5	25	16	48	17.75

separation cases. All the important parameters relating to the cases studied are also given in the table. To study the effect of increment size, convergence criterion etc. on the response of vertical anchor the computer runs are performed with D/B ratio fixed at 1.5.

The anchor is modelled by continuum elements. To investigate the effect of relative stiffness (K_r) variation of anchor, on load deformation response and ultimate capacity, the analysis is carried out by specifying $K_r = 1.0, 10.0$ and 50.0 in computer runs, R.No.1, R.No.2 and R.No.3 respectively. Von-Mises criterion was used. Figure 5.2 shows the load deformation response curves for the three K_r values. The dimensionless ratio P/CB is plotted against normalised deflection δ_c/B , δ_c being the horizontal displacement at the centre of vertical anchor. Curve for K_r value equal to 1.0 shows a larger value of horizontal anchor displacement for all loads. The load deformation curve for K_r equal to 10 and K_r equal to 50 almost coincide. The three curves at limit load merge, at the numerical limit load of 95 KN/m. Hence, for the case of shallow anchor ($D/B = 1.5$) investigated, the numerically obtained limit load is not affected by the variation in relative stiffness ($K_r = 1.0$ to $K_r = 50.0$), of the anchor.

In Table 5.2, the results of R.No.2 for $K_r = 10$ are summarised. The horizontal concentrated load applied, and the resulting horizontal displacement at the centre of anchor and the number of iterations applied to satisfy the criterion of convergence

Table 5.2

Elasto-plastic undrained analysis - Vertical strip, Von-Mises criterion

$$E = 1.0 \times 10^4 \text{ KN/m}^2$$

$$K_r = 10.0$$

$$G = 20 \text{ KN/m}^2$$

$$K_o = 1.0$$

$$\nu = 0.48$$

$$H/B = 4.0, D/B = 1.5, \text{ Full bonding}$$

Load (KN/m)	δ_c (m)	Number of iterations
5	0.0414×10^{-2}	1
50	0.4139×10^{-2}	1
55	0.4567×10^{-2}	4
60	0.5033×10^{-2}	6
65	0.5543×10^{-2}	10
70	0.6171×10^{-2}	14
75	0.6837×10^{-2}	16
80	0.8410×10^{-2}	30
85	0.9106×10^{-2}	42
90	1.135×10^{-2}	69
95	1.960×10^{-2}	200

are given in the table. A constant magnitude of incremental load of 5 KN/m is used throughout the analysis. The behaviour is elastic upto 50 KN/m. The first stress point yields at 55 KN/m. From 55 KN/m to 95 KN/m, the load deformation response is non-linear, as is evident from Fig. 5.2, as well as from the values reported in Table 5.2. The number of iterations carried out within the increment to satisfy the criterion of convergence increases with higher load. At 95 KN/m, the number of iterations completed is equal to the maximum limit on iterations specified and hence it is presumed that the numerical limit load is reached. Specification of a smaller limiting value on number of iterations, say 50, may bring in saving in computer time but will give the limit load as 90 KN/m, a lower value. Hence, in the incremental iterative technique like 'initial stress' method, the choice of the limiting number of iterations is an important aspect both from the considerations of accuracy of limit load obtained and the cost of the elasto-plastic analysis.

$K_0 = 0.5$ is specified in R.No. 6, making the initial stress magnitudes of σ_x and σ_z different from σ_y . An embedment ratio of $D/B = 1.5$, with Von-Mises model is employed for this study. The load at which the first soil stress point yields, and the ultimate capacity of the anchor are unaffected by the presence of initial stresses which are anisotropic. The numerical value of failure load was obtained as 95 KN/m. It is observed that the number of iterations needed to satisfy the convergence requirement

is more than for the case when $K_c = 1.0$, especially in the last few increments of load.

For full adhesion between anchor and soil around it, the anchor embedment ratios (D/B) equal to 1.0, 1.5 and 2.0 are carried out in R.No. 4, R.No. 2 and R.No. 5 respectively. $K_r=10$ is used in all the three cases. The load displacement response curves for the three cases analysed are shown in Fig. 5.3. The elastic horizontal deflection of the anchor decreases with increase in anchor embedment ratio. For D/B ratios 1.0, 1.5 and 2.0, the loads at first yield of a point inside the soil medium are 50 KN/m, 55 KN/m and 65 KN/m. The limit loads obtained from the elastoplastic analysis are 75 KN/m, 95 KN/m and 120 KN/m for $D/B = 1.0$, 1.5 and 2.0. These results of limit load indicate clearly that the failure load on the vertical anchor (where a complete adhesion between the anchor and the soil is assumed) increases with embedment ratio (D/B).

For a continuous anchor block in plastic clay with $\phi = 0$, and $C > 0$, and where the anchor extends to the top surface ($D/B = 1.0$) according to Coulomb and Rankine theories, the maximum resistance to lateral displacement is expressed by (97),

$$P = 2 CD + \frac{\gamma D^2}{2} \quad (5.2)$$

The above expression for P considers only the passive resistance of soil from one side of the anchor as it is displaced horizontally. If the contribution from weight is neglected, the lateral

resistance works out to be 20 KN/m only. In the elasto-plastic analysis using Von-Mises criterion, for $D/B = 1.0$, the numerical limit load obtained is 75 KN/m, if full adhesion between anchor and soil surrounding it is assumed. This value works out to be 3.75 times the load obtained from the eqn.(5.2), neglecting weight of the material. For full bonding of anchor and the soil, the elements in front and in rear of the anchor are stressed and are effective in deciding the response and limit load on anchor. Equation (5.2) uses soil resistance on one side of the anchor only. For continuous anchor blocks which are deeply buried beneath plastic saturated clay ($\phi = 0$ case), the limit load per unit length is reported by Hansen (38) as,

$$P = 11.4 CD \quad (5.3)$$

This value works out to be 114 KN/m for the anchor analysed. For $D/B = 1.5$ and $D/B = 2.0$, the limit loads obtained from finite element analysis are 95 KN/m and 120 KN/m respectively. This indicates that even for $D/B = 2.0$, the limit load obtained from finite element elasto-plastic progressive deformation analysis under full bonding case is greater than the upper bound load suggested for very deep anchors by Hansen (38).

Figures 5.6, 5.7 and 5.8 show the propagation of yielded points with load upto failure for $D/B = 1.0$, 1.5 and 2.0 respectively. For $D/B = 1$, Figs. 5.6a, 5.6b and 5.6c show the points which have reached plastic state at 60 KN/m, 70 KN/m and

75 KN/m (failure load). The points on either side of the anchor near the surface yield first. The zone that yields with subsequent increments in load spread on either side of anchor in a symmetrical manner. The plastic zones at collapse load are localised on either side of the anchor symmetrically and the extent of the zone at the surface being about 2.5 D on both sides of anchor axis. The points yielded extend below anchor level also. Figs. 5.7a, 5.7b and 5.7c show the yielded points for $P = 70 \text{ KN/m}$, 90 KN/m and 95 KN/m for $D/B = 1.5$. For this case the points near the bottom of anchor, yield first. As load on anchor increases the points yielded spread and extent towards top and sides of anchor. It can be observed generally that for $D/B = 1.5$, the zone of yielding is larger when compared to $D/B = 1.0$. Figs. 5.8a, 5.8b and 5.8c give the points which have reached the plastic state for $P = 80 \text{ KN/m}$, 100 KN/m and 120 KN/m (failure load) respectively. The points which yield first are the ones near the bottom of the anchor and they spread out towards the sides and extend to the top and bottom. A symmetrical pattern in yielded zones on either side of anchor is seen at all stages of loading and the zone of yielding at failure is larger than for $D/B = 1.0$ and $D/B = 1.5$.

For $K_r = 10.0$ and $D/B = 1.5$ in R.No.2, the load in one increment is kept as 5 KN/m. This is increased to 10 KN/m and 20 KN/m per increment in R.No. 7 and R.No. 8 respectively. It is seen that the load at which the first point yields is increased to

60 KN/m. For loads greater than this, the deformation response is such that the points lie on the curve for $D/B = 1.5$ shown in Fig. 5.3, which is obtained keeping the load per increment as 5 KN/m. The failure load obtained is 100 KN/m in both the cases, which is within the limits of accuracy expected with the use of a larger increment of load. Hence, using initial stress method for elasto-plastic non-linear undrained analysis, even under number of increments of load, the deformations obtained lie on the load deformation curve obtained with finer increments in load. Numerical limit load is not significantly affected by specifying a larger incremental load.

The criterion for convergence on absolute maximum value of residual load vector is kept at 1 percent of the load applied in one increment. In R.No. 9 and R.No. 10, the effect of a stricter criterion on convergence equal to 0.1 percent and 0.01 percent are set keeping all other parameters same. It is observed that for the case investigated for $D/B = 1.5$, the 0.1 percent criterion does not influence the limit load of 95 KN/m obtained. But the number of iterations needed to satisfy the criterion within an increment is found to be considerably larger and hence, the computer time needed for the solution of the elasto-plastic problem is also more. By setting a convergence criterion equal to 0.01 percent makes the limit load to 90 KN/m which is about 5 percent less than the limit load obtained with a 1 percent criterion.

Mesh-3 (Fig. 5.1c) is a coarser mesh with 193 nodes and 54 elements. In this arrangement the vertical spacing of the nodes is fixed at the same distance as in Mesh-1 (Fig. 5.1a), but the horizontal spacing of nodal points are altered. For $D/B = 1.5$ and $K_r = 10$, Mesh-3 is used in R.No. 11 to study how the response and limit loads are affected by the use of a coarser mesh. The yield load is 60 KN/m. The limit load from this case is 105 KN/m, which is 10.5 percent greater than the corresponding load for Mesh-1. This shows that the limit load has definitely improved with a finer mesh and the trend observed from the two mesh arrangements studied for vertical anchor is that the limit load is reduced with the use of a finer mesh.

In R.No. 12 , R.No. 13 , R.No. 14 and R.No. 15 , the elastic perfectly plastic Tresca model is used for carrying out the undrained analysis. The relative stiffness of $K_r = 10$ and convergence criterion of 1 percent is fixed in all the computer runs. For full bonding between anchor and the soil, the analysis is carried out for embedment ratios of $D/B = 1.0, 1.5$ and 2.0 . The load deformation response curves for the vertical anchor are given in Fig. 5.4. The response curves start with a straight line elastic segment, become non-linear after the onset of yield, and then become asymptotic to x-axis at collapse state. The results obtained indicate that the load at which the first point yields for $D/B = 1.0, 1.5$ and 2.0 are 45 KN/m, 50 KN/m and 60 KN/m respectively. These loads are less than the corresponding loads

using Von-Mises criterion. The collapse loads obtained for all the three embedment ratio considered, are less than those obtained using Von-Mises model. It is also observed that for K_0 set equal to 0.5, the initial stresses (for $D/B = 1.5$), do not influence the load at which the first point yields nor the ultimate load.

From experimental results on anchor blocks (48), it is noted that there is no contact between anchor and the soil behind the anchor at failure. A full separation of the anchor from the soil behind it is modelled by incorporating interface elements of negligible normal stiffness. In R.No. 16, R.No. 17, R.No. 18 and R.No. 19, at all load levels separation is assumed. For $D/B = 1.0$, 1.5 and 2.0, the load deformation responses are plotted in Fig.5.5. The elastic deflection in the horizontal direction at the centre of anchor decreases with increase in embedment ratio. The response curves show a straight line portion (elastic state) and a non-linear segment which finally becomes asymptotic with x-axis at limit state. The ultimate load on anchor increases with increase in embedment ratio D/B . The loads at failure obtained are 36 KN/m, 54 KN/m and 68 KN/m respectively for $D/B = 1.0$, 1.5 and 2.0. These limit loads obtained for the case of full separation are less when compared to the full bonding case for all the D/B ratios investigated. For $D/B = 1.5$, the load obtained is 54 KN/m which is only 0.57 times the load obtained for the full bonding case.

Equation (5.2) gives the maximum passive resistance from one side of the soil on the anchor wall to be 20 KN/m only, for the anchor extending to the surface of the soil. The corresponding result from elasto-plastic analysis for $D/B = 1.0$, gives an ultimate limit load of 36 KN/m using Von-Mises criterion. The limit load obtained from the elasto-plastic analysis using Von-Mises criterion is larger than that obtained from resistance calculated using passive earth pressure theories. In Fig. 5.11, the experimental curve obtained by tests on anchor blocks in plastic clay (48) and the theoretical results are given. The limit load obtained for $D/B = 2.0$ are less than the higher limit obtained from experiments equal to 9.5 CB (Fig. 5.11). Even with full separation, the limit loads obtained are more than the experimentally observed values for anchor blocks for the same D/B ratios. The cases analysed in this work are for anchor slabs whose B/t ratio works out to be 5, where t is the thickness of continuous anchor slab. For square blocks, the response will also be affected by the bonding of more number of elements with the anchor above and below.

Figures 5.9a, 5.9b and 5.9c show the points yielded at the failure load for $D/B = 1.0$, $D/B = 1.5$ and $D/B = 2.0$ respectively. For $D/B = 1.0$, the points in front of the anchor near the ground surface yield first. The zone that has yielded is localised in front of the anchor and also extend to the bottom of the anchor. The zone of yield indicates that a curved rupture surface used in

passive resistance calculation is a reasonably good approximation. For $D/B = 1.5$, the zone that has yielded is mainly in front of the anchor extending to a level below the anchor also. The points that have yielded at failure load are more in number and the zone of yield is larger than for $D/B = 1.0$. The points extend to the surface. For $D/B = 2.0$, the zone that has yielded is larger than for $D/B = 1.0$ and $D/B = 1.5$ and the yielded points spread to the surface of the ground.

Figure 5.10 shows the velocity field for the vertical anchor for full separation case. At failure, a mechanism which is localised to the front of the anchor and extending to top and which is curved is indicated for $D/B = 1.5$. When the anchor is separated from the soil behind it, practically, the plastic zone and the movements are concentrated to the front of the anchor.

R.No. 20 and R.No. 21 use Tresca criterion. The load deformation response curve for the full separation case investigated is given in Fig. 5.4. When compared with the results for same $D/B = 1.5$ for full bonding case, the elastic displacement at centre of anchor are more for this case. The load at first yield and the limit load are smaller, the collapse load being only 48 KN/m in comparison to the 85 KN/m obtained for full bonding case. The load at which the first point yields appear to be slightly smaller, but the collapse load appears to be unaffected by the presence of initial stresses.

5.4 Conclusions :

Based on the elasto-plastic undrained analysis of the shallow vertical plate anchor, using the Von-Mises and Tresca material models in finite element method, the following inferences are made :

Both Von-Mises and Tresca perfectly plastic models can be used with displacement finite element method to trace the load deformation history upto collapse. The 'initial stress' technique (108) which is used to solve the non-linear problem is found to be satisfactory. The limited cases investigated show that the Von-Mises model predicts higher load for first yield and higher limit load in comparison to Tresca model. The load displacement curves from Tresca model fall below those obtained using Von-Mises model.

For the embedment ratios corresponding to shallow anchor range, the relative stiffness of the anchor does not appear to influence the collapse load obtained using Von-Mises perfectly plastic model. But the deformation history below collapse may be affected by a lower anchor stiffness.

If 'initial stress' method is used for the solution of the non-linear elasto-plastic problem to obtain collapse load, the maximum number of iterations specified within an increment has to be decided carefully because specification of a lower limit may show a decrease in collapse load. A convergence criterion equal to one percent, specified on the absolute maximum value of

the residual load vector appears to be a reasonable one. A stricter criterion may increase the cost of the computer analysis and can result in giving a reduced limit load as well. The refinement of mesh used for the analysis will definitely affect the ultimate load at least up to certain stage of refinement. From the cases analysed, it is seen that the numerical limit load obtained from a fine mesh is smaller in magnitude than from a coarse mesh for the same problem. If the same maximum number of iterations are specified within a load increment, the use of a larger load per increment does not appear to affect either the load displacement diagram or the numerical limit load significantly.

The load deformation response, pattern and spread of plastic zone and collapse load obtained from the elasto-plastic analysis are affected by the type of bonding behind the anchor. Although only case of full bonding between anchor and soil surrounding and full separation behind the anchor are investigated here, it is seen that the interface condition is an important parameter to be considered in any realistic simulation of vertical anchor behaviour. The ultimate loads obtained for the full bonding cases are more than the loads obtained for full separation cases.

The embedment ratio (D/B) of the vertical anchor is an important parameter which affects deformation response, the load at first yield as well as the collapse load for the range of

D/B investigated. The elastic horizontal deflection at anchor centre decreases with increase in embedment depth. The collapse load obtained from elasto-plastic analysis increases with increase in embedment depth, both for full bonding and full separation cases investigated.

The yield zone is symmetrical at all stages of loading for full bonding case. The zones extend upto the ground surface and are localised around the anchor. The plastic zone for full separation case is limited to the front of the anchor and the extent of the plastic zone at collapse increases as embedment ratio increases.

The collapse load obtained from a full separation case from using either Von-Mises or Tresca perfectly plastic models are greater than the values obtained from the conventional earth pressure theories for $\phi = 0$ case for a vertical anchor extending to the surface.

The velocity field, obtained from elasto-plastic analysis for $D/B = 1.5$ indicates that a localised region in front of the anchor deform considerably. The pattern suggests an envelope of a curved boundary and straight line used for passive earth pressure calculation for $\phi = 0$ case is reasonable.

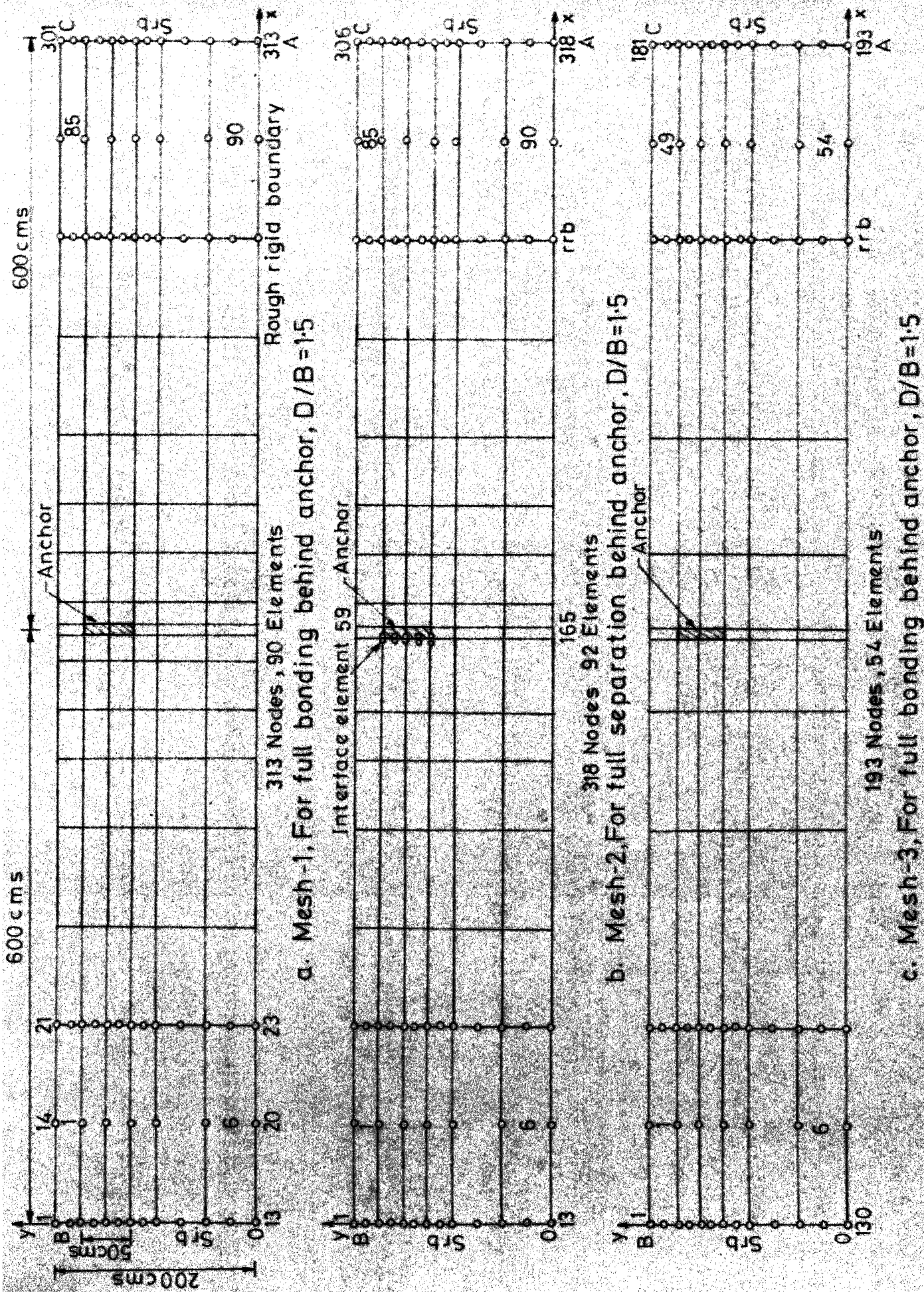


FIG-5-1 DISCRETISED MODEL OF SOIL LAYER AND ANCHOR, ELASTO-PLASTIC ANALYSIS

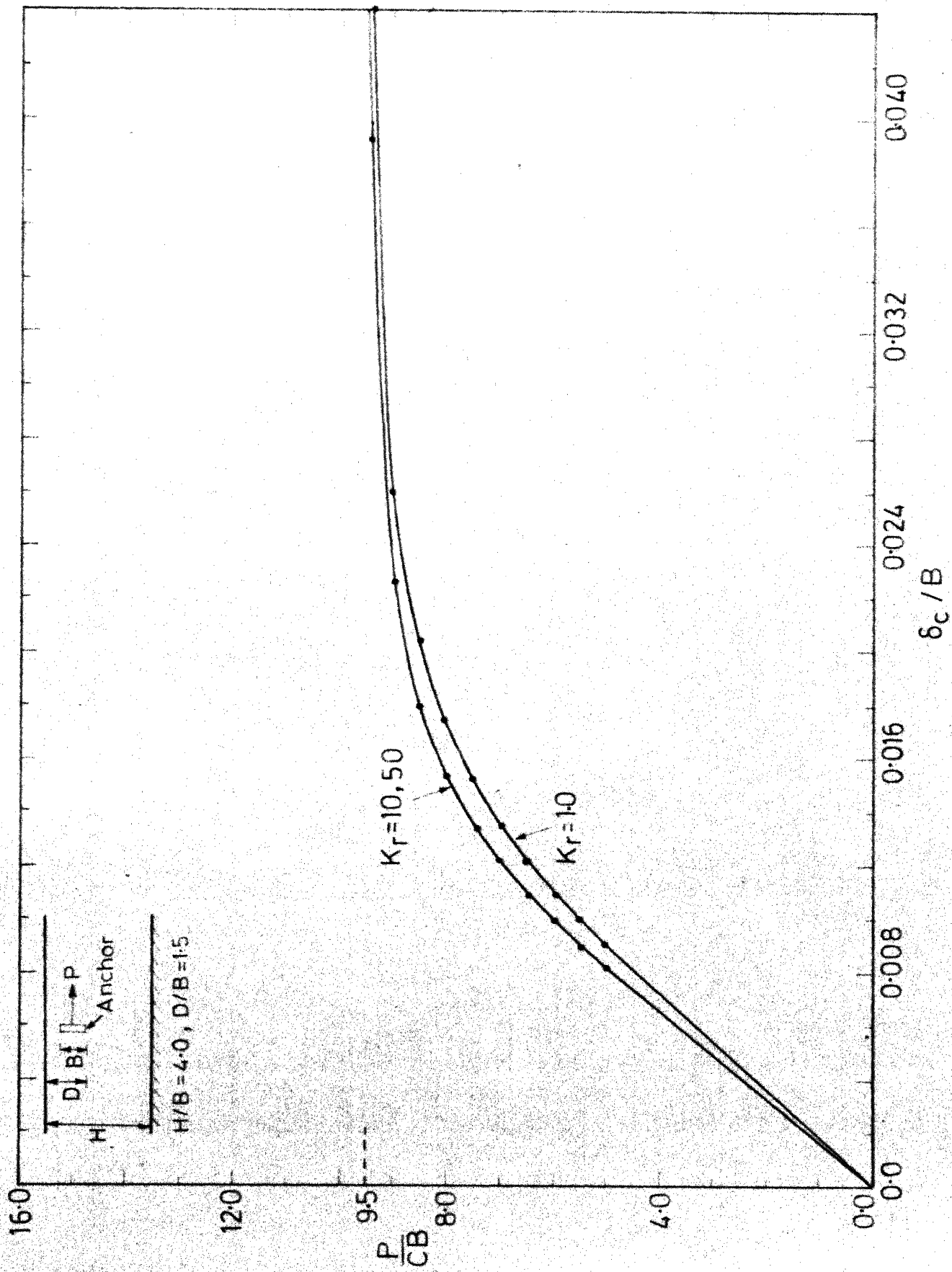


FIG.5.2 LOAD DISPLACEMENT RESPONSE OF VERTICAL ANCHOR FOR $K_r = 1, 10, 50$
(FULL BONDING, VON-MISES MODEL)

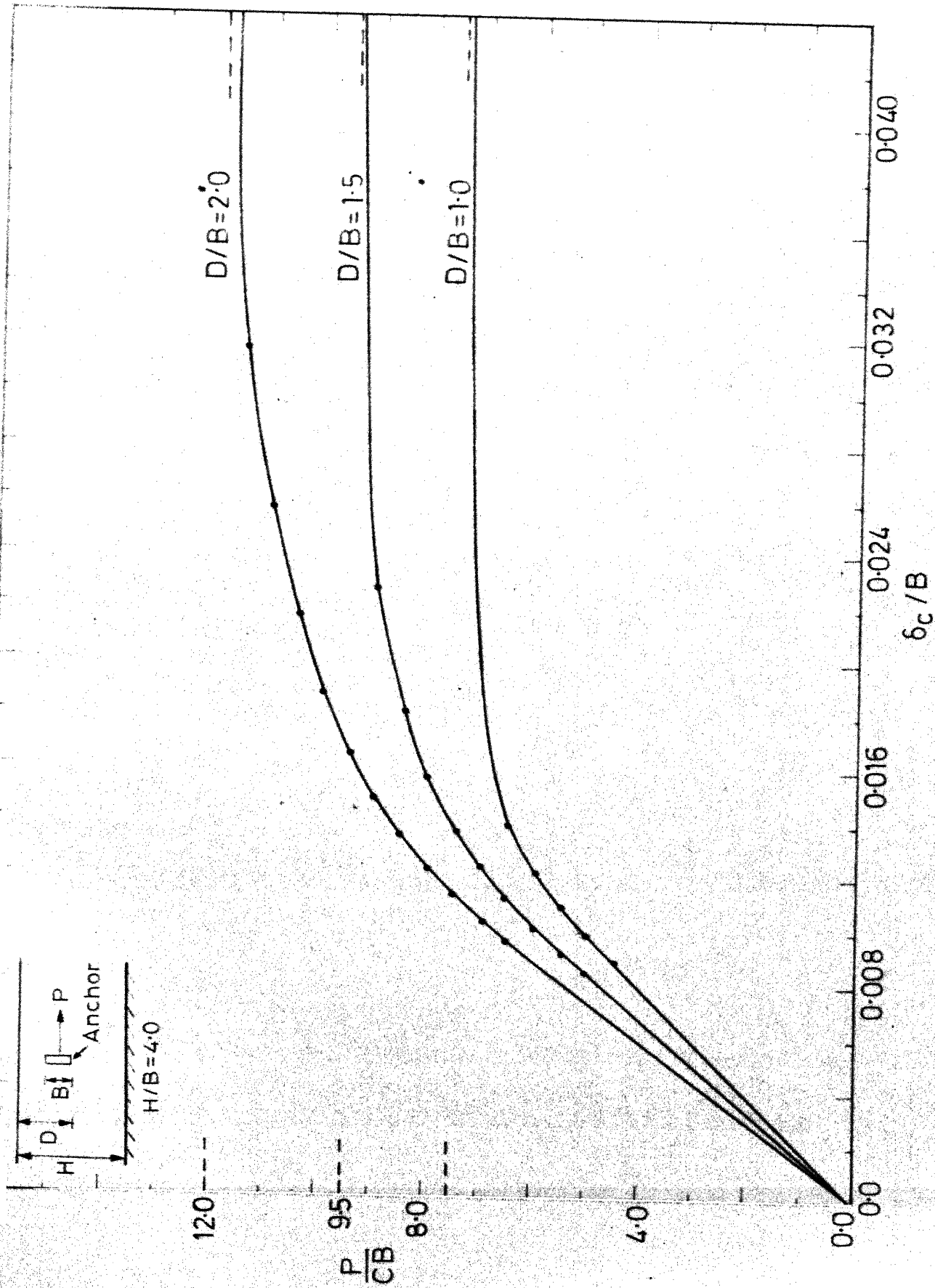


FIG.53 LOAD DISPLACEMENT RESPONSE OF VERTICAL ANCHOR FOR $D/B=1.0, 1.5, 2.0$
(FULL BONDING, VON-MISES MODEL)

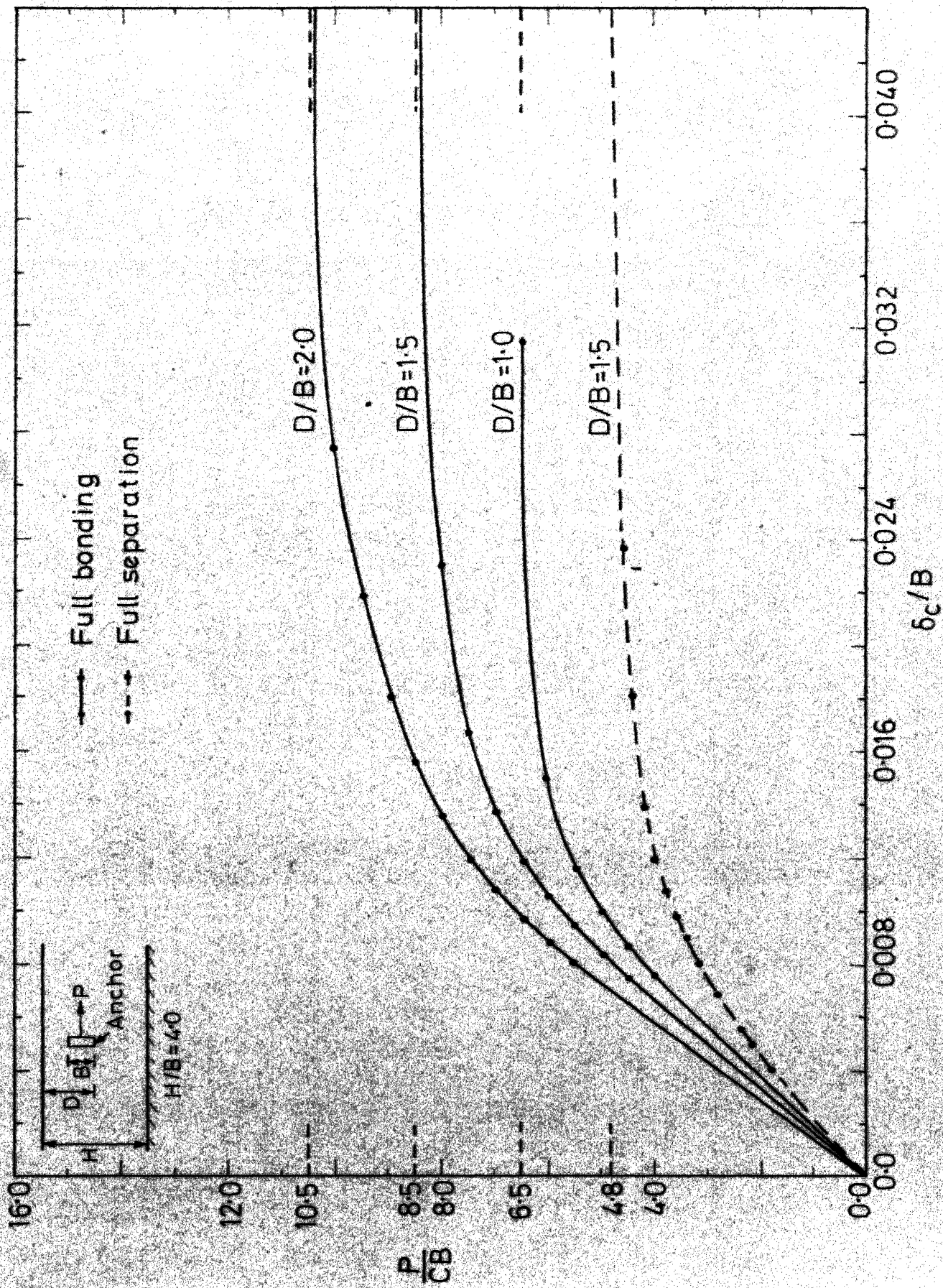


FIG.5-4 LOAD DISPLACEMENT RESPONSE OF VERTICAL ANCHOR FOR $D/B=1.0, 1.5, 2.0$
(TRESCA-MODEL)

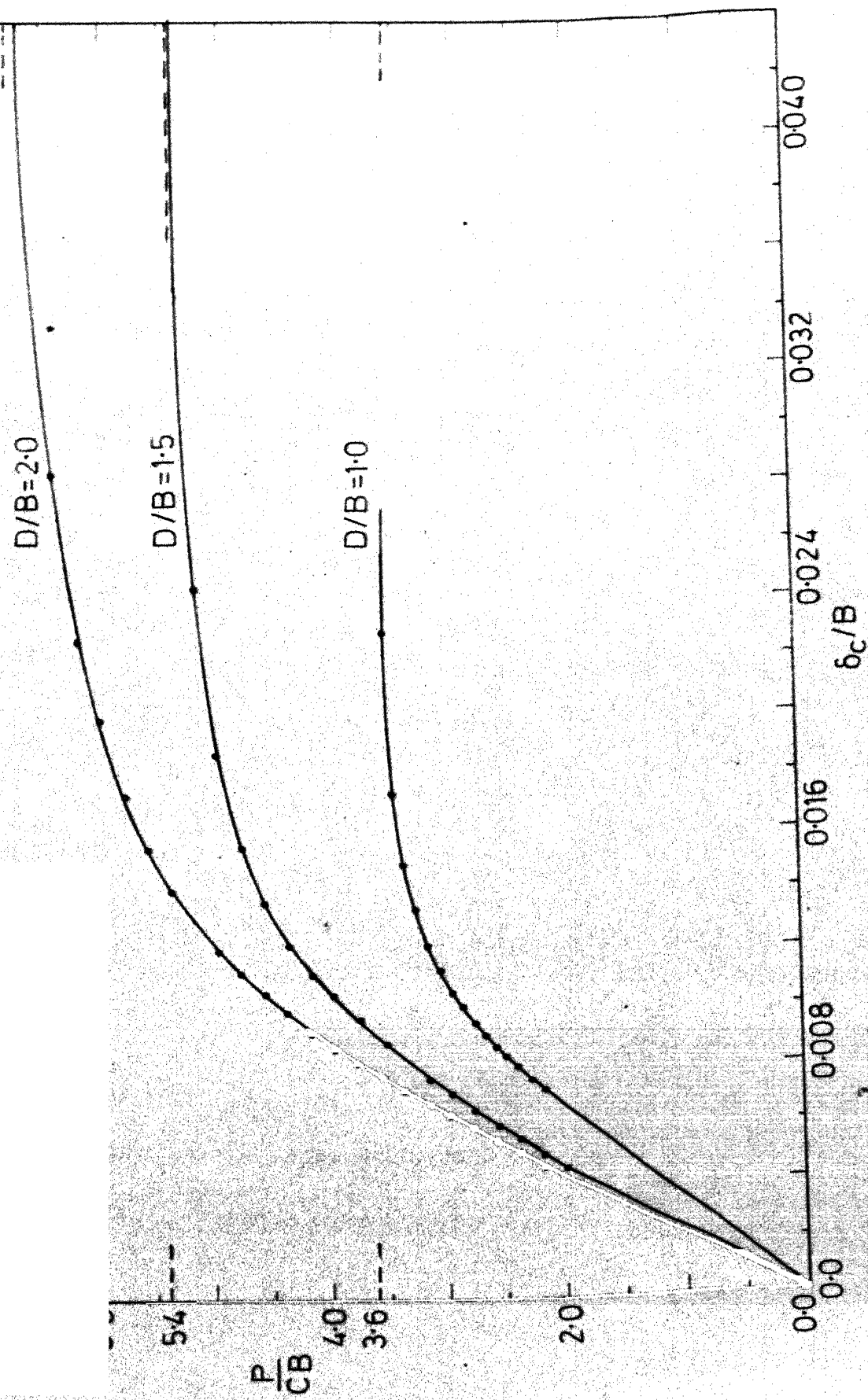
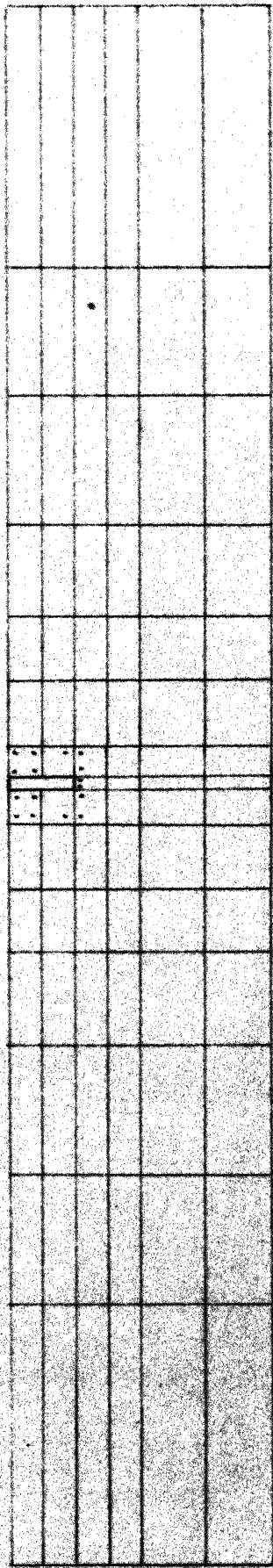
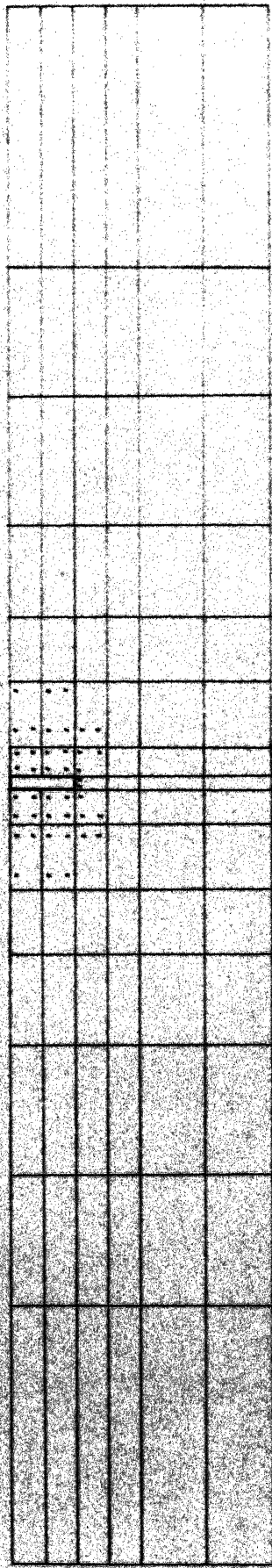


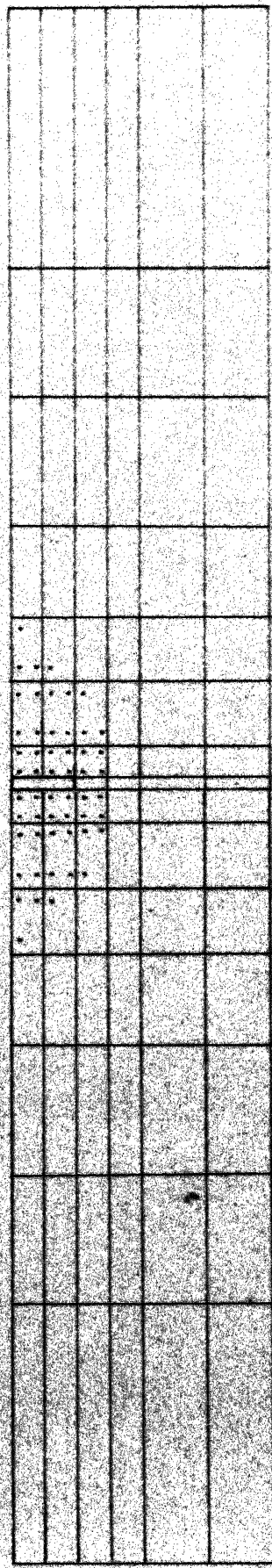
FIG.5.5 LOAD DISPLACEMENT RESPONSE OF VERTICAL ANCHOR FOR $D/B=1.0, 1.5, 2.0$
(FULL SEPARATION, VON-MISES MODEL)



a. $P = 60 \text{ kN/m}$



b. $P = 70 \text{ kN/m}$



c. $P = 75 \text{ kN/m}$ (Failure load)

FIG. 5.6 SPREAD OF PLASTIC ZONE (VERTICAL ANCHOR, $D/B = 1.0$, FULL BONDING, VON-MISES MODEL)

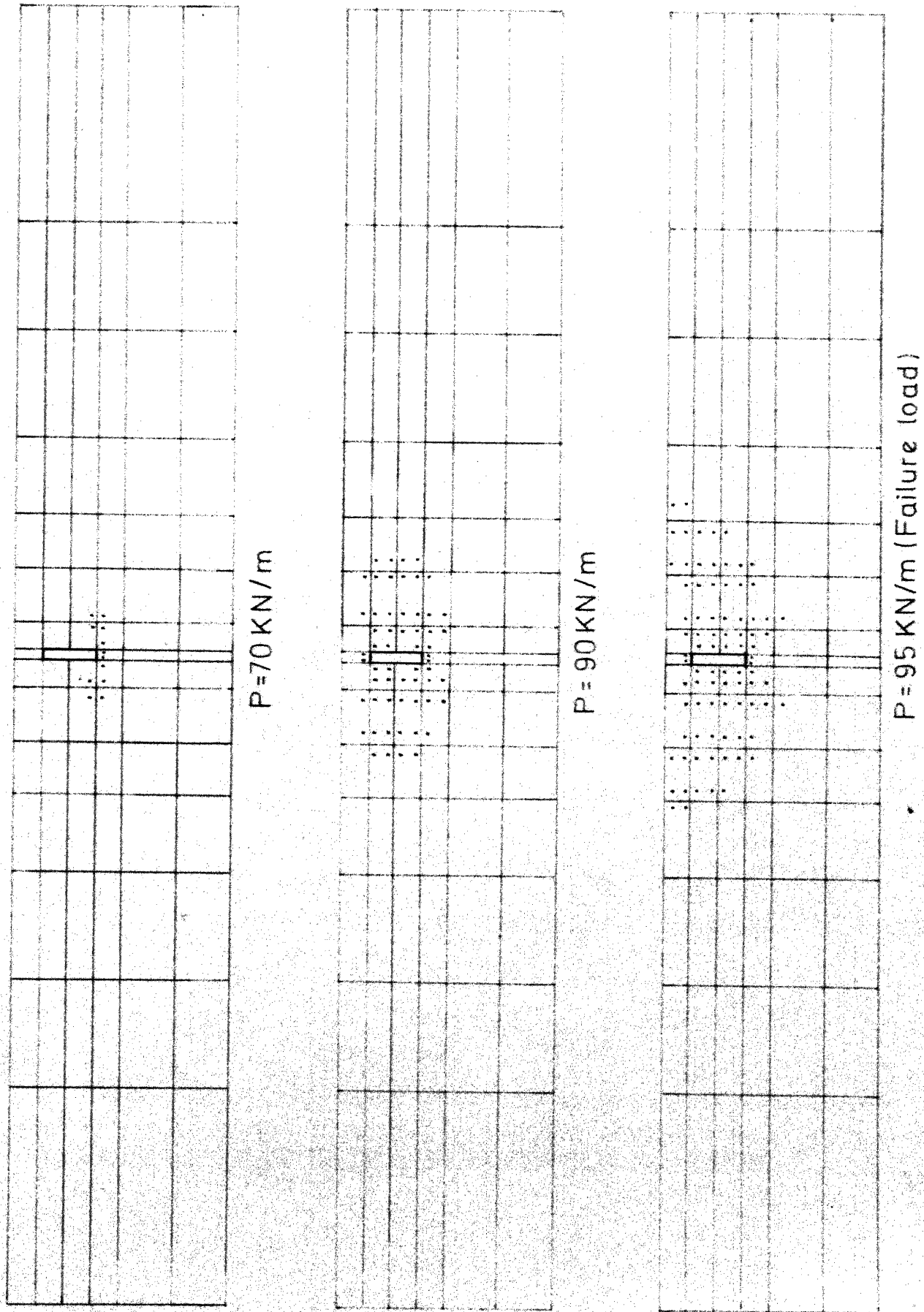
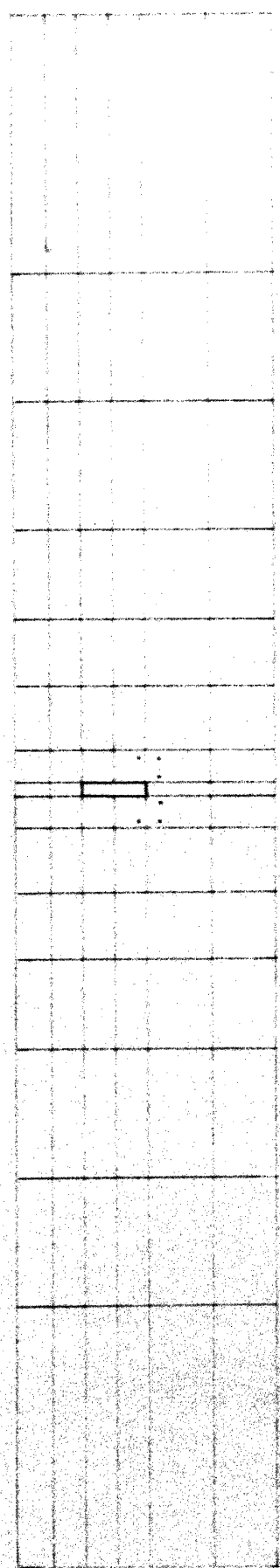
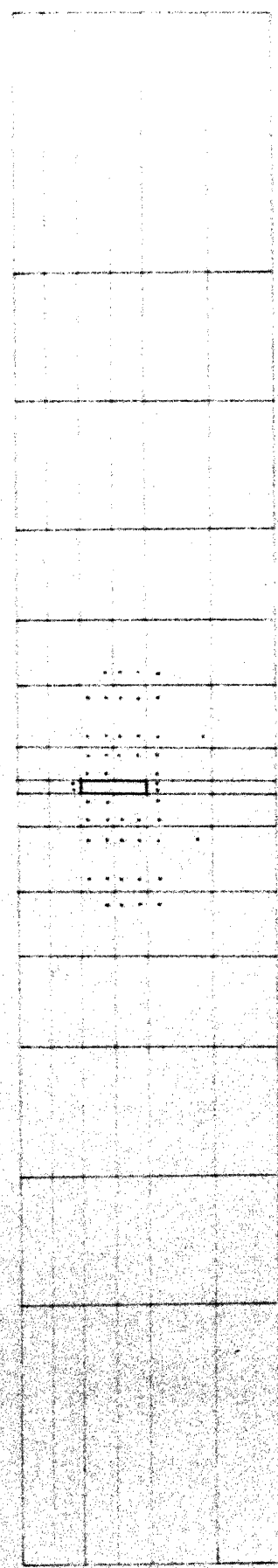


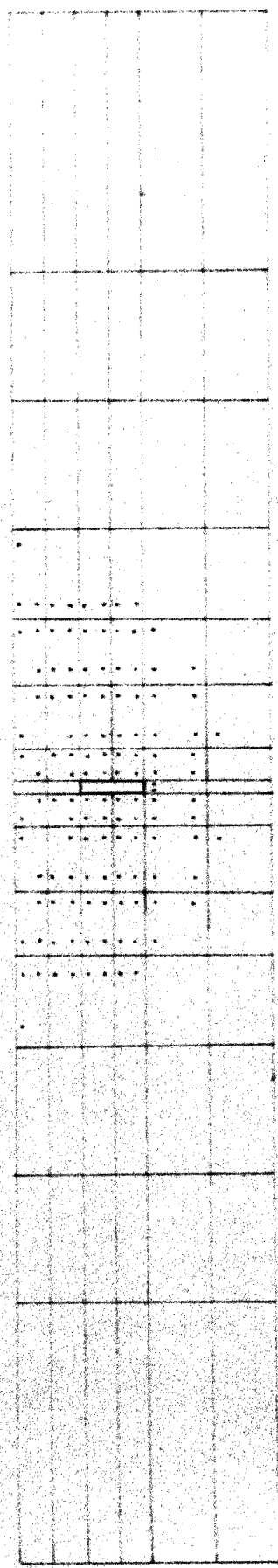
FIG.5.7 SPREAD OF PLASTIC ZONE (VERTICAL ANCHOR, $D/B=1.5$. FULL BONDING, VON-MISES MODEL)



$P = 80 \text{ kN/m}$

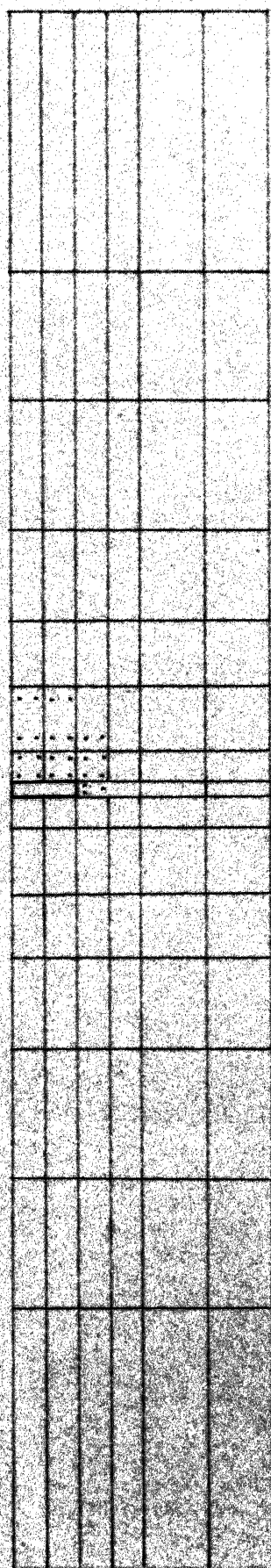


$P = 100 \text{ kN/m}$

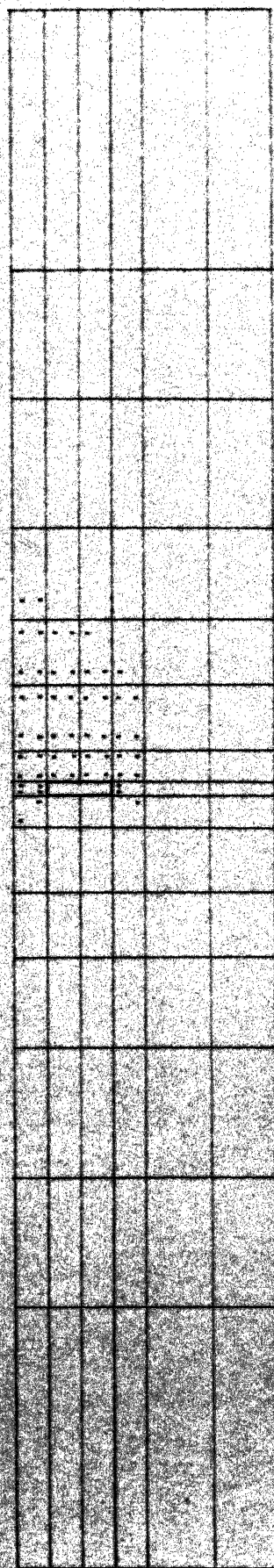


$P = 120 \text{ kN/m}$

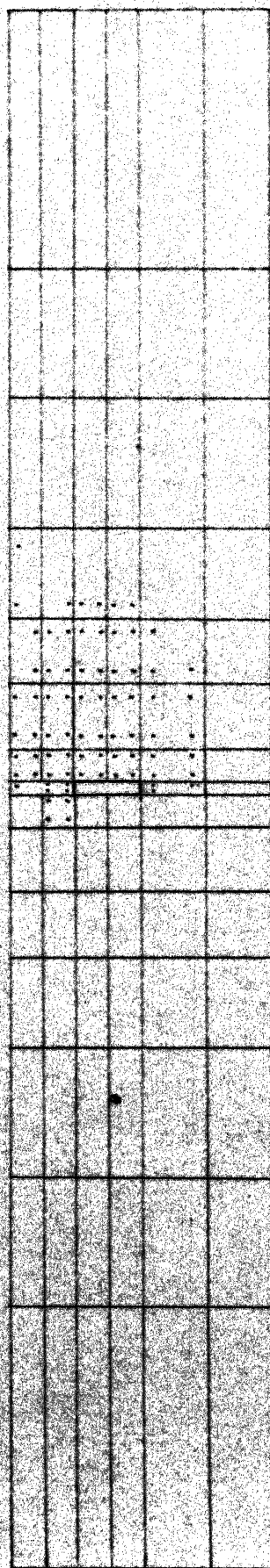
FIG-58 SPREAD OF PLASTIC ZONE (VERTICAL ANCHOR, $D/B=2.0$, FULL BONDING, VON-MISES MODEL)



a. $H/B = 4.0$, $D/B = 1.0$ $P = 36 \text{ kN/m}$ (Failure load)



b. $H/B = 4.0$, $D/B = 1.5$ $P = 54 \text{ kN/m}$ (Failure load)



c. $H/B = 4.0$, $D/B = 2.0$ $P = 68 \text{ kN/m}$ (Failure load)

FIG. 5.9 YIELD ZONE AT FAILURE LOAD (VERTICAL ANCHOR, $D/B = 1.0, 1.5, 2.0$; FULL SEPARATION, VON-MISES MODEL)

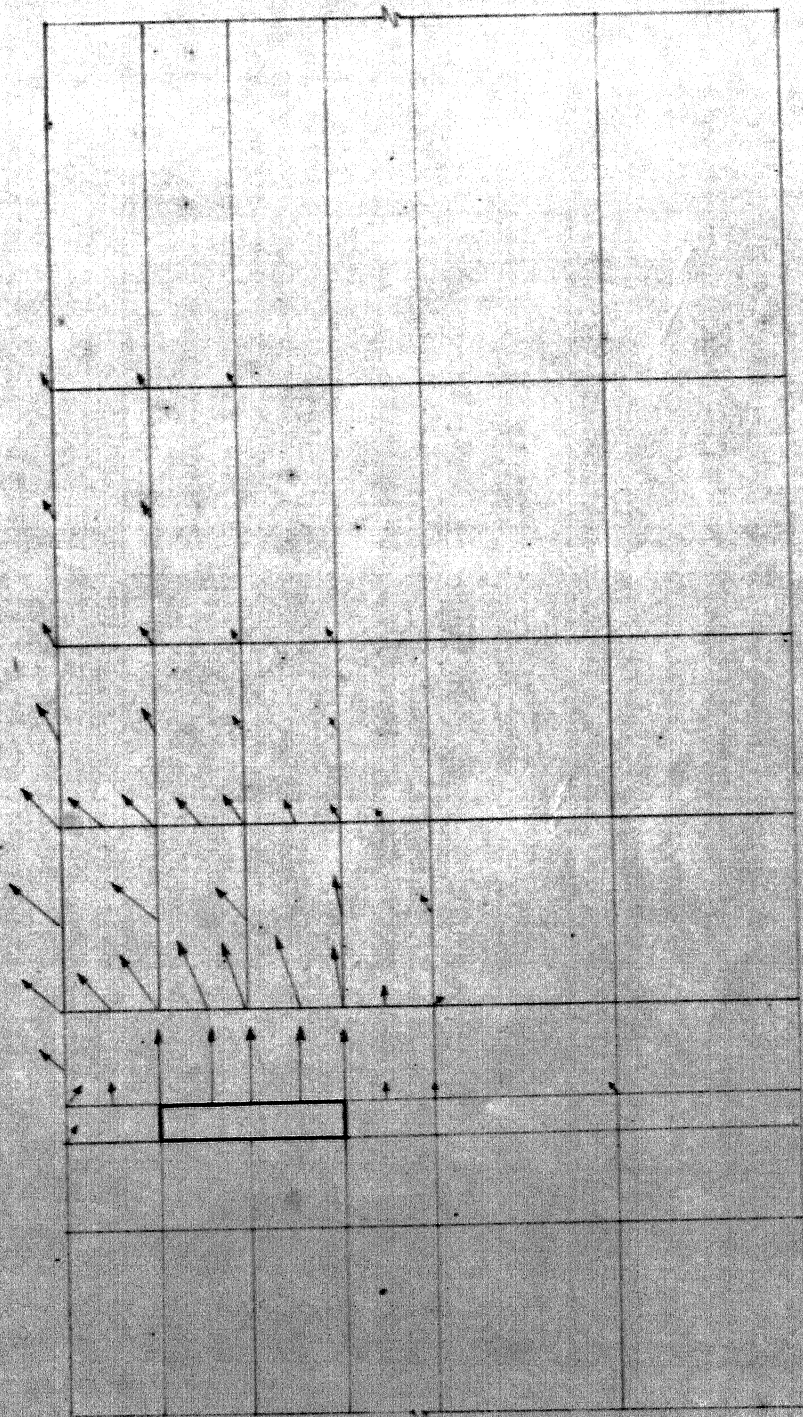


FIG. 5.10 VELOCITY FIELD AT COLLAPSE LOAD (VERTICAL ANCHOR,
FULL SEPARATION, VON-MISES MODEL, $D/B=1.5$)

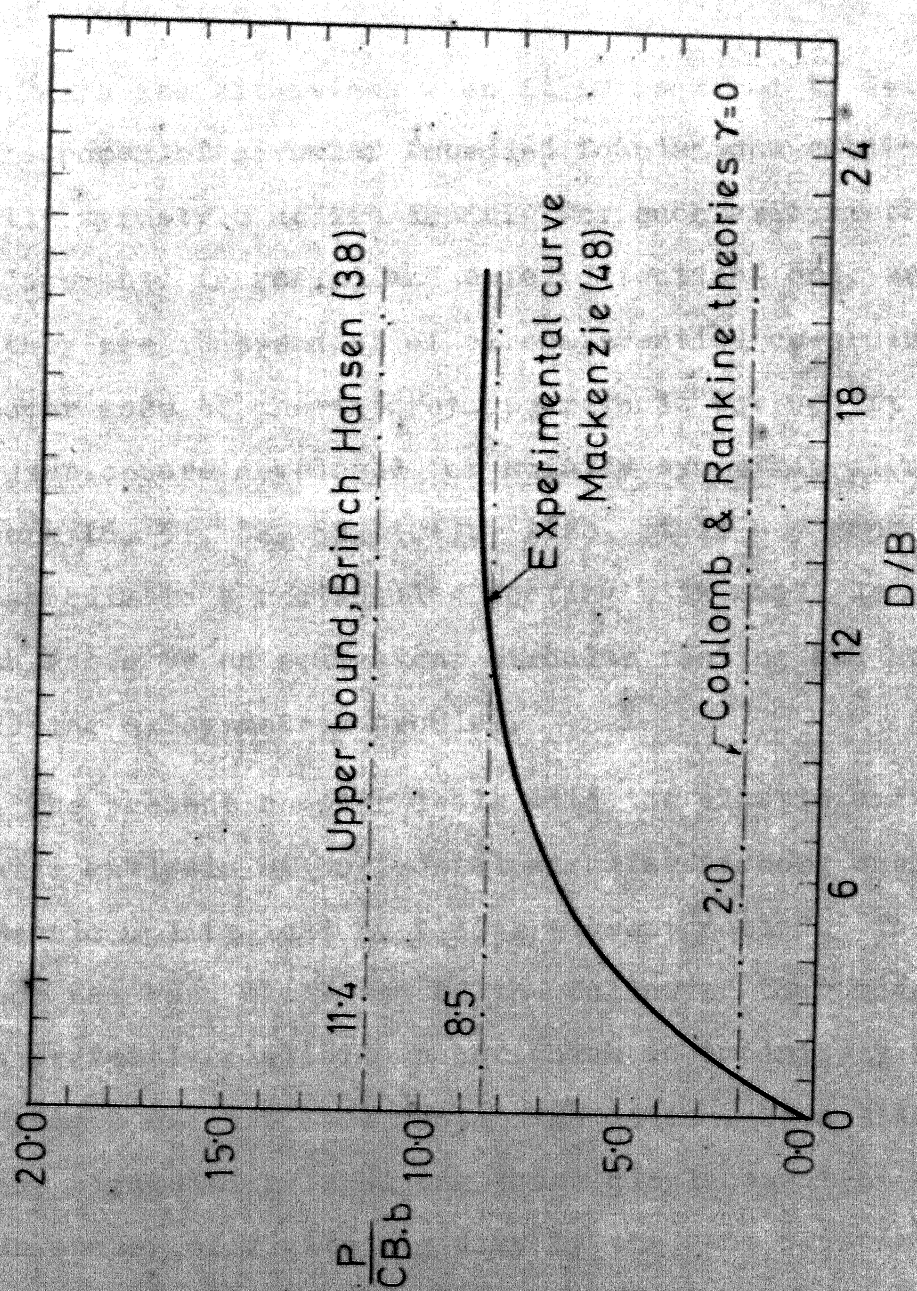


FIG. 5.11 RESISTANCE OF PLASTIC CLAY TO ANCHOR BLOCKS. SUMMARY OF EXPERIMENTAL AND THEORETICAL RESULTS

elements. Under small loads it is usually assumed that a full bonding of anchor bottom and soil exists. Study of limiting case of separation of anchor from the soil below is also carried out since this is an important aspect which effects all the response parameters of this soil structure interaction problem.

The elastic response of a flexible circular anchor subjected to uniform pressure and a rigid anchor embedded in an elastic layer of limited depth has been investigated under different embedment ratios and Poisson's ratios. For studying the effect of relative stiffness of anchor with the use of continuum element and plate bending element a specific embedment ratio ($D/B = 1.0$) and layer depth ($H/B = 2.0$) has been chosen. A comparison of these models has been done based on the anchor response obtained from the studies.

For the undrained progressive deformation analysis of anchor uplift problem the Von-Mises perfectly plastic model has been used. Perfectly plastic Tresca model is used for comparison. Some important aspects studied are the effects of anchor rigidity, interface separation, convergence criterion, magnitude of incremental load, refinement of mesh etc. on the load deformation response and limit load. For simulating drained behaviour Mohr-Coulomb associated perfectly plastic model is chosen and the results obtained compared with shallow anchor theories.

6.2 Finite Element Model :

6.2.1 Elastic Analysis :

Four noded axisymmetric ring elements are used for discretising soil layer. The finite element meshes are the same as used for plane-strain analysis and are shown in Figs. 4.2 and 4.3. The number of nodal points are 630 and number of elements 580 for the Mesh-1 (Fig. 4.2) and is used for the full bonding case. Mesh-2 in Fig. 4.3, has 641 nodes and 590 elements and is used in cases where interface separation below anchor is simulated. The bottom of elastic soil layer has a rough rigid boundary and side boundary is a smooth rigid one. The diameter of anchor (B) is fixed at 100 cms. The soil layer depth is kept at 200 cms for $H/B = 2.0$ and 400 cms for $H/B = 4.0$. As indicated in Fig. 4.2, the distance of side boundary from the centre line is kept as 400 cms.

The separation of circular anchor for the soil layer beneath it is modelled by providing four noded interface elements with very low values of normal and shear stiffnesses. The elastic analysis of circular anchor is carried out for the following four cases.

a) Flexible Anchor Subjected to Uniform Pressure : At the level where the circular anchor is embedded a uniform uplift load is applied.

b) Rigid Anchor : A rigid circular anchor is simulated by applying equal vertical upward displacement at the level where the circular anchor is placed. The equivalent nodal forces are summed up to obtain the uplift load. The rigid circular anchor is considered infinitely thin in comparison to soil elements.

c) Circular Anchor of Finite Rigidity, Continuum Elements : The anchor thickness is fixed as 20 cms. 20 axisymmetric ring elements in two layers are used to discretise the anchor. The relative stiffness of anchor for analysis is as specified by Borowicka (69), (i.e.)

$$K_r = \frac{1}{6} \frac{(1 - \nu_p^2)}{(1 - \nu_p^2)} \frac{E_p (2t/B)^3}{E} \quad (6.1)$$

where

E, ν = elastic moduli of soil

E_p, ν_p = elastic moduli of anchor material

t = thickness of anchor

B = diameter of the anchor

The Poisson's ratio of anchor plate material is taken as 0.3. The analysis is carried out for $\nu = 0.3$ and $\nu = 0.49$. The relative stiffness considered for analyses varied from 0.01 to 10.0. The loads applied on anchor are (i) uniform uplift pressure, (ii) concentrated uplift load at centre of anchor.

d) Circular Anchor of Finite Rigidity, Plate Elements : The axisymmetric plate bending element is a line element. The relative stiffness is fixed as specified in eqn. (6.1). 10 elements

are used to simulate the anchor. The Poisson's ratio of soil is taken as 0.3 and 0.49 and that of plate material is taken as 0.3. The anchor is analysed for a uniform upward uplift pressure and the range of relative stiffness (K_r) considered varied from 0.01 to 100.

The cases (a), (b) and (c) given above are analysed using computer program 'ISOAXI' developed for the purpose. The general features of this program are same as for 'ISOPIN', the details of which are given in Appendix A. This program uses the 4 noded ring element and 4 noded interface element to simulate the interface. For analysis of the cases (d) where an axisymmetric plate bending element is used to simulate the anchor, the program 'ISOPLJ' is developed. This is a modification of 'ISOAXI', with provision for including plate bending element also into analysis. The two programs 'ISOAXI' and 'ISOPLJ' are developed in DEC-1090 system at I.I.T. Kanpur, Computer Centre. All the computer runs needed for the elastic analyses are carried out in DEC-1090 system.

6.2.2 Elasto-Plastic Analysis

Eight noded axisymmetric ring elements are used for the discretisation of soil layer and the circular anchor. The arrangement of mesh chosen for the axisymmetric analysis of anchor problem is the same as used for plane-strain case. For the full bonding cases, Figs. 4.30a, 4.30c and 4.30d give the three finite element meshes. Mesh-1 has 72 elements and 251 nodes, Mesh-3 has

40 elements and 147 nodes and Mesh-3 has 20 elements and 79 nodes. Mesh-2 which incorporates 6 noded axisymmetric interface element also has 256 nodes and 74 elements and is shown in Fig. 4.3Cb. The diameter and thickness of the circular anchor are chosen as 100 cms and 25 cms for analysis. Equation (6.1) is used to calculate the relative stiffness of the anchor. The soil layer depth is fixed at 200 cms. The lateral boundary is at a distance of 400 cms from centre of anchor. 6 noded axisymmetric ring elements are used to model the interface.

'Initial stress' method is used to solve non-linear problem with a 1 percent convergence criterion on residual load vector. The maximum number of iterations within an increment is limited to 200 and if the iterations executed in an increment is equal to this value, it is presumed that the failure state has reached. The stiffness matrix of the ring element is formed by numerical integration (2x2). The strains and the stresses at the four Gauss sampling points are calculated from the displacements and stresses are checked for yield at each point.

Undrained Analysis : For the Von-Mises and Tresca models an undrained soil modulus of $(E_u) 1 \times 10^4 \text{ KN/m}^2$, Poisson's ratio (ν) of 0.48 and an undrained shear strength (C_u) of 20 KN/m^2 are specified. The elastic modulus of anchor is fixed based on eqn. (6.1). For a K_r value equal to 10, it works out to be $5.675 \times 10^6 \text{ KN/m}^2$. A high value of cohesion is set for foundation

material to ensure that the material of foundation do not yield. To study the effect of initial stresses on response, K_0 is taken as equal to 0.5 and the weight of soil is chosen at 16 KN/m^3 .

Drained Analysis : The drained modulus (E) and Poisson's ratio (ν) of the soil are assumed as $2 \times 10^5 \text{ KN/m}^2$ and 0.3 respectively for the Mohr-Coulomb associated plasticity model used for this analysis. For $K_r = 10$, E_p works out to be $9.60 \times 10^7 \text{ KN/m}^2$. The unit weight of the soil and the foundation material are chosen as 16 KN/m^3 and 24 KN/m^3 respectively.

Computer Programs : Two computer programs ELPIA1, ELPIA2 are developed in DEC-1090 system for the elasto-plastic analysis of the axisymmetric problems using 'initial stress' computational process. For Von-Mises plasticity model explicit expression for elasto-plastic matrix in incremental form is available and is used in ELPIA1. ELPIA2 employs Tresca and Mohr-Coulomb models and follows the calculation procedure shown in Section 3.4 with specification of convenient form of invariants to derive elasto-plastic matrix. The general features of computational process and capabilities of these programs ELPIA1 and ELPIA2 which are developed for the solution of the axisymmetric elasto-plastic problem are the same as ELPIP1 outlined in Appendix B.

Testing of Programs : The example of a long thick walled cylinder subjected to an internal pressure (p) and zero

external pressure is chosen to check the program ELPIA1 and ELPIA2. An analytical solution of this simple problem in the elastic and elasto-plastic range is available in literature (39,40) for Von-Mises and Tresca criteria. The following properties of material of cylinder are specified.

$$E = 6.09 \times 10^4 \text{ N/cm}^2, \quad \nu = 0.3, \quad c = 6.09 \text{ N/cm}^2, \quad a = 2.54 \text{ cms.}$$

For the finite element solution of the problem with Von-Mises criterion ELPIA1 is used and with Tresca criterion ELPIA2 is used. This test problem is analysed to check the elasto-plastic formulation employed and also the numerical methods developed. The elastic horizontal displacement at A (u_A), internal pressure needed to cause the first yield and the limit load are checked with the analytical results available (39,40). Fig. 6.15 presents the load deformation response curve plotted with non-dimensional parameters p/c versus $2Gu_A/Ca$ where G is the shear modulus of the material. The load deformation response curve and the limit load obtained are very close to the results from analytical solution. Fig. 6.16 shows the elasto-plastic stress distribution through thickness of the thick walled cylinder at $p = 8.44 \text{ N/cm}^2$. The variation of radial, axial and tangential stress are plotted for the Von-Mises and Tresca criteria. These variations obtained from the finite element analysis are in close agreement with the reported results (39,40).

6.3 Results and Discussions :

6.3.1 Elastic Analysis :

a) Flexible Anchor : Elastic analysis of flexible anchor subjected to uniform uplift load has been carried out for $H/B = 2.0$ and $H/B = 4.0$. The embedment ratios (D/B) investigated are 0.5, 1.0 and 1.5 for $H/B = 2.0$ and for $H/B = 4.0$, the embedment ratios are 1.0, 2.0 and 3.0. Poisson's ratios of 0.2, 0.3, 0.4 and 0.49 are used. Full bonding and full separation between anchor and soil are considered in the elastic analysis.

Table 6.1 summarises the results for vertical displacements in the form of influence factors for full bonding case. The influence factors for vertical displacement at centre of anchor, at edge of anchor and at surface directly above the centre of anchor are presented. It is seen from the results presented that the elastic vertical displacement response of circular anchor decreases with increase in embedment depth. Depth of elastic layer below anchor level is also an important parameter. For $H/B = 2.0$ and $D/B = 1.0$, $I_c = 0.361$, whereas for $H/B = 4.0$ and $D/B = 1.0$, $I_c = 0.462$ for $\nu = 0.3$. It is seen that the Poisson's ratio of the elastic layer, embedment depth and the layer depth of anchor significantly influence the elastic response of anchor. The variation of vertical displacement along the centre line of anchor for $\nu = 0.2, 0.3, 0.4$ and 0.49 is shown in Figs. 6.1, 6.2, 6.3 for $D/B = 0.5, 1.0$ and 1.5 respectively.

Table 6.1

Influence factors for vertical displacement of
flexible circle, uniformly distributed
uplift load

Full bonding

$$\rho = \frac{pB}{E} I$$

a. $H/B = 2.0$

D/B	I_c			I_e			I_{cs}		
	0.5	1.0	1.5	0.5	1.0	1.5	0.5	1.0	1.5
0.2	0.498	0.368	0.267	0.310	0.216	0.138	0.414	0.187	0.072
0.3	0.492	0.361	0.253	0.300	0.207	0.127	0.404	0.181	0.066
0.4	0.465	0.332	0.216	0.275	0.184	0.102	0.382	0.167	0.057
0.49	0.397	0.264	0.135	0.224	0.135	0.054	0.342	0.144	0.040

b. $H/B = 4.0$

D/B	I_c			I_e			I_{cs}		
	1.0	2.0	3.0	1.0	2.0	3.0	1.0	2.0	3.0
0.2	0.463	0.388	0.332	0.304	0.237	0.185	0.267	0.104	0.038
0.3	0.462	0.385	0.325	0.300	0.233	0.179	0.262	0.099	0.035
0.4	0.440	0.363	0.297	0.283	0.216	0.158	0.248	0.091	0.029
0.49	0.369	0.293	0.212	0.236	0.171	0.104	0.225	0.074	0.019

- I_c - Influence factor for vertical deflection at centre of circle
 I_e - Influence factor for vertical deflection at edge of circle
 I_{cs} - Influence factor for vertical deflection at the surface above centre

The maximum displacement occurs at the level of anchor and decreases with depth below anchor.

For the case of full separation the results of elastic analysis of flexible strip are summarised in Table 6.2. The vertical displacement of anchor can be observed to increase considerably by the anchor breakaway. For $H/B = 2.0$, $D/B = 1.0$, $\nu = 0.3$ the vertical displacement for full separation case is about 2.24 times that for the full bonding case. Fig. 6.4 shows the variation of vertical displacement along the centre line for $H/B = 2.0$ and $D/B = 1.0$. The vertical displacements of nodal points directly below the anchor are very small. For $D/B = 0.5$, and 1.5 also, the same general pattern of variation of vertical displacement as shown in Fig. 6.4 is observed although it is not plotted.

The vertical stress variation along the centre line with depth is shown in Fig. 6.5, for the full bonding case. For the axisymmetric element the stresses are found at four Gauss integration points. The average of the vertical stress of two Gauss points nearest to the centre line are plotted as the vertical stress on the centre line of the anchor. The uniform intensity of upward load produces compressive vertical stress (σ_z) in elements above anchor and tensile stress in elements below anchor level. The elements directly above anchor have dimensionless stress ratio (σ_z/p) magnitudes of the order of 0.30 to 0.40 for the D/B ratios 0.5, 1.0 and 1.5 investigated.

Table 6.2

Influence factors for vertical displacement of flexible
circle, uniformly distributed uplift load

Full separation

$$\rho = \frac{pB}{E} I$$

a. $H/B = 2.0$

D/B	I_c			I_e			I_{cs}		
	0.5	1.0	1.5	0.5	1.0	1.5	0.5	1.0	1.5
0.2	1.350	0.838	0.721	0.587	0.373	0.292	1.073	0.370	0.167
0.3	1.306	0.808	0.693	0.578	0.366	0.285	1.031	0.356	0.160
0.4	1.220	0.750	0.641	0.544	0.340	0.262	0.960	0.331	0.146
0.49	1.009	0.629	0.535	0.427	0.260	0.191	0.789	0.278	0.117

b. $H/B = 4.0$

D/B	I_c			I_e			I_{cs}		
	1.0	2.0	3.0	1.0	2.0	3.0	1.0	2.0	3.0
0.2	0.886	0.737	0.690	0.429	0.330	0.285	0.422	0.145	0.062
0.3	0.862	0.714	0.666	0.427	0.327	0.281	0.410	0.140	0.057
0.4	0.807	0.663	0.616	0.405	0.306	0.260	0.384	0.128	0.050
0.49	0.677	0.545	0.499	0.329	0.237	0.191	0.329	0.099	0.037

- I_c - Influence factor for vertical deflection at centre of circle
 I_e - Influence factor for vertical deflection at edge of circle
 I_{cs} - Influence factor for vertical deflection at the surface above centre.

The variation of vertical stress with depth along centre line for full separation case is shown in Fig. 6.6 for D/B ratios equal to 0.5, 1.0 and 1.5. σ_z/p for elements above the level of anchor are compressive and nearest to the anchor the value of σ_z/p approaches unity. The vertical stress for elements directly below the anchor level are smaller in magnitude. The pattern of vertical stress variation along the centre line of anchor is affected to a significant extent by the anchor breakaway.

The variation of the vertical contact stress along the length of anchor above and below it is shown in Fig. 6.7 for $\nu = 0.3$. The stresses at the integration points located nearest to the anchor are plotted as the vertical contact stress (σ_z). For full bonding and full separation cases indicated, the σ_z/p almost remains constant along the length of anchor and reduces towards the edge of the anchor.

b) Rigid anchor : The results from finite element analysis of rigid anchor simulation are presented in Table 6.3 and Table 6.4 for full bonding and full separation cases respectively. Influence factors for vertical displacement of anchor at the centre and at the surface directly above the centre of anchor for $H/B = 2.0$ and $D/B = 0.5, 1.0, 1.5$ are given in the tables. Poisson's ratios considered are 0.2, 0.3, 0.4 and 0.49. The vertical displacement of anchor decreases with increase in Poisson's ratio and as the embedment ratio increases. The

Table 6.3

Influence factors for vertical displacement
of rigid circle

Full bonding

H/B = 2.0

$$\rho = \frac{p_{av} B}{E} I$$

D/B	I_c			I_{cs}			$I_{c(av)}$		
	0.5	1.0	1.5	0.5	1.0	1.5	0.5	1.0	1.5
0.2	0.367	0.269	0.188	0.352	0.176	0.069	0.404	0.292	0.203
0.3	0.358	0.261	0.177	0.340	0.169	0.064	0.396	0.284	0.190
0.4	0.331	0.236	0.149	0.316	0.155	0.055	0.370	0.258	0.159
0.49	0.263	0.171	0.085	0.263	0.129	0.038	0.311	0.199	0.095

Table 6.4

Influence factors for vertical displacement of
rigid circle

Full separation

H/B = 2.0

$$\rho = \frac{p_{av} B}{E} I$$

D/B	I_c			I_{cs}			$I_{c(av)}$		
	0.5	1.0	1.5	0.5	1.0	1.5	0.5	1.0	1.5
0.2	0.698	0.495	0.413	0.681	0.300	0.139	0.969	0.606	0.507
0.3	0.684	0.484	0.402	0.662	0.291	0.134	0.942	0.587	0.489
0.4	0.640	0.448	0.369	0.618	0.271	0.122	0.882	0.545	0.452
0.49	0.478	0.333	0.265	0.473	0.217	0.091	0.718	0.445	0.363

I_c - Influence factor for vertical deflection at centre of circle

I_{cs} - Influence factor for vertical deflection at the surface above centre

$I_{c(av)}$ - Influence factor calculated from flexible anchor analysis as $(I_c + I_e)/2$.

variation of vertical displacement of rigid circular anchor with depth is shown in Figs. 6.1, 6.2 and 6.3 for full bonding and in Fig. 6.4 for full breakaway. Table 6.3 and Table 6.4 also give values of $I_{c(av)}$. $I_{c(av)}$ is obtained from taking average of centre and edge influence values from flexible strip analysis. For full bonding situation these values obtained are higher than the rigid anchor results and can be considered as an approximation.

The variation of vertical stress above and below the circular anchor for full bonding and full separation cases are shown in Fig. 6.7 for $\nu = 0.3$. For full bonding case the vertical contact stress at centre above and below the anchor is less when compared to a fully flexible anchor. The dimensionless ratio σ_z/p increases towards the edge of the anchor. For the case of full separation from soil below it, the ratio σ_z/p increases from 0.3 near the centre to 1.65 near the edge of anchor. It can be also observed that the contact stress (σ_z) in soil obtained at integration points nearest to anchor shows a smooth variation in all the cases.

c) Anchor of finite Stiffness, Continuum Element : The results for vertical central displacement of anchor and maximum differential vertical displacement are presented in Table 6.5 for K_r values ranging from 0.01 to 100. Loading cases investigated are (i) a uniform upward load and (ii) a central concentrated load. Values of Poisson's ratio of soil are taken as 0.3 and 0.49. Figs. 6.8 and 6.9 show the variation of central vertical

Table 6.5

Influence factors for vertical displacement of circular anchor - continuum element and plate element discretisation

$$= \frac{\bar{p} B}{E} I \quad \bar{p} = p \text{ for uniform load} \quad H/B = 2.0$$

$$\bar{p} = P/A \text{ for concentrated load} \quad D/B = 1.0$$

*continuum element : ** plate element

K_r		Load:uniform full bonding		Load:uniform full separation		Load:conc. full bonding		Load:conc. full separation	
		I_c	I_d	I_c	I_d	I_c	I_d	I_c	I_d
0.01	$v=0.3$	0.365*	0.157	0.654	0.342	8.968	8.817	9.615	9.342
	$v_p=0.3$	0.360**	0.144	0.791	0.397	-	-	-	-
0.10	-do-	0.283	0.088	0.511	0.196	2.062	1.903	2.425	2.126
		0.331	0.096	0.636	0.192	-	-	-	-
1.00	-do-	0.228	0.028	0.367	0.045	0.457	0.268	0.610	0.293
		0.277	0.021	0.508	0.030	-	-	-	-
10.0	-do-	0.207	0.003	0.328	0.005	0.232	0.029	0.353	0.031
		0.248	0.002	0.481	0.003	-	-	-	-
100	-do-	0.205	0.0003	0.323	0.0005	0.207	0.003	0.325	0.003
		0.234	0.0003	0.428	0.0003	-	-	-	-
0.01	$v=0.49$	0.289	0.145	0.556	0.315	6.165	6.070	6.778	6.567
	$v_p=0.30$	0.262	0.123	0.614	0.340	-	-	-	-
0.10	-do-	0.214	0.086	0.429	0.180	1.661	0.679	1.988	1.748
		0.238	0.086	0.482	0.176	-	-	-	-
1.00	-do-	0.154	0.026	0.292	0.043	0.347	0.228	0.497	0.248
		0.182	0.020	0.350	0.030	-	-	-	-
10.0	-do-	0.132	0.003	0.254	0.005	0.153	0.025	0.275	0.027
		0.173	0.002	0.335	0.003	-	-	-	-
100	-do-	0.129	0.0003	0.249	0.0005	0.131	0.003	0.251	0.003
		0.167	0.0002	0.322	0.0002	-	-	-	-

I_c - Influence factor for vertical displacement at centre of anchor
 I_d - Influence factor for differential displacement between centre and edge.

displacement of anchor for full bonding and full separation cases. The results obtained for flexible and rigid anchors are also shown in the same figures for comparison. For $\nu = 0.3$ and full bonding, the influence factor for vertical displacement (I_c) varies from 0.365 to 0.205 as K_r varies from 0.01 to 100 for a uniform uplift load. For concentrated central load for the same case the variation of I_c is from 8.968 to 0.207. The variation of I_c with K_r is sharp in the lower ranges of K_r especially for concentrated load but this range may not be of practical importance in the case of foundations. For a uniform uplift load, from 10 to 100 (Table 6.5), the vertical displacement response does not vary much with K_r values. But for the concentrated upward load, there is considerable reduction in vertical displacement from $K_r = 10$ to $K_r = 100$. At $K_r = 100$, there is practically no difference in vertical displacement response because of the mode of application of load. The same observation is true for $\nu = 0.49$ and also for full separation cases. For $\nu = 0.3$ and full bonding case the influence factor for maximum differential displacement (I_d) of anchor varies from 0.157 to 0.0003 as K_r varies from 0.01 to 100 for uniform load (Table 6.5). The change in magnitude of I_d is very small for uniform load as K_r varies from 10 to 100. With concentrated central load, there is reduction in the values of I_d from $K_r = 10$ to $K_r = 100$. This can be observed for $\nu = 0.49$ for full bonding case and full separation cases investigated also.

It can also be seen from Fig. 6.8 and Fig. 6.9 that the influence factor for vertical deflection of rigid anchor simulation is higher than the anchor simulation with continuum elements with even $K_r = 1$ in all the cases investigated. This clearly brings out the fact that rigid anchor simulation carried out by specification of equal nodal displacements gives displacements which does not correctly reflect the effects of structural rigidity of a finite anchor geometry. Hence in embedded foundations, it is more advisable to simulate it by the use of continuum elements of finite rigidity.

Figure 6.10 shows the variation of vertical contact stress distribution above and below anchor for $\nu = 0.3$. The variation of σ_z/\bar{p} versus X/B is plotted for $\nu = 0.3$. The variation of σ_z/\bar{p} along the length, for $K_r = 100$ almost coincides with the curves for $K_r = 10$ except that the edge stresses are slightly higher. For $K_r = 10$, the variation of σ_z/\bar{p} curves for uniform load and concentrated load are very close. These general trends of variation of σ_z are also observed for $\nu = 0.49$.

d) Anchor of Finite Stiffness, Plate Element : The results for central vertical displacement and maximum differential vertical displacement of circular anchor for variation of relative stiffness from $K_r = 0.01$ to $K_r = 100$ are presented in Table 6.5. Full bonding and full separation of the anchor plate from underlying soil are the two interface conditions investigated. The load applied on the anchor is uniformly distributed.

Fig. 6.11 shows the variation of central displacement of anchor as K_r varies from 0.01 to 100. For the case of full bonding, the influence factor for vertical displacement of anchor (I_c) varies from 0.360 to 0.234 for $\nu = 0.3$ and 0.262 to 0.167 for $\nu = 0.49$. It is also noted that there is reduction in I_c , as K_r increases from 10 to 100 in all the cases analysed. If the anchor discretisation by plate elements and the continuum elements are compared it is observed that the central vertical displacement obtained by use of plate elements are higher. The points corresponding to $K_r = 0.01$ and flexible anchor case plots near each other. It is observed that for $K_r = 100$, the I_c values are less than those from the rigid anchor simulation in all the cases investigated (Fig. 6.11).

The vertical stress variation above and below the anchor for $\nu = 0.3$ is shown in Fig. 6.12 as a plot of dimensionless ratio σ_z/p versus X/B . The above variation is plotted for the full separation and full bonding cases for $K_r = 0.01$ and $K_r = 10$. For $K_r = 100$, the variation of σ_z/p in all cases almost coincides with the values for $K_r = 10$. It can be observed that the vertical stress at the edge of anchor is more than the one obtained from continuum element discretisation for full separation case. The variation of σ_z/p for rigid anchor simulation with full separation (Fig. 6.7) and by the plate elements with K_r equal to 10 (Fig. 6.12) show the same trends.

The variation of radial bending moment along the length of anchor for a uniform load is shown in Figs. 6.13 and 6.14 for full bonding and full separation cases respectively. The dimensionless ratio M_r/pB^2 is plotted against X/B for $K_r = 0.01, 0.1, 1.0$ and 10.0 . For $K_r \geq 0.1$, the radial moment is maximum at the centre of anchor. The radial bending moment in anchor increases with K_r . The increase in M_r/pB^2 at the centre from $K_r = 0.1$ to $K_r = 1$ is much more than from increase from $K_r = 1$ to 10 . Poisson's ratio equal to 0.49 gives higher maximum moments than for $\nu = 0.3$, for both full bonding and full separation cases. Comparing the results for cases of full bonding and full separation of the anchor from underlying soil, it is noted that the maximum radial bending moment at the centre of anchor for full separation case is higher. For $K_r = 10$ and $\nu = 0.3$, the ratio of maximum radial moments for the full separation and the full bonding cases works out to be 1.36 .

6.3.2 Elasto-Plastic Analysis :

a) Undrained Analysis : The results of the elasto-plastic analysis of the circular anchor are summarised in Table 6.6. The perfectly plastic Von-Mises and Tresca models are used for undrained analysis.

Relative stiffness values equal to $1, 10$ and 100 are used with Von-Mises model in R.No.1, R.No.2 and R.No.3 in Table 6.6. The load at which first point yields is altered with change in K_r from 1 to 10 . For all the three values of K_r , the ultimate

Table 6.6

Elasto-plastic undrained analysis - circular anchor

R.No.	Model	Mesh	Properties	Conv. crit. ()	K _r	K _o	No. of incr.	P _y (KN)	P _u (KN)	CPU time in DEC-1090 (mts)
1	Von-Mises	1	Full bonding E=10 ⁴ KN/m ² C=20KN/m ² ν=0.48	1	1.0	1.0	27	70	270	25.58
2	-do-	1		1	10.0	1.0	27	110	270	15.30
3	-do-	1		1	100.0	1.0	27	100	270	14.67
4	-do-	1		1	10.0	0.5	27	100	270	15.10
5	-do-	3		1	10.0	1.0	32	140	320	10.73
6	-do-	4		1	10.0	1.0	42	180	420	4.82
7	-do-	1		0.1	10.0	1.0	25	110	250	14.08
8	-do-	1		0.01	10.0	1.0	24	110	240	14.23
9	-do-	1		1	10.0	1.0	14	120	280	10.67
10	-do-	1		1	10.0	1.0	6	150	300	6.67
11	Tresca	1		1	10.0	1.0	25	90	250	13.50
12	Von-Mises	2	Full separation	1	10.0	1.0	25	40	100	13.51
13	-do-	2		1	10.0	0.5	25	40	100	14.02
14	-do-	2		1	100.0	1.0	25	40	100	13.05
15	Tresca	2		1	10.0	1.0	22	36	85	13.40

uplift load is obtained as 270 KN. In Fig. 6.17 the load deformation response of the anchor for the three values of K_r are given. The non-dimensional ratios, P/CB^2 are plotted against δ_c/B . The deformation response shows an initial straight portion and a non-linear segment which becomes asymptotic with x-axis at ultimate stage. From the response curve for $K_r = 1$ and $K_r = 10$, it is evident that the elastic response of anchor and non-linear elasto-plastic deformations are dependent on the relative stiffness value K_r .

Table 6.7 gives the load and the corresponding central vertical displacement of anchor and the number of iterations executed to satisfy the convergence criterion. Upto a load of 100 KN, all the elements are elastic. At 110 KN, the first yield takes place. After that with each subsequent load increment, more points yield and the number of iterations for meeting convergence requirements also increase. If the maximum number of iterations were limited to 50, the limit load would have been obtained as 240 KN and if limited to 100, the limit load would have been obtained as 250 KN. The limit load is influenced by the maximum number of iterations specified.

The effect of initial stresses due to weight are considered by specifying $K_0 = 0.5$ and $\gamma = 16 \text{ KN/m}^3$ in R.No.4. It is seen from the results of the analysis that the load at which the first point yields is reduced from 110 KN to 100 KN, but the ultimate uplift load obtained is 270 KN. Its value is unaffected by the

Table 6.7

Elasto-plastic undrained analysis - circular anchor

Von-Mises criterion

 $E=1 \times 10^4 \text{ KN/m}^2$ $C=20 \text{ KN/m}^2$ $\nu=0.48$ $K_r = 10.0$ $K_o = 1.0$

Full bonding

Load (KN)	δ (m ^c)	Number of iterations
10	0.0201×10^{-2}	1
100	0.2009×10^{-2}	1
110	0.2221×10^{-2}	3
120	0.2443×10^{-2}	4
130	0.2685×10^{-2}	5
140	0.2969×10^{-2}	6
150	0.3291×10^{-2}	8
160	0.3654×10^{-2}	9
170	0.4059×10^{-2}	11
180	0.4488×10^{-2}	12
190	0.4955×10^{-2}	14
200	0.5521×10^{-2}	18
210	0.6220×10^{-2}	23
220	0.7056×10^{-2}	28
230	0.8267×10^{-2}	46
240	1.0030×10^{-2}	70
250	1.2400×10^{-2}	101
260	1.5940×10^{-2}	154
270	2.0820×10^{-2}	200

presence of initial stresses in the soil due to the weight.

Mesh-3 and Mesh-4 are used to study the effect of mesh refinement on ultimate uplift load obtained from elasto-plastic analysis. The limit loads obtained with Mesh-3 and Mesh-4 are 18.5 percent and 35.7 percent higher respectively in comparison with the loads obtained by use of Mesh-1 which is the finest one used. With mesh refinement the ultimate load obtained becomes smaller. The reduction in uplift load with a mesh refinement is considerable for the axisymmetric case.

A convergence criterion of 1 percent on maximum magnitude of the residual load vector is used in R.No.2. Stricter criteria of 0.1 and 0.01 percent are used in R.No. 7 and R.No.8. A reduction in uplift load of 20 KN and 30 KN are observed due to the use of the stricter criteria. The convergence criterion specified in elasto-plastic analysis directly effects the limit load obtained.

The load increment for R.No. 2 is set equal to 10 KN. In R.No. 9 and R.No. 10, the load per increment is kept equal to 20 KN and 50 KN respectively. The deformation response obtained from these follow the same curve as shown in Fig. 6.27 for load increment equal to 10 KN/m. The limit load obtained is within the limits of refinements expected with such increments. The loads obtained are higher than for a finer increment.

The use of Tresca model with same relative stiffness value for elasto-plastic undrained analysis shows that the load at

first yield is reduced from 100 KN to 90 KN. The limit load obtained is 250 KN which is 7.5 percent less than the load obtained with the use of Von-Mises model.

Full separation of the circular anchor from the soil below it changes the load deformation behaviour, load at first yield and also the ultimate uplift load obtained. Fig. 6.17 shows the load deformation response for the anchor with full separation. The load at which the first point yields is 40 KN is only 0.40 of the corresponding load for full bonding case. The ultimate uplift load obtained for full separation case is only 0.37 of the load for full bonding case. For the full separation case, the presence of initial stresses due to weight does not affect the yield load nor ultimate breakout load. The Tresca model gives an ultimate uplift load which is 15 percent smaller than for the Von-Mises model.

The spread of plastic zone with increase in load are shown in Fig. 6.18a for full bonding case and in Fig. 6.18b for full separation case. For full bonding case because of the force transmitted through the base, more points below the anchor reaches plastic state first. For case of full separation more points above the anchor yield and at limit load the yielded points are localised above the anchor. The velocity field (Fig. 6.19b) for full separation of the anchor indicates a mechanism in which the nodal points directly above the anchor and on the sides participate.

For $\phi = 0$, case and $D/B = 1.0$, the following table presents the magnitude of load calculated using various shallow circular anchor theories presented in Chapter 7.

Table 6.8

Results from circular anchor theories

	F_c	F_q	$\frac{\pi}{4} B^2 C F_c$ (KN)	$P_u = \frac{\pi}{4} B^2 (C F_c + \gamma D F_q)$ (KN)
CIR-1				
Vesic(101)	3.80	1.0	59.66	72.22
Balla (6)	5.03	1.64	78.97	99.57
Meyerhof and Adams (58)				
Mariupol'skii (51)	4.00	1.00	62.80	75.36
Matsuo (52)	4.72	1.00	74.10	86.66

The limit loads obtained by elasto-plastic analysis using Von-Mises criterion and Tresca criterion are 270 KN and 250 KN respectively for full bonding case and 100 KN and 85 KN for the case of full breakaway of anchor from underlying soil. The full bonding case gives values of numerical limit loads much higher than predicted by all the approximate circular anchor theories.

For $K_0 = 1$, the Von-Mises and Tresca models gave the same ultimate loads even if the weight of the material is considered

in analysis. If it is assumed that the uplift load obtained from elasto-plastic undrained analysis gives the contribution from cohesion only, then it has to be compared with the load ' $\frac{\pi}{4} B^2 C F_c$ ' (given in Table 6.8) obtained from approximate theories. The magnitude of the limit load obtained from elasto-plastic analysis using both Von-Mises and Tresca criteria are higher than the contribution due to cohesion calculated from approximate anchor theories. This is observed for strip anchor analysis also.

b) Drained Analysis : Mohr-Coulomb perfectly plastic model is used in this analysis. The results and details of different cases investigated are given in Table 6.9 .

Table 6.9

Elasto-plastic Drained Analysis - Mohr-Coulomb Model

$K_r = 10.0$ $E = 2 \times 10^5 \text{ KN/m}^2$
 $K_o = 1.0$ $\nu = 0.30, \gamma = 16 \text{ KN/m}^3$
 Convergence criterion=1 percent

R.No.	Mesh	Properties	No.of incr.	P_{yield} (KN)	P_u (KN)	CPU time (min)
1	1	Full bonding $C=0, \phi = 30^\circ$	20	40	200	38.21
2	2	Full separation $C=0, \phi = 30^\circ$	16	8	64	42.41
3	2	Full separation $C=20 \text{ KN/m}^2,$ $\phi = 30^\circ$	21	48	168	28.95

The uplift load from conventional shallow anchor theories and elasto-plastic analysis are given in Table 6.10 for the same case for the purposes of comparison.

Table 6.10
Comparison of Breakout Load

D/B = 1.0

Theory	C=0, $\phi = 30^\circ$	C=20 KN/m ² , $\phi = 30^\circ$
1. CIR-1 Vesic (101)	26.50	92.28
2. Balla (6)	36.92	111.02
3. Meyerhof and Adams (58)	28.88	91.68
4. Mariupol'skii (51)	21.60	95.55
5. Matsuo (52)	25.25	115.53
6. Earthcone (44) $\beta = 20^\circ$	24.00	24.00
7. Elasto-plastic analysis, full separation	64.00	168.00

The ultimate uplift load obtained from elasto-plastic analysis for the full bonding case and full separation cases obtained from R.No.1 and R.No.2 (Table 6.9) are found to differ by a large amount. The uplift load obtained for the full bonding situation is very high when compared to the results from conventional anchor theories also. The breakout load from full separation case of anchor for a purely frictional soil (C=0) and

C , ϕ soil are also seen to be more than the results obtained from the conventional theories.

6.4 Conclusions :

From the finite element elastic and elasto-plastic analysis of circular anchors subjected to axisymmetric uplift loads the following inferences are made :

The elastic vertical deformation response of shallow flexible circular anchor subjected to uniform uplift load is effected by the embedment depth of anchor and Poisson's ratio of the soil medium within which the anchor is embedded. For a specific layer depth of soil the vertical displacement of anchor decreases with increase in embedment ratio. The distribution of stress in the soil medium in which it is embedded and the deformation response of anchor are significantly influenced by the anchor break-away. The rigid anchor elastic behaviour also shows the same trends. The vertical contact stress distribution above the rigid circular anchor for the case of full separation from soil below it shows a variation of stress along the length of anchor similar to that obtained for the case of a rigid surface footing.

Discretisation of shallow circular anchor by continuum element shows that the displacement response of anchor subjected to uniform and concentrated loads are influenced by variation in relative stiffness (K_r) considerably in the lower ranges of K_r value. The variation in central vertical displacement is more

pronounced in the case of concentrated central load than due to a uniform uplift load. The mode of load application, i.e. uniform or concentrated does not affect the deformation response and contact vertical stress distribution for relative stiffness value equal to 100. The vertical contact stress above the anchor is compressive and below the anchor is tensile for full bonding and full separation cases but the tensile stresses in full breakaway situation are very small. The anchor breakaway influences the variation of stress inside the soil medium significantly.

The anchor discretisation by circular plate bending elements yields higher values of deformation response for $K_r \geq 1$ in comparison to continuum element discretisation of anchor. The elastic deformation response of anchor, the variation in radial bending moment and stress distribution within the soil medium are considerably influenced by anchor breakaway. The maximum radial bending moment in anchor increases with relative stiffness of anchor. The magnitude of maximum radial bending moment obtained at the plate centre for $\nu = 0.49$ is more than for $\nu = 0.3$. For full breakaway condition the resulting radial moments are also found to be more.

The elastic central vertical deflection from a rigid anchor simulation gives deformations larger than those obtained either by continuum element or plate element discretisations of anchor for $K_r \geq 10$. This clearly brings out the fact that for

embedded foundations subject to uplift loads the rigid anchor behaviour simulated by specifying nodal displacement in displacement finite element analysis does not give realistic results. Continuum elements and axisymmetric plate bending elements can model finite rigidity of circular anchor. But plate element is a line element and for the practical ranges of K_r , the deformations predicted with the use of plate elements are found to be higher when compared to the continuum element discretisation of anchor.

Elasto-plastic undrained progressive deformation analysis of circular anchor upto collapse can be carried out by using Von-Mises or Tresca plasticity models using finite element method. The maximum number of iterations specified in elasto-plastic analysis has a direct bearing on the limit loads obtained, if 'initial stress' method is used for the elasto-plastic analysis. For Tresca criterion the load at which the first point reaches plastic state and the collapse loads obtained are smaller than those obtained from Von-Mises model. The stiffness of the anchor effects the load deformation response curve but does not significantly effect the load at which the first point yields nor the breakout loads.

The deformation response of the circular anchor, the load at which the first point starts yielding and the collapse load of the anchor are effected significantly by anchor breakaway below the base. The breakout load obtained with full bonding

between anchor and the soil below it is much higher when compared to conventional circular anchor theories. For full separation case the magnitude of loads obtained using Von-Mises and Tresca models are nearer to those predicted by the conventional theories.

The magnitude of the ultimate uplift load in a purely frictional soil ($C = 0$) is effected significantly by the interface separation. The ratio of $P_{ultimate}/P_{yield}$ is large using these criterion. This indicates onset of yield at smaller loads. It is observed that the results from elastoplastic analysis for frictional soil ($C = 0$) and $C-\phi$ soil for full breakaway condition are larger than the corresponding loads obtained from shallow anchor theories.

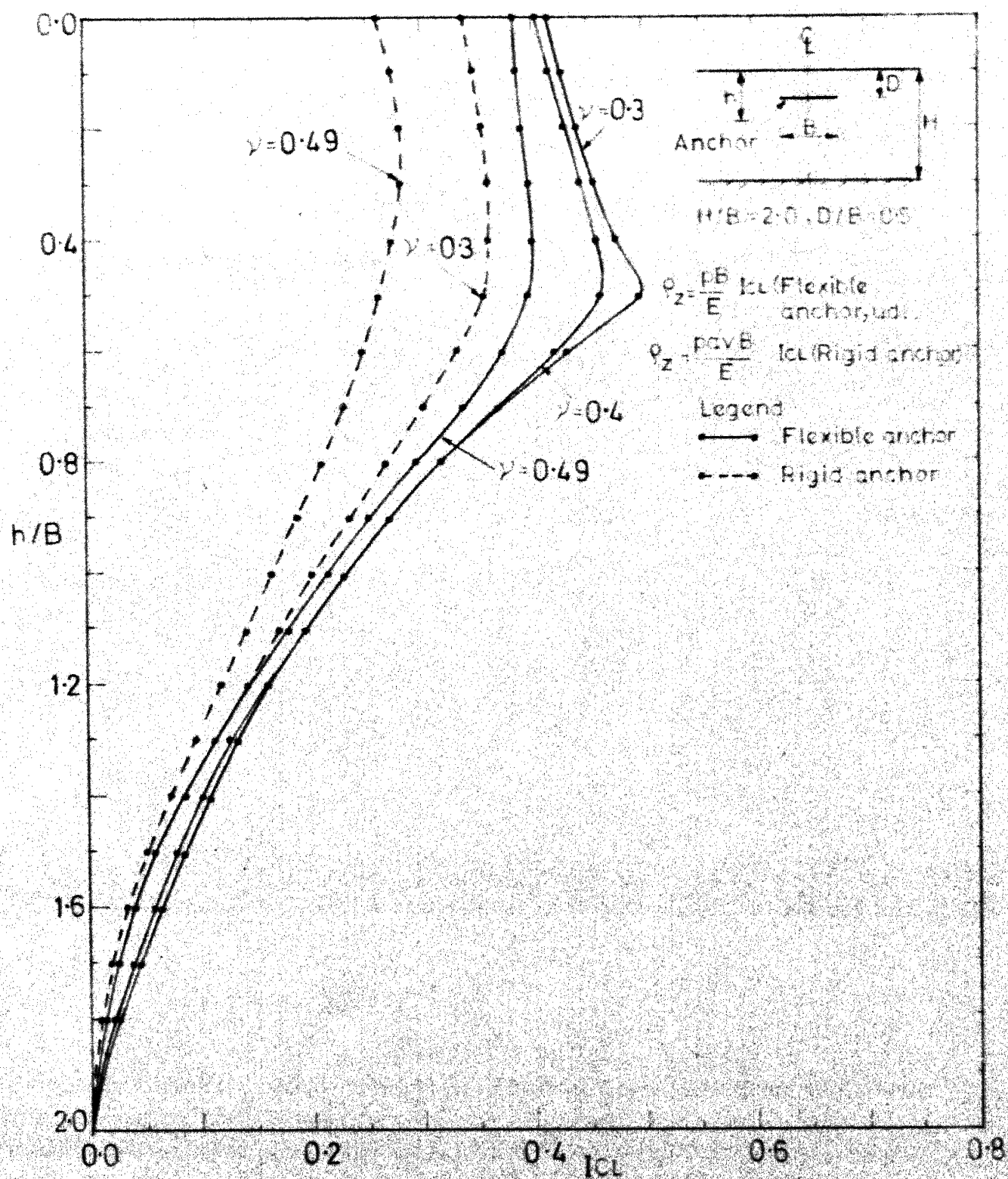


FIG. 6-1 VARIATION OF VERTICAL DISPLACEMENT WITH DEPTH
(CIRCULAR ANCHOR, FULL BONDING, $H/B = 2.0$, $D/B = 0.5$)

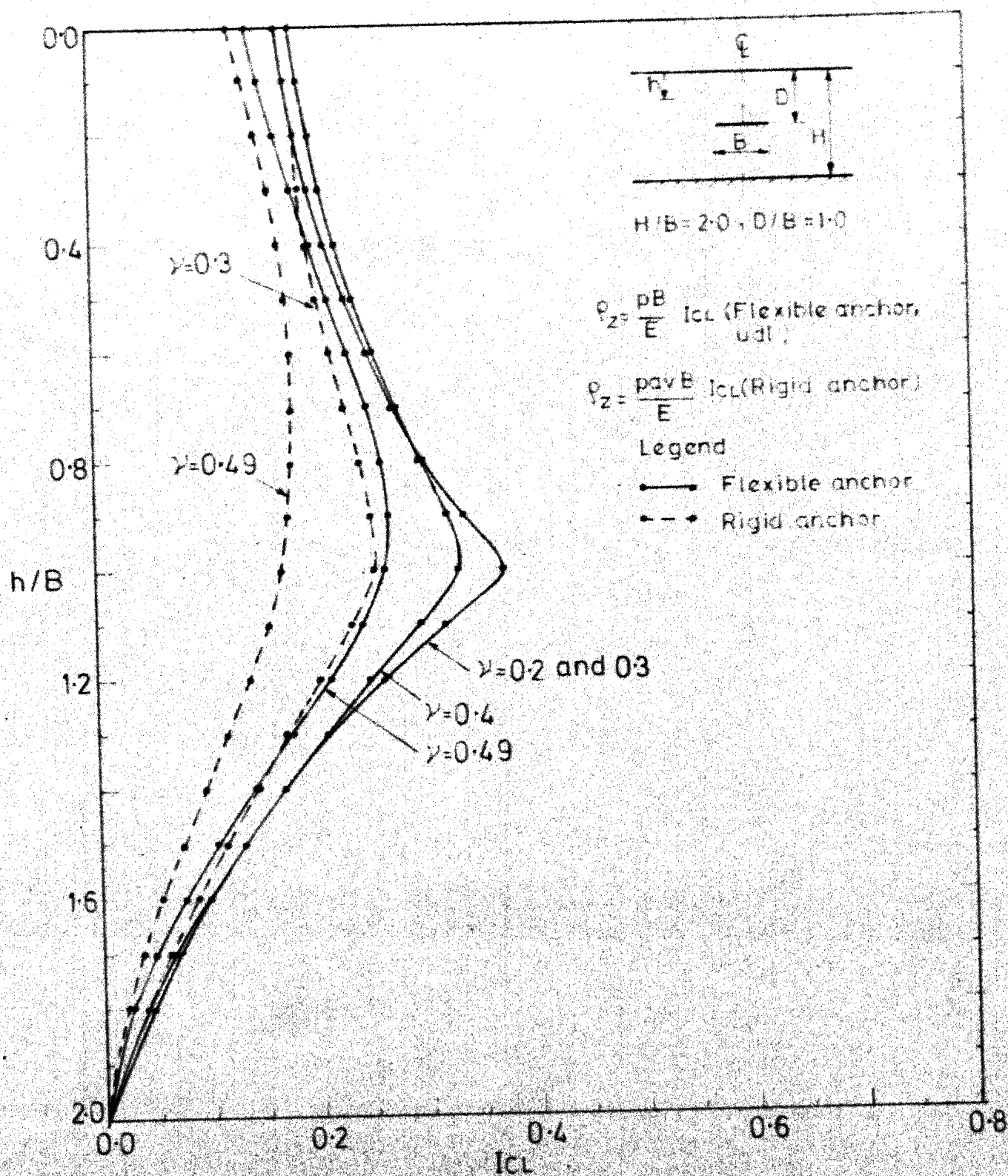


FIG.6.2 VARIATION OF VERTICAL DISPLACEMENT WITH DEPTH (CIRCULAR ANCHOR, FULL BONDING, $H/B=2.0, D/B=1.0$)

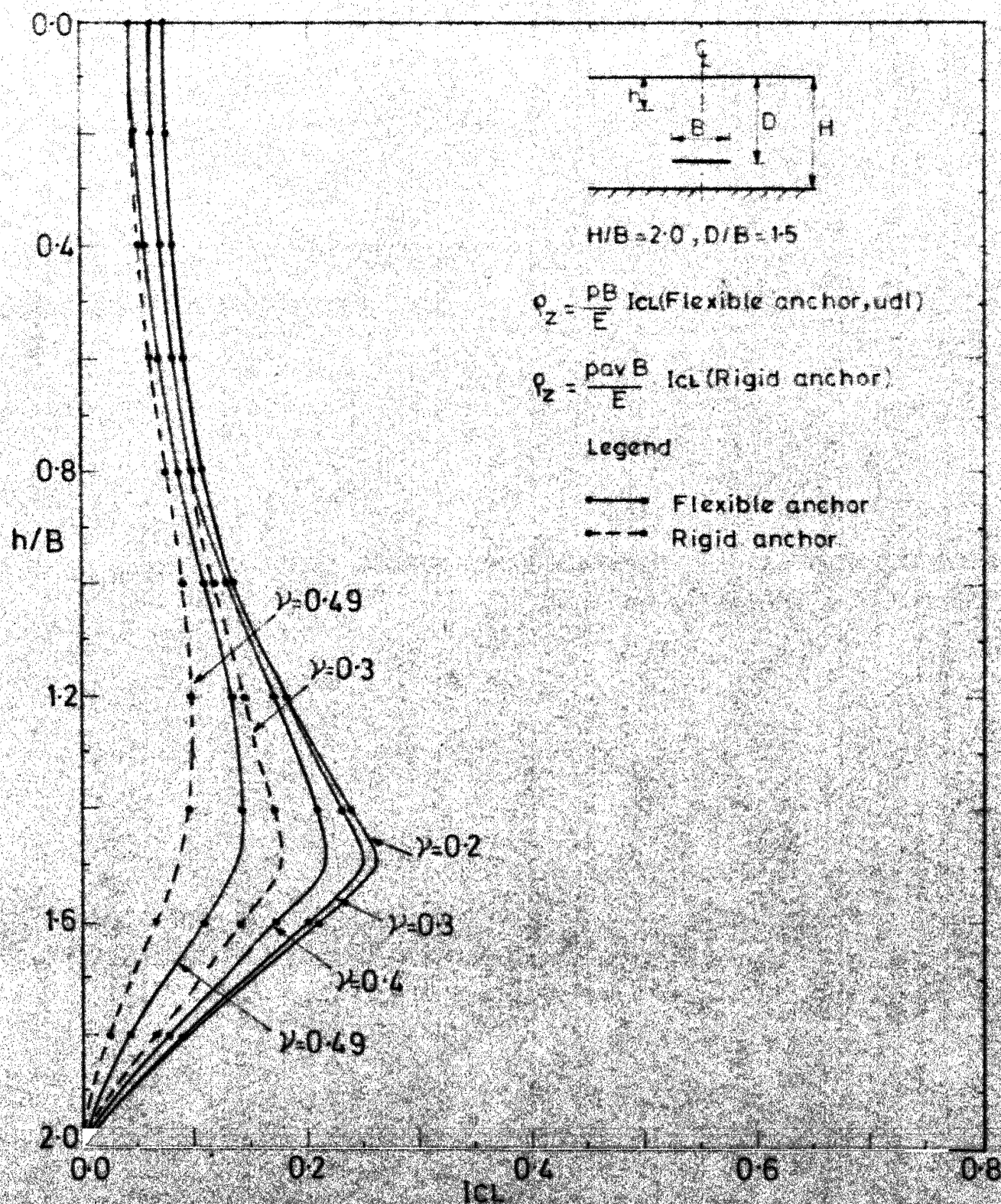


FIG-6.3 VARIATION OF VERTICAL DISPLACEMENT WITH DEPTH (CIRCULAR ANCHOR, FULL BONDING, $H/B=2.0$, $D/B=1.5$)

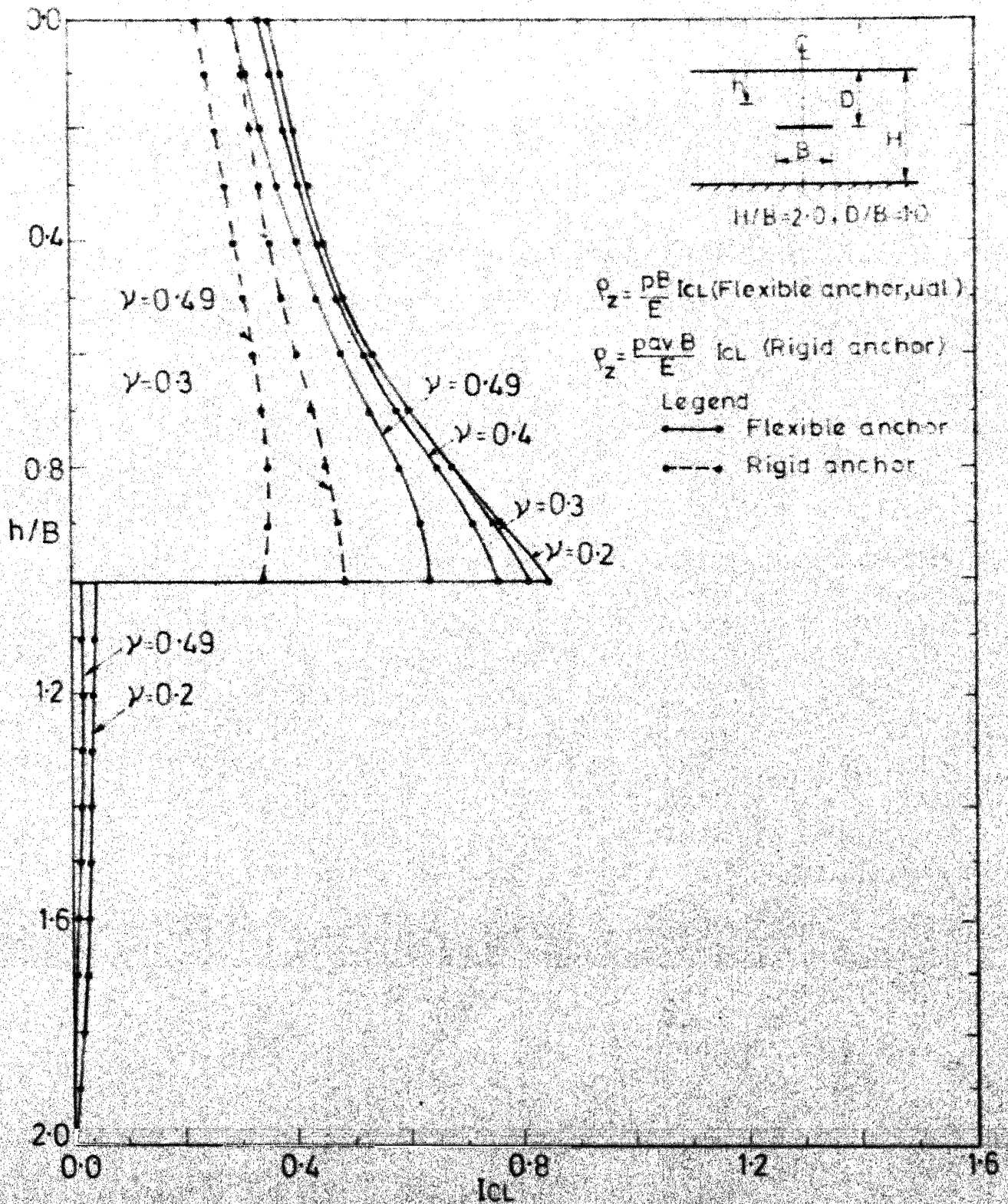


FIG.64 VARIATION OF VERTICAL DISPLACEMENT WITH DEPTH
(CIRCULAR ANCHOR, FULL SEPARATION, $H/B=2.0$, $D/B=1.0$)

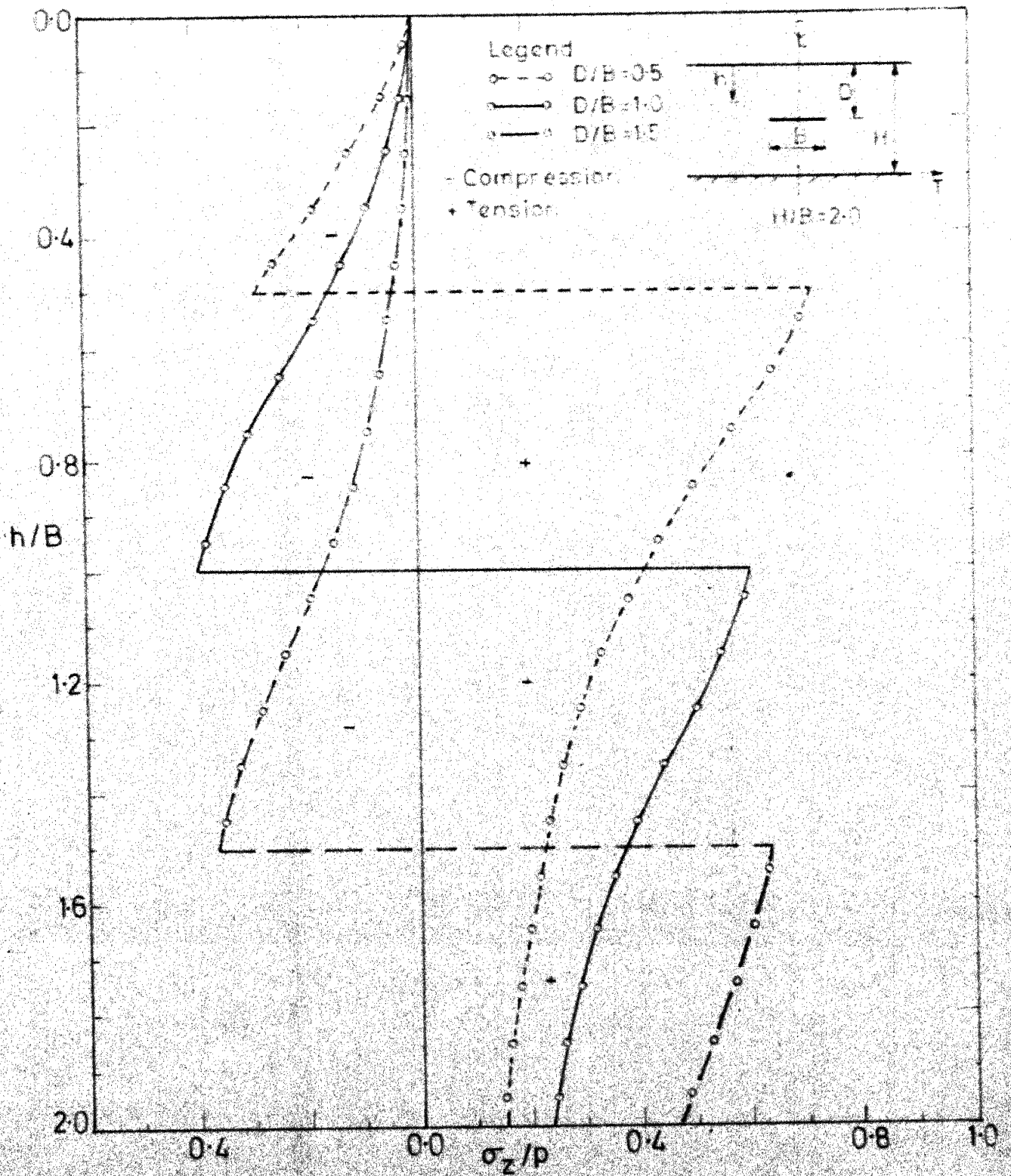


FIG 6.5 VARIATION OF VERTICAL STRESS WITH DEPTH
(CIRCULAR ANCHOR, FULL BONDING, $H/B = 2.0$)

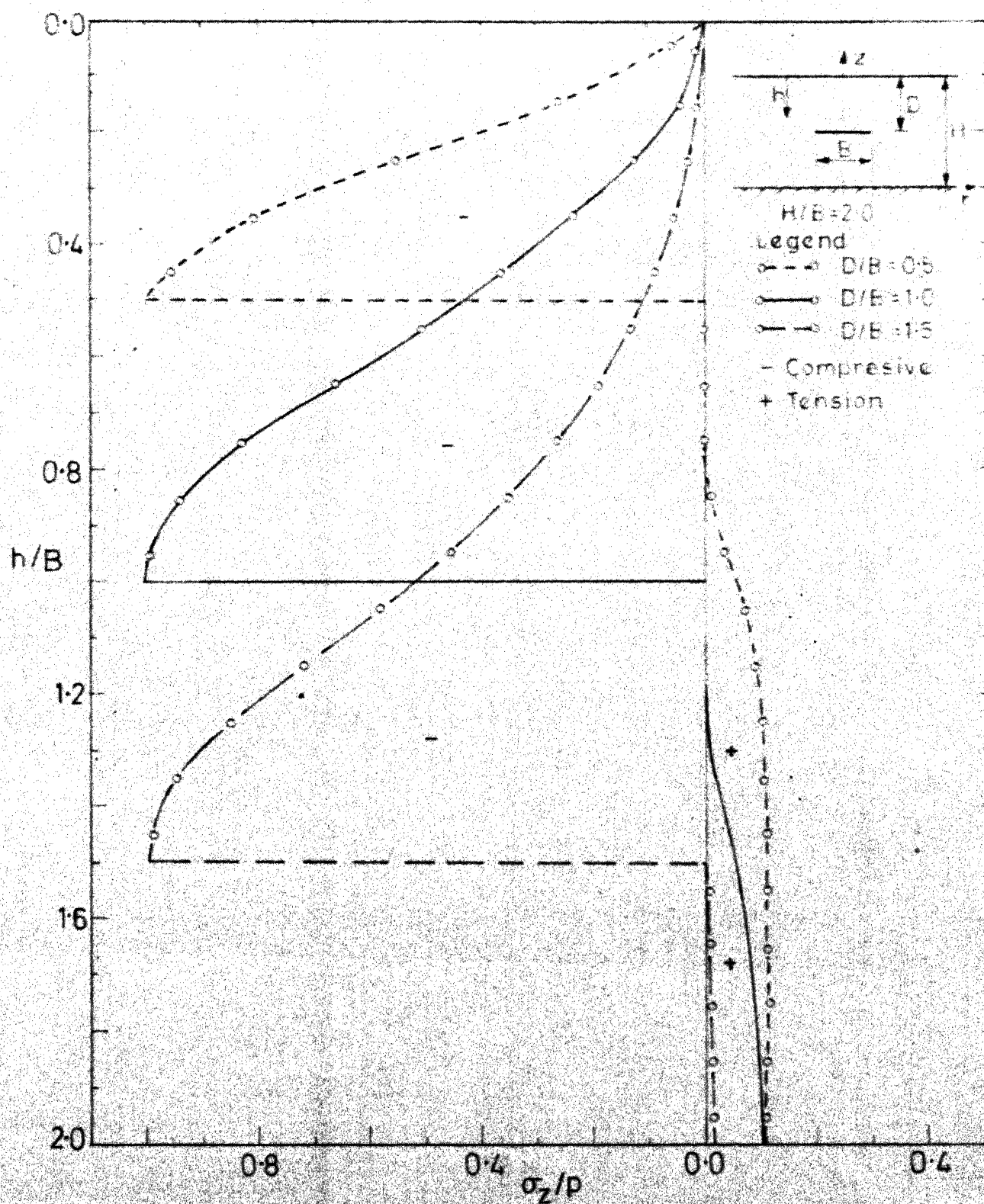


FIG.66 VARIATION OF VERTICAL STRESS WITH DEPTH
(CIRCULAR ANCHOR, FULL SEPARATION, $H/B = 2.0$)

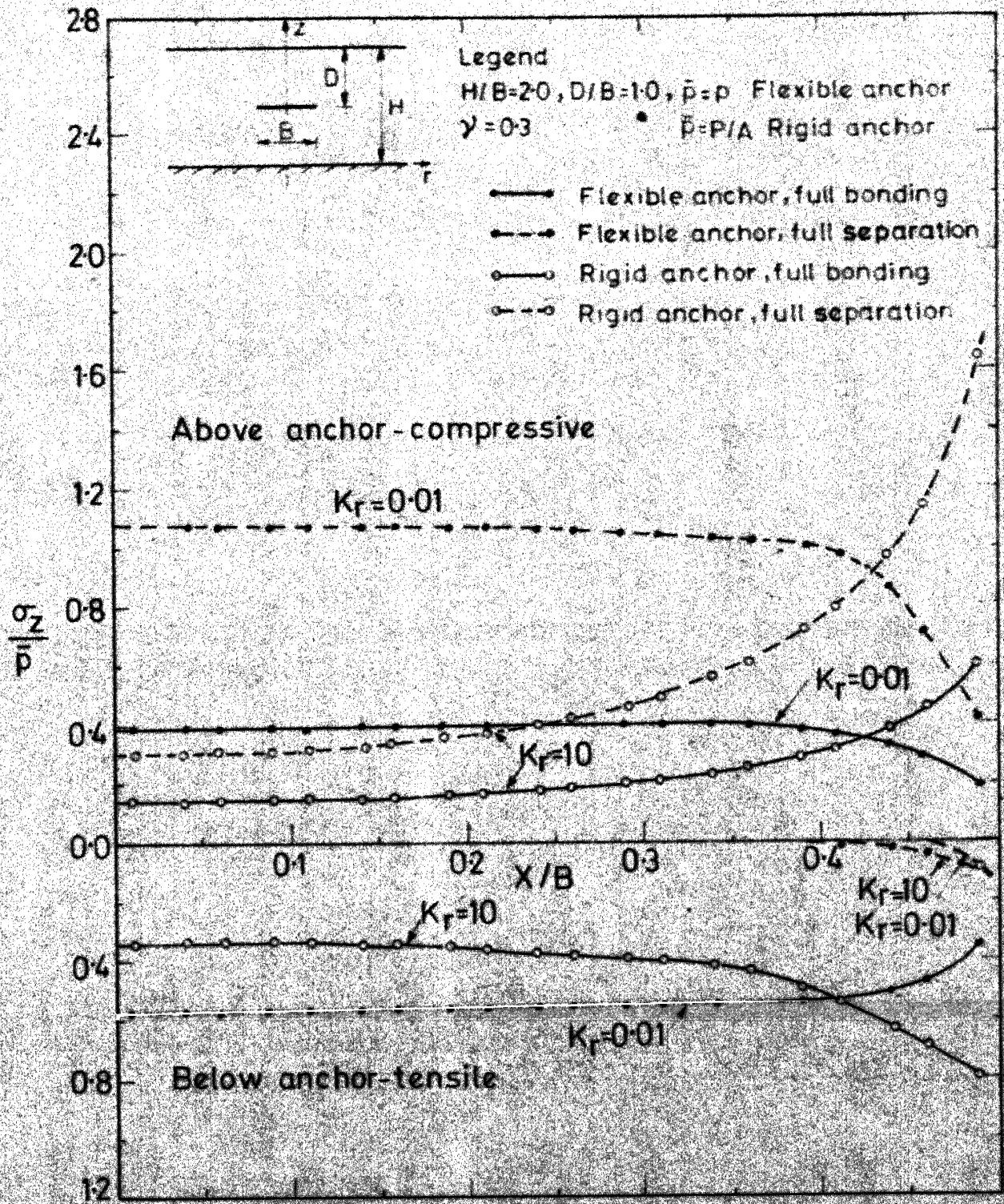


FIG.57 VARIATION OF VERTICAL CONTACT STRESS DISTRIBUTION (CIRCULAR ANCHOR, FLEXIBLE & RIGID, $\nu=0.3$)

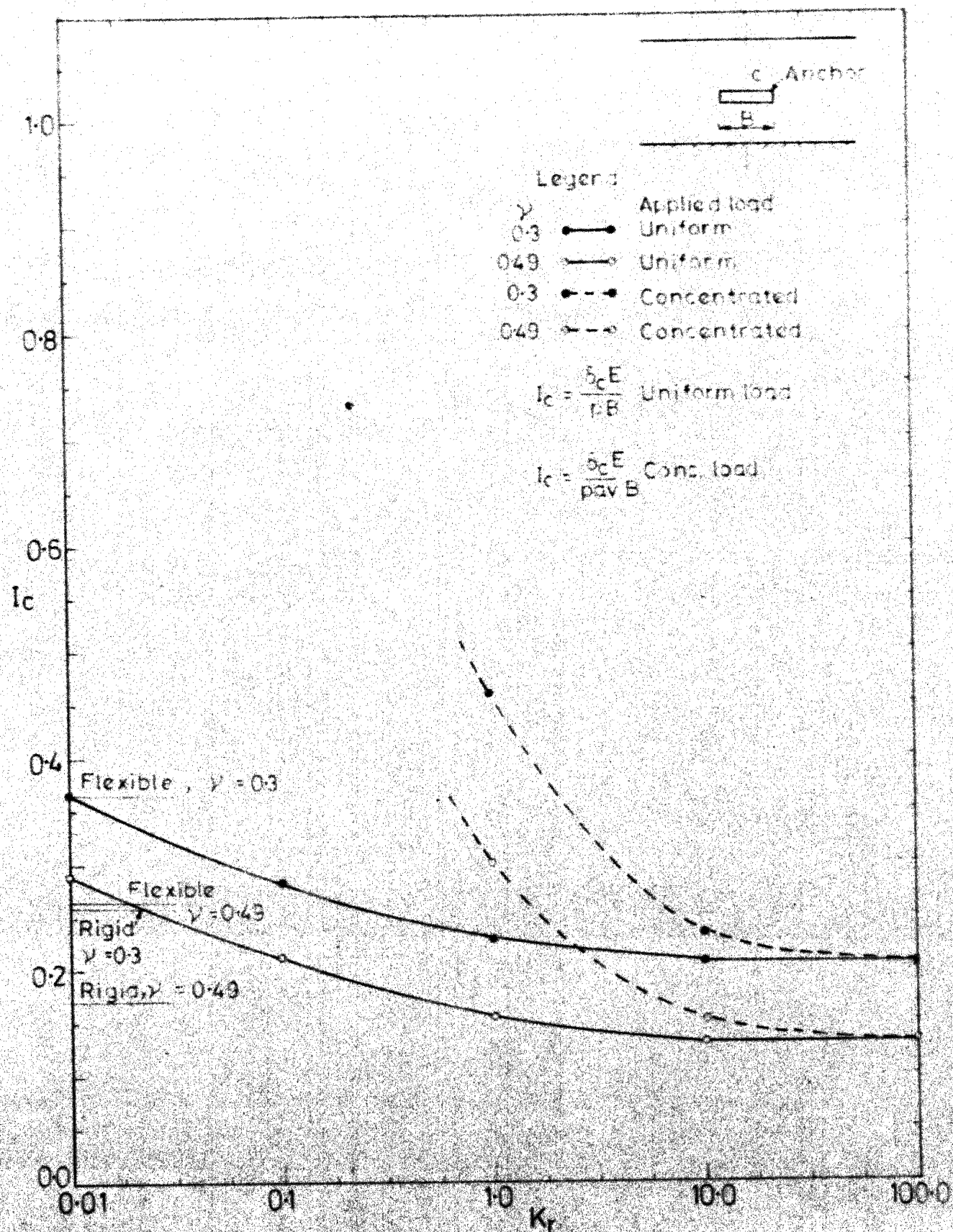


FIG. 6.8 VARIATION OF CENTRAL VERTICAL DISPLACEMENT WITH K (CIRCULAR ANCHOR, FULL BONDING, CONTINUUM ELEMENT)

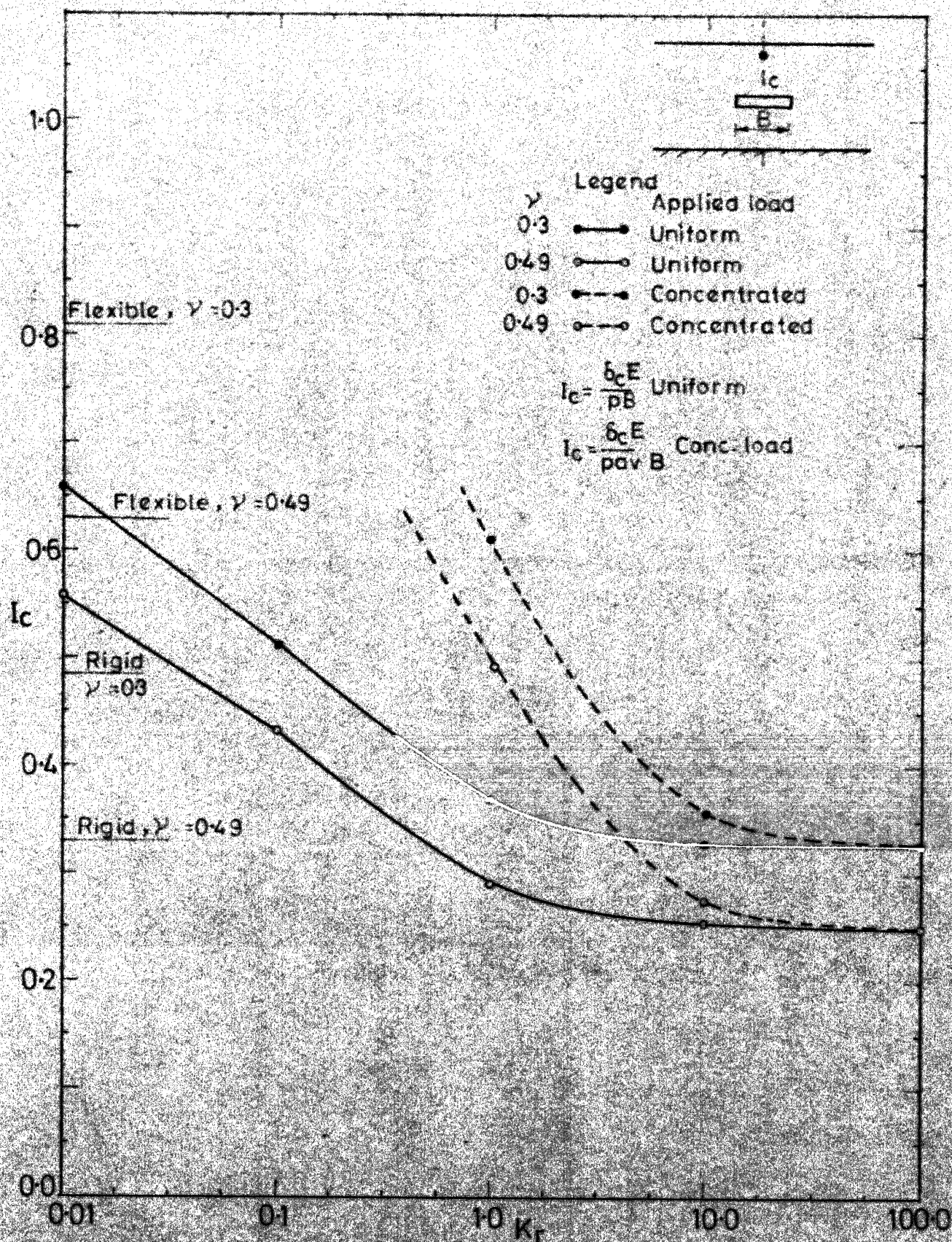


FIG. 6-9 VARIATION OF CENTRAL VERTICAL DISPLACEMENT WITH K_r
(CIRCULAR ANCHOR, FULL SEPARATION, CONTINUUM ELEMENT)

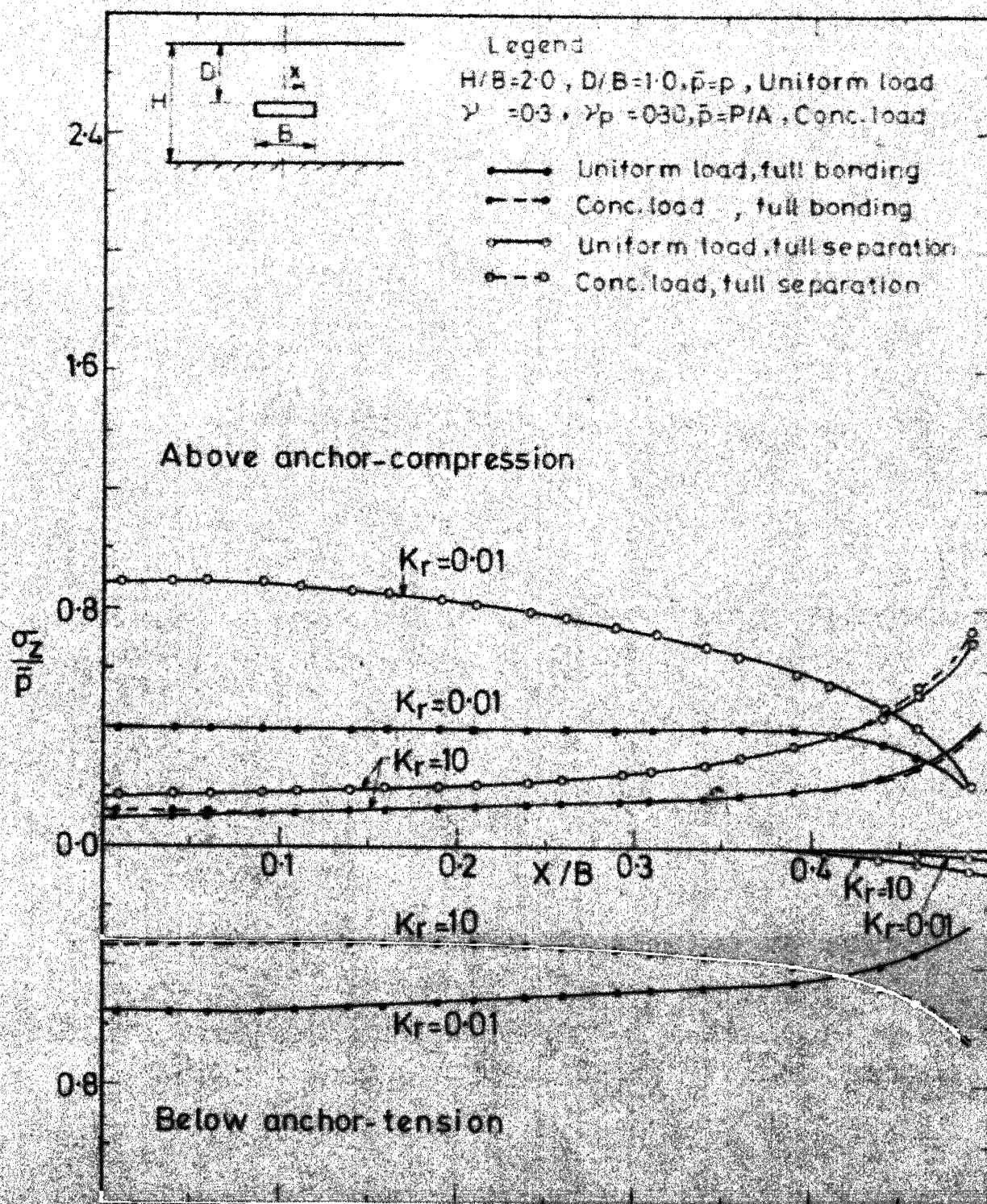


FIG.6-10 VARIATION OF VERTICAL CONTACT STRESS DISTRIBUTION (CIRCULAR ANCHOR, CONTINUUM ELEMENT, $\gamma=0.3$)

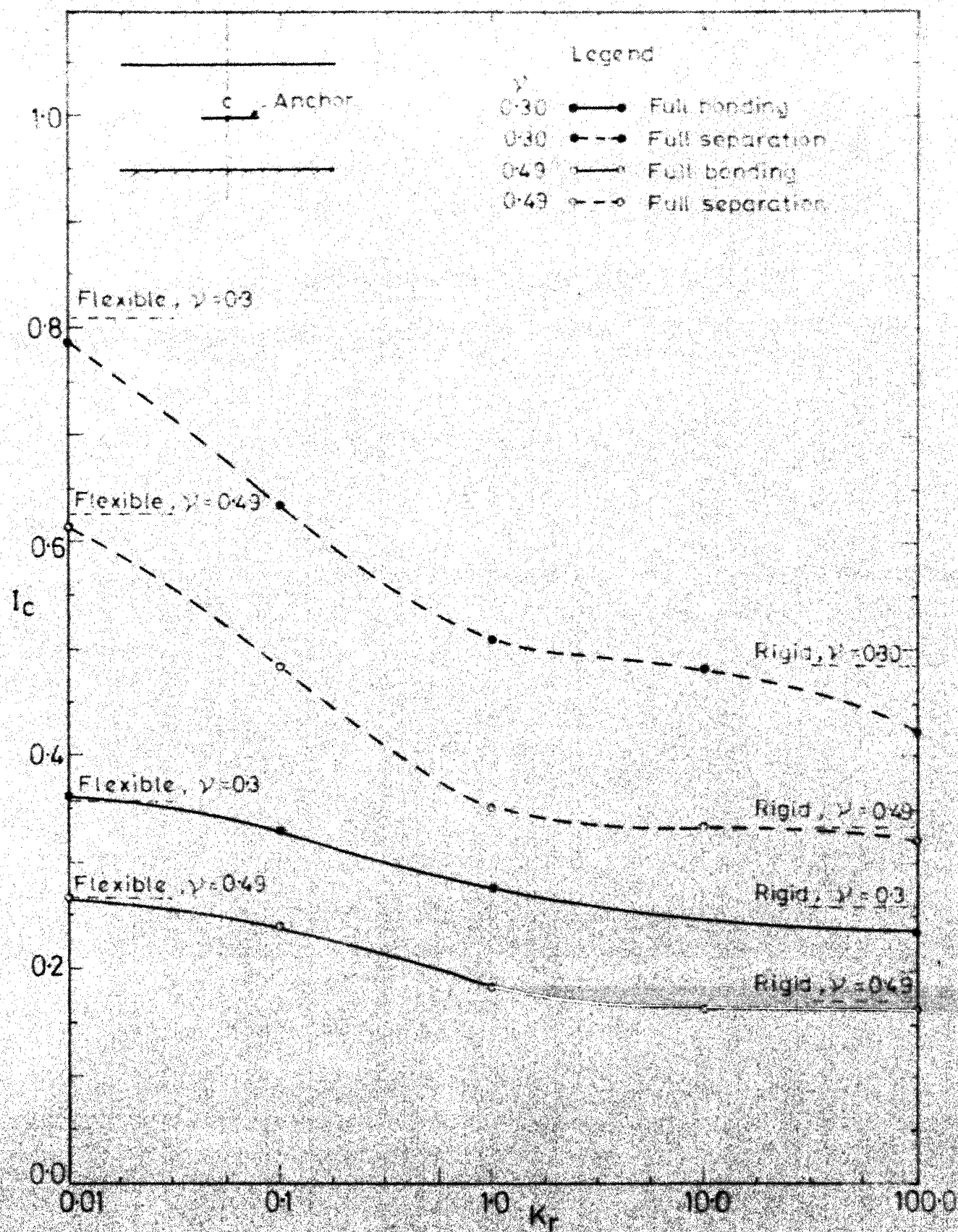


FIG. 6.11 VARIATION OF CENTRAL VERTICAL DISPLACEMENT WITH K_r (CIRCULAR ANCHOR, PLATE ELEMENT)

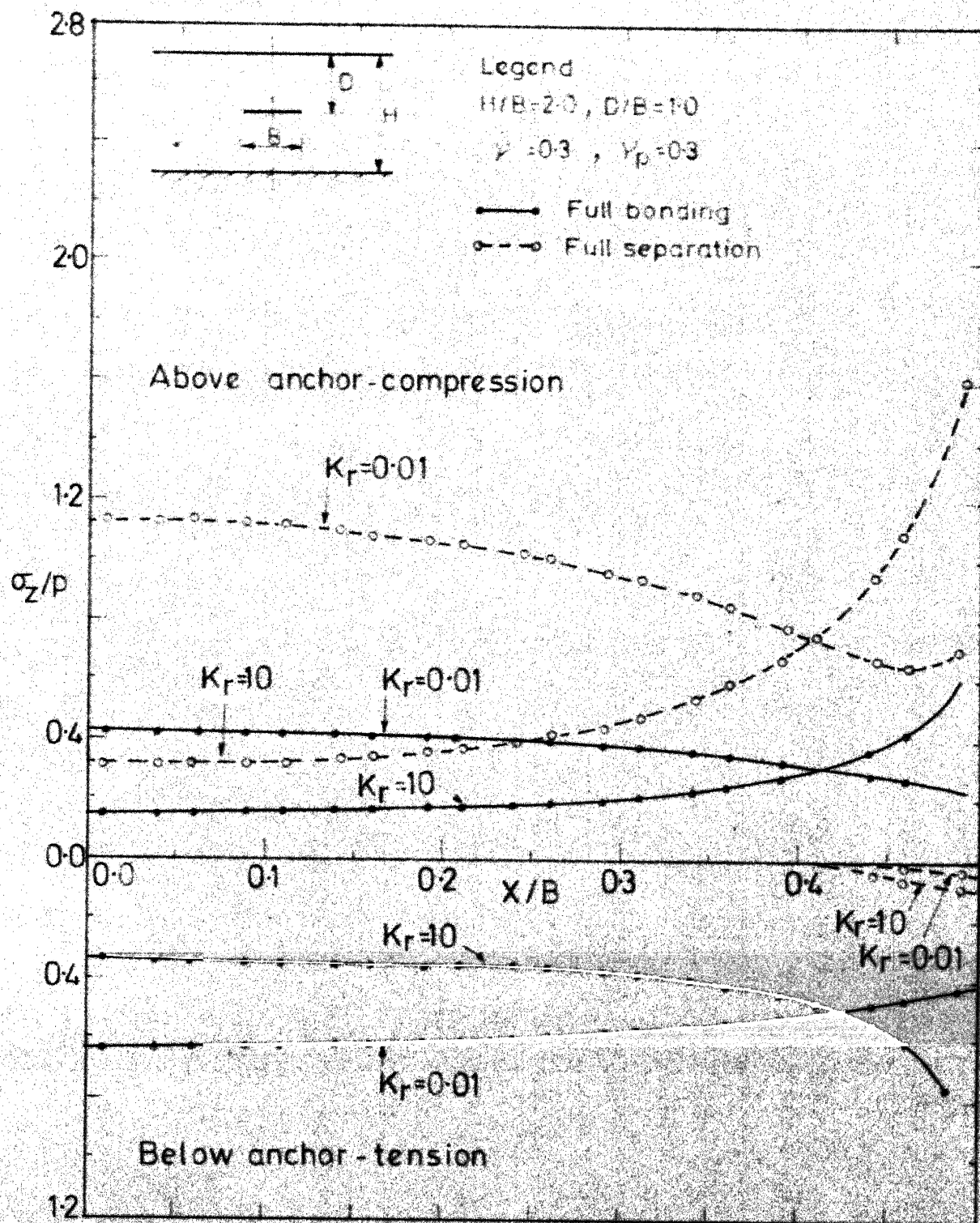


FIG. 6-12 VARIATION OF VERTICAL CONTACT STRESS DISTRIBUTION (CIRCULAR ANCHOR, PLATE ELEMENT, $\nu=0.3$)

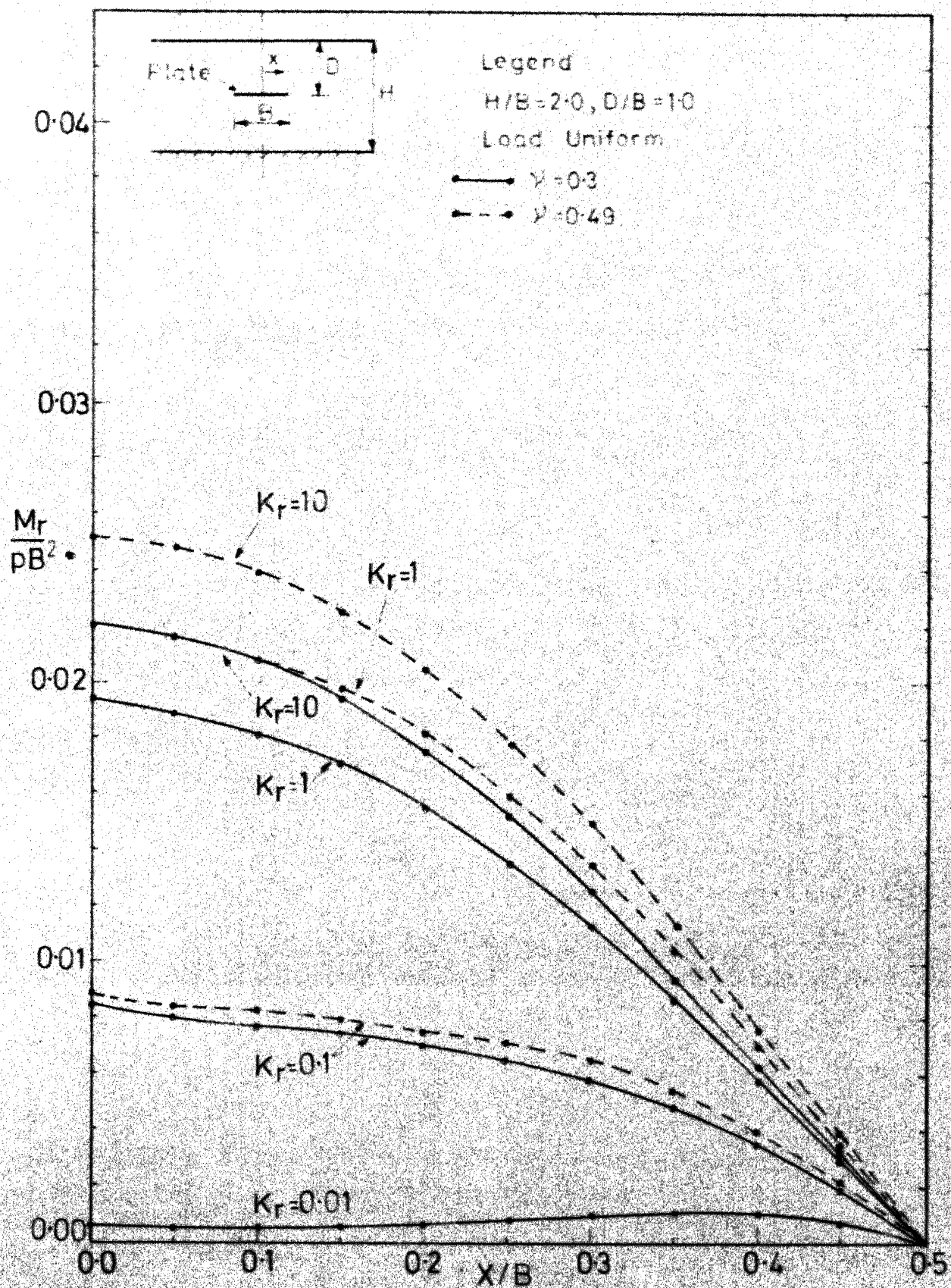


FIG. 6-13 RADIAL BENDING MOMENT DISTRIBUTION
(CIRCULAR ANCHOR, PLATE ELEMENT, UNIFORM
LOAD, FULL BONDING)

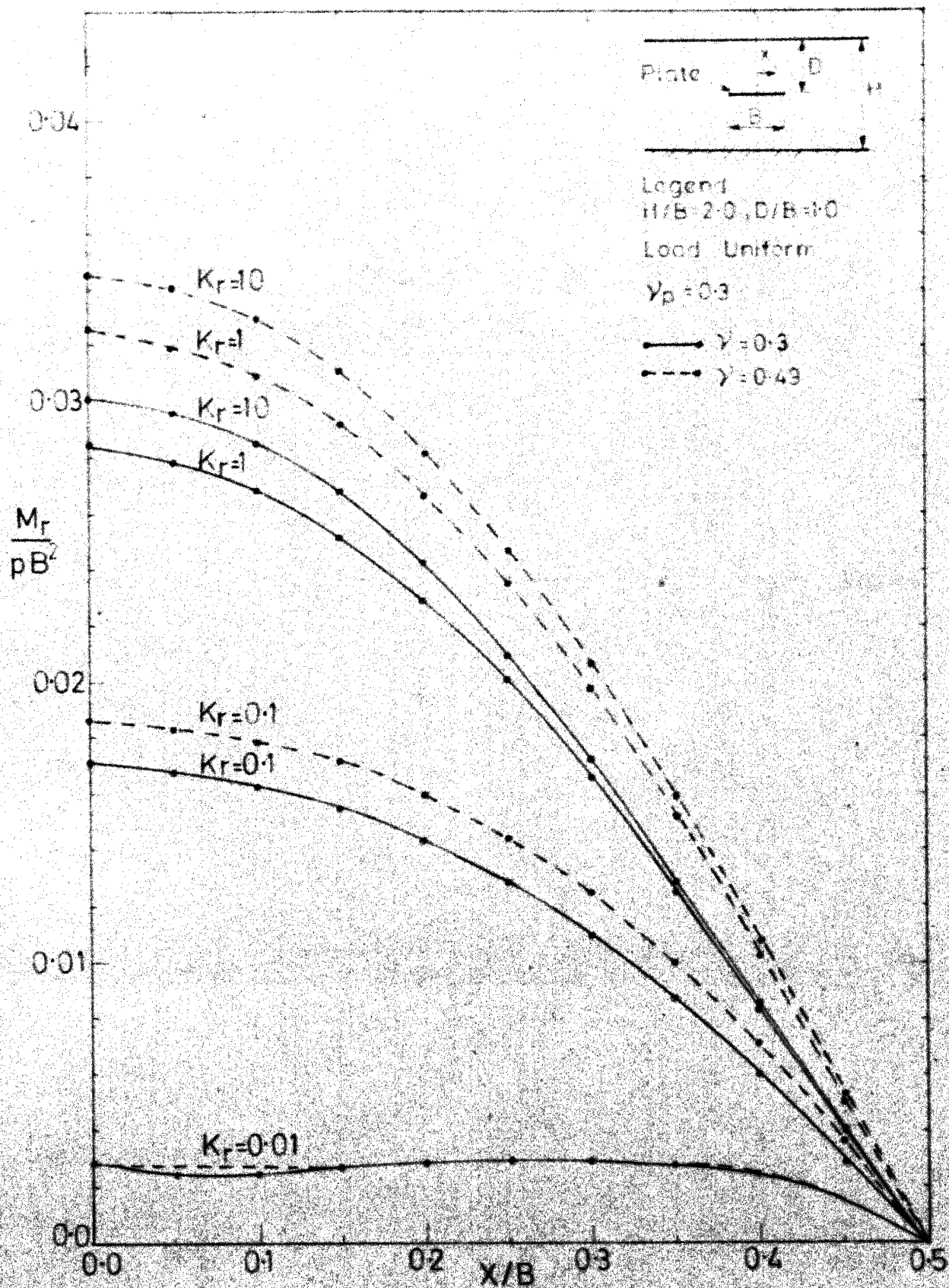
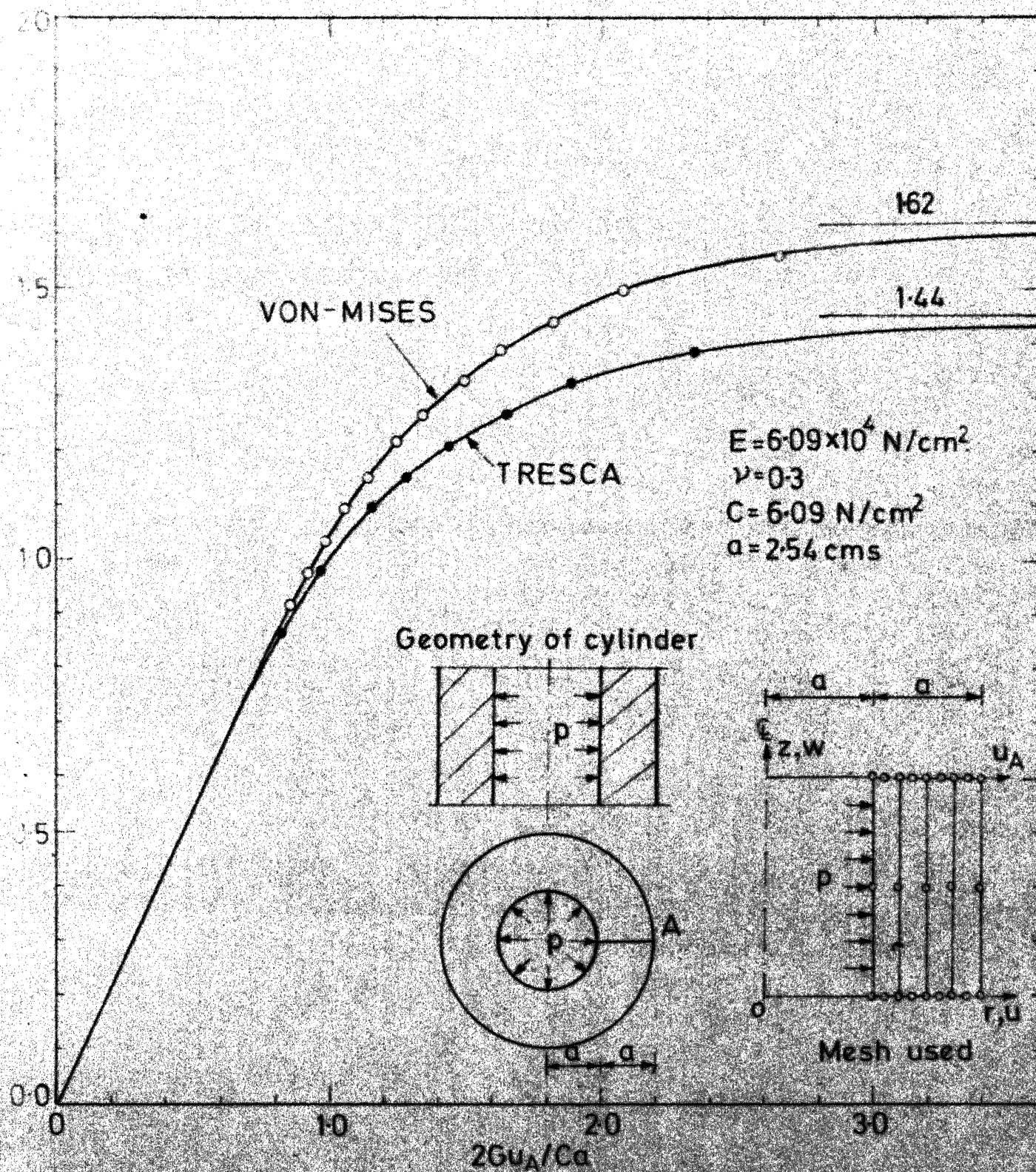


FIG. 6-14 RADIAL BENDING MOMENT DISTRIBUTION
 (CIRCULAR ANCHOR, PLATE ELEMENT, UNIFORM
 LOAD, FULL SEPARATION)



G. 6-15 ELASTO-PLASTIC DISPLACEMENT RESPONSE OF THICK WALLED CYLINDER (VON-MISES, TRESCA CRITERIA)

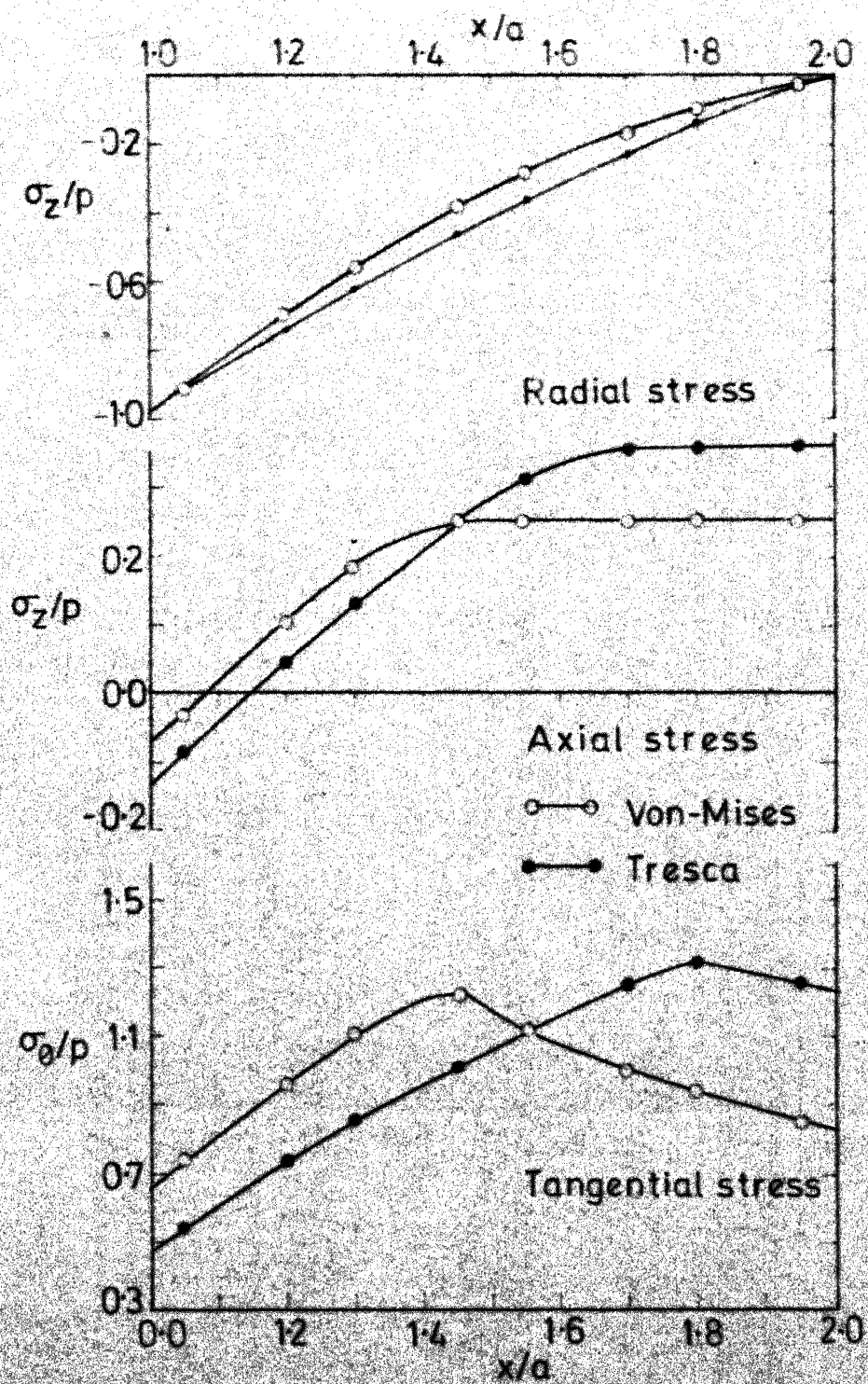


FIG. 6.16 ELASTO-PLASTIC STRESS DISTRIBUTION THROUGH THICKNESS OF THICK WALLED CYLINDER AT $p = 8.44 \text{ N/cm}^2$

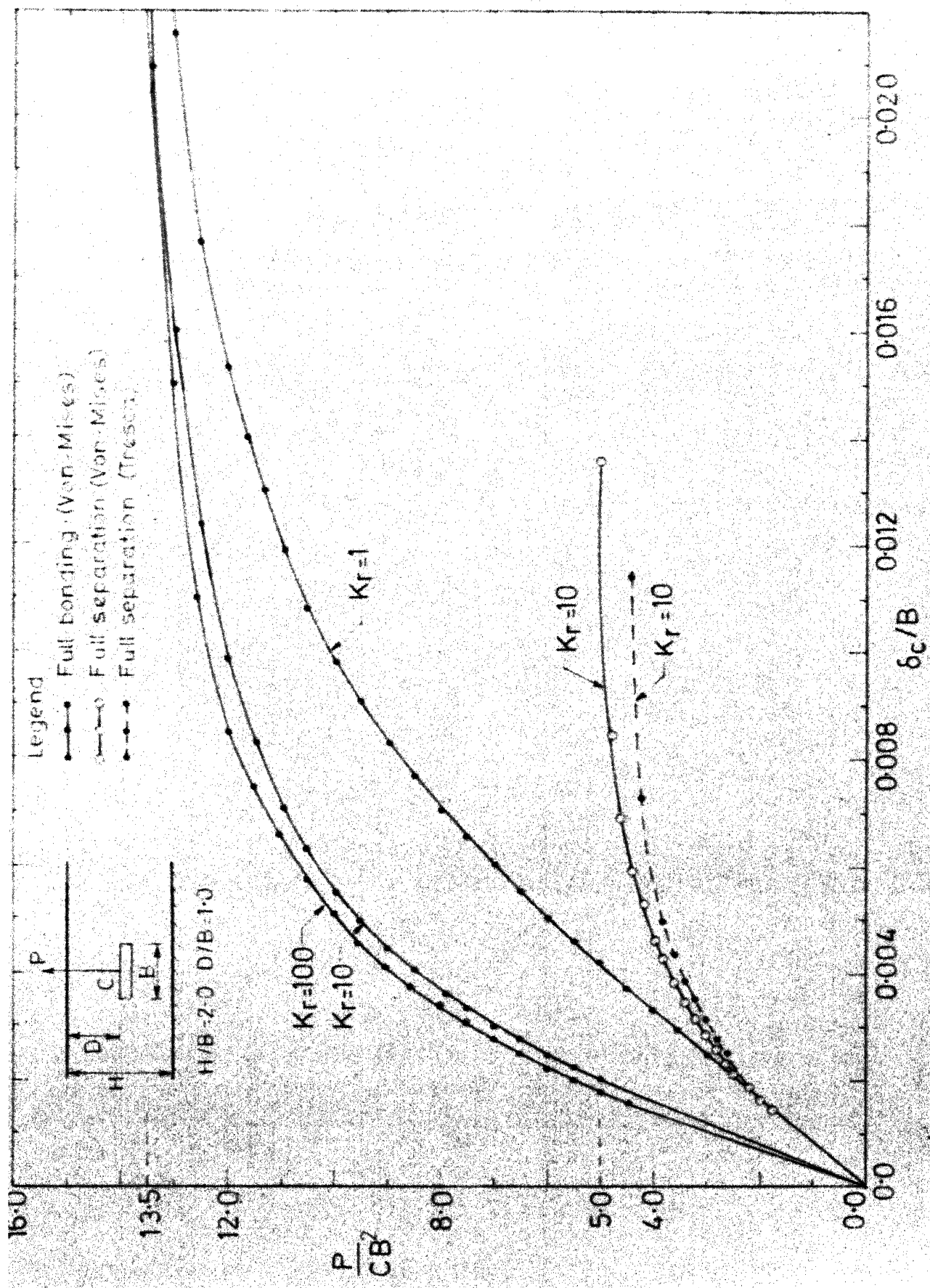
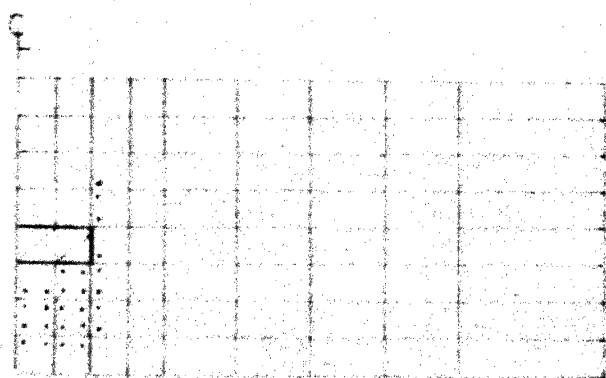
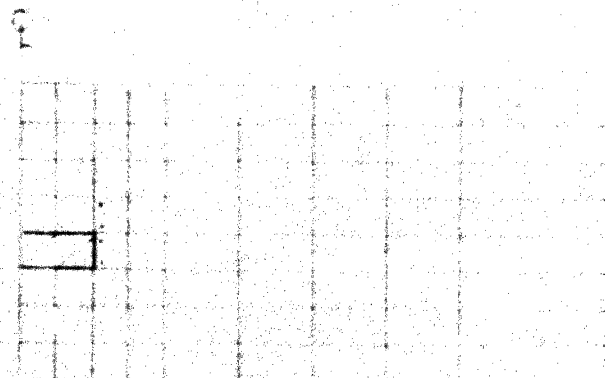


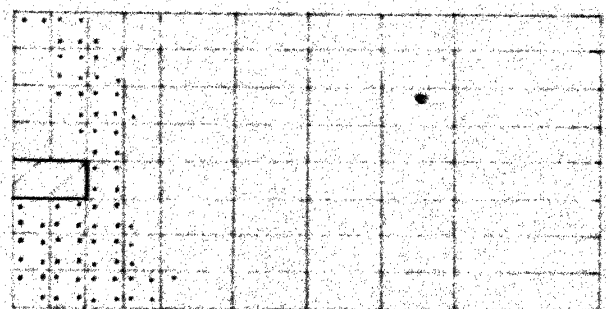
FIG. 6.17 LOAD DISPLACEMENT RESPONSE (CIRCULAR ANCHOR, VON-MISES AND TRESCA MODELS)



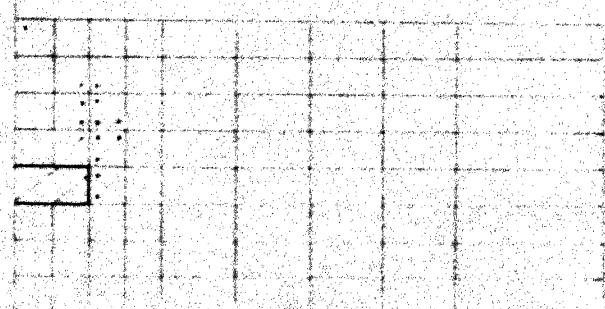
a.1 180 kN



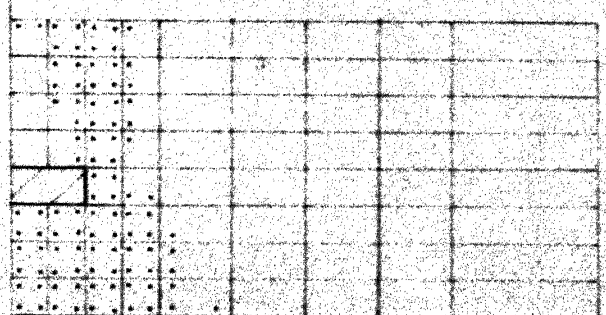
b.1 72 kN



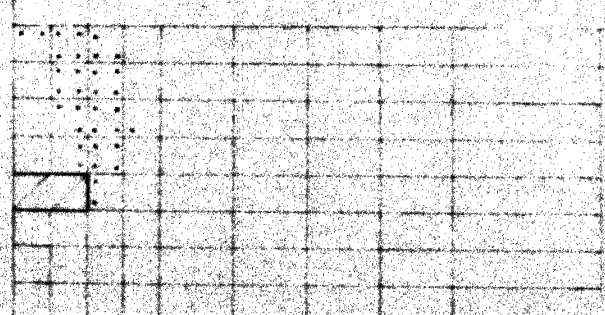
a.2 240 kN



b.2 88 kN



a.3 270 kN (Failure load)

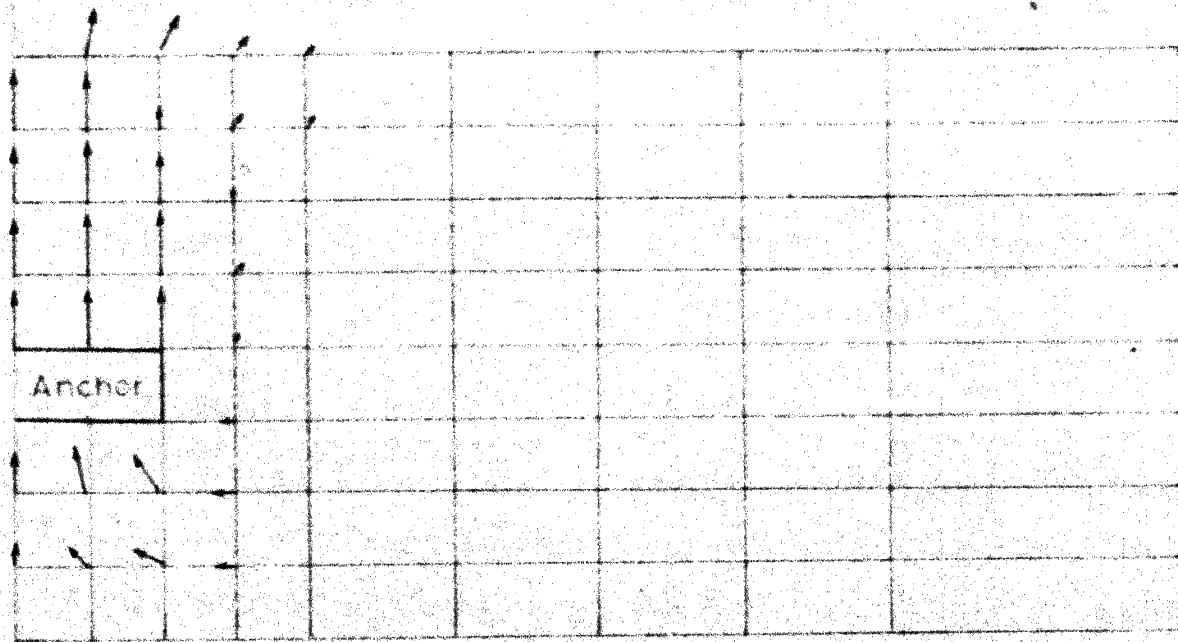


b.3 100 kN (Failure load)

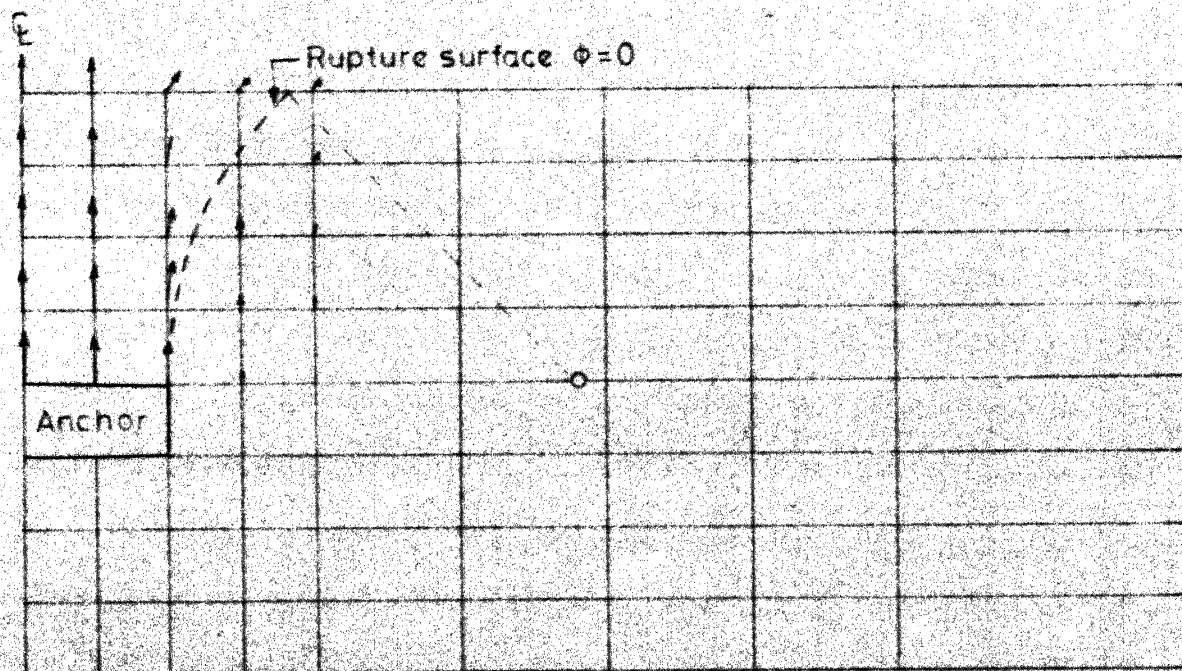
a. Full bonding

b. Full separation

FIG. 6-18 SPREAD OF PLASTIC ZONE (CIRCULAR ANCHOR)
VON-MISES MODEL



a. Full bonding case



b. Full separation case

FIG. 6-19 VELOCITY FIELD AT LIMIT LOAD (VON-MISES CRITERION)

CHAPTER 7

THEORETICAL RESULTS ON BREAKOUT RESISTANCE OF HORIZONTAL STRIP AND CIRCULAR ANCHORS

7.1 General :

A reasonable estimate of breakout resistance of plate anchors is essential for carrying out their successful design. The results of theoretical formulation for estimate of capacity of anchors should also be available in a form which can be readily used by the designer. Formulations for the calculation of ultimate uplift capacity of shallow horizontal strip and circular plate anchors are presented. The results from the methods are presented in the form of breakout factors so that they can be used with ease and also compared with results from other theories. To check the correctness of the results using Balla's theory (6), the problem has been reformulated and the uplift coefficients recomputed. Results from Balla (6), Meyerhof and Adams (58), Mariupol'skii (51) Matsuo (52) are presented in the form of breakout factors for easier comparison and use.

Figure 7.1 shows the general geometry, the rupture lines and the symbols used in the derivations. It is assumed that the shape of the rupture line is circular. The wedge of soil 1234 is sheared due to uplift load. It is also assumed that the lines of rupture intersect top free surface at statically correct angles of $\pi/4 - \phi/2$. Based on experimental observations and kinematic

considerations, the lines of rupture are also assumed to meet the anchor edge vertically at 2 and 3.

The uplift capacity of the foundation is the sum of the dead weight of foundation, the weight of soil enclosed within the lines of rupture, the ground surface and the top of the foundation and the soil resistance mobilised along the rupture lines.

$$V_f = W_f + W_s + T_v \quad (7.1a)$$

where

V_f = gross ultimate uplift capacity

W_f = weight of foundation, which is the sum of the weight of base slab and the product of the volume of the foundation stem and difference in densities of foundation material and soil

W_s = weight of soil enclosed in 1234

T_v = contribution to uplift capacity from soil resistance mobilised along the lines of rupture.

$$V_f = W_f + P_u \quad (7.1b)$$

where W_f is given by

$$W_f = W_b + V_s(\gamma_f - \gamma) \quad (7.2)$$

W_b = weight of base slab

V_s = volume of foundation stem

γ_f = density of material of foundation

γ = density of soil.

W_f depends on the foundation geometry and material densities and can be estimated for each specific case.

In all computations listed in this chapter, the ultimate uplift capacity, P_u , is calculated as given below :

$$P_u = W_s + T_v \quad (7.3)$$

7.2 Horizontal Strip Anchor :

In the calculation of breakout resistance it is assumed that as the strip plate anchor is subjected to vertical uplift force, definite rupture lines of circular shape are developed as shown in Fig. 7.1. The rupture lines meet the strip edge vertically, curves out and intersects the ground at an angle of $(\pi/4 - \phi/2)(\alpha_1)$. P_u , the ultimate uplift capacity of the strip per unit length, is computed as,

$$P_u = W_s + T_v$$

Two theories, namely, Strip Theory - 1 (ST-1) and Strip Theory 2 (ST-2) are considered. In Strip Theory - 1 (ST-1), all calculations are carried out on the assumption that the vertical component of the shearing resistance on the rupture surface contributes to soil resistance (T_v) mobilisation against uplift (Fig. 7.3). For Strip Theory - 2 (ST-2) it is assumed that the vertical component of cohesion and the vertical component of the resultant (p) of shearing resistance and normal force on the rupture surfaces contributes to T_v (Fig. 7.4).

7.2.1 Strip Theory - 1 (ST-1) :

The ultimate uplift load can be expressed as

$$P_u = W_s + T_v$$

Evaluation of W_s : Referring to Figs. 7.2 and 7.3,

$$W_s = 2T_1 = 2(T_4 - T_2 - T_3) \quad (7.4a)$$

T_1, T_2, T_3 and T_4 are weights of areas marked in Fig. 7.2, multiplied by unit length in lateral direction.

$$T_2 = \frac{\gamma}{2} D^2 \tan \alpha_1 \quad (7.4b)$$

$$T_3 = \frac{\gamma}{2} \left(\frac{D}{\cos \alpha_1} \right)^2 \alpha_2 \quad (7.4c)$$

$$T_4 = \gamma D \left(\frac{B}{2} + \frac{D}{\cos \alpha_1} \right) \quad (7.4d)$$

where

$$\alpha_1 = \frac{\pi}{4} - \frac{\phi}{2} \quad (7.4e)$$

$$\alpha_2 = \frac{\pi}{4} + \frac{\phi}{2} \quad (7.4f)$$

$$W_s = \gamma D^2 \left[\frac{B}{D} + 2/\cos \alpha_1 - \tan \alpha_1 - \alpha_2/\cos^2 \alpha_1 \right] \quad (7.5)$$

Evaluation of T_v : Kotter's equation for circular rupture line in terms of shear stress (τ_f) on it is

$$\frac{d\tau_f}{d\alpha} + 2\tau_f \tan \phi - r \gamma \sin(\alpha+\phi) \sin \phi = 0 \quad (7.6)$$

The solution of the above differential equation gives the following result.

$$\tau_f = A e^{-\alpha 2 \tan \phi} + \frac{\gamma r \sin \phi}{1+4 \tan^2 \phi} [2 \tan \phi \sin(\alpha+\phi) - \cos(\alpha+\phi)] \quad (7.7)$$

At ground level, $\alpha = \frac{\pi}{4} - \frac{\phi}{2}$, $\tau_f = C + C \sin \phi$

Using the above conditions, the constant A is evaluated as,

$$A = \gamma r e^{2 \tan \phi \alpha_1} \left[\frac{C}{r\gamma} (1 + \sin \phi) - \frac{\sin \phi}{1 + 4 \tan^2 \phi} (2 \tan \phi \sin \alpha_2 - \cos \alpha_2) \right] \quad (7.8)$$

and

$$\begin{aligned} \tau_f = \gamma r e^{2 \tan \phi \alpha_1} & \left[\frac{C}{r\gamma} (1 + \sin \phi) - \right. \\ & \left. - \frac{\sin \phi}{1 + 4 \tan^2 \phi} (2 \tan \phi \sin \alpha_2 - \cos \alpha_2) \right] e^{-\alpha 2 \tan \phi} \\ & + \frac{\gamma r \sin \phi}{1 + 4 \tan^2 \phi} [2 \tan \phi \sin(\alpha + \phi) - \cos(\alpha + \phi)] \end{aligned} \quad (7.9)$$

Equation (7.9) for τ_f , gives the variation of τ_f on the rupture lines, under the assumptions made.

The vertical component of the force on an arc length of ds due to τ_f can be expressed as

$$dT_v = 2(\tau_f r d\alpha) \sin \alpha \quad (7.10)$$

Hence

$$T_v = 2r \int_{\alpha_1}^{\pi/2} \tau_f \sin \alpha d\alpha \quad (7.11)$$

Substituting for τ_f from eqn. (7.9) into eqn. (7.11) and carrying out the necessary integration, the resulting expression is

$$\begin{aligned}
T_v = & \gamma D^2 \frac{C}{\gamma D} \frac{2 e^{2 \tan \phi \alpha_1} (1 + \sin \phi)}{\cos \alpha_1} \left[\frac{e^{-\alpha_1 2 \tan \phi}}{1 + 4 \tan^2 \phi} (2 \tan \phi \sin \alpha_1 + \cos \alpha_1) \right. \\
& - \left. \frac{e^{-\pi \tan \phi}}{1 + 4 \tan^2 \phi} \right] + \gamma D^2 \frac{2 e^{2 \tan \phi \alpha_1}}{\cos^2 \alpha_1} \left[\frac{\sin \phi}{1 + 4 \tan^2 \phi} (\cos \alpha_2 \right. \\
& - \left. 2 \tan \phi \sin \alpha_2) \right] \left[\frac{e^{-\alpha_1 2 \tan \phi}}{1 + 4 \tan^2 \phi} (2 \tan \phi \sin \alpha_1 + \cos \alpha_1) \right. \\
& - \left. \frac{e^{-\pi \tan \phi}}{1 + 4 \tan^2 \phi} \right] + \gamma D^2 \frac{2 \sin \phi}{\cos^2 \alpha_1 (1 + 4 \tan^2 \phi)} \left[\sin \phi \left(\alpha_2 + \frac{\cos \phi}{2} \right) \right. \\
& + \left. \frac{\tan \phi \sin \phi}{2} (1 + \sin \phi) - \cos \phi (1 + \sin \phi) + \frac{\sin \phi}{2} \left(\alpha_2 + \frac{\cos \phi}{2} \right) \right]
\end{aligned}
\tag{7.12}$$

$$P_u = \gamma D^2 (F_1 + \frac{C}{\gamma D} F_2 + F_3) \tag{7.13}$$

where F_1, F_2 and F_3 are non-dimensional factors which are functions of ϕ and D/B . The factor F_1 gives the contribution due to weight of wedge of soil and F_2, F_3 corresponds to contribution from T_v .

The calculation of P_u is simplified if the results are given in the form of breakout factors suggested by Vesic (101), i.e.

$$P_u = B(p_u) \tag{7.14a}$$

$$p_u = C F_c + \gamma D F_q \tag{7.14b}$$

F_c, F_q are breakout factors which are functions of ϕ and D/B given by

$$F_c = \frac{D}{B} F_2 \tag{7.15}$$

$$F_q = \frac{D}{B} (F_1 + F_3) \tag{7.16}$$

For specific values of ϕ and D/B , F_c and F_q can be read from table or graph and P_u can be calculated using eqn. (7.14). Once P_u is found, the gross uplift load can be obtained as

$$V_f = W_f + P_u$$

The non-dimensional breakout factors F_c, F_q for strip theory-1 (ST-1) are calculated by developing a simple computer program and the numerical values of factors are tabulated in Table 7.1 for a range of D/B and ϕ values. The variation of F_c with variation in ϕ and D/B is plotted in Fig. 7.5 and the variation of F_q with variation in ϕ and D/B is plotted in Fig. 7.6.

7.2.2 Strip Theory-2 (ST-2) :

The ultimate uplift load can be again expressed as

$$P_u = W_s + T_v$$

where W_s is given in eqn. (7.5).

Evaluation of T_v : Kotter's equation for circular rupture line in terms of p is,

$$\frac{dp}{d\alpha} + 2p \tan \phi - \gamma r \sin(\alpha + \phi) + 2C \sec \phi = 0 \quad (7.17)$$

The solution of the above differential equation is,

$$p = A e^{-\alpha 2 \tan \phi} + \frac{\gamma r}{1+4 \tan^2 \phi} [2 \tan \phi \sin(\alpha + \phi) - \cos(\alpha + \phi)] - \frac{C}{\sin \phi} \quad (7.18)$$

At ground level, $\alpha = \frac{\pi}{4} - \frac{\phi}{2}$, $\tau_f = C(1 + \sin \phi)$, $p = C$

Making use of the above conditions, in eqn. (7.18)

$$A = \left[\left(C + \frac{C}{\sin \phi} \right) - \frac{\gamma r}{1+4 \tan^2 \phi} (2 \tan \phi \sin \alpha_2 - \cos \alpha_2) \right] e^{\alpha_1 2 \tan \phi} \quad (7.19)$$

$$p = \left[\left(C + \frac{C}{\sin \phi} \right) - \frac{\gamma r}{1+4 \tan^2 \phi} (2 \tan \phi \sin \alpha_2 - \cos \alpha_2) \right] e^{\alpha_1 2 \tan \phi} e^{-\alpha 2 \tan \phi} \\ + \frac{\gamma r}{1+4 \tan^2 \phi} [2 \tan \phi \sin(\alpha + \phi) - \cos(\alpha + \phi)] - \frac{C}{\sin \phi} \quad (7.20)$$

$$dT_v = -2p r d\alpha \cos(\alpha + \phi) + 2 Cr d\alpha \sin \alpha \quad (7.21)$$

$$T_v = \int_{\alpha_1}^{\pi/2} -2p r \cos(\alpha + \phi) d\alpha + \int_{\alpha_1}^{\pi/2} 2Cr d\alpha \sin \alpha \quad (7.22)$$

Substituting for p, in eqn. (7.22)

$$T_v = 2 \int_{\alpha_1}^{\pi/2} \left[\left(C + \frac{C}{\sin \phi} \right) - \frac{\gamma r}{1+4 \tan^2 \phi} (2 \tan \phi \sin \alpha_2 - \cos \alpha_2) \right] e^{\alpha_1 2 \tan \phi} e^{-\alpha 2 \tan \phi} (\sin \alpha \sin \phi - \cos \alpha \cos \phi) r d\alpha \\ - 2 \int_{\alpha_1}^{\pi/2} \left\{ \frac{\gamma r}{1+4 \tan^2 \phi} [2 \tan \phi \sin(\alpha + \phi) - \cos(\alpha + \phi)] - \frac{C}{\sin \phi} \right\} \cos(\alpha + \phi) r d\alpha + 2 \int_{\alpha_1}^{\pi/2} Cr \sin \alpha d\alpha \quad (7.23)$$

$$P_u = W_s + T_v$$

$$\text{i.e., } P_u = \gamma D^2 [F_1 + \frac{C}{\gamma D} F_2 + F_3]$$

where F_1, F_2 and F_3 are non-dimensional factors which are functions of ϕ and D/B . The factor F_1 gives the contribution due to weight of enclosed wedge of soil and F_2, F_3 corresponds to contribution from T_v . Accordingly,

$$F_1 = \left(\frac{B}{D} + \frac{2}{\cos \alpha_1} - \tan \alpha_1 - \frac{\alpha_2}{\cos^2 \alpha_1} \right) \quad (7.24)$$

$$F_2 = 2.0 + \frac{2}{\cos \alpha_1} \left(1 + \frac{1}{\sin \phi} \right) e^{\alpha_1 2 \tan \phi} [e^{-\pi \tan \phi} (-\cos \phi - 2 \sin \phi \tan \phi) + \cos \phi \frac{e^{-\alpha_1 2 \tan \phi}}{1+4 \tan^2 \phi} (\sin \alpha_1 - 2 \tan \phi \cos \alpha_1) + \sin \phi \frac{e^{-\alpha_1 2 \tan \phi}}{1+4 \tan^2 \phi} (\cos \alpha_1 + 2 \tan \phi \sin \alpha_1)] + \frac{2}{\sin \phi \cos \alpha_1} (\cos \phi - \sin \alpha_1 \cos \phi - \cos \alpha_1 \sin \phi) \quad (7.25)$$

$$F_3 = \frac{2.0}{\cos^2 \alpha_1 (1+4 \tan^2 \phi)} (\cos \alpha_2 - 2 \tan \phi \sin \alpha_2) e^{\alpha_1 2 \tan \phi} \left[\frac{e^{-\pi \tan \phi}}{1+4 \tan^2 \phi} (-\cos \phi - 2 \sin \phi \tan \phi) + \frac{\cos \phi e^{-\alpha_1 2 \tan \phi}}{1+4 \tan^2 \phi} (\sin \alpha_1 - 2 \tan \phi \cos \alpha_1) \right] + \frac{\sin \phi e^{-\alpha_1 2 \tan \phi}}{1+4 \tan^2 \phi} (\cos \alpha_1 + 2 \tan \phi \sin \alpha_1) + \frac{\tan \phi}{\cos^2 \alpha_1 (1+4 \tan^2 \phi)} \tan \phi [\cos \phi \sin 2\phi - \cos 2\phi (1+\sin \phi)] + \frac{1}{\cos^2 \alpha_1 (1+4 \tan^2 \phi)} \left(\alpha_2 + \frac{\sin 2\phi}{2} - \frac{\cos \phi}{2} \right) \quad (7.26)$$

The expression derived above for P_u is not valid for the case $\phi = 0$, as some of the terms will become indeterminate.

For $\phi = 0$, Kotter's equation reduces to

$$\frac{d\sigma}{d\alpha} + 2C - \gamma r \sin \alpha = 0 \quad (7.27)$$

at ground level $\alpha = 45^\circ$, $\sigma = C$

Therefore,

$$\sigma = 2C\alpha + \gamma r \cos \alpha - \frac{\pi C}{2} - \frac{\gamma r}{\sqrt{2}} + C \quad (7.28)$$

$$T_v = 2 \int_{\pi/4}^{\pi/2} -(\sigma) r d\alpha \cos \alpha + 2 \int_{\pi/4}^{\pi/2} C r d\alpha \sin \alpha \quad (7.29)$$

$$P_u = \gamma D^2 (F_1 + \frac{C}{\gamma D} F_2 + F_3)$$

$$F_1 = (\frac{B}{D} + \frac{2}{\cos \pi/4} - \tan \pi/4 - \frac{\pi/4}{\cos^2 \alpha_1}) \quad (7.30)$$

$$F_2 = 0.729 \quad ; \quad F_3 = 0.519.$$

$$P_u = B(p_u)$$

$$p_u = (CF_c + \gamma D F_q)$$

F_c and F_q are non-dimensional breakout factors which are functions of ϕ and D/B which can be expressed as

$$F_c = \frac{D}{B} F_2$$

$$F_q = \frac{D}{B} (F_1 + F_3)$$

$$V_f = P_u + W_f$$

The non-dimensional breakout factors F_c , F_q for Strip Theory - 2 (ST-2) are calculated using a computer program for a range of ϕ and D/B values and are presented in Table 7.2. The variation of F_c with variation in ϕ and D/B is plotted in Fig. 7.7 and the variation of F_q with variation in ϕ and D/B is plotted in Fig. 7.8.

7.2.3 Breakout Factors Using Meyerhof and Adams's Theory (58) :

For shallow anchors, the ultimate uplift capacity is given by

$$P_u = 2CD + \gamma D (D K_u \tan \phi) \quad (7.31)$$

where K_u = nominal uplift coefficient of earth pressure on vertical plane through strip edge. For all practical purposes, it can be taken as a constant and equal to 0.95. Accordingly, eqn. (7.31) can be written as

$$P_u = B \left[C \frac{2D}{B} + \gamma D (0.95 \frac{D}{B} \tan \phi) \right] \quad (7.32)$$

and using eqn. (7.14b),

$$F_c = 2 \frac{D}{B} \quad (7.33)$$

$$F_q = 0.95 \frac{D}{B} \tan \phi \quad (7.34)$$

The computed values for F_c and F_q for strip anchor are tabulated in Table 7.3.

7.2.4 Comparison of Strip Anchor Theories :

The numerical values of F_c and F_q calculated for Strip Theory - 2 (ST-2) on comparison with Vesic's (101) reported values for F_c and F_q are seen to be identical. Vesic has derived the strip breakout resistance from modifications in solutions of the problem of a linear charge expanding a cylindrical cavity of infinite length, close to the surface, the axis of the cavity being parallel to the horizontal surface of a semi-infinite, homogeneous, isotropic solid possessing both cohesion and internal friction. The direct formulation used here for ST-2 and the Vesic's theory for long rectangular plates gives same numerical results.

Figure 7.9 presents values of F_q for two different values of ϕ equal to 30° and 45° , for a range of D/B values. The F_q values for $\phi = 0$ are also plotted in the same diagram for comparison. For the case, $C = 0$, $P_u = B\gamma D F_q$. The variation of F_q with D/B for all values of ϕ is linear for ST-1, ST-2 and for Meyerhof and Adams's Theories. The graph also shows the plot of F_q versus D/B by considering only the weight of earth trapezoid above the strip as contributing to uplift capacity. The inclination of the side of trapezoid from vertical is assumed as β . The plot is made for $\beta = 20^\circ$.

For $\phi = 0$, case,

$$p_u = (C F_c + \gamma D F_q)$$

$$F_u = \frac{p_u - \gamma D}{C} \quad (7.35a)$$

$$F_u = \frac{C F_c + \gamma D (F_q - 1)}{C} \quad (7.35b)$$

F_u , is the ultimate uplift capacity factor, considered equivalent to bearing capacity factor, N_c . For $\phi = 0$ case, if F_q factor works out to be equal to unity, F_u is nothing but F_c . Plot of F_u versus D/B for ST-1, ST-2 and Meyerhof and Adams's theories are shown in Fig. 7.10. For ST-1, F_u becomes a function of $\frac{C}{\gamma B}$ as well as D/B and curves are plotted for two $\frac{C}{\gamma B}$ values of 0.5 and 4.0.

7.3 Circular Anchors :

The circular anchor subjected to central vertical load is an axially symmetric problem and presents more difficulties in

solution than a strip anchor. An equivalent of Kotter's equation does not exist for axially symmetric problems. Additional assumptions are needed to get solution of the problem. The assumptions made are : (i) the normal and shear distributions as well as statically correct angles along the slip surfaces are equivalent to those found in the corresponding two-dimensional cases, (ii) the slip surface is a part of torus, formed by revolution of the circular rupture line around axis of symmetry, (iii) the slip surface meets the surface of the anchor edge vertically and the soil surface at $(\pi/4 - \phi/2)$ as in the two-dimensional cases.

7.3.1 Circular Anchor Theory - 1 (CIR-1) :

The formulation for ultimate uplift capacity is done under the following assumptions. The soil resistance against uplift along the rupture surface is taken as the sum of the vertical components of force due to cohesion and the vertical component of the resultant of normal and shear force on rupture surface as was done in the derivation of Strip Theory - 2 (ST-2). Accordingly, the ultimate uplift capacity of the anchor is,

$$P_u = W_s + T_v$$

Referring to Fig. 7.2

$$W_s = T_1 = (T_4 - T_2 - T_3) \quad (7.36)$$

$$W_s = \gamma D^3 \left[\pi \left(\frac{B}{2D} + \frac{1}{\cos \alpha_1} \right)^2 + \frac{\pi \alpha_2}{\cos^2 \alpha_1} \left(\frac{B}{2D} + \frac{1}{\cos \alpha_1} - \frac{2}{3} \frac{\sin \alpha_2}{\alpha_2 \cos \alpha_1} \right) + \pi \tan \alpha_1 \left(\frac{B}{2D} + \frac{1}{\cos \alpha_1} + \frac{\tan \alpha_1}{3} \right) \right] \quad (7.37)$$

Solution for p and its variation along rupture surface is already derived in Sec. 7.2.2. Referring to Figs. 7.4 and 7.11.

$$dT_v = (C r d\alpha) \sin \alpha \rho d\beta - p r d\alpha \cos(\alpha + \phi) \rho d\beta \quad (7.38)$$

$$\rho = r \left(\frac{B}{2r} + 1 - \sin \alpha \right) \quad (7.39)$$

$$P_v = 2\pi r^2 C \int_{\alpha_1}^{\pi/2} \left[\left(\frac{B}{2r} + 1 \right) \sin \alpha - \sin^2 \alpha \right] d\alpha - 2\pi r^2 \int_{\alpha_1}^{\pi/2} \left[\left(\frac{B}{2r} + 1 \right) \cos \phi \cos \alpha - \left(\frac{B}{2r} + 1 \right) \sin \alpha \sin \phi - \cos \phi \sin \alpha \cos \alpha + \sin \phi \sin^2 \alpha \right] p d\alpha \quad (7.40)$$

Substituting for p , from eqn. (7.20) into eqn. (7.40) and carrying out the necessary integration, the resulting expressions are :

$$P_v = \gamma D^3 \left[F_1(\phi, \lambda) + \frac{C}{\gamma D} F_2(\phi, \lambda) + F_3(\phi, \lambda) \right] \quad (7.41)$$

$$F_2 = Q_0 + Q_1 M_1 + Q_3 \quad (7.42)$$

$$F_3 = Q_2 M_1 + Q_4 M_2 + Q_5 M_3 \quad (7.43)$$

where

$$Q_0 = \frac{2\pi}{\cos^2 \alpha_1} \left[\left(\frac{B \cos \alpha_1}{2D} + 1 \right) \cos \alpha_1 - \frac{1}{2} (\alpha_2 + \frac{\cos \phi}{2}) \right] \quad (7.44)$$

$$Q_1 = \frac{-2\pi}{\cos^2 \alpha_1} \left(1 + \frac{1}{\sin \phi} \right) e^{2\alpha_1 \tan \phi} \quad (7.45)$$

$$Q_2 = \frac{-2\pi e^{2\alpha_1 \tan \phi}}{\cos^3 \alpha_1 (1 + 4 \tan^2 \phi)} [\cos \alpha_2 - 2 \tan \phi \sin \alpha_2] \quad (7.46)$$

$$Q_3 = \frac{-2\pi}{\cos \alpha_1} \left[\left(\frac{B}{2D} \cos \alpha_1 + 1 \right) (\sin \alpha_1 - 1) \cot \phi + \right. \\ \left. \left(\frac{B}{2D} \cos \alpha_1 + 1 \right) \cos \alpha_1 + \frac{\cos \phi}{4 \sin \phi} (1 + \sin \phi) + 0.5 \left(-\alpha_2 - \frac{\cos \phi}{2} \right) \right] \quad (7.47)$$

$$Q_4 = - \frac{4\pi \sin \phi}{\cos^3 \alpha_1 (1 + 4 \tan^2 \phi)} - \frac{2\pi \sin \phi}{\cos^3 \alpha_1 (1 + 4 \tan^2 \phi)} \quad (7.48)$$

$$Q_5 = - \frac{4\pi \tan \phi \sin \phi}{\cos^3 \alpha_1 (1 + 4 \tan^2 \phi)} + \frac{2\pi \cos \phi}{\cos^3 \alpha_1 (1 + 4 \tan^2 \phi)} \quad (7.49)$$

$$M_1 = \left(\frac{B}{2D} \cos \alpha_1 + 1 \right) \cos \phi \left[\frac{e^{-\pi \tan \phi}}{1 + 4 \tan^2 \phi} - \frac{e^{-2\alpha_1 \tan \phi}}{1 + 4 \tan^2 \phi} (\sin \alpha_1 - \right. \\ \left. 2 \tan \phi \cos \alpha_1) \right] + \left(\frac{B}{2D} \cos \alpha_1 + 1 \right) \sin \phi \left[\frac{e^{-\pi \tan \phi} (2 \tan \phi)}{1 + 4 \tan^2 \phi} - \right. \\ \left. \frac{e^{-2\alpha_1 \tan \phi}}{1 + 4 \tan^2 \phi} (\cos \alpha_1 + 2 \tan \phi \sin \alpha_1) \right] + \frac{\cos \phi}{4} \left[\frac{e^{-\pi \tan \phi}}{1 + \tan^2 \phi} - \right. \\ \left. \frac{e^{-2\alpha_1 \tan \phi}}{1 + \tan^2 \phi} 2 \sin \phi \right] + \frac{\sin \phi}{4} \left[\frac{e^{-\pi \tan \phi}}{\tan \phi} - \frac{e^{-\pi \tan \phi}}{1 + \tan^2 \phi} \tan \phi + \right. \\ \left. \frac{e^{-2\alpha_1 \tan \phi}}{\tan \phi} + \frac{e^{-2\alpha_1 \tan \phi}}{1 + \tan^2 \phi} (\cos \phi - \tan \phi \sin \phi) \right] \quad (7.50)$$

$$M_2 = \left(\frac{B}{2D} \cos \alpha_1 + 1 \right) (1 + \sin \phi) \frac{\cos \phi}{4} - \left(\frac{B}{2D} \cos \alpha_1 + 1 \right) \left(\alpha_2 + \right. \\ \left. \frac{\cos \phi}{2} \right) \frac{\sin \phi}{2} + \frac{\cos \phi}{3} (\sin^3 \alpha_1 - 1) + \sin \phi \left(\cos \alpha_1 - \frac{\cos^3 \alpha_1}{3} \right) \quad (7.51)$$

$$M_3 = \left(\frac{B}{2D} \cos \alpha_1 + 1 \right) \left(\alpha_2 - \frac{\cos \phi}{2} \right) \frac{\cos \phi}{2} - \left(\frac{B}{2D} \cos \alpha_1 + 1 \right) (1 + \sin \phi) \frac{\sin \phi}{4} - \frac{\cos \phi}{3} \cos^3 \alpha_1 + \frac{\sin \phi}{3} (1 - \sin^3 \alpha_1) \quad (7.52)$$

For $\phi = 0$, some terms in the above expressions will be indeterminate. T_v is separately calculated for $\phi = 0$ case as follows :

$$\sigma = 2C\alpha + \gamma r \cos \alpha - \frac{\pi C}{2} - \frac{\gamma r}{\sqrt{2}} + C$$

$$dT_v = -\sigma r d\alpha \cos \alpha \left(\frac{B}{2} + r - r \sin \alpha\right) d\beta + Cr d\alpha \sin \alpha \left(\frac{B}{2} + r - r \sin \alpha\right) d\beta \quad (7.53)$$

$$T_v = -2\pi r^2 \int_{\pi/4}^{\pi/2} \left(\frac{B}{2r} + 1 - \sin \alpha\right) (2C\alpha \cos \alpha + \gamma r \cos^2 \alpha - \frac{\pi C}{2} \cos \alpha - \frac{\gamma r}{\sqrt{2}} \cos \alpha + C \cos \alpha) d\alpha + 2\pi r^2 C \int_{\pi/4}^{\pi/2} \left[\left(\frac{B}{2r} + 1\right) \sin \alpha - \sin^2 \alpha\right] d\alpha \quad (7.54)$$

$$F_2 = 4\pi \left[\left(\frac{B}{4D} + \frac{1}{\sqrt{2}}\right) - \frac{\pi}{8} - \frac{1}{4}\right] \quad (7.55)$$

$$F_3 = -4\pi \left[\left(\frac{B}{2\sqrt{2}D} + 1\right) \left(\frac{\pi}{2} - \sqrt{2} + 1 - \frac{1}{\sqrt{2}} - \frac{\pi}{8}\right) - 4\pi \sqrt{2} \left[\left(\frac{B}{2\sqrt{2}D} + 1\right) \left(\frac{\pi}{8} - \frac{1}{\sqrt{2}} + \frac{1}{4}\right) + \frac{1}{12\sqrt{2}}\right]\right] \quad (7.56)$$

$$F_1 = \pi \left(\frac{B}{2D} + \frac{1}{\cos \alpha_1}\right)^2 + \frac{\pi \alpha_2}{\cos^2 \alpha_1} \left(\frac{B}{2D} + \frac{1}{\cos \alpha_1} - \frac{2}{3} \frac{\sin \alpha_2}{\alpha_2 \cos \alpha_1}\right) + \pi \tan \alpha_1 \left(\frac{B}{2D} + \frac{1}{\cos \alpha_1} - \frac{\tan \alpha_1}{3}\right) \quad (7.57)$$

To obtain the results in the form of breakout factors,

$$\frac{P_u}{\pi/4 B^2} = p_u = C F_c + \gamma D F_q \quad (7.58)$$

$$F_c = \frac{4}{\pi} \frac{D^2}{B^2} (F_2) \quad (7.59)$$

$$F_q = \frac{4}{\pi} \frac{D^2}{B^2} (F_1 + F_3) \quad (7.60)$$

where F_c and F_q are circular anchor breakout factors.

The gross ultimate uplift load $V_f = W_f + P_u$

where

$$P_u = \frac{\pi}{4} B^2 p_u \quad (7.61)$$

$$p_u = CF_c + \gamma D F_q$$

The non-dimensional breakout factors for circular anchor F_c and F_q as per the above formulation (CIR-1) are calculated using a computer program and the results are given in Table 7.4. For a range of ϕ and D/B values, the factors have been tabulated. The variation of F_c and F_q with change in ϕ and D/B are plotted in graphical form in Figs. 7.12 and 7.13.

7.3.2 Balla's Theory-Recomputation of Factors :

Balla (6) derived his theory under the general assumptions listed in Sec. 7.3. The contribution to uplift capacity from resistance mobilised along the rupture surface is taken as due to the vertical component of shearing resistance on the rupture surface. Balla presented the results of his computations in the form,

$$P_u = \gamma D^3 [F_1(\phi, \lambda) + \frac{C}{\gamma D} F_2(\phi, \lambda) + F_3(\phi, \lambda)]$$

Vesic (101) has pointed out that Balla's work contains errors in numerical values of F_2 and F_3 . The coefficients F_1, F_2 and F_3 are calculated from an independent computation of Balla's theory, to check whether the reported values are correct. Calculation of breakout resistance and the comparison with other theories

become easier if the results are expressed in terms of circular anchor breakout factors, F_c and F_q . The ultimate uplift capacity of the anchor can be expressed as,

$$P_u = W_s + T_v$$

The solution for τ_f for two-dimensional case is already obtained in eqn. (7.9).

Referring to Fig. 7.11,

$$dT_v = \tau_f r d\alpha \sin \alpha \rho d\beta \quad (7.62)$$

$$\rho = r \left(\frac{B}{2r} + 1 - \sin \alpha \right)$$

$$r = \frac{D}{\cos \alpha_1}$$

$$T_v = 2\pi r^2 \int_{\alpha_1}^{\pi/2} \tau_f [\sin \alpha \left(\frac{B}{2r} + 1 \right) - \sin^2 \alpha] d\alpha \quad (7.63)$$

Carrying out the integration,

$$T_v = \gamma D^3 \left[\frac{C}{\gamma D} F_2(\phi, \lambda) + F_3(\phi, \lambda) \right]$$

where

$$\begin{aligned} F_2(\phi, \lambda) = & \frac{2\pi e^{2 \tan \phi \alpha_1}}{\cos^2 \alpha_1} (1 + \sin \phi) \left[\frac{B \cos \alpha_1}{2D(1+4 \tan^2 \phi)} + \right. \\ & \left. \frac{1}{(1+4 \tan^2 \phi)} \right] [-e^{-\pi \tan \phi} 2 \tan \phi + \\ & e^{-\alpha_1 2 \tan \phi} (2 \tan \phi \sin \alpha_1 + \cos \alpha_1)] + \\ & e^{-\pi \tan \phi} \left(\frac{\tan \phi}{4+4 \tan^2 \phi} + \frac{1}{4 \tan \phi} \right) - e^{-2\alpha_1 \tan \phi} \left[\frac{\cos \phi}{4+4 \tan^2 \phi} - \right. \\ & \left. \frac{\tan \phi \sin \phi}{4+4 \tan^2 \phi} + \frac{1}{4 \tan \phi} \right] \end{aligned} \quad (7.64)$$

$$\begin{aligned}
F_3(\phi, \lambda) = & \frac{2\pi e^{2\alpha_1 \tan \phi} \sin \phi}{\cos^3 \alpha_1 (1 + 4 \tan^2 \phi)} (\cos \alpha_2 - \\
& - 2 \tan \phi \sin \alpha_2) \left\{ \left[\frac{B}{2D} \frac{\cos \alpha_1}{(1 + 4 \tan^2 \phi)} + \frac{1}{1 + 4 \tan^2 \phi} \right] \right. \\
& \left. [-e^{-\pi \tan \phi} 2 \tan \phi + e^{-2\alpha_1 \tan \phi} (2 \tan \phi \sin \alpha_1 + \cos \alpha_1)] + \right. \\
& \left. e^{-\pi \tan \phi} \left(\frac{\tan \phi}{4 + 4 \tan^2 \phi} + \frac{1}{4 \tan \phi} \right) - e^{-2\alpha_1 \tan \phi} \left[\frac{\cos \phi}{4 + 4 \tan \phi} - \right. \right. \\
& \left. \left. \frac{\tan \phi \sin \phi}{(4 + 4 \tan^2 \phi)} + \frac{1}{4 \tan \phi} \right] \right\} \quad (7.65)
\end{aligned}$$

For $\phi = 0$ case, T_v is separately calculated as follows :

$$dT_v = Cr \, d\alpha \sin \alpha \, d\beta \quad (7.66)$$

$$\begin{aligned}
T_v &= 2\pi r^2 C \int_{\pi/4}^{\pi/2} \left[\left(\frac{B}{2r} + 1 \right) \sin \alpha - \sin^2 \alpha \right] d\alpha \\
&= \gamma D^3 \frac{C}{\gamma D} 4\pi \left[\left(\frac{B}{4D} + \frac{1}{\sqrt{2}} \right) - \frac{\pi}{8} - \frac{1}{4} \right] \quad (7.67)
\end{aligned}$$

Expression for $F_1(\phi, \lambda)$ is the same as given in eqn. (7.57).

$$P_u = \gamma D^3 [F_1(\phi, \lambda) + \frac{C}{\gamma D} F_2(\phi, \lambda) + F_3(\phi, \lambda)]$$

Numerical values of F_1, F_2 and F_3 derived above are calculated by developing a computer program for the purpose. Table 7.5 gives the values of the factors F_1, F_2 and F_3 for the range of D/B and ϕ values reported by Balla and those computed from the above expressions. A comparison of the two values clearly shows that there is no numerical errors in the factors reported by Balla (6), as observed by Vesic (101).

The results of Balla's theory are calculated in the form of

circular anchor breakout factors also, as presented below

$$\frac{P_u}{\pi/4 B^2} = p_u = C F_c + \gamma D F_q$$

$$F_c = \frac{4}{\pi} \frac{D^2}{B^2} (F_2)$$

$$F_q = \frac{4}{\pi} \frac{D^2}{B^2} (F_1 + F_3)$$

F_c and F_q are circular anchor breakout factors. Table 7.6 gives the values of F_c and F_q factors for Balla's theory for a range of D/B and ϕ values. Figs. 7.14 and 7.15 give the variation of F_c and F_q with D/B and ϕ in a graphical form.

7.3.3 Breakout Factors Using Meyerhof and Adams's Theory :

For shallow anchors, the expressions for ultimate uplift capacity (58) is :

$$P_u = \pi C B D + \gamma D (0.5 \pi B D K_u \tan \phi) + \frac{\pi}{4} B^2 D \gamma \quad (7.68)$$

Rearranging the above equation,

$$\frac{P_u}{\pi/4 B^2} = C \left(4 \frac{D}{B}\right) + \gamma D \left(2 s \frac{D}{B} K_u \tan \phi + 1\right) \quad (7.69)$$

$$F_c = 4 \frac{D}{B} \quad (7.70)$$

$$F_q = \left(2 s \frac{D}{B} K_u \tan \phi + 1\right) \quad (7.71)$$

The earth pressure coefficients ' sK_u ' for the calculation are read from the graphical plot of ' sK_u ' versus D/B ratio for each ϕ value (58). The values tabulated are for shallow anchors.

Table 7.7 summarises the results of calculations.

7.3.4 Breakout Factors Using Mariupol'skii's Theory :

The ultimate uplift capacity for shallow anchors is given by :

$$P_u = \frac{\pi}{4} (B^2 - B_0^2) \frac{C + 4 \frac{D}{B} + \gamma D \left[1 - \left(\frac{B_0}{B} \right)^2 + 2K' \tan \phi \frac{D}{B} \right]}{1 - \left(\frac{B_0}{B} \right)^2 - 2n \frac{D}{B}} \quad (7.72)$$

The terms B_0^2 and $\left(\frac{B_0}{B} \right)^2$ are neglected when compared to other terms in the expression for purposes of computation. K' is the coefficient of lateral earth pressure and is taken as 0.4 in this calculation. $n = 0.0025 \phi$, (ϕ in degrees) is an empirical function of ϕ . So the expression used for the calculation is,

$$\frac{P_u}{\pi/4 B^2} = \frac{C + 4 \frac{D}{B}}{1 - (0.005 \phi) \frac{D}{B}} + \gamma D \frac{(1 + 0.8 \tan \phi \frac{D}{B})}{1 - (0.005 \phi) \frac{D}{B}} \quad (7.73)$$

$$F_c = \frac{4 \frac{D}{B}}{1 - (0.005 \phi) \frac{D}{B}} \quad (7.74)$$

$$F_q = \frac{1 + 0.8 \tan \phi \frac{D}{B}}{1 - (0.005 \phi) \frac{D}{B}} \quad (7.75)$$

Table 7.8 gives the breakout factors for shallow circular anchor by Mariupol'skii's Theory under the above assumptions.

7.3.5 Breakout Factors for Matsuo's Theory :

Matsuo (52) presented the final results of his analysis in the form given below (Fig. 2.4e).

$$P_u = \gamma B_2^3 K_1 + C B_2^2 K_2 \quad (7.76)$$

$$K_1 = \pi[(a-1)(a^2 F_1 + a F_2 + ab F_3 + b F_4 + F_5) + b] \quad (7.77)$$

$$K_2 = \pi[(a-1)(a F_6 + F_7) + b(b \tan \alpha_2 + 2)] \quad (7.78)$$

$$a = \frac{X_0}{B_2}, \quad b = \frac{D_2}{B_2}, \quad \alpha_2 = 45^\circ + \phi/2.$$

where $F_1, F_2, F_3, F_4, F_5, F_6$ and F_7 are as specified by Matsuo (52).

Using $\theta_0 = 60^\circ$, as recommended by Matsuo,

$$B_2 = D \left[\frac{B}{2D} + \left(\frac{\sin(75 - \phi/2)}{\sin 60} - \frac{\sin \alpha_2}{\sin 60 e^{60 \tan \phi}} \right) \sin \alpha_2 \right] \quad (7.79)$$

$$a = \left[\frac{B}{2D} + \frac{\sin(75 - \phi/2) \sin \alpha_2}{\sin 60} \right] / \left[\frac{B}{2D} + \left(\frac{\sin(75 - \phi/2)}{\sin 60} - \frac{\sin(45 + \phi/2)}{\sin 60 e^{60 \tan \phi}} \right) \right] \quad (7.80)$$

$$b = \left\{ \left[\frac{\sin(75 - \phi/2)}{\sin 60} - \frac{\sin \alpha_2}{\sin 60 e^{60 \tan \phi}} \right] \cos \alpha_2 \right\} / \left\{ \frac{B}{2D} + \left[\frac{\sin(75 - \phi/2)}{\sin 60} - \frac{\sin \alpha_2}{\sin 60 e^{60 \tan \phi}} \right] \sin \alpha_2 \right\} \quad (7.81)$$

$$FACT1 = B_2^3 K_1 \quad (7.82)$$

$$FACT2 = B_2^2 K_2 \quad (7.83)$$

$$p_u = CF_c + \gamma D F_q$$

$$p_u = C \left(\frac{D^2}{B^2} \frac{4}{\pi} FACT2 \right) + \gamma D \left(\frac{4}{\pi} \frac{D^2}{B^2} FACT1 \right) \quad (7.84)$$

$$F_c = \frac{D^2}{B^2} \frac{4}{\pi} FACT2 \quad (7.85)$$

$$F_q = \frac{D^2}{B^2} \frac{4}{\pi} FACT1 \quad (7.86)$$

The expressions above have been programmed. The results of calculation are given in Table 7.9. F_c and F_q factors are tabulated against D/B and ϕ values.

7.3.6 Breakout Factors - Earth Cone Method :

Indian Standards (44) do not specify about circular anchors. However, for a rectangular foundation it is specified that the uplift can be considered to be resisted by the weight of an inverted frustrum of pyramid of earth on the footing pad with the sides inclined at an angle of 20° to 30° to vertical. For a circular anchor the inverted frustrum of cone is considered. If the side inclination of cone from vertical is considered as β , (semi-apex angle of the inverted cone),

$$\text{Weight of soil inside the cone} = \gamma D \frac{\pi B^2}{4} \left[1 + \frac{4}{3} \frac{D^2}{B^2} \tan^2 \beta + \frac{2D}{B} \tan \beta \right] \quad (7.87)$$

Breakout factor F_q is given by

$$F_q = \left(1 + \frac{4}{3} \frac{D^2}{B^2} \tan^2 \beta + \frac{2D}{B} \tan \beta \right) \quad (7.88)$$

Table 7.10 presents F_q values for a range of β and D/B values. Indian Standards specify β equal to 20° for cohesionless materials and β equal to 30° for firm cohesive materials, for pyramids, in connection with rectangular foundation.

7.3.7 Comparison of Different Theories :

The numerical values of F_c and F_q calculated for circular anchor by Circular Anchor Theory-1 (CIR-1) on comparison with

Vesic's (101) reported values for F_c and F_q are seen to agree with each other. Vesic has derived the circular plate breakout factors from the modifications in the solution of the problem of a point charge expanding into a spherical cavity close to the surface of a semi-infinite, homogeneous, isotropic solid possessing both cohesion and internal friction. The direct formulation used in CIR-1 and the Vesic's theory for circular plate anchor gives the same results.

Figure 7.16 gives values of F_q for two different values of ϕ equal to 30° and 45° for a range of D/B values. F_q versus D/B plot is made for theories, CIR-1 (Vesic), Balla, Meyerhof and Adams, Mariupol'skii, and Matsuo. The plot also shows the variation of F_q versus D/B by considering only the weight of an earth cone above the circular anchor contributing against uplift. Inclination of side of the conical frustum is taken as 20° . The model test results reported by Sutherland (95) for $\phi = 45^\circ$ and $\phi = 31^\circ$ are also superposed to get a comparative idea of predictions by different theories.

For $\phi = 0$ case,

$$F_u = \frac{CF_c + \gamma D(F_q - 1)}{C}$$

where F_u is the ultimate uplift capacity factor. Plot of F_u versus D/B for theories, CIR-1 (Vesic), Balla, Meyerhof and Adams, Mariupol'skii, Matsuo are made in Fig. 7.17. Theories in which $F_q = 1$, for $\phi = 0$, F_u is equal to F_c . For Balla's

that the breakout factors obtained are same. F_c decreases with increase in ϕ , for $\phi = 10^\circ$ to $\phi = 50^\circ$. $\phi = 0$, gives F_c values closer to $\phi = 10^\circ$ but numerically slightly smaller. D/B values appear to effect F_c more than angle of internal friction. Plot of breakout factor F_q versus D/B in Fig. 7.8 shows that F_q increases with ϕ . For $\phi = 0$, $F_q = 1$, irrespective of D/B ratio. Observation of magnitude of F_q factor for $\phi = 30^\circ$ and $\phi = 45^\circ$, shows that its variation is not considerable over this range of values of angle of internal friction. For $\phi = 0$, $F_q = 1$ for all D/B values and hence the ultimate uplift capacity factor (F_u) is a unique function of D/B and is numerically equal to the breakout factor F_c .

Results of Meyerhof and Adams (58) for strip anchor recomputed in the form of breakout factors show the following general trends (Table 7.3). The plots of F_c and F_q with D/B for all values of ϕ are linear as in the case of Strip Theory-1 and Strip Theory-2. The magnitude of F_c is dependent on D/B ratio only. F_c variation is independent of angle of internal friction. F_q increases with increase in both D/B ratio and ϕ value. For $\phi = 0$, $F_q = 1$, for all D/B values. Meyerhof and Adams's theory distinguishes shallow and deep anchor behaviour.

Rowe and Davis (83) derived the lower and upper bound solutions for the ultimate uplift load of a horizontal deeply embedded strip anchor at infinite depth in a purely cohesive

material. The lower bound on the bases of well known Prandtl's solution was obtained as $P_u = 10.28 \text{ CB}$ and the upper bound was obtained as $P_u = 11.42 \text{ CB}$.

For deep anchors in purely cohesive material, the limiting value of F_c by Meyerhof and Adams's theory (58) is equal to the bearing capacity factor N_c for deep foundations (55). The magnitude of N_c factors for deep strip foundation in clay ($\phi = 0$) are,

$$N_c = 2\pi + 2 = 8.28 \quad (C_a = 0)$$

$$N_c = \frac{5\pi}{2} + 1 = 8.85 \quad (C_a = C).$$

If $N_c = 8.28$ is considered as the limiting value of F_c for shallow anchors, then D/B ratio upto which the anchor can be considered as shallow is about 4. This is obtained on the assumption that the shaft friction is neglected.

Referring to the plot of F_q versus D/B in Fig. 7.9, it is clearly evident that for Strip Theory-1, Strip Theory-2 (Vesic) for a range of ϕ varying from 30° to 45° , F_q factor is not very much sensitive to ϕ values. Meyerhof and Adams's theory (58) shows a greater variation of F_q with ϕ . The F_q factors found from only considering the weight of earth trapezoid with $\beta = 20^\circ$, plots below F_q values for $\phi = 30^\circ$, calculated by all the other theories and hence gives a more conservative estimate of capacity than all the other three theories.

For $\phi = 45^\circ$, the Meyerhof and Adams's theory gives highest value of F_q and ST-2 (Vesic) the lowest. ST-1 results, plot in between but nearer to Meyerhof and Adams's theory. For $\phi = 30^\circ$, ST-1 shows highest value of F_q and ST-2 (Vesic) the least values. Meyerhof and Adams's theory plots nearer to ST-2 (Vesic) values. Strip Theory-1 (ST-1) which is derived on the assumption that the vertical component of the shearing resistance on the rupture surface contributes to soil resistance against uplift, gives higher values of F_q factors, than those obtained from Strip Theory-2 (ST-2), which is derived under the assumption that the vertical component of C and p contributes to the resistance against uplift.

Figure 7.10 shows a plot of F_u versus D/B in which ST-1, ST-2 (Vesic) and Meyerhof and Adams's theory are compared for $\phi = 0$ case. For the range of $\frac{C}{\gamma B}$ values used for the computation of F_u in ST-1, the uplift capacity factor F_u is maximum for ST-1. F_u is least for ST-2 (Vesic). The results of Rowe and Davis (83) and Meyerhof (58) for deep anchors are also shown in the figure for specifying the shallow anchor range of D/B .

7.4.2 Circular Anchor :

The breakout factors computed from Circular Anchor Theory-1 (CIR-1) shows that the direct formulation for circular plate anchor, starting from Kotter's equation employed and limited results reported by Vesic (101), give the same values. The plot

of F_c versus D/B is non-linear for all values of ϕ and plot of F_q versus D/B is non-linear for all values of $\phi > 0$. (Figs. 7.12 and 7.13). For $\phi = 0$, $F_q = 1$, for CIR-1. From Table 7.4 and Fig. 7.12, it is clear that for shallow anchor range of D/B , and ϕ values ranging from 20° to 50° , F_c values are not very much sensitive to changes in ϕ value. The variation of F_c with embedment ratio is more. F_q factor increases with ϕ and D/B .

The uplift capacity factors $F_1(\phi, \lambda)$, $F_2(\phi, \lambda)$ and $F_3(\phi, \lambda)$ reported by Balla (6) and the recomputed values of the above factors (Table 7.5) show that there are no numerical errors in the values reported by Balla as pointed out by Vesic (101). The results of Balla's theory is made more effective for comparison with other theories and calculation of uplift load as it is presented in Table 7.6 in the form of breakout factors F_c and F_q . The plot of F_c versus D/B is non-linear (Fig. 7.14) and F_c decreases with ϕ for ϕ ranging from 20° to 50° . F_q factor increases with ϕ as shown in Fig. 7.15.

A comparison of F_q factors reported in Tables 7.4 and 7.6 shows that Balla's theory, which is derived on the assumption that the vertical component of the shearing resistance on the rupture surface contributes to soil resistance against uplift gives higher values of F_q than given by CIR-1 (Vesic) which is derived on the basis that the vertical component of C and p contributes to the uplift resistance. So the uplift capacity of foundations for cohesionless soils, calculated on the basis

of Balla's theory for all values of D/B and ϕ are greater than those obtained by CIR-1 (Vesic).

The breakout factors from Meyerhof and Adams's theory (58) for shallow circular anchors (Table 7.7) show that F_c does not depend on ϕ . It is a function of D/B only. For $\phi = 0$, F_c values are limited to bearing capacity factor for deep foundation, N_c . Value of N_c as suggested by Meyerhof (55) are as follows,

$$N_c = 9.34 \quad (C_a = 0)$$

$$N_c = 9.74 \quad (C_a = C)$$

Assuming $N_c = 9.34$ to be valid, it can be seen (Fig. 7.17) that when embedment ratio reaches a value equal to approximately 2.3, the maximum value of F_c is reached. F_q factors from Meyerhof theory are more sensitive to changes in values of ϕ in the range of 30° to 45° . For $\phi = 0$, F_q is equal to unity.

Table 7.8 summarises the results of Mariupolskii's theory (51) for shallow anchors. It is seen that F_c and F_q increase with ϕ and D/B ratio. The breakout factors reported are for specific value of K' equal to 0.4 and neglecting $(\frac{B_0}{B})^2$ terms. The relationship between n and ϕ reported in the paper is used. The denominator, $(1 - 2n \frac{D}{B})$ in eqn. (7.72), for higher values of ϕ and D/B becomes very small and F_q factors work out to be very large.

The results based on Matsuo's theory (52), are condensed in the form of non-dimensional breakout factors F_c and F_q in Table 7.9. The theory as was presented originally needs seven factors to be read from graphs and used in the final equations [eqns. (7.76), (7.77) and (7.78)], to obtain the uplift load. Breakout factors F_c and F_q computed and reported herein make the computation of ultimate uplift calculation much simpler.

In Table 7.10, the F_q factors for earth cone with $\beta = 20^\circ$ are presented. Indian Standards (44) specify $\beta = 20^\circ$ for cohesionless soils. Variation of F_q with D/B is non-linear.

Referring to Fig. 7.16, in which a comparison of various circular anchor theories for cohesionless soils is done, the following observations can be made. The F_q factors for $\phi = 30^\circ$ and $\phi = 45^\circ$ computed from Balla's Theory do not show the scatter as obtained from experimental results of Sutherland (95). For $\phi = 30^\circ$ (loose sand), F_q values and hence uplift capacity predicted by this theory is higher than all the other theories, the results of which are presented in Fig. 7.16. The F_q factors for $\phi = 45^\circ$, plot below the experimental results by Sutherland as is evident from Fig. 7.16. The results from CIR-1 (Vesic) show that the F_q factors for $\phi = 30^\circ$ and $\phi = 45^\circ$ are less than the values predicted by Balla's theory for $\phi = 30^\circ$. This means that the capacity of circular anchor computed for cohesionless soil with $\phi = 45^\circ$ using CIR-1 (Vesic) will be less than the value using Balla's theory with $\phi = 30^\circ$. The plot of F_q versus

D/B for $\phi = 30^\circ$, is closer to the experimental curve of Sutherland (95). Matsuo's theory gives results of F_q for $\phi = 30^\circ$ and $\phi = 45^\circ$ which plot close to the curves from CIR-1 (Vesic) for the same angles of internal friction. F_q values computed from earth cone method for circular anchors plot close to the values of CIR-1 and Matsuo (52) for $\phi = 30^\circ$. Hence, use of this method for higher ϕ values may result in a conservative design.

F_c factors from theories CIR-1 (Vesic), Meyerhof and Adams (58), Mariupol'skii (51) and Matsuo (52) for $\phi = 0$ case are equal to the uplift capacity factor F_u as shown in Fig.

7.17. For Balla's theory (6) F_u is a function of D/B and $C/\gamma B$ and hence is different from F_c . Meyerhof and Adams's and Mariupol'skii's results give the same values of F_c and the values can be seen to be the lowest. F_u versus D/B plot (Fig. 7.17) shows that for both $\frac{C}{\gamma B} = 0.5$ and $\frac{C}{\gamma B} = 4.0$, the F_u values given by Balla's theory are greater than those given by other theories.

A comparison of anchor pull out results with theoretical prediction using CIR-1 (Vesic), Balla, Meyerhof and Adams, Mariupol'skii, Matsuo and Earth cone method is done in Table 7.11 and Table 7.12. Table 7.11, deals with laboratory small scale tests and Table 7.12, deals with results from large scale laboratory and field tests. The size of anchor and relevant details of soil are also given. This comparison is attempted

to check the reliability of prediction of uplift load by various theories.

Balla's results for $B = 9$ cms are calculated for $C = 0.49 \text{ KN/m}^2$ and $C = 0$ and tabulated in Table 7.11. Balla (6) has assumed a cohesion value for the soil arbitrarily as $\frac{1}{10}$ of the cohesion measured on the wet side for the material of his tests. The paper (6) also claims close agreement between theory and model test results. But the values of the uplift load with $C = 0.49 \text{ KN/m}^2$ and $C = 0$, on comparison clearly show that the results are close only because of the trace cohesion of 0.49 KN/m^2 assumed for sand. For sands whether an assumption of an arbitrary cohesion value like this can be made is a debatable point.

It is generally seen on comparison of predicted uplift load using various theories and the results of small scale laboratory and field tests that for ϕ values greater than 40° the theories underestimate the uplift load in the shallow anchor range. This will result in a conservative design, but on the safe side. The results also show that in the range of ϕ values nearer to 30° , some theories like Balla's, overestimate the uplift load for shallow anchors. In the overall sense for both low and high values of ϕ , the predictions from Meyerhof and Adams's (58) theory seems to fit the experimental observations better than other theories. The earth cone method (44) gives conservative estimate of uplift capacity especially in the shallow anchor range of D/B and for high values of angles of internal friction.

7.5 Conclusions :

7.5.1 Horizontal Strip Anchor :

i) By presenting results in the form of breakout factors, it is possible to compare theoretical prediction by different theories and also use the results easily for computation of the uplift capacity. The variation of the breakout factors F_c and F_q with embedment ratio for Strip Theory-1, Strip Theory-2 (Vesic) and also Meyerhof and Adams's theory is linear.

ii) The theory for cohesionless soil derived on the assumption that the vertical component of the shearing resistance on the rupture surface contributes to the soil resistance against uplift (ST-1), gives higher breakout loads than the theory (ST-2), which is derived under the assumption that the vertical component of the resultant of shearing resistance and normal force on the rupture surface (p) contributes to the soil resistance against uplift.

iii) The ultimate uplift capacity factor, F_u for $\phi = 0$ case, is a unique function of D/B for Strip Theory-2 (Vesic) and Meyerhof and Adams's theory. For Strip Theory-1, F_u is a function of $\frac{C}{\gamma B}$ and D/B .

iv) Meyerhof and Adams's theory for shallow strip anchor shows a greater spread of F_q factors for $\phi = 30^\circ$ and $\phi = 45^\circ$ in a plot of F_q versus D/B ratio. The results of ST-1 and

ST-2 (Vesic) show a lack of sensitiveness in prediction of F_q factor and hence uplift load due to variation of ϕ for sands in the range of 30° to 45° .

v) The direct formulation used in ST-2 and Vesic's derivation for strip plate from the modification of the solution of the problem of a linear charge expanding a cylindrical cavity of infinite length, closer to the surface gives the same breakout factors.

7.5.2 Circular Anchor :

i) Presentation of anchor pullout resistance in the form of circular anchor breakout factors make the estimation of uplift load straight forward and gives a common base for comparison of results from different theories.

ii) For cohesionless soil, Balla's theory (6) derived on the assumption that the vertical component of the shearing resistance on the rupture surface contributes to the soil resistance against uplift, gives higher values of breakout loads than predicted by theory CIR-1, which is derived on the assumption that the vertical component of the resultant of shearing resistance and normal force on the rupture surface contributes to the soil resistance against uplift load.

iii) The results of direct formulation done for circular anchor in theory CIR-1 and the Vesic's theory (101), for circular plate anchor which is based on the modification of the solution of a

problem of a point charge expanding into a spherical cavity close to the surface of a semi-infinite, homogeneous isotropic solid possessing both cohesion and internal friction, gives the same breakout factors.

iv) The numerical values of the uplift capacity factors reported by Balla (6) in his paper do not contain any numerical errors.

v) Results from CIR-1 (Vesic) and Balla's theory shows a lack of sensitiveness in uplift loads for cohesionless soils in the range of ϕ from 30° to 45° which is not in conformity with experimentally observed facts by Sutherland (95).

vi) The ultimate uplift capacity factor, F_u plots as a function of D/B only for theories like, CIR-1 (Vesic), Meyerhof and Adams, Mariupol'skii and Matsuo. For Balla's theory F_u is a function of D/B and $C/\gamma B$.

vii) Earth cone method with $\beta = 20^\circ$, as recommended by Indian Standards (44) for cohesionless soils gives the ultimate load on the conservative side for shallow circular anchors in sand, especially for high values of ϕ .

viii) A comparison of experimental results from laboratory, field and theoretical predictions show the results from Meyerhof and Adams's theory (58) is closer to the experimentally obtained values, when the full range of values of angle of internal friction and cohesion are considered.

Table 7.1

Breakout factors for strip plate anchor - F_c and F_q for ST-1

ϕ	D/B								
	0.5	1.0	1.5	2.0	2.5	3.0	4.0	5.0	10.00
0°	1.00	2.00	3.00	4.00	5.00	6.00	8.00	10.00	20.00
	1.13	1.26	1.39	1.52	1.64	1.77	2.03	2.29	3.58
10°	1.00	2.00	2.99	3.99	4.99	5.99	7.99	9.99	19.99
	1.23	1.46	1.69	1.91	2.14	3.37	2.83	3.29	5.57
20°	0.94	1.87	2.81	3.75	4.68	5.62	7.49	9.37	18.73
	1.32	1.64	1.96	2.27	2.59	2.91	3.55	4.18	7.37
25°	0.88	1.77	2.65	3.53	4.42	5.30	7.06	8.83	17.66
	1.36	1.71	2.07	2.42	2.78	3.14	3.85	4.56	8.12
30°	0.82	1.63	2.45	3.26	4.08	4.89	6.53	8.16	16.31
	1.39	1.77	2.16	2.55	2.93	3.32	4.09	4.87	8.74
35°	0.74	1.47	2.21	2.95	3.68	4.42	5.89	7.37	14.73
	1.41	1.82	2.23	2.64	3.05	3.46	4.28	5.10	9.21
40°	0.65	1.30	1.95	2.59	3.24	3.89	5.19	6.49	12.97
	1.43	1.85	2.28	2.70	3.13	3.55	4.40	5.25	9.51
45°	0.55	1.11	1.66	2.22	2.77	3.33	4.43	5.54	11.08
	1.43	1.86	2.30	2.73	3.16	3.59	4.45	5.32	9.63
50°	0.46	0.91	1.37	1.83	2.29	2.74	3.66	4.57	9.14
	1.43	1.86	2.29	2.71	3.14	3.57	4.43	5.29	9.57

First Number : F_c $p_u = CF_c + \gamma D F_q$ Second Number : F_q $P_u = B p_u$
 $V_f = W_f + P_u$

Table 7.2

Breakout factors for strip plate anchor - F_c and F_q for ST-2

ϕ	0.5	1.0	1.5	2.0	D/B 2.5	3.0	4.0	5.0	10.0
0°	0.81	1.61	2.42	3.23	4.04	4.84	6.46	8.07	16.15
	1.00	1.00	1.00	1.00	1.00	1.00	1.00	1.00	1.00
10°	0.84	1.69	2.53	3.37	4.22	5.06	6.74	8.43	16.86
	1.08	1.17	1.25	1.33	1.42	1.50	1.66	1.83	2.66
20°	0.84	1.68	2.51	3.35	4.19	5.02	6.70	8.37	16.75
	1.17	1.32	1.50	1.66	1.83	1.99	2.32	2.65	4.30
25°	0.82	1.64	2.46	3.27	4.09	4.91	6.55	8.18	16.37
	1.20	1.41	1.61	1.81	2.01	2.22	2.62	3.03	5.06
30°	0.79	1.58	2.37	3.16	3.95	4.73	6.31	7.89	15.78
	1.24	1.47	1.71	1.95	2.19	2.42	2.90	3.37	5.74
35°	0.75	1.50	2.25	3.00	3.75	4.50	6.00	7.50	15.00
	1.27	1.53	1.80	2.07	2.33	2.60	3.13	3.67	6.33
40°	0.70	1.40	2.11	2.81	3.51	4.21	5.60	7.02	14.00
	1.29	1.58	1.87	2.16	2.45	2.75	3.33	3.91	6.82
45°	0.65	1.29	1.94	2.58	3.23	3.88	5.17	6.46	12.92
	1.31	1.62	1.93	2.24	2.55	2.85	3.47	4.09	7.18
50°	0.58	1.17	1.75	2.34	2.92	3.50	4.67	5.84	11.68
	1.32	1.64	1.96	2.28	2.60	2.92	3.56	4.20	7.41

First Number : F_c Second -Number: F_q

$$p_u = CF_c + \gamma D F_q$$

$$P_u = B p_u$$

$$V_f = W_f + P_u$$

Table 7.3

Breakout factors for strip plate anchor - F_c and F_q for
Meyerhof and Adams's theory(58)

ϕ	D/B								
	0.5	1.0	1.5	2.0	2.5	3.0	4.0	5.0	10.0
0°	1.00	2.00	3.00	4.00	5.00	6.00	8.00	10.00	20.00
	1.00	1.00	1.00	1.00	1.00	1.00	1.00	1.00	1.00
20°	1.00	2.00	3.00	4.00	5.00	6.00	8.00	10.00	20.00
	1.17	1.35	1.52	1.69	1.86	2.04	2.38	2.73	4.46
25°	1.00	2.00	3.00	4.00	5.00	6.00	8.00	10.00	20.00
	1.22	1.44	1.66	1.89	2.11	2.33	2.77	3.31	5.43
30°	1.00	2.00	3.00	4.00	5.00	6.00	8.00	10.00	20.00
	1.27	1.55	1.82	2.10	2.37	2.65	3.19	3.74	6.49
35°	1.00	2.00	3.00	4.00	5.00	6.00	8.00	10.00	20.00
	1.33	1.67	2.00	2.83	2.66	3.00	3.66	4.33	7.75
40°	1.00	2.00	3.00	4.00	5.00	6.00	8.00	10.00	20.00
	1.40	1.80	2.20	2.59	2.99	3.39	4.19	4.99	8.97
45°	1.00	2.00	3.00	4.00	5.00	6.00	8.00	10.00	20.00
	1.48	1.95	2.43	2.90	3.38	3.85	4.80	5.75	10.50
50°	1.00	2.00	3.00	4.00	5.00	6.00	8.00	10.00	20.00
	1.57	2.13	2.70	3.26	3.83	4.40	5.53	6.66	12.32

First Number : F_c $p_u = CF_c + \gamma D F_q$

Second Number : F_q $P_u = B p_u$

$$V_f = W_f + P_u$$

For $\phi = 0$, F_c is limited to N_c value equal to 9.

For C, ϕ soils, the values for F_q given, are only valid upto a certain critical value of D/B presented in Table 2.1.

Table 7.4

Breakout factors for circular plate anchor F_c and F_q for CIR-1

ϕ	D/B								
	0.5	1.0	1.5	2.0	2.5	3.0	4.0	5.0	10.0
0°	1.76	3.80	6.12	8.72	11.61	14.79	21.98	30.32	89.00
	1.00	1.00	1.00	1.00	1.00	1.00	1.00	1.00	1.00
10°	1.87	4.10	6.69	9.64	12.96	16.63	25.08	34.97	106.10
	1.18	1.37	1.59	1.83	2.08	2.36	2.98	3.67	8.36
20°	1.90	4.23	7.01	10.24	13.90	18.01	27.55	38.86	122.00
	1.35	1.76	2.21	2.71	3.25	3.85	5.18	6.70	17.21
25°	1.88	4.24	7.07	10.39	14.19	18.47	28.50	40.40	128.80
	1.44	1.94	2.51	3.14	3.84	4.60	6.32	8.29	22.06
30°	1.84	4.19	7.06	10.44	14.34	18.76	29.14	41.58	134.80
	1.52	2.11	2.80	3.56	4.41	5.34	7.45	9.90	27.10
35°	1.77	4.09	6.96	10.38	14.34	18.85	29.51	42.36	139.40
	1.59	2.27	3.06	3.96	4.95	6.05	8.56	11.58	32.24
40°	1.69	3.95	6.78	10.11	14.17	18.73	29.55	42.66	142.60
	1.64	2.41	3.30	4.32	5.45	6.72	9.61	13.00	37.35
45°	1.59	3.76	6.53	9.89	13.83	18.37	29.21	42.42	143.80
	1.69	2.53	3.51	4.63	5.90	7.31	10.58	14.42	42.32
50°	1.47	3.53	6.19	9.45	13.31	17.76	28.46	41.55	142.80
	1.72	2.61	3.67	4.89	6.28	9.83	11.43	15.70	46.98

First Number : F_c Second Number : F_q

$$P_u = CF_c + \gamma D F_q$$

$$P_u = \pi/4 B^2 p_u$$

$$V_f = W_f + P_u$$

Table 7.5

Uplift capacity factors $F_1(\phi, \lambda)$, $F_2(\phi, \lambda)$ and $F_3(\phi, \lambda)$
for circular plate anchor - Balla's Theory (6)

		D/B = 1		D/B = 2		D/B = 3		D/B = 4	
		B*	C*	B*	C*	B*	C*	B*	C*
0°	F ₁	1.29	1.29	0.50	0.50	0.32	0.32	0.25	0.25
	F ₂	3.96	3.95	2.39	2.38	1.86	1.86	1.60	1.60
	F ₃	0.00	0.00	0.00	0.00	0.00	0.00	0.00	0.00
10°	F ₁	1.35	1.35	0.54	0.54	0.36	0.36	0.29	0.28
	F ₂	4.07	4.11	2.50	2.50	1.98	2.01	1.71	1.75
	F ₃	0.30	0.31	0.17	0.18	0.12	0.13	0.10	0.11
20°	F ₁	1.41	1.42	0.58	0.59	0.40	0.40	0.33	0.32
	F ₂	4.06	4.03	2.53	2.56	2.09	2.07	1.84	1.82
	F ₃	0.59	0.60	0.33	0.34	0.25	0.26	0.21	0.22
30°	F ₁	1.47	1.48	0.62	0.63	0.44	0.43	0.37	0.36
	F ₂	3.70	3.71	2.42	2.43	2.00	2.00	1.78	1.79
	F ₃	0.83	0.83	0.48	0.48	0.36	0.37	0.31	0.31
40°	F ₁	1.53	1.55	0.66	0.68	0.48	0.47	0.41	0.39
	F ₂	3.13	3.16	2.12	2.14	1.78	1.80	1.61	1.63
	F ₃	0.94	0.95	0.56	0.57	0.43	0.44	0.37	0.37

B* : The values presented in Balla's paper (6)

C* : Recomputed values of the factors

$$P_u = \gamma D^3 \left(F_1 + \frac{C}{\gamma D} F_2 + F_3 \right)$$

Table 7.6

Breakout factors for circular plate anchor - F_c and F_q for
Balla's Theory (6)

ϕ	D/B								
	0.5	1.0	1.5	2.0	2.5	3.0	4.0	5.0	10.0
0°	2.26	5.03	8.32	12.12	16.44	21.28	32.49	45.77	143.11
	1.29	1.64	2.05	2.53	3.06	3.66	5.05	6.68	18.55
10°	2.31	5.23	8.76	12.91	17.68	23.06	35.67	50.73	162.90
	1.51	2.12	2.83	3.64	4.55	5.57	7.91	10.65	30.46
20°	2.22	5.13	8.73	13.02	18.01	23.68	37.11	53.29	175.70
	1.71	2.57	3.57	4.73	6.03	7.48	10.81	14.74	43.24
25°	2.12	4.96	8.52	12.79	17.78	23.48	37.04	53.46	178.50
	1.80	1.77	3.91	5.22	6.71	8.36	12.19	16.71	49.61
30°	1.99	4.72	8.18	12.36	17.27	22.92	36.39	52.78	178.50
	1.87	2.94	4.20	5.67	7.32	9.17	13.47	18.55	55.72
35°	1.84	4.41	7.70	11.73	16.49	21.97	35.13	51.21	175.40
	1.93	3.08	4.45	6.04	7.85	9.88	14.60	20.20	61.39
40°	1.65	4.02	7.11	10.91	15.42	20.65	33.25	48.71	168.90
	1.97	3.19	4.64	6.34	8.28	10.46	15.55	21.61	66.41
45°	1.45	3.59	6.40	9.90	14.09	18.96	30.75	45.28	158.90
	1.99	3.25	4.77	6.55	8.59	10.89	16.27	22.71	70.58
50°	1.23	3.10	5.61	8.75	12.52	16.93	27.67	40.94	145.50
	2.00	3.27	4.82	6.65	8.75	11.14	16.74	23.45	73.67

First Number : F_c

$$P_u = CF_c + \gamma D F_q$$

Second Number : F_q

$$P_u = \pi/4 B^2 p_u$$

$$V_f = W_f + P_u$$

Table 7.7

Breakout factors for circular plate anchor - F_c and F_q for
Meyerhof and Adams's Theory(58)

ϕ	D/B								
	0.5	1.0	2.0	3.0	4.0	5.0	6.0	7.0	8.0
0°	2.00	4.00	8.00	12.00	16.00	20.00	24.00	28.00	32.00
	1.00	1.00	1.00	1.00	1.00	1.00	1.00	1.00	1.00
30°	2.00	4.00	8.00	12.00	16.00				
	1.61	2.30	3.89	5.76	7.93				
35°	2.00	4.00	8.00	12.00	16.00	20.00			
	1.78	2.74	5.15	8.23	11.98	16.40			
40°	2.00	4.00	8.00	12.00	16.00	20.00	24.00		
	1.99	3.27	6.73	11.38	17.21	24.24	32.45		
42°	2.00	4.00	8.00	12.00	16.00	20.00	24.00	28.00	
	2.07	3.47	7.29	12.44	18.94	26.77	35.94	46.60	
45°	2.00	4.00	8.00	12.00	16.00	20.00	24.00	28.00	32.00
	2.24	3.94	8.78	15.50	24.11	34.61	46.99	61.28	77.45

First Number : F_c

$$p_u = CF_c + \gamma D F_q$$

Second Number : F_q

$$P_u = \pi/4 B^2 p_u$$

$$V_f = W_f + P_u$$

For $\phi = 0$, F_c value should be limited to the bearing capacity factor N_c for deep footings (55).

$$F_q = [2(sK_u) \frac{D}{B} \tan \phi + 1]$$

' sK_u ' values are taken from graphs given in Ref. 58 and may not be very accurate as they are read from the graph.

Table 7.8

Breakout factors for circular plate anchor - F_c and F_q for
Mariupol'skii's Theory (51)

ϕ	D/B								
	0.5	1.0	1.5	2.0	2.5	3.0	4.0	5.0	10.0
0°	2.00	4.00	6.00	8.00	10.00	12.00	16.00	20.00	40.00
	1.00	1.00	1.00	1.00	1.00	1.00	1.00	1.00	1.00
10°	2.05	4.21	6.49	8.89	11.43	14.12	20.00	26.67	80.00
	1.10	1.20	1.31	1.42	1.55	1.67	1.96	2.27	4.82
20°	2.11	4.44	7.06	10.00	13.33	17.14	26.67	40.00	-
	1.21	1.43	1.69	1.98	2.30	2.68	3.61	4.91	-
25°	2.13	4.57	7.38	10.67	14.55	19.20	32.00	53.33	-
	1.27	1.57	1.92	2.33	2.81	3.39	4.98	7.64	-
30°	2.16	4.71	7.74	11.43	16.00	21.82	40.00	80.00	-
	1.33	1.72	2.18	2.75	3.45	4.34	7.12	13.24	-
35°	2.19	4.85	8.14	12.31	17.78	25.26	53.33	160.00	-
	1.40	1.89	2.49	3.26	4.27	5.64	10.80	30.41	-
40°	2.22	5.00	8.57	13.33	20.00	30.00	80.00	-	-
	1.48	2.09	2.87	3.90	5.36	7.53	13.43	-	-
45°	2.25	5.16	9.06	14.55	22.86	36.92	160.00	-	-
	1.58	2.32	3.32	4.73	6.86	10.46	42.00	-	-
50°	2.29	5.33	9.60	16.00	26.67	48.00	-	-	-
	1.69	2.60	3.89	5.81	9.02	15.44	-	-	-

First Number : F_c

Second Number : F_q

$$P_u = CF_c + \gamma D F_q$$

$$P_u = \pi/4 B^2 p_u$$

$$V_f = W_f + P_u$$

Table 7.9
Breakout factors for circular plate anchor - F_c and F_q for
Matsuo's Theory (52)

ϕ	D/B								
	0.5	1.0	1.5	2.0	2.5	3.0	4.0	5.0	10.0
0°	2.18	4.72	7.62	10.88	14.50	18.48	27.51	37.99	111.94
	1.00	1.00	1.00	1.00	1.00	1.00	1.00	1.01	1.03
10°	2.27	5.07	8.40	12.26	16.66	21.59	33.06	46.65	146.61
	1.15	1.31	1.47	1.64	1.82	2.00	2.38	2.79	5.22
20°	2.35	5.41	9.17	13.64	18.81	24.68	38.55	55.23	180.93
	1.31	1.64	2.00	2.40	2.82	3.26	4.24	5.33	12.49
25°	2.39	5.58	9.55	14.31	19.87	26.21	41.27	59.48	197.92
	1.39	1.82	2.30	2.82	3.39	4.01	5.38	6.93	17.41
30°	2.44	5.75	9.93	14.99	20.92	27.72	43.95	63.67	214.69
	1.47	2.01	2.62	3.29	4.03	4.84	6.66	8.75	23.26
35°	2.48	5.91	10.30	15.64	21.94	29.20	46.58	67.78	231.11
	1.56	2.20	2.95	3.79	4.72	5.75	8.09	10.81	30.10
40°	2.52	6.07	10.66	16.28	22.94	30.63	49.12	71.74	246.98
	1.64	2.41	3.30	4.32	5.47	6.74	9.67	13.11	37.90
45°	2.55	6.22	10.99	16.88	23.87	31.98	51.51	75.49	261.96
	1.72	2.61	3.66	4.88	6.25	7.80	11.37	15.60	46.58
50°	2.59	6.36	11.30	17.42	24.73	33.21	53.70	78.90	275.62
	1.80	2.81	4.02	5.42	7.06	8.89	13.15	18.24	55.92

First Number : F_c

$$p_u = CF_c + \gamma D F_q$$

Second Number : F_q

$$P_u = \pi/4 B^2 p_u$$

$$V_f = W_f + P_u$$

Table 7.10

Breakout factors for circular plate anchor - F_q for Earth Cone
Method (44)

R	D/B								
	0.5	1.0	1.5	2.0	2.5	3.0	4.0	5.0	10.0
0°	1.00	1.00	1.00	1.00	1.00	1.00	1.00	1.00	1.00
10°	1.19	1.39	1.62	1.87	2.14	2.43	3.07	3.80	8.67
20°	1.41	1.91	2.49	3.16	3.92	4.77	6.74	9.06	25.94
30°	1.69	2.60	3.73	5.09	6.66	8.46	12.73	17.89	56.99
40°	2.07	3.62	5.63	8.11	11.06	14.48	22.73	37.36	111.66

$$p_u = \gamma D F_q$$

$$P_u = \pi/4 B^2 p_u$$

$$V_f = W_f + P_u$$

Table 7.11
Comparison of circular anchor pull-out results with theory -
Small scale laboratory tests

Investigator and details	B (cm)	D (cm)	D/B	Expt (N)	Predicted ultimate uplift load in N					
					A*	B*	C*	D*	E*	F*
Adams and Hayes (1) dense silica sand $\phi = 34^\circ$ $\gamma = 16.69 \text{ KN/m}^3$	11.48	5.08	0.44	16.9	12.1	14.8	13.5	11.7	11.8	11.9
	11.48	10.16	0.89	53.3	36.4	48.6	42.7	30.4	35.3	31.2
	11.48	15.24	1.33	111.1	77.3	103.4	89.3	58.4	69.2	60.1
	11.48	20.32	1.77	206.6	120.5	181.2	153.8	98.2	115.1	99.8
Balla (6)** air dry sand $C=0.49 \text{ KN/m}^2$ $\phi = 37^\circ$ $\gamma=16.68 \text{ KN/m}^3$	9.00	4.00	0.44	16.7	10.8	12.13	12.4	11.8	12.7	5.7
					6.0	7.3	6.9	5.8	5.9	
	9.00	9.00	1.00	50.0	34.9	43.2	36.1	34.0	40.4	18.2
					22.3	29.9	23.6	18.7	21.8	
	9.00	14.00	1.55	103.0	70.9	94.2	86.2	67.3	81.4	37.9
					48.3	69.7	66.9	40.2	47.2	
	9.00	19.00	2.11	191.3	122.3	171.5	151.1	118.0	139.1	67.0
					87.4	132.7	124.8	74.9	85.1	
	9.00	24.00	2.67	309.0	190.9	278.7	243.8	196.7	217.2	107.0
					141.5	222.8	210.5	130.9	137.4	
	9.00	29.00	3.22	397.3	277.5	418.5	398.8	322.5	309.8	159.3
					211.9	343.1	358.7	223.2	205.5	
12.00	6.00	19.00	3.16	147.2	88.6	129.9	109.1	83.0	103.4	45.4
					60.3	97.4	91.6	40.9	58.5	
	12.00	19.00	1.58	220.7	159.8	216.4	176.0	148.2	175.4	92.8
					118.7	171.7	164.7	98.7	115.8	

333

contd...

Investigator and details	B (cm)	D (cm)	D/B	Expt (N)	Predicted ultimate uplift load in N					
					A*	B*	C*	D*	E*	F*
Baker and Kondner (5) air dry uni- form silica sand $\phi = 42^\circ$ $\gamma = 17.62 \text{ kN/m}^3$	7.62	7.62	1.0	24.4	15.1	19.7	21.3	13.3	15.2	14.9
	7.62	15.24	2.0	79.6	54.5	78.8	89.2	51.5	55.6	38.7
	7.62	22.86	3.0	220.4	127.9	195.6	228.5	156.9	131.5	87.6
	7.62	30.48	4.0	423.5	245.2	388.7	463.9	593.9	253.2	165.1
	7.62	38.10	5.0	744.8	415.8	676.3	819.6	-	431.2	277.4
	7.62	45.72	6.0	1197.0	649.5	1076.8	1320.4	-	675.6	430.9
	7.62	53.34	7.0	1724.6	967.6	1630.0	1997.3	-	1030.6	632.3
Clemence and Veesaert (15) uniformly graded dry sand $\phi = 41^\circ$ $\gamma = 16.66 \text{ kN/m}^3$	7.62	22.36	3.0	258.1	118.8	183.4	206.8	141.4	120.7	82.8
	7.62	30.48	4.0	479.1	277.2	363.8	418.6	443.4	231.6	156.1
	7.62	38.10	5.0	903.4	384.7	632.5	738.2	-	393.4	262.3
	7.62	45.72	6.0	1468.5	600.2	1006.7	1187.7	-	615.4	407.4
	7.62	53.34	7.0	2376.3	893.2	1523.0	-	-	917.6	597.9
	12.70	12.70	1.0	89.0	65.3	85.8	90.4	57.3	65.4	51.2
	12.70	25.40	2.0	378.3	234.9	342.4	375.7	218.0	237.4	169.4
	12.70	38.10	3.0	1032.4	550.1	849.1	957.6	652.6	558.8	383.5

contd.....

Investigator and details	B (cm)	D (cm)	D/B	Expt (N)	Predicted ultimate uplift load in N					
					A*	B*	C*	D*	E*	F*
Esquivel	7.62	11.43	1.5	17.8	20.4	29.7	26.3	16.61	19.7	16.61
Diaz (28)	7.62	22.86	3.0	61.8	80.7	131.9	110.5	75.26	76.7	63.64
loose sand	7.62	34.29	4.5	100.0	200.0	348.3	284.0	412.40	189.1	158.10
$\phi = 35^\circ$	7.62	45.72	6.0	132.0	395.2	712.0	-	-	371.2	286.30
$\gamma = 12.80 \text{ kN/m}^3$	7.62	74.68	9.8	269.3	1405.3	2675.6	-	-	1311.6	1094.10
Esquivel	7.62	11.43	1.5	60.4	26.7	36.8	44.5	24.50	27.4	19.40
Diaz (28)	7.62	22.86	3.0	275.2	110.5	167.5	209.9	144.80	114.9	74.40
dense sand	7.62	34.29	4.5	761.1	281.3	448.2	585.4	-	295.3	184.70
$\phi = 43^\circ$	7.62	45.72	6.0	1599.8	563.6	923.9	1235.9	-	595.1	365.80
$\gamma = 14.96 \text{ kN/m}^3$	7.62	60.96	8.0	3261.8	1170.0	1966.6	-	-	1241.8	753.90
	7.62	74.68	9.8	4424.6	2056.2	3516.9	-	-	2190.7	1278.80

contd....

Investigator and details	B (cm)	D (cm)	D/B	Expt (N)	Predicted ultimate uplift load in N					
					A*	B*	C*	D*	E*	F*
Sutherland*** (95) dense sand $\phi = 45^\circ$	3.81	-	1.0	4.8	2.5	3.3	3.9	2.3	2.6	1.91
	to	-	2.0	10.1	4.6	6.6	8.8	4.7	4.9	3.20
	15.24	-	3.0	19.3	7.3	10.9	15.5	10.5	7.8	4.80
		-	4.0	29.8	10.6	16.3	24.1	42.0	11.4	6.70
		-	5.0	36.9	14.4	22.7	34.6	-	15.6	9.10
Sutherland (95) $\phi = 31^\circ$	3.81	-	1.0	2.5	2.2	3.0	2.4	1.8	2.1	1.90
	to	-	2.0	3.8	3.6	5.8	4.1	2.9	3.4	3.20
	15.24	-	3.0	5.4	5.5	9.3	6.3	4.6	5.0	4.80
		-	4.0	7.7	7.7	13.7	8.7	7.9	6.9	6.70
		-	5.0	11.0	10.2	18.9	-	16.7	9.1	9.10

** two predicted values are given, the first one for $C = 0.49 \text{ kN/m}^2$ and second for $C = 0.0$

*** experimental F_q factors and predicted F_q values are tabulated.

A* - CIR-1 (Vesic) B* - Balla C* - Meyerhof and Adams

D* - Mariupol'skii E* - Matsuo F* - Earth cone

Comparison of anchor pull-out results with theory - Large scale tests in laboratory and field

Investigator and details	B (m)	D (m)	D/B	Expt (KN)	Predicted ultimate uplift load in KN				
					A*	B*	C*	D*	F*
Brown Boveri from Balla(6) sand $\phi = 36^\circ$ $\gamma = 19.13 \text{ KN/m}^3$	1.90 1.90	1.50 1.45	0.79 0.76	203.1 204.1	162.3 153.4	210.9 196.2	172.4 160.3	138.4 131.4	167.3 152.3
Felitz $\gamma = 16.28$ from $\gamma = 13.05$ Balla $\gamma = 15.70$ (6) $\phi = 30^\circ$	1.30 1.10 1.40	2.50 2.70 2.50	1.92 2.45 1.79	201.1 240.3 229.6	171.7 144.8 195.2	293.0 239.6 204.0	203.3 158.4 213.8	143.2 112.9 150.9	171.6 132.5 181.2
Sutherland(95) sand $\phi = 42^\circ$ $\gamma = 10.38 \text{ KN/m}^3$ (effective)	2.39 2.39 2.39	2.44 4.58 5.19	1.02 1.91 2.17	447.9 1791.8 2518.5	283.6 906.6 1172.8	371.9 1303.1 1717.8	403.0 1481.6 1973.6	250.8 845.9 1137.8	286.8 924.6 1199.0
sand $\phi = 35^\circ$ $\gamma = 10.38 \text{ KN/m}^3$	2.39 2.39	6.41 7.02	2.68 2.94	2309.4 2866.9	1585.7 1935.1	2562.0 3150.9	2162.6 2630.1	1405.9 1782.0	1520.0 1839.8
Kananyan(46) $C = 4.91 \text{ KN/m}^2$ $\phi = 32^\circ$ $\gamma = 15.99 \text{ KN/m}^3$	0.40 0.60 0.80 1.00 1.20	1.00 1.00 1.00 1.00 1.00	2.50 1.67 1.25 1.00 0.82	19.6 25.1 33.6 41.3 50.1	18.2 25.7 34.0 43.4 53.3	25.6 34.7 44.5 55.4 66.5	17.4 26.2 36.1 49.8 57.8	17.8 24.0 31.8 37.7 50.3	21.8 29.8 38.7 48.6 58.9
A* - CIR-1 (Vesic)		B* - Balla	C* - Meyerhof and Adams						
D* - Mariupol'skii		E* - Matsuo	F* - Earth cone						

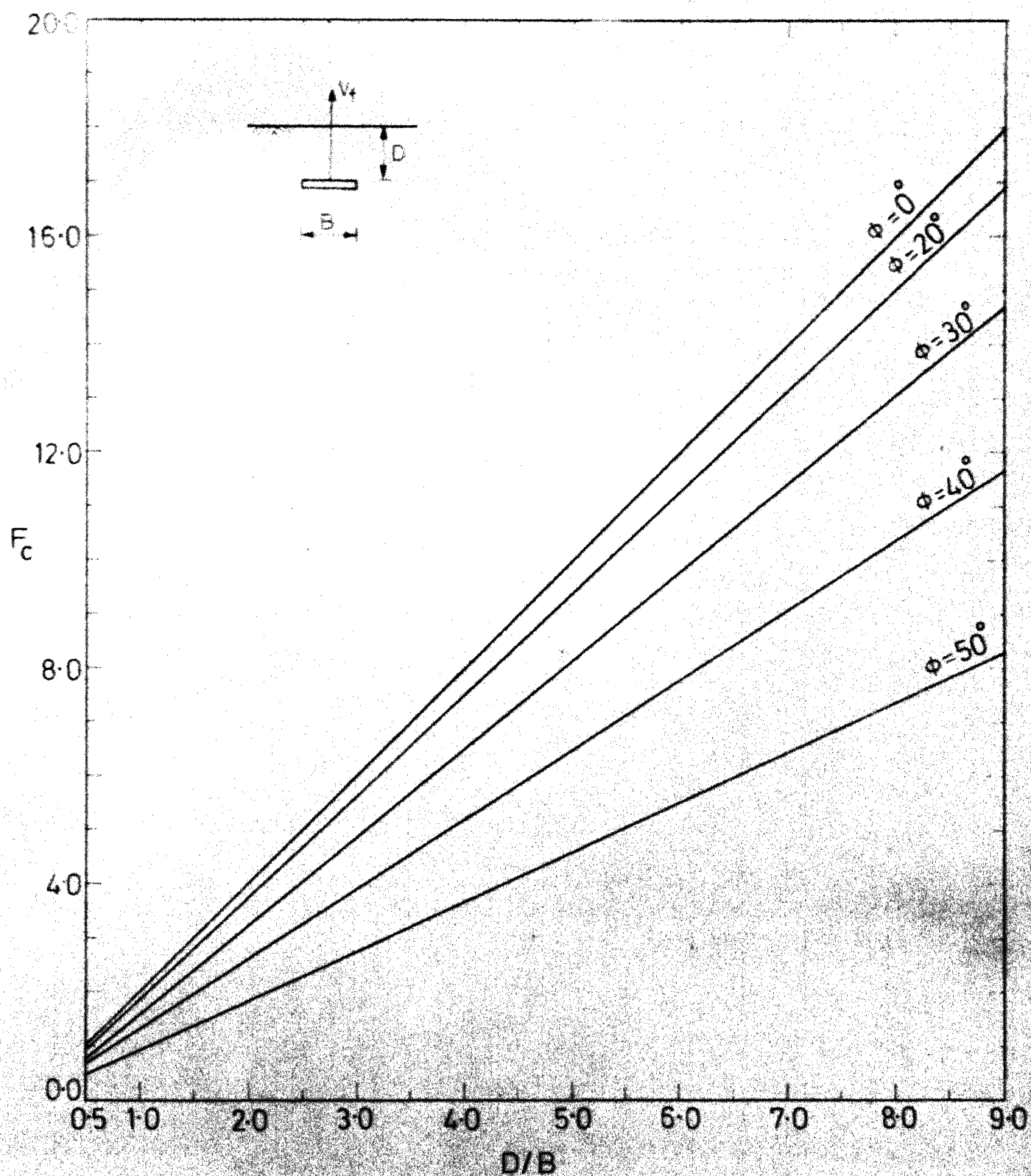


FIG.7-5 BREAKOUT FACTORS FOR HORIZONTAL STRIP, F_c FOR ST-1

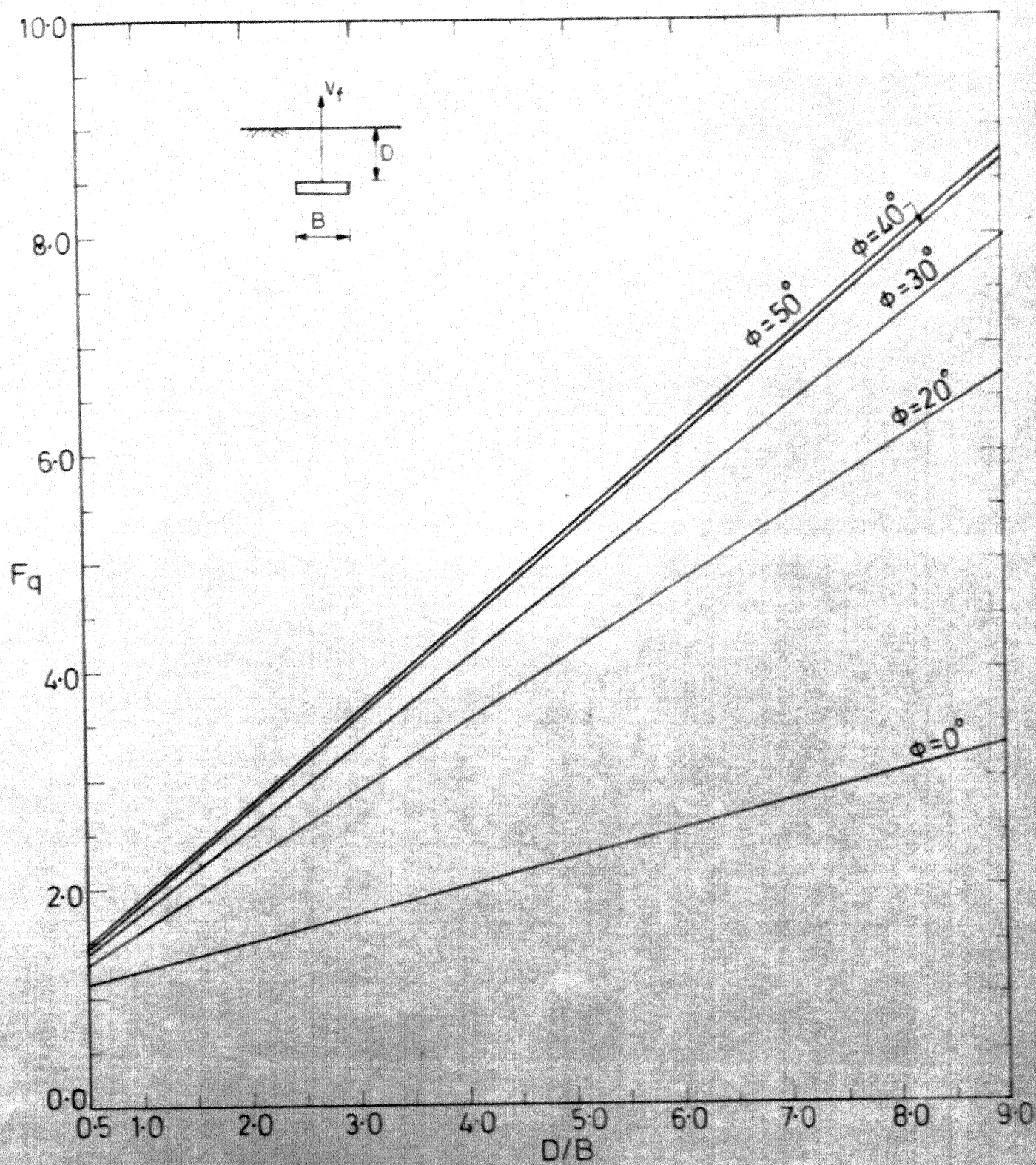
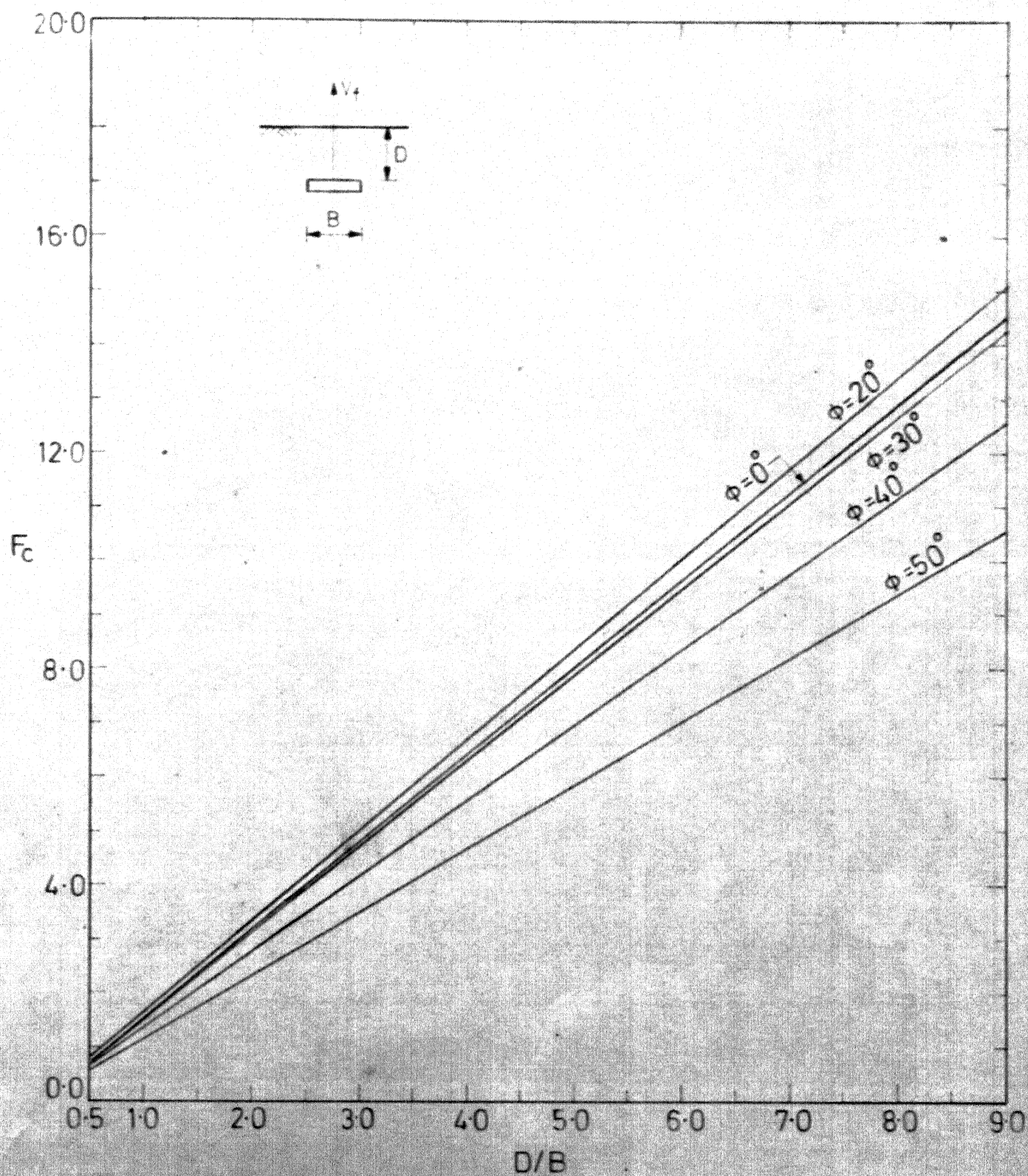
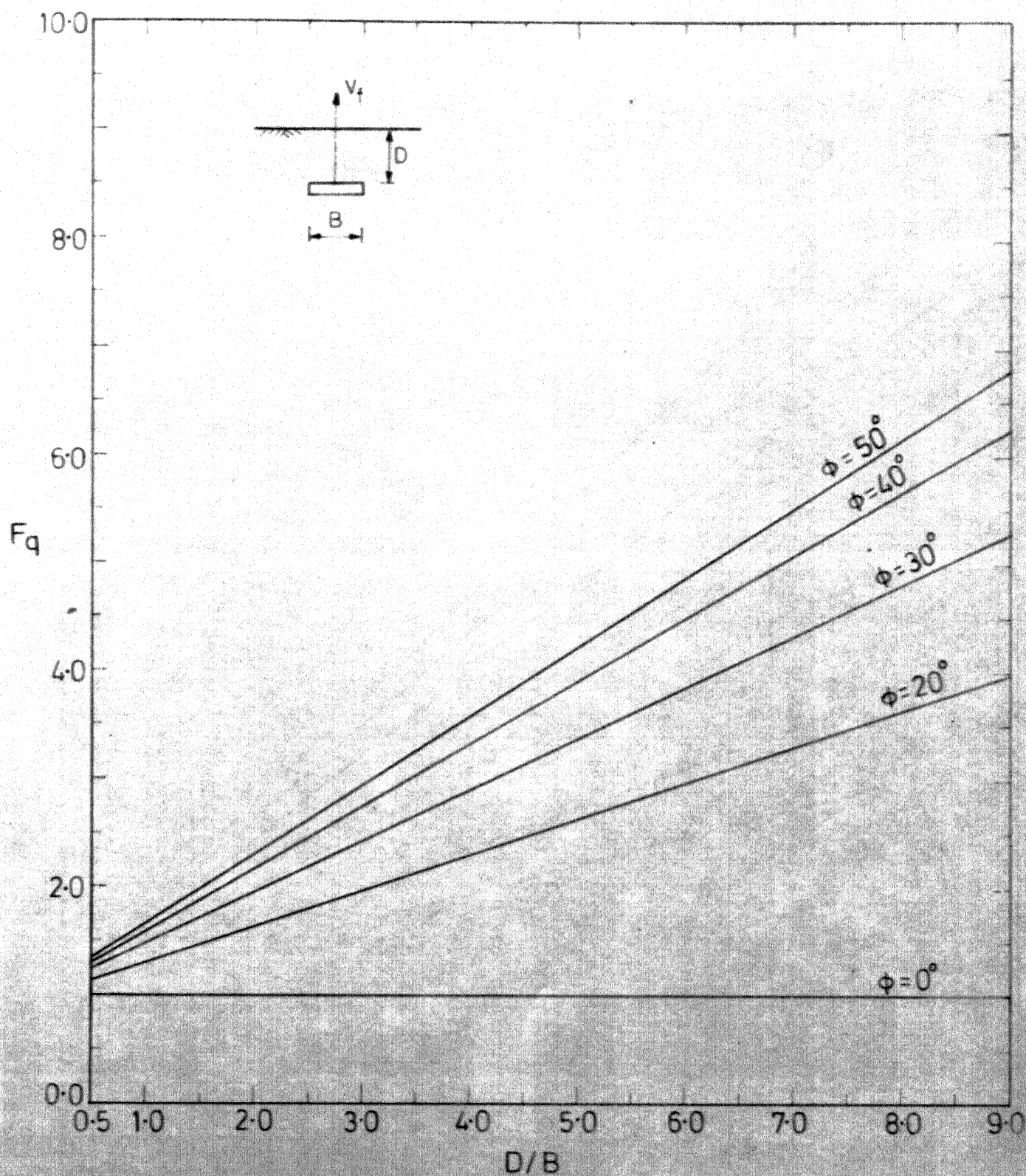
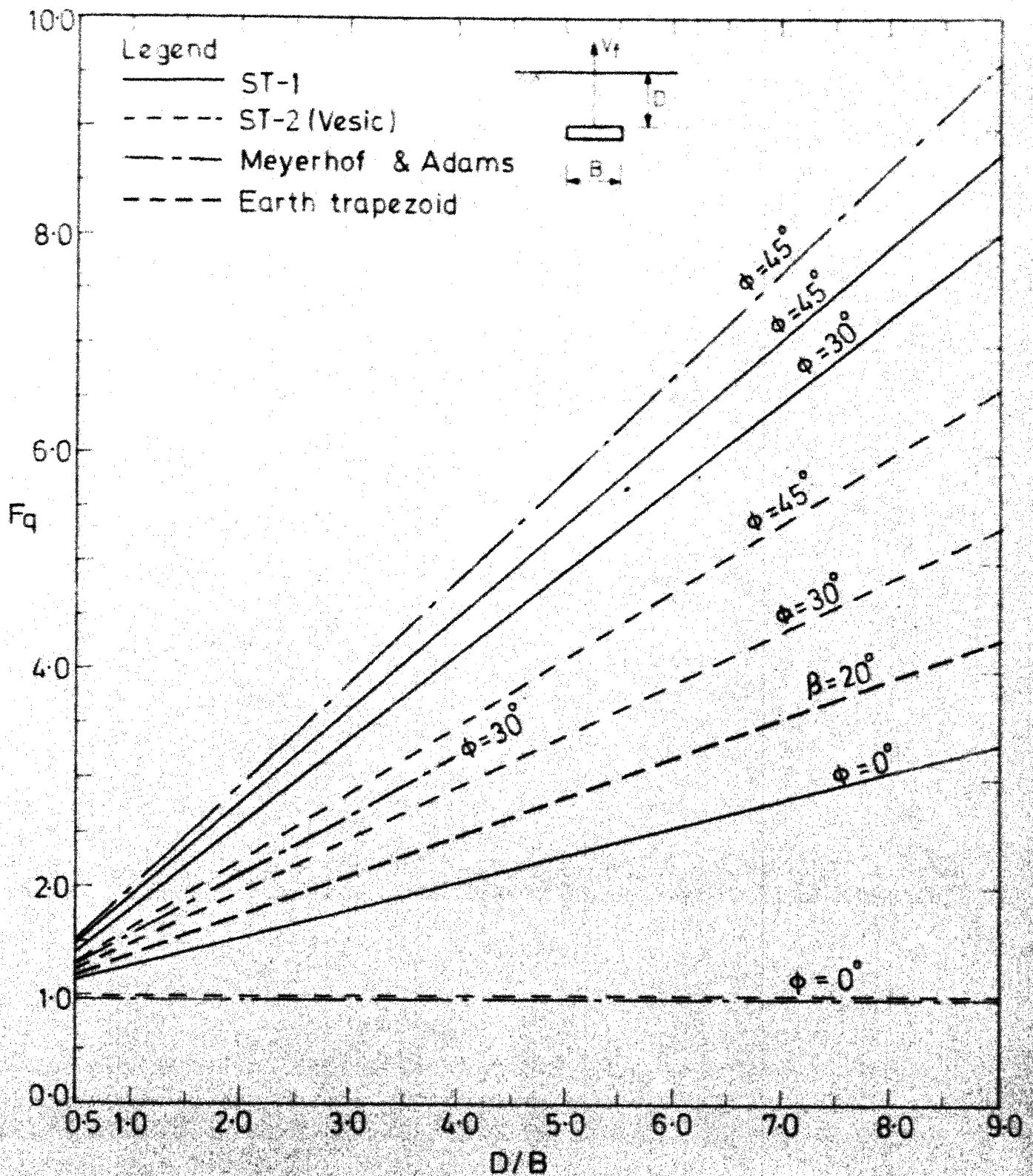
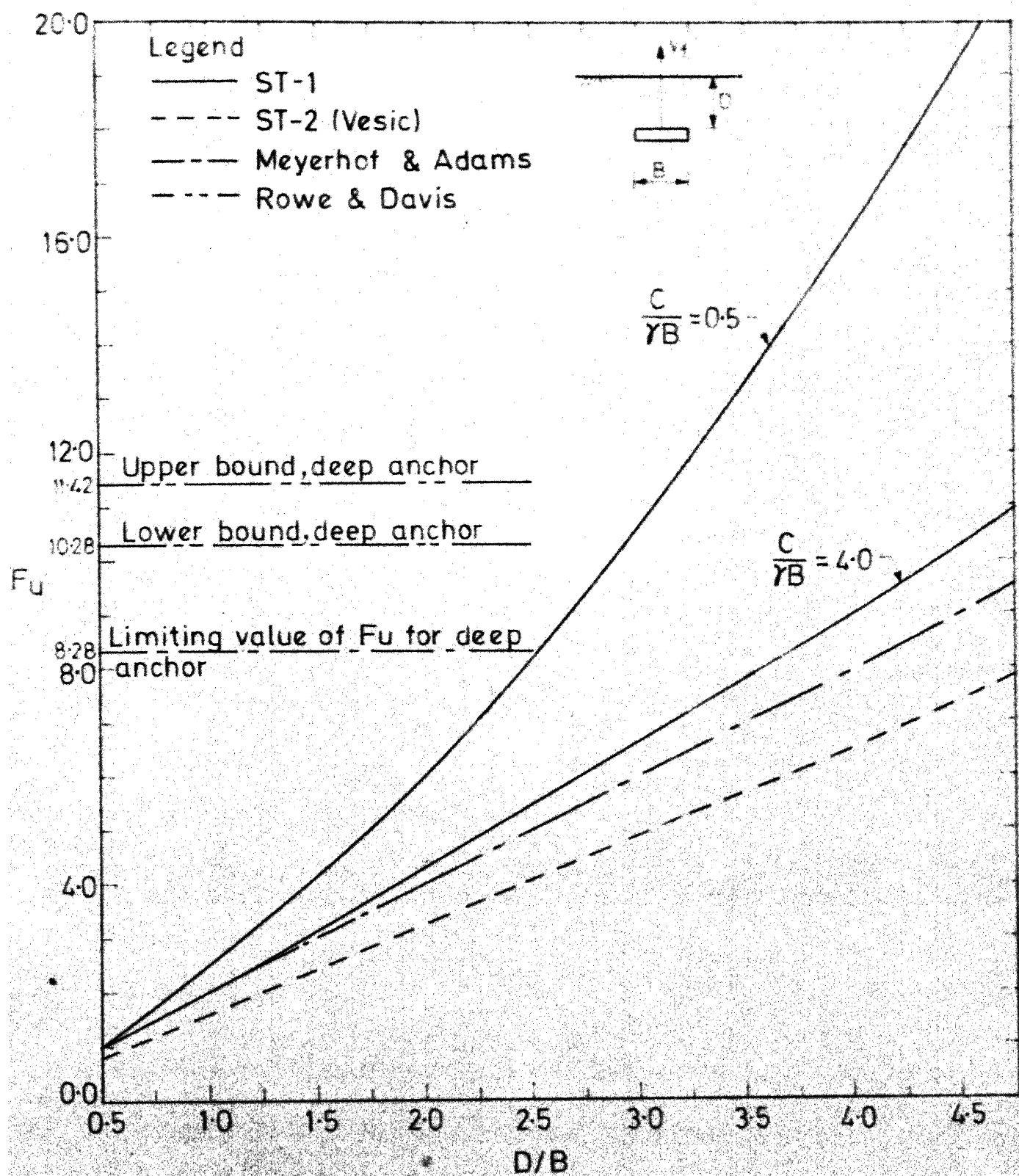


FIG.7-6 BREAKOUT FACTORS FOR HORIZONTAL STRIP, F_q FOR ST-1

FIG.7-7 BREAKOUT FACTORS FOR HORIZONTAL STRIP, F_c FOR ST-2

FIG.7.8 BREAKOUT FACTORS FOR HORIZONTAL STRIP, F_q FOR ST-2



FIG.7-10 COMPARISON OF STRIP ANCHOR THEORIES. $\phi=0$

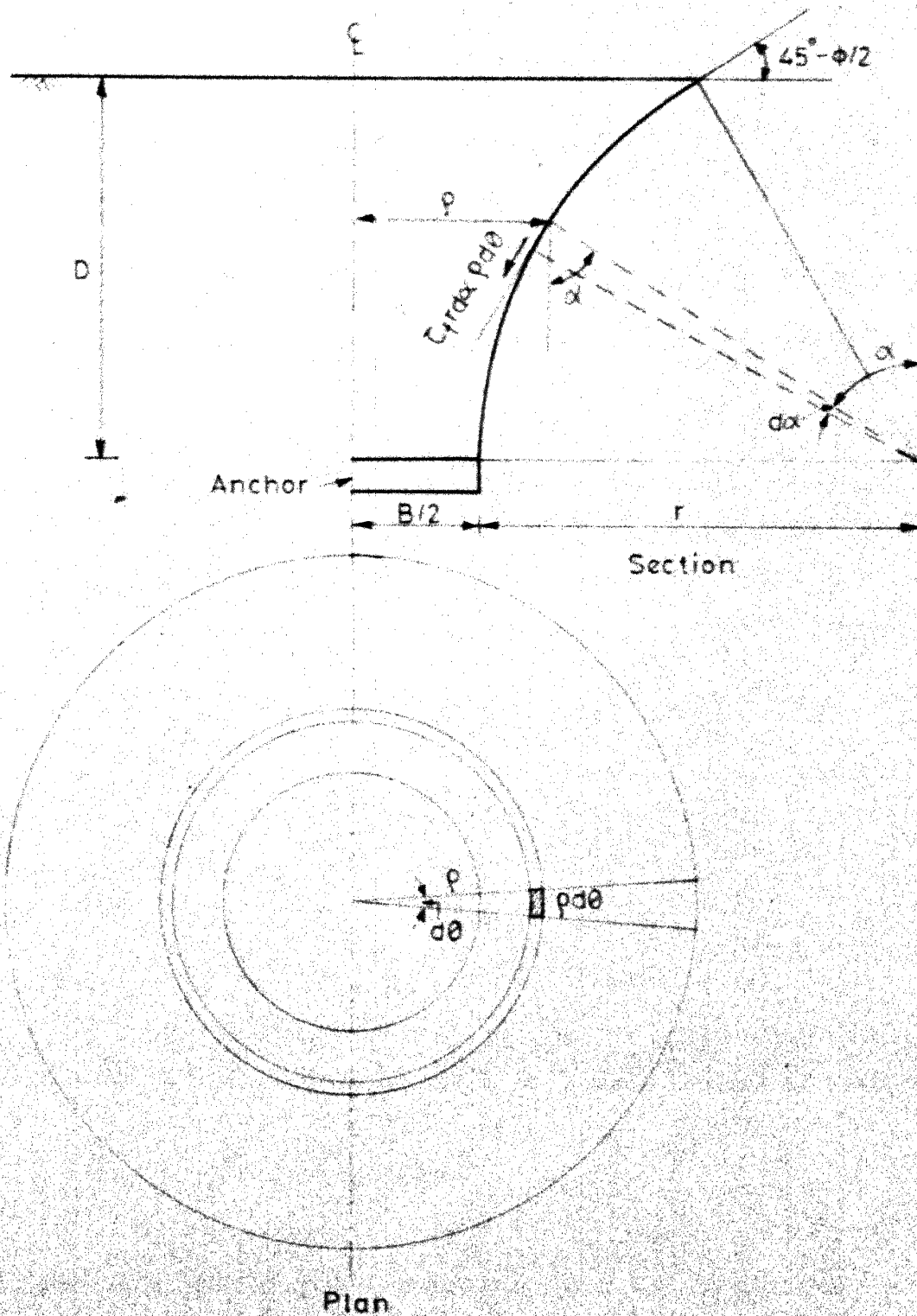


FIG. 7-11 SHEARING RESISTANCE ON RUPTURE SURFACE
CIRCULAR ANCHOR-BALLA'S THEORY

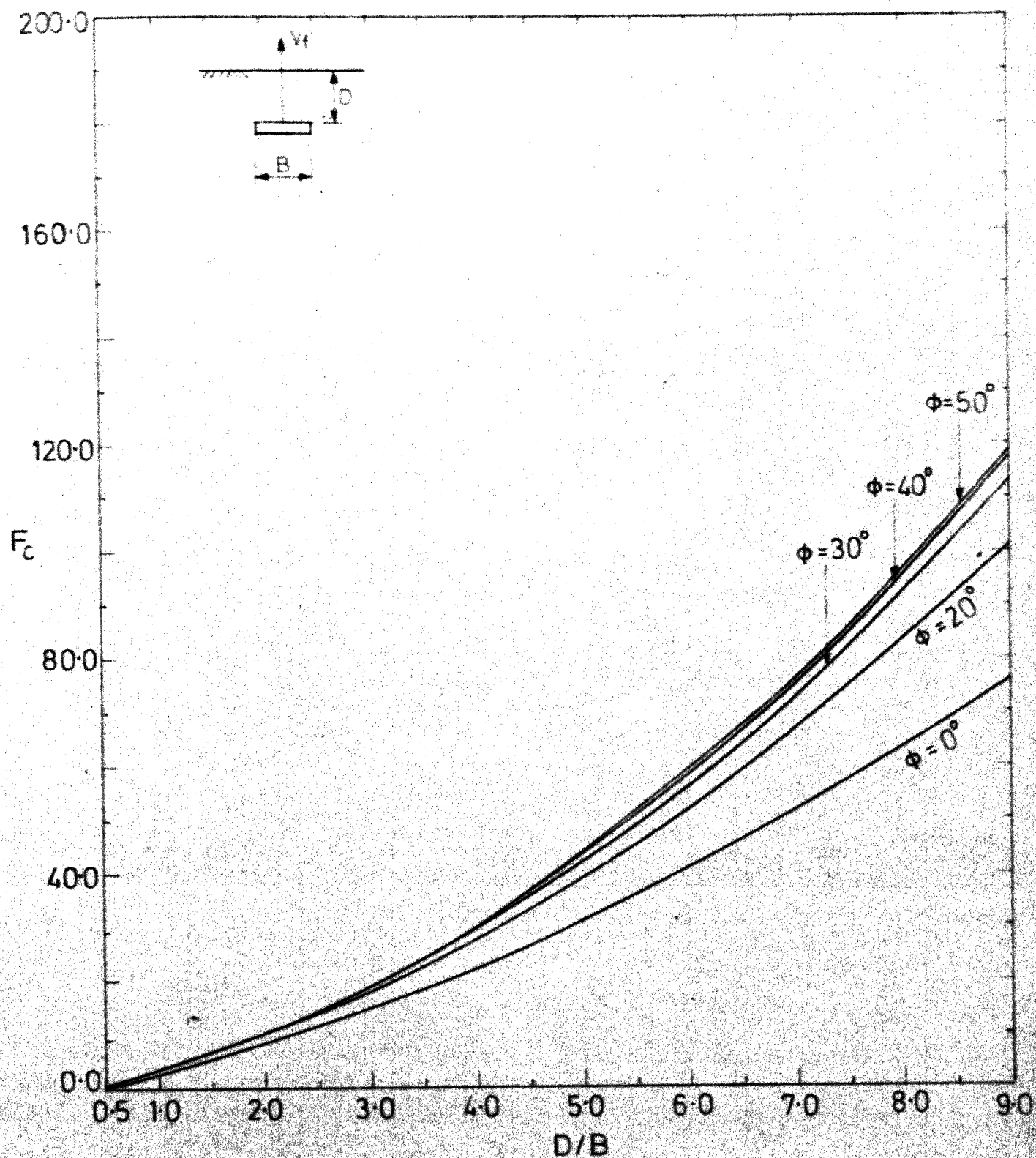


FIG.7.12 BREAKOUT FACTORS FOR CIRCULAR ANCHOR, F_c FOR CIR-1

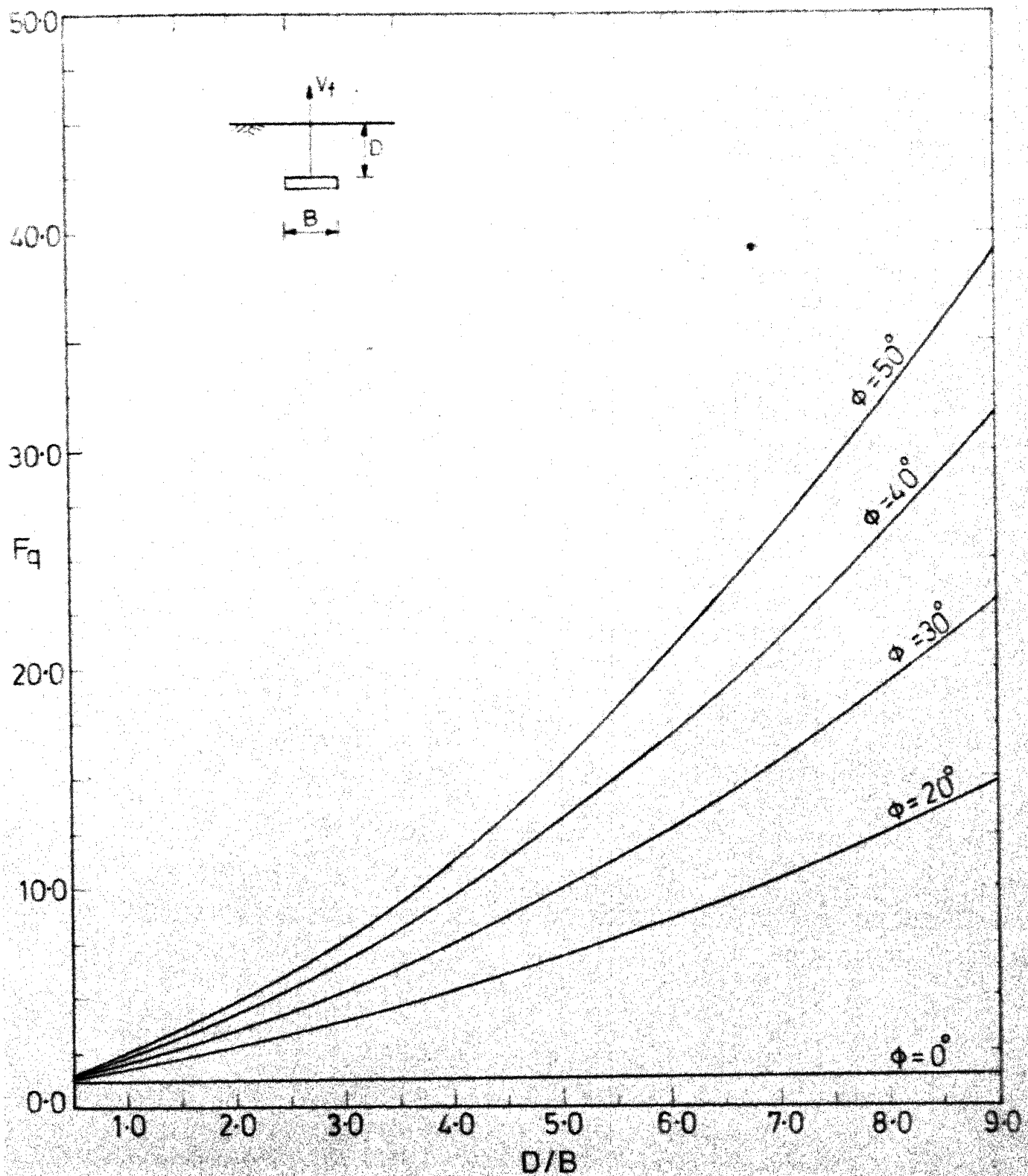
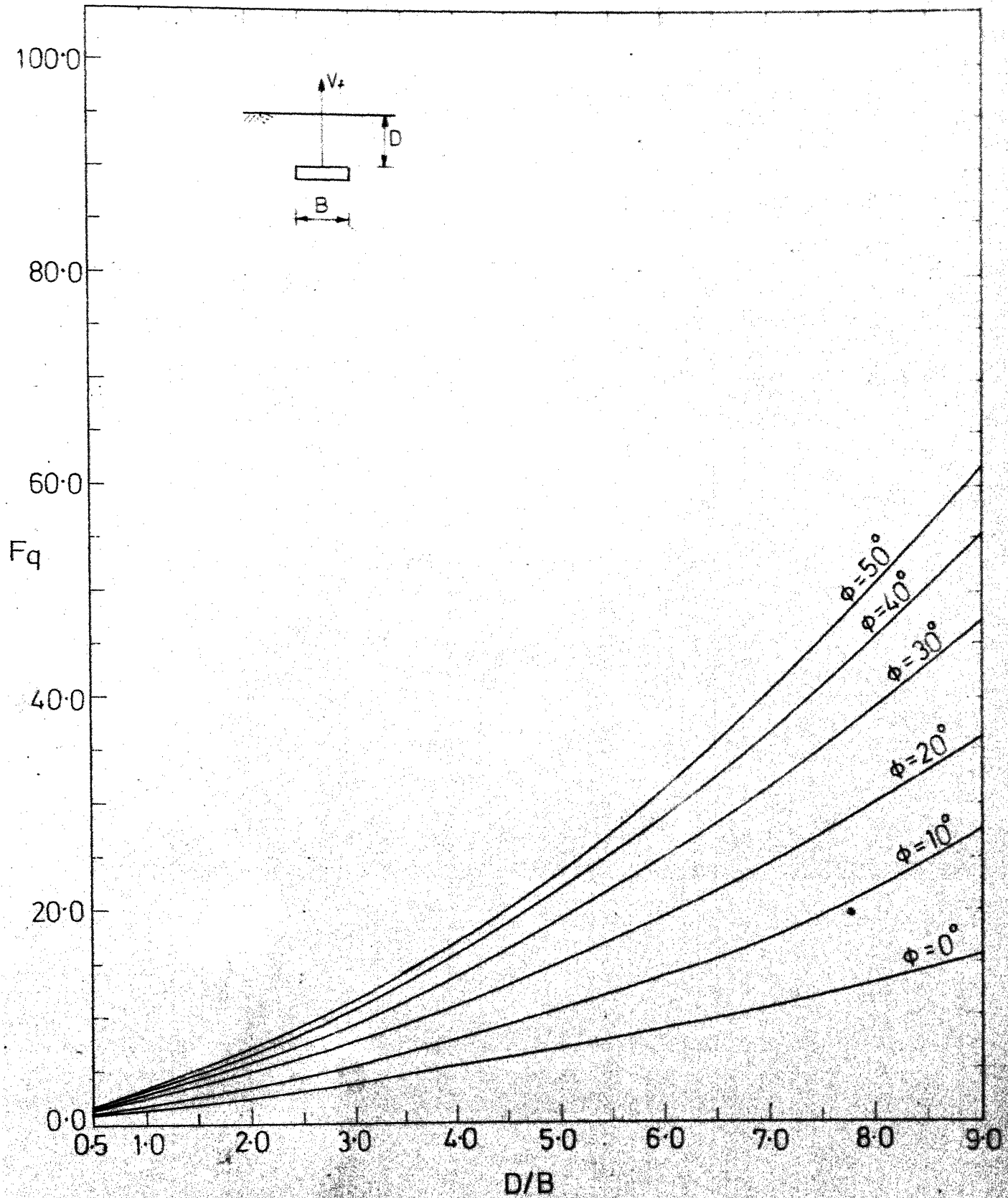
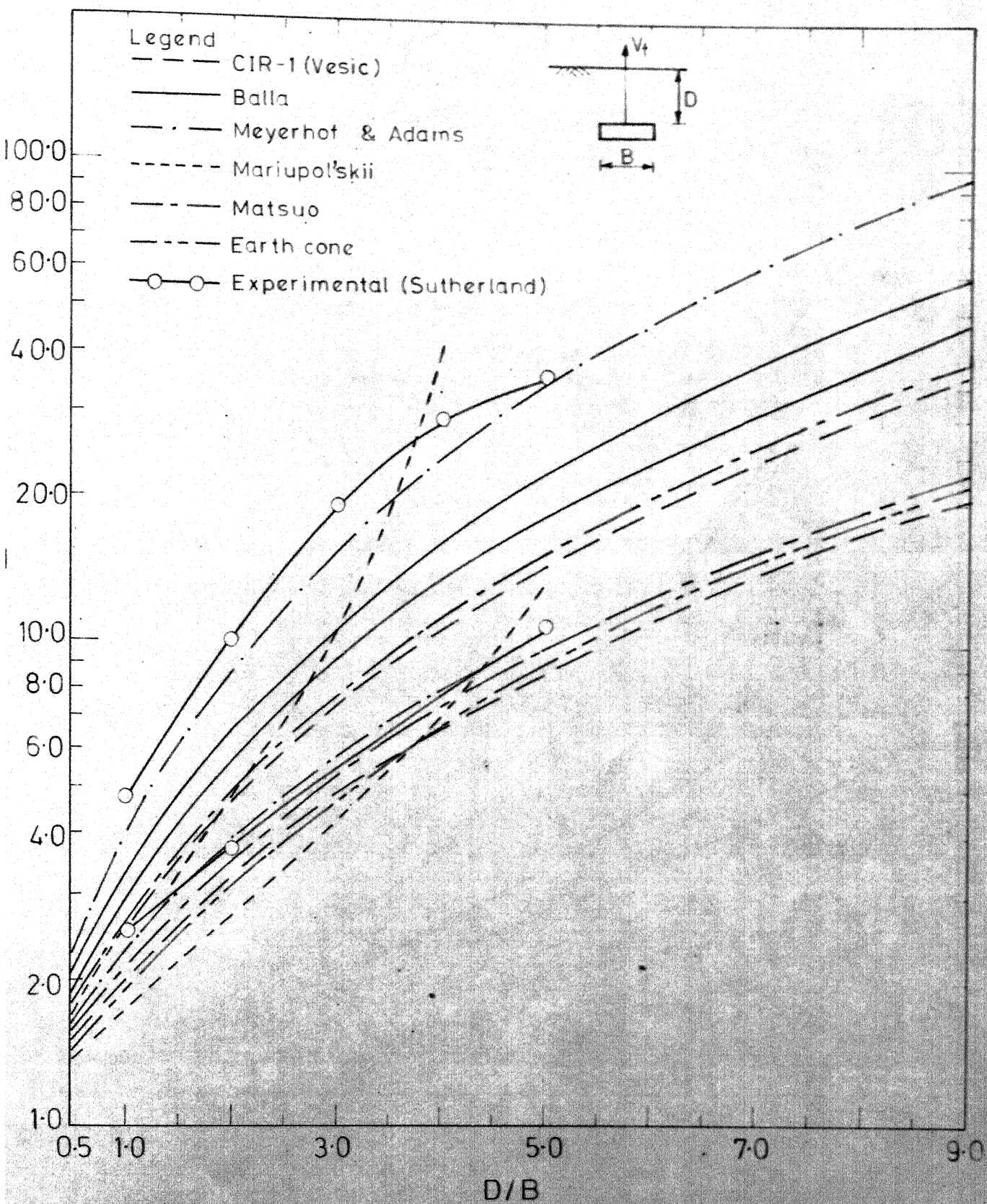
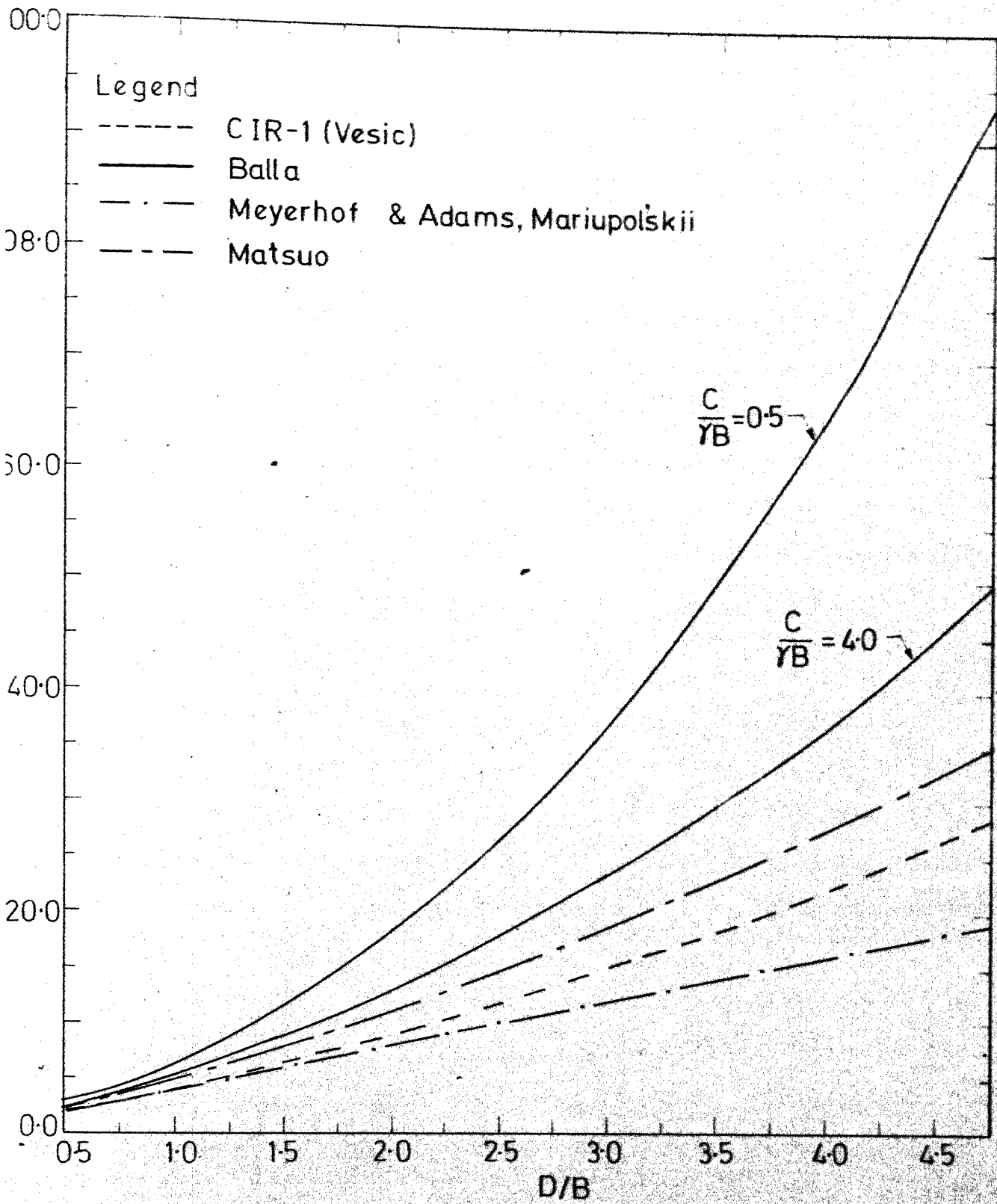


FIG. 7.13 BREAKOUT FACTORS FOR CIRCULAR ANCHOR, F_q FOR CIR-1

FIG. 7.15 BREAKOUT FACTORS FOR CIRCULAR ANCHOR, F_q FOR

FIG.7-16 COMPARISON OF CIRCULAR ANCHOR THEORIES, $C=0$

FIG. 7-17 COMPARISON OF CIRCULAR ANCHOR THEORIES, $\phi=0$

CHAPTER 8

CONCLUSIONS AND RECOMMENDATIONS

8.1 Introduction :

The relevant conclusions on the finite element analysis of horizontal strip, vertical strip and horizontal circular anchors considered in the present investigation have already been discussed at the end of each chapter. Conclusions regarding the approximate anchor theories derived and modified are made at the end of Chapter 7. General conclusions from the present study are outlined in Section 8.2 below. Recommendations for future work have been listed in Section 8.3.

8.2 Conclusions :

Analytical studies have been conducted in this investigation for the response of plate anchors embedded inside soil medium subjected to static loads. Elastic and elasto-plastic deformation analysis of horizontal anchors (strip and circular) and elasto-plastic undrained analysis of vertical strip anchors are carried out following the basic concepts outlined in Chapter 3 for the general finite element formulation and using analytical models and methods proposed. On the basis of the results obtained from the analyses it can be concluded that the performance of analytical models used for the elastic analysis and non-linear elasto-plastic progressive deformation analysis of the anchor problem are very much promising. The recasting

of theoretical results for horizontal strip and circular anchors in the form of breakout factors (101) gives a common basis for comparison.

From the elastic analysis of horizontal strip and circular anchors it can be concluded that the response of embedded objects under uplift loads are significantly effected by factors like embedment ratio, layer depth below the anchor, the type of loading applied, Poisson's ratio of the material and interface condition below the anchor. For a layer of limited soil depth analysed, the vertical deformation decreases with anchor embedment ratio. The anchor breakaway effects significantly the deformation response as well as the stress distributions above and below the anchor. The simulation of a rigid anchor by specification of equal nodal displacements in displacement finite element analysis gives vertical displacement response which is not realistic. In the higher ranges of K_r (10 to 100) the vertical deformation at the centre of anchor due to discretisation of anchor by continuum elements and structural elements (beam-column element and plate bending elements) are less in comparison to the deformation from rigid anchor simulation. For the practical ranges of relative stiffness (K_r) values investigated, the bending moments in the anchor are found to be higher for higher Poisson's ratio of the material. The anchor breakaway at the base significantly increases the bending moments in the anchor. Specification of finite stiffness

of anchor by use of continuum elements and structural elements results in different vertical response factors.

Elasto-plastic undrained progressive deformation analysis of anchor problem upto collapse can be carried out by implementing Von-Mises or Tresca plasticity models in displacement finite element analysis. The 'initial stress' computational technique used for the solution of the non-linear problem is found to be satisfactory. In an incremental iterative technique like the 'initial stress' method, the maximum number of iterations allowed within an increment and the limit on convergence specified in the analysis will effect the numerical limit load as well as the computer time for carrying out the non-linear analysis. In all the cases investigated, the Tresca plasticity model gives a deformation response curve for anchor which falls below that obtained by using Von-Mises model. The load at which the first point inside the soil medium reaches plastic state and the collapse loads obtained are smaller for the Tresca model. It can generally be concluded that for the case of anchors embedded inside the soil, the anchor stiffness effects the load deformation response curve but does not significantly alter the numerical limit loads obtained.

The deformation response, the load at first yield and the numerical limit loads obtained from elasto-plastic analysis using Von-Mises and Tresca criteria are effected considerably by anchor breakaway from soil below it. The full bonding

situation gives collapse loads which are very high in comparison to the prediction from horizontal strip and circular anchor theories. The plastic zones at failure, obtained for the full break-away situation is limited in extent and appears to be localised to points above the anchor level.

The progressive deformation behaviour of anchor embedded inside a frictional soil medium can be traced by finite element elasto-plastic non-linear analysis using associated Mohr-Coulomb criterion. The onset of yield is at very low loads and hence the ratio of ultimate load to load at first yield is high. The full bonding of anchor to soil below gives loads which are unrealistically large in comparison to the values predicted by conventional horizontal strip and circular anchor theories. Hence any analysis carried out without due consideration of the anchor soil interface condition may give loads on the unsafe side for the plate anchor problem.

By presenting results in the form of breakout factors, it is possible to compare as well as use efficiently the results of theoretical prediction by different approximate anchor theories for horizontal strip and circular anchors. For cohesionless soils, the theories (ST-1, Balla) derived on the assumption that the vertical component of the shearing resistance on the rupture surface contributes to the soil resistance against uplift, gives higher breakout loads than the theories (ST-2, CIR-1, Vesic) which are derived on the assumption that the vertical component

of the resultant of the shearing resistance and normal force on the rupture surface (p) contributes to the soil resistance against uplift. A comparison of the experimental results with theoretical predictions presented in this work for circular anchors will give confidence in the use of appropriate shallow anchor theories for uplift load calculation. Earth cone method as suggested by Indian Standards will give uplift loads on the conservative side for shallow circular anchors in sand especially for higher values of angle of internal friction. When the full range of values of angle of internal friction and cohesion are considered, the predictions for uplift load of circular anchor by Meyerhof and Adams's theory appears to be closer to the experimentally obtained results.

8.3 Recommendations :

Various aspects of the problems which have been studied in the preceeding chapters are limited to the static vertical load on shallow horizontal anchors and static horizontal load on shallow vertical anchors. Most of the practical problems relate to finding the uplift loads on rectangular embedded foundations subjected to inclined uplift loads. A three dimensional analysis of the problem may be needed for this.

The plasticity models used for the elasto-plastic analysis are the classical models for purely cohesive and frictional materials. The recent formulations on constitutive relations for soils can be made use of in selection and implementation of

Anchors in ocean environment are subjected to cyclic loadings and even in tower foundations load reversals can occur because of the wind loads. Both these aspects can be studied with the use of appropriate constitutive laws and appropriate modifications by the use of the finite element method.

REFERENCES

1. Adams, J.I., and Hayes, I., "The Uplift Capacity of Shallow Foundations", Ontario Hydro Research Quarterly, Vol. 19, No.1, 1967, pp. 1-12.
2. Ali, M.S., "Fullout Resistance of Anchor Plates and Anchor Piles in Soft Bentonite Clay", Duke Soil Mechanics Series No. 17, School of Engineering, Duke University, Durham, 1968. (From Ref. 101).
3. Allen, D.N. de G., and Southwell, R., "Relaxation Methods Applied to Engineering Problems, XIV. Plastic Straining in Two-Dimensional Stress Systems", Philosophical Transactions, Royal Society, London, Series A, Vol. 242, 1950, pp.379-414.
4. Ang, A.H.S., and Harper, G.N., "Analysis of Contained Plastic Flow in Plane Solids", Journal of Engineering Mechanics Division, ASCE, Vol. 90, No. EM5, 1964, pp. 397-418.
5. Baker, W.H., and Kondner, R.L., "Fullout Load Capacity of a Circular Earth Anchor Buried in Sand", National Academy of Sciences, Highway Research Record, 108, 1966, pp.1-10.
6. Balla, A., "The Resistance to Breakingout of Mushroom Foundations for Pylons", Proceedings, 5th International Conference on Soil Mechanics and Foundation Engineering, Paris, Vol.1, 1961, pp. 569-576.
7. Bathe, K.J., and Wilson, E.L., Numerical Methods in Finite Element Analysis, Prentice Hall India Pvt.Ltd., New Delhi, 1978.
8. Bemben, S.M., and Kupferman, M., "The Vertical Holding Capacity of Marine Anchors in Sand and Clay Subjected to Static and Cyclic Loading", CR 72.007, Naval Civil Engineering Laboratory, Port Hueneme, California, November, 1971.
9. Bhatnagar, R.S., "Fullout Resistance of Anchors in Silty Clay", Duke Soil Mechanics Series No.18, School of Engineering, Duke University, Durham, 1968. (From Ref. 101).
10. Boonlualohr, P., Valliappan, S., and Lee, I.K., "Elastic-Plastic Analysis of Shallow Foundations", Proceedings, International Conference on Finite Element Methods in Engineering, University of New South Wales, Australia, 1974, pp. 479-492.

11. Bosakov, S.V., "Analysis of Deep Anchor Plates of Finite Rigidity", Osnovaniya, Fundamenty i Mekhanika Gruntov, No.6, 1977, pp. 23-24 (English Translation Available from Engineering Consultants Bureau, New York in 'Soil Mechanics and Foundation Engineering').
12. Buragohain, D.N., and Shah, V.L., "Curved Interface Elements for Interaction Problems", Proceedings, International Symposium on Soil Structure Interaction, Dept. of Civil Engg., Roorkee, India, 1977, pp. 197-201.
13. Butterfield, R., and Banerjee, P.K., "A Rigid Disc Embedded in an Elastic Half Space", Geotechnical Engineering, Vol. 2, No.1, 1971, pp. 35-52.
14. Chapman, C.R., and Groth, N.N., "Computer Evaluation of Deformation Due to Sub-Surface Loads in a Semi-Infinite Elastic Medium", B.E. Thesis, University of Sydney, Australia, 1969. (From Ref. 69).
15. Chickanagappa, L.S., "Some Studies on Stresses and Displacements in Elastic Half Space", Ph.D. Thesis, Bangalore University, February, 1976.
16. Clemence, S.P., and Veesaert, C.J., "Dynamic Pullout Resistance of Anchors in Sand", Proceedings, International Symposium on Soil Structure Interaction, Dept. of Civil Engg., Roorkee, India, 1977, pp. 389-397.
17. Das, B.M., "Pullout Resistance of Vertical Anchors", Journal of the Geotechnical Engineering Division, ASCE, Vol. 101, No. GT1, 1975, pp. 87-91.
18. Das, B.M., "Model Tests for Uplift Capacity of Foundations in Clay", Soil and Foundations, Vol. 18, No.2, 1978, pp. 17-24.
19. Das, B.M., and Seeley, G.R., "Breakout Resistance of Shallow Horizontal Anchors", Technical Note, Journal of Geotechnical Engineering Division, ASCE, Vol. 101, No. GT9, 1975, pp. 999-1003.
20. Das, B.M., and Seeley, G.R., "Inclined Load Resistance of Anchors in Sand", Technical Note, Journal of Geotechnical Engineering Division, ASCE, Vol. 101, No. GT9, 1975, pp. 995-998.
21. Davidson, H.L., and Chen, W.F., "Non-linear Response of Undrained Clay to Footings", Computers and Structures, Vol.7, 1977, pp. 539-546.

22. Davie, J.R., and Sutherland, H.B., "Uplift Resistance of Cohesive Soils", *Journal of Geotechnical Engineering Division*, ASCE, Vol. 103, No. GT9, September 1977, pp. 935-952.
23. Davis, E.H., "Theories of Plasticity and the Failure of Soil Masses", *Soil Mechanics, Selected Topics*, ed. I.K. Lee, London, Butterworths, 1968, pp. 341-380.
24. Desai, C.S., and Abel, J.F., *Introduction to the Finite Element Method*, Affiliated East-West Press Pvt.Ltd., New Delhi, 1972.
25. DiMaggio, F.L., and Sandler, I.S., "Material Model for Granular Soils", *Journal of Engineering Mechanics Division*, ASCE, Vol. 97, No. EM3, 1971, pp. 935-950.
26. Douglas, D.J., and Davis, E.H., "The Movement of Buried Footings Due to Moment and Horizontal Load and the Movement of Anchor Plates", *Geotechnique*, Vol. 14, No.2, 1964, pp. 115-132.
27. Drucker, D.C., and Prager, W., "Soil Mechanics and Plastic Analysis of Limit Design", *Quarterly of Applied Mathematics*, Vol. 10, 1952, pp. 157-165.
28. Esquivel-Diaz, R.F., "Pullout Resistance of Deeply Buried Anchors in Sand", *Soil Mechanics Series No.8*, School of Engineering, Duke University, Durham, 1967.
29. Fernandez, R.M., and Christian, J.T., "Finite Element Analysis of Large Strains in Soils", *NASA Research Report*, R71-37, 1971.
30. Fotiyeva, N.N., and Litkin, V.A., "Design of Deep Anchor Plates", *Osnovaniya, Fundamenty i Mekhanika Gruntov*, No.5, 1969, pp. 8-10, (English Translation Available from Engineering Consultants Bureau, New York in 'Soil Mechanics and Foundation Engineering').
31. Fox, E.N., "The Mean Elastic Settlement of a Uniformly Loaded Area at a Depth Below the Ground Surface", *Proceedings, 2nd International Conference on Soil Mechanics and Foundation Engineering*, Vol. 1, 1948, pp.129.
32. Geddes, J.D., "Vertical Stress Components Produced by Axially Symmetric Sub-Surface Loadings", *Canadian Geotechnical Journal*, Vol. 12, 1975, pp. 482-497.
33. Ghaboussi, J., Wilson, E.L., and Isenberg, J., "Finite Elements for Rock Joints and Interfaces", *Journal of Soil Mechanics and Foundation Engineering*, Vol. 99, No.SM10, 1973, pp. 833-843.

34. Goodman, R.E., Taylor, R.L., and Brekke, T.L., "A Model for the Mechanics of Jointed Rock", Journal of Soil Mechanics and Foundation Division, ASCE, Vol. 94, No.SM3, 1968, pp. 637-659.
35. Hagmann, A.J., "Prediction of Stress and Strain Under Drained Loading Conditions", MIT, Cambridge, Mass., Department of Civil Engineering, Report, R71-3, January, 1971.
36. Hanna, T.H., Sparks, R., and Yilmaz, M., "Anchor Behaviour in Sand", Journal of Soil Mechanics and Foundation Division, ASCE, Vol. 98, No.SM11, 1972, 1187-1208.
37. Hansen, J.B., Earth Pressure Calculations, Danish Technical Press, Copenhagen, Denmark, 1953.
38. Hansen, J.B., "The Stabilizing Effects of Piles in Clay", CN-POST, No.3, Christiani and Nielsen, Copenhagen, n.d. (From Ref. 97).
39. Hill, R., The Mathematical Theory of Elasticity, Oxford University Press, 1950.
40. Hodge, P.G., White, G.N., and Providence, R.I., "A Quantitative Comparison of Flow and Deformation Theory of Plasticity", Journal of Applied Mechanics, 17, 1950, pp. 180-184.
41. Høeg, K., "Finite Element Analysis of Strain Softening Clay", Journal of the Soil Mechanics and Foundation Division, ASCE, Vol. 98, No. SM1, January 1972, pp. 43-58.
42. Høeg, K., "Deformation Computations in Geotechnical Engineering", NR-123, Norwegian Geotechnical Institute, Oslo, 1978, pp. 1-19.
43. Høeg, K., Christian, J.T., and Whitman, R.V., "Settlement of Strip Load on Elastic-Plastic Soil", Journal of the Soil Mechanics and Foundation Division, ASCE, Vol. 94, No.SM2, March, 1968, pp. 431-445.
44. IS 4091-1967, "Indian Standard Code of Practice for Design and Construction of Foundations for Transmission Towers and Poles".
45. Jacobs, J.A., "Relaxation Methods Applied to Problems of Plastic Flow", Philosophical Magazine, Series 7, Vol. 41, 1950, pp. 349-361, 458-467.

46. Kananyan, A.S., "Experimental Investigation of the Stability of Bases of Anchor Foundations", Osnovaniya, Fundamenty i Mekhanika Gruntov, Vol.4, No.6, 1966, pp. 9-12 (English Translation Available from Engineering Consultants Bureau, New York in 'Soil Mechanics and Foundation Engineering').
47. Lade, P.V., and Duncan, J.M., "Elasto-Plastic Stress Strain Theory for Cohesionless Soil", Journal of Geotechnical Engineering Division, ASCE, Vol. 101, No. GT10, 1975, pp. 1037-1053.
48. Mackenzie, T.R., "Strength of Dead man Anchors in Clay", Master's Thesis, Princeton University, 1955 (from Ref. 97).
49. Mahtab, M.A., and Goodman, R.E., "Three-Dimensional Finite Element Analysis of Jointed Rock Slopes", Proceedings, Second Congress, International Society on Rock Mechanics, Belgrade, Vol. 3, 1970, pp. 7-12.
50. Marcal, P.V., and King, I.P., "Elastic-Plastic Analysis of Two-Dimensional Stress Systems by the Finite Element Method", International Journal of Mechanical Sciences, Vol. 9, 1967, pp. 143-155.
51. Mariupol'skii, L.G., "The Bearing Capacity of Anchor Foundations", Osnovaniya, Fundamenty i Mekhanika Gruntov, Vol.3, No.1, 1965, pp. 14-18 (English Translation Available from Engineering Consultants Bureau, New York in 'Soil Mechanics and Foundation Engineering').
52. Matsuo, M., "Study on the Uplift Resistance of Footing (I)", Soil and Foundation, Vol. 7, No.4, 1967, pp. 1-37.
53. Matsuo, M., "Study on the Uplift Resistance of Footing (II)", Soil and Foundation, Vol. 8, No.1, 1968, pp. 18-48.
54. Melan, E., "Der Spannungszustand der durch eine Einzelkraft in Innern beanspruchten Halbschiebe", Z. Angew. Math. Mech., Vol. 12, 1932.
55. Meyerhof G.G., "The Ultimate Bearing Capacity of Foundations", Geotechnique, Vol.2, No.4, 1951, pp. 301-332.
56. Meyerhof G.G., "The Uplift Capacity of Foundations Under Oblique Loads", Canadian Geotechnical Journal, Vol. 10, No.1, 1973, pp. 64-70.
57. Meyerhof G.G., "Uplift Resistance of Inclined Anchors and Piles", Proceedings, 8th International Conference on Soil Mechanics and Foundation Engineering, Moscow, Vol.2, 1973, pp. 167-172.

58. Meyerhof G.G., and Adams, J.I., "The Ultimate Uplift Capacity of Foundations", Canadian Geotechnical Journal, Vol. 5, No.4, 1968, pp. 225-244.
59. Mindlin, R.D., "Force at a Point in the Interior of a Semi-infinite Solid", Journal of Applied Physics, Vol. 7, No.5, 1936, pp. 195-202.
60. Mors, H., "Das Verhalten Von Mastgrundungen bei Zugbeanspruchung", Bautechnik, Vol. 36, No.10, 1959, pp. 367-378.
61. Muga, B.J., "Ocean Bottom Breakout Forces", Technical Report R-591, Naval Civil Engineering Laboratory, Port Hueneme, California, 1968.
62. Nayak, G.C., and Zienkiewicz, O.C., "Convenient Form of Stress Invariants for Elasticity", Journal of Structural Division, ASCE, Vol. 98, 1972, 949-954.
63. Nayak, G.C., and Zienkiewicz, O.C., "Elasto-Plastic Stress Analysis, A Generalisation for Various Constitutive Relations Including Strain Softening", International Journal of Numerical Methods in Engineering, Vol. 5, 1972, pp. 113-135.
64. Neely, J.W., Stuart, J.G., and Graham, J., "Failure Loads on Vertical Anchor Plates in Sand", Journal of Soil Mechanics and Foundation Division, ASCE, Vol. 99, No. SM9, 1973, pp. 669-685.
65. Nishida, Y., "Vertical Stress and Vertical Deformations of Ground Under a Deep Circular Uniform Pressure in the Semi-infinite", Proceedings, 1st Congress, International Society of Rock Mechanics, Vol.2, 1966, pp. 493-498.
66. Paramasivam, V., "Finite Element Analysis of Axi-symmetric Plates", Proceedings, International Conference on Finite Element Methods in Engineering, Coimbatore, India, 1974, pp. 198-213.
67. Pardoen, G.C., "Static, Vibration and Buckling Analysis of Axisymmetric Circular Plates Using Finite Elements", Computers and Structures, Vol.3, 1973, pp. 355-375.
68. Pope, G.G., "The Application of the Matrix Displacement Method in Plane Elasto-Plastic Problems", Proceedings, Conference on Matrix Methods in Structural Mechanics, Wright - Patterson Air Force Base, AFFDL-TR-66-80, pp. 635-654.

69. Poulos, H.G., and Davis, E.H., *Elastic Solutions for Soil and Rock Mechanics*, John Wiley & Sons, Inc., New York, 1974.
70. Prevost, J.H., "Mathematical Modelling of Monotonic and Cyclic Undrained Clay Behaviour", *International Journal for Numerical and Analytical Methods in Geomechanics*, Vol.1, No.2, 1977, pp. 195-216.
71. Prevost, J.H., and Höeg, K., "Effective Stress-Strain Strength Model for Soils", *Journal of Geotechnical Engineering Division*, ASCE, Vol. 101, No. 673, 1975, pp. 259-278.
72. Prevost, J.H., and Höeg, K., "Plasticity Model for Undrained Stress Strain Behaviour", *Proceedings, 9th International Conference on Soil Mechanics and Foundation Engineering*, Tokyo, Vol.1, 1977, pp. 255-261.
73. Przemieniecki, J.S., *Theory of Matrix Structural Analysis*, McGraw-Hill Book Co., New York, 1968.
74. Repnikov, L.N., and Gorbunov-Posadov, M.I., "Calculation of Anchor Plate for the Ground Consolidation Stage", *Osnovaniya, Fundamenty i Mekhanika Gruntov*, No.5, 1969, pp.6-8. (English Translation Available from Engineering Consultants Bureau, New York in 'Soil Mechanics and Foundation Engineering').
75. Reyes, S.F., and Deere, D.U., "Elastic-Plastic Analysis of Underground Openings by the Finite Element Method", *Proceedings, 1st International Congress on Rock Mechanics*, Vol. 11, Lisbon, 1966, 477-483.
76. Roscoe, K.H., "The Influence of Strains in Soil Mechanics", *Tenth Rankine Lecture, Geotechnique*, Vol. 20, No.2, 1970, pp. 129-170.
77. Roscoe, K.H., and Burland, J.B., "On the Generalised Stress Strain Behaviour of 'Wet' Clay", *Engineering Plasticity*, J. Heyman and F.A. Leckie, eds., Cambridge University Press, London, 1968, pp. 535-609.
78. Roscoe, K.H., Schofield, A.N., and Thurairajah, A., "Yielding of Clays in States Welter than Critical", *Geotechnique*, Vol. 13, No.3, 1963, pp. 211-240.
79. Roscoe, K.H., Schofield, A.N., and Wroth, C.P., "On the Yielding of Soils", *Geotechnique*, Vol. 8, No.1, pp.22-53, 1958.

80. Rowe, R.K., and Booker, J.R., "A Method for Analysis of Horizontally Embedded Anchors in an Elastic Soil", International Journal of Numerical and Analytical Methods in Geomechanics, Vol. 3, No.2, 1979, pp. 187-203.
81. Rowe, R.K., and Booker, J.R., "The Analysis of Inclined Anchor Plates", Proceedings, 3rd International Conference on Numerical Methods in Geomechanics, Aachen, 1979, pp. 1227-1236.
82. Rowe, R.K., Booker, J.R., and Balaam, N.P., "Application of Initial Stress Method to Soil Structure Interaction", Research Report No. R294, School of Civil Engineering, University of Sydney, 1976.
83. Rowe, R.K., and Davis, E.H., "Application of the Finite Element Method to the Prediction of Collapse Loads", Research Report No. R310, School of Civil Engineering, University of Sydney, 1977.
84. Sandler, I.S., DiMaggio, F.L., and Baladi, G.Y., "Generalised Cap Model for Geologic Materials", Journal of Geotechnical Engineering Division, ASCE, Vol. 102, No.GT7, 1976, pp. 683-699.
85. Schafer, H., "A Contribution to the Solution of Contact Problems by Joint Elements", Computer Methods in Applied Mechanics and Engineering, Vol. 6, 1975, pp. 335-354.
86. Schofield, A., and Wroth, P., Critical State Soil Mechanics, McGraw-Hill, New York, 1968.
87. Selvadurai, A.P.S., "The Load Deflection Characteristics of a Deep Rigid Anchor in an Elastic Medium", Geotechnique, Vol.26, No.4, 1976, pp. 603-612.
88. Sharma, H.D., Nayak, G.C., and Maheshwari, J.B., "Generalisation of Sequential Non-linear Analysis, A Study of Rock fill Dam with Joint Elements", Numerical Methods in Geomechanics, ASCE, Vol. 2, 1976, pp. 663-685.
89. Shieh, W.Y.J., and Sandhu, R.S., "Application of Elasto-Plastic Analysis in Earth Structures", ASCE National Water Resources Engineering Meeting, Memphis, Tenn., Preprint 1077, January 1970, pp. 1-21.
90. Skopek, J., "The Influence of Foundation Depth on Stress Distribution", Proceedings, 5th International Conference on Soil Mechanics and Foundation Engineering, Paris, Vol. 1, 1961, pp. 815.

91. Smith, I.M. and Hobbs, R., "Finite Element Analysis of Centrifugal and Built up Slopes", *Geotechnique*, Vol. 24, No.4, 1974, 531-559.
92. Smith, I.M., and Kay, S., "Stress Analysis of Contractive or Dilative Soils", *Journal of Soil Mechanics and Foundation Division*, ASCE, Vol. 97, No. SM7, 1971, pp. 981-997.
93. Sokolov'skii, V.V., *Statics of Granular Media*, Pergamon Press, New York, 1965.
94. Stricklin, J.A., and Haisler, W.E., "Formulations and Solution Procedures for Non-linear Structural Analysis", *Computers and Structures*, Vol. 7, No.1, 125-136, 1977.
95. Sutherland, H.B., "Model Studies for Shaft Raising Through Cohesionless Soils", *Proceedings, Sixth International Conference on Soil Mechanics and Foundation Engineering*, Montreal, Canada, Vol. 2, 1965, pp. 410-413.
96. Timoshenko, S.P., and Woinowsky-Krieger, S., *Theory of Plates and Shells*, McGraw-Hill, 2nd ed., 1959.
97. Tschebotarioff, G.P., *Foundations, Retaining and Earth Structures*, McGraw-Hill, 2nd ed., 1973.
98. Turner, E.Z., "Uplift Resistance of Transmission Tower Footings", *Journal of Power Division*, ASCE, Vol. 88, No. P02, 1962, pp. 17-33.
99. Valliappan, S., Discussion, *Journal of Soil Mechanics and Foundation Division*, ASCE, Vol. 95, No. SM2, March 1969, pp. 676-678.
100. Varma, B.S., Khadilkar, B.S., and Chandrasekaran, V.S., "Circular Footing on Transversely Isotropic Soil", *Proceedings, International Symposium on Soil Structure Interaction*, Dept. of Civil Engg., Roorkee, India, 1977, pp. 265-270.
101. Vesic, A.S., "Breakout Resistance of Objects Embedded in Ocean Bottom", *Journal of Soil Mechanics and Foundation Division*, ASCE, Vol. 97, No. SM9, 1971, pp. 1183-1205.
102. Vesic, A.S., Wilson, W.E., Clough, G.W., and Tai, T.L., "Theoretical Studies of Cratering Mechanisms Affecting the Stability of Cratered Slopes", *Final Report, Phase II, Project No. A-655, Engineering Experiment Station, Georgia Institute of Technology, Atlanta, Georgia.*

103. Yamada, Y., and Yoshimura, N., "Plastic Stress-Strain Matrix and its Application for the Solution of Elastic-Plastic Problems by the Finite Element Method", International Journal of Mechanical Sciences, Vol. 10, 1968, pp. 343-354.
104. Zienkiewicz, O.C., The Finite Element Method, McGraw-Hill Book Company (UK) Limited, 3rd Expanded and Revised Edition, 1977.
105. Zienkiewicz, O.C., Best, B., Dullage, C., and Stagg, K.G., "Analysis of Non-linear Problems in Rock Mechanics with Particular Reference to Jointed Rock Systems", Proceedings, Second Congress, International Society on Rock Mechanics, Belgrade, 1970, pp. 8-14.
106. Zienkiewicz, O.C., Humpheson, C., and Lewis, R.W., "Associated and Non-Associated Visco-plasticity and Plasticity in Soil Mechanics", Geotechnique, Vol. 25, No.4, 1975, pp. 671-689.
107. Zienkiewicz, O.C., and Naylor, D.J., "The Adoption of Critical State Soil Mechanics for Use in Finite Elements", Proceedings, Roseoe Memorial Symposium, Cambridge, 1972, pp. 537-547.
108. Zienkiewicz, O.C., Valliappan, S., and King, I.P., "Elasto-Plastic Solutions of Engineering Problems. 'Initial Stress' Finite Element Approach", International Journal of Numerical Methods in Engineering, Vol. 1, 1969, pp. 75-100.

Appendix A

a. PROGRAM : ISOPLN

This computer program is developed at IIT Kanpur, in DEC-1090 system. It can be used for two dimensional analysis of plane stress and plane strain problems. The 4 noded quadrilateral linear isoparametric element has been used to discretise the continuum. The program incorporates a data generating facility for nodes and elements whereby only a minimum amount of information need be input to specify problem geometry. Depending on the core storage requirements of the problem, and the maximum core available necessary modifications can be made. The program uses in-core storage and uses Cholesky decomposition to solve the resulting banded symmetric linear set of equations. In the form that it is developed it can take 650 nodes, 600 elements, 20 surface tractions and 10 different materials.

Most of the computational steps are carried out in the various subroutines of the program. Main routine controls important subroutines.

MAIN	reads the title of the problem,
	calls DATAIN, computes number of equations, semi-
	bandwidth and prints it,
	calls ASEMBL, to form and assemble overall stiffness
	matrix, load vector and to apply geometric
	boundary conditions,

MAIN calls CHOLLES to solve overall equilibrium equations
 and prints resulting displacements,
 calls STRESS to calculate stresses.

DATAIN reads and prints input data

ASEMBL initialises overall stiffness matrix,
 calls element stiffness matrix routine ISO4PL,
 assembles global stiffness matrix, forms global
 load vector,
 calls GEOMBC to apply geometric boundary conditions.

ISO4PL initialises element stiffness matrix,
 forms stress strain matrix,
 calls SHAPE to form elements of strain-displacement
 matrix and Jacobian determinant at integration
 point
 Forms stiffness matrix and body forces vector if
 needed

SHAPE Calculates shape function, X and Y derivatives of
 shape function and determinant of Jacobian

GEOMBC Applies prescribed displacement boundary conditions
 at nodes

CHOLLES Carries out the triangularisation of the banded symmetric matrix by Cholesky decomposition in DECOM and solves for the displacement vector by back substitution in RESOLV.

STRESS Computes from nodal displacements element strains; calculates elements stresses at centroidal point and principal stresses. Prints out the stresses and principal stresses at element centroids.

b. PROGRAM : ISOPLJ

The program has same general features of ISOPIN. It has provision to include 4 noded interface elements. From ASEMBL, JO14PL are called.

JO14PL Calculates the element stiffness matrix of the 4 noded interface element in local co-ordinates and transforms it to global co-ordinates.

Joint forces are calculated in stress routine.

c. PROGRAM : ISOBMJ

The program has same general features of ISO4PL. It has provision to include beam-column element and joint element. From assembly routine ASEMBL, Subroutine BEAM and JO14PL are called.

BEAM Calculates the element stiffness matrix of the beam-column element in local co-ordinates and transforms to global co-ordinate systems.

Internal forces in beam are calculated in STRESS routine.

Appendix B

PROGRAM ELPIPL

This computer program is developed at IIT, Kanpur in DEC-1090 system. The program can be used for the two-dimensional plane strain elasto-plastic analysis using Von-Mises model. The 8 noded parabolic isoparametric element is used to discretise the continuum. 6 noded interface elements model interface. 'Initial stress' method is used for non-linear elasto-plastic analysis. The program incorporates a data generating facility for nodes and elements. Assembly and solution are performed in-core.

Most of the computational steps are carried out in various subroutines of the program. Main routine controls various subroutines. Flow charts for MAIN, ASEMBL and STRESS are presented in Figs. B.1, B.2 and B.3 respectively.

MAIN	reads title of the problem, calls DATAIN, calls ASEMBL, CHOLBS, STRESS calls PRINTR to print final results.
DATAIN	reads and prints maximum number of increments, maximum number of iterations and convergence criterion, reads and prints material properties, reads, generated and prints nodal point data, element data, reads and prints surface traction data.

ASEMBL initialises global stiffness matrix, load vector
 and total displacement vector,
 calls IS08PL, JOI6PL and assembles global stiffness
 matrix, assembles load vector,
 calls GEOMBC

IS08PL initialises element stiffness matrix,
 forms stress strain matrix,
 calls SHAPE to form elements of strain displacement
 matrix and Jacobian determinant at integration point,
 stores elements of B matrix and determinant of
 Jacobian for all integration points in all elements
 in INCR = 1, ITER = 1.

JOI6PL calculates the element stiffness matrix of the 6 noded
 interface element in local co-ordinates and transforms
 to global

SHAPE calculates shape function, X and Y derivatives of
 shape function and determinant of Jacobian for the
 8 noded element

GEOMBC applies prescribed boundary condition at nodes

CHOLES carries out the triangularisation of the banded
 symmetric matrix by Cholesky decomposition for
 INCR=1, ITER=1,
 Solves for displacement vector by back substitution
 for all iterations

STRESS initialises the total stress, strain vectors or
 assigns initial stresses due to gravity loads,
 selects incremental nodal displacements,
 calculates incremental strains and stresses,
 checks for yield at integration points,
 calls ELPLAS if element has yielded,
 computes correction stress vector if yielded and
 find residual load vector,
 calls PRINTR once solution converges

ELPLAS calculates the elasto-plastic matrix for the current
 stress
 value at each integration point using Von-Mises model

PRINTR prints load increment, number of iterations performed
 prints applied load,
 prints total displacements and incremental displacements at nodal points,
 prints co-ordinates of integration point, condition of
 the point (elastic or plastic), stress and principal
 stress.

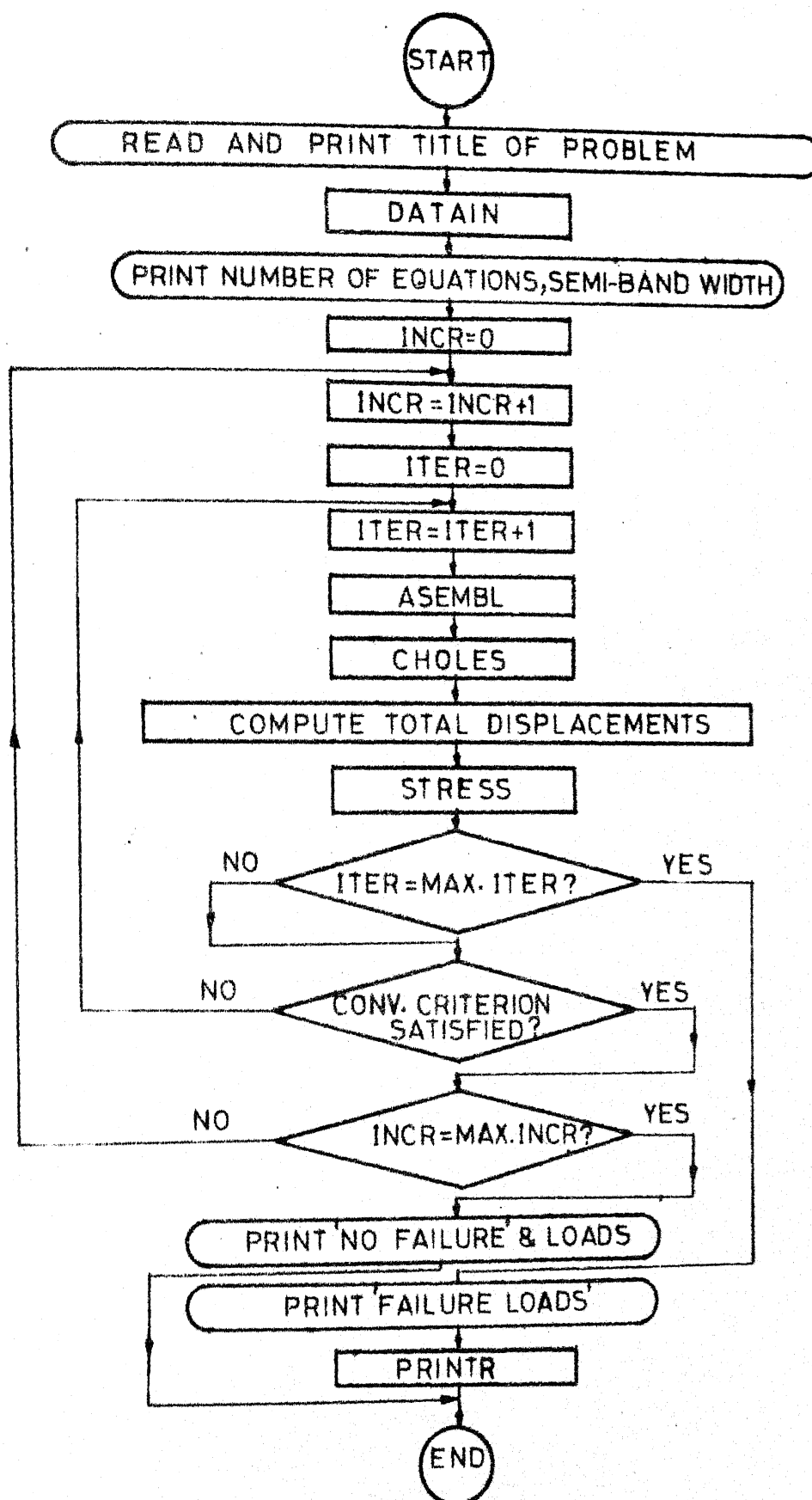


FIG. B.1 FLOW CHART: MAIN
PROGRAM : ELPLP1

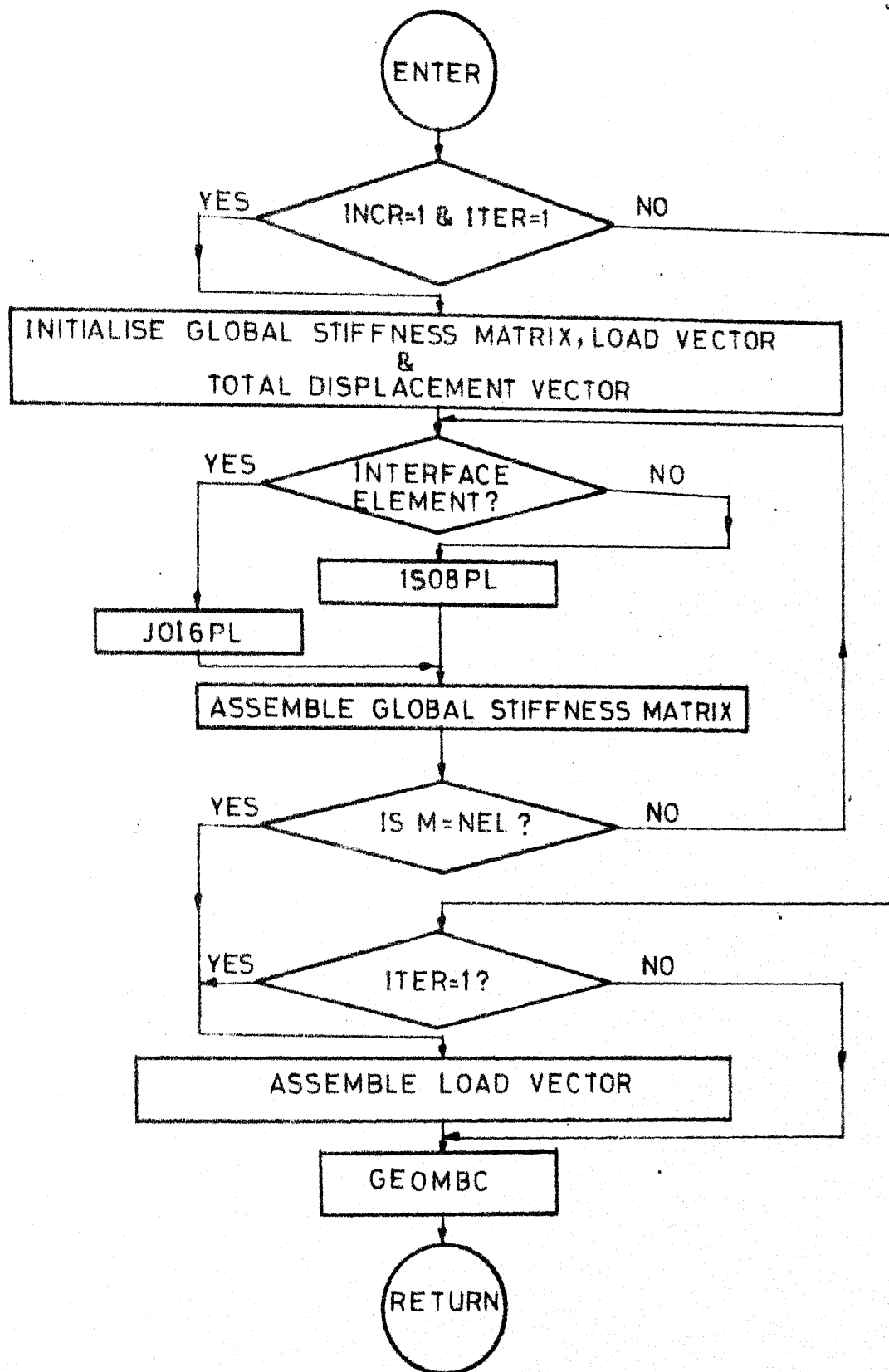


FIG. B2 FLOW CHART:ASEMBL
PROGRAM :ELPLP1

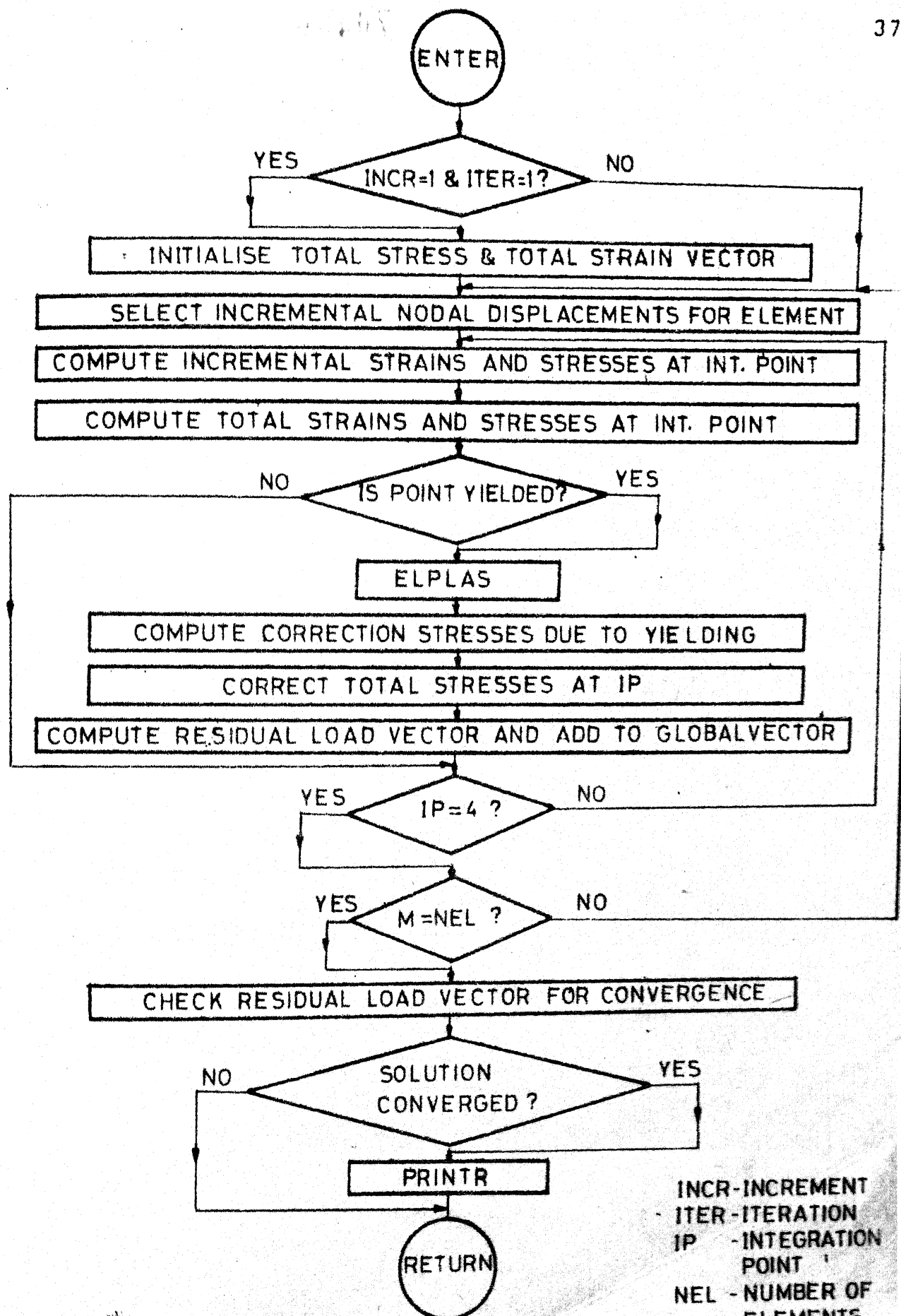


FIG. B.3 FLOW CHART: STRESS PROGRAM :ELPLP1

A70490

CE-1981-D-VII-FIN